Proteomics approach to understand HIV-Mycobacteria co-infection

Thesis submitted for the degree of

DOCTOR OF PHILOSOPHY

By

Ganji Rakesh

(09LBPH18)

Supervisor

Dr. Sharmistha Banerjee

Department of Biochemistry

School of Life Sciences

University of Hyderabad-500046

India

Department of Biochemistry

School of Life Sciences

University of Hyderabad

Hyderabad 500 046

India

CERTIFICATE

This is to certify that this thesis entitled **"Proteomics approach to understand HIV-Mycobacteria co-infection"** submitted to the University of Hyderabad by Mr Ganji Rakesh, for the degree of Doctor of Philosophy, is based on the studies carried out by him under my supervision. I declare to the best of my knowledge that this work has not been submitted earlier for the award of degree or diploma from any other University or Institution.

Dr. Sharmistha Banerjee

Supervisor

Head

Department of Biochemistry

Dean

School of Life Sciences

Department of Biochemistry
School of Life Sciences
University of Hyderabad
Hyderabad 500 046
India

DECLARATION

I, Ganji Rakesh, hereby declare that the work presented in my thesis is entirely original and was carried out by me in the Department of Biochemistry, University of Hyderabad, under the supervision of **Dr. Sharmistha Banerjee.** I further declare that this work has not been submitted earlier, in part or in full, for the award of degree or diploma to this University or from any other University or Institution.

Dr. Sharmistha Banerjee
Supervisor

Ganji Rakesh

Date:

Place: Department of Biochemistry,
School of Life Sciences,
University of Hyderabad,
Hyderabad - 500 046

Department of Biochemistry
School of Life Sciences
University of Hyderabad
Hyderabad 500 046
India

DECLARATION

I, Ganji Rakesh, hereby declare that the work presented in my thesis is entirely original, plagiarism free and was carried out by me in the Department of Biochemistry, University of Hyderabad, under the supervision of **Dr. Sharmistha Banerjee.** I further declare that this work has not been submitted earlier, in part or in full, for the award of degree or diploma to this University or from any other University or Institution. I hereby agree that my thesis can be deposited in shodganga/INFLIBNET.

A report on plagiarism statistics from the University Librarian has been enclosed.

Dr. Sharmistha Banerjee
Supervisor

Ganji Rakesh

Date:

Place: Department of Biochemistry,
School of Life Sciences,
University of Hyderabad,
Hyderabad - 500 046

TABLE OF CONTENTS

Acknowledgements

First and foremost I thank my supervisor **Dr Sharmistha Banerjee** for her constant guidance and support throughout my Ph.D. I am amazed by her understanding of science and skills to analyse the data. I am truly inspired by her commitment to science or any other responsibility that comes her way. She always has a different positive perspective towards a problem which makes it easy to solve or worry less about the problem. I am always grateful for her confidence and trust on me as I had a great freedom to plan and execute my ideas in research without any pressure. This made me to identify my own strength and drawbacks, and particularly boosted my self-confidence. She has been a great support through the rough roads to finish my PhD. I believe from my heart that she is a dream supervisor for a student who wants to do research and I am lucky to be one of those who had an opportunity to work with her. I am always grateful to my supervisor for everything.

I am always thankful to my doctoral committee members: **Dr. Krishnaveni Mishra** and **Dr. Naresh Babu V Sepuri** for their critical comments and invaluable suggestions on my PhD work.

I would like to thank Heads of Department of Biochemistry (**Prof. N. Siva Kumar**, Prof. O.H. Setty, and Prof. K.V.A Ramaiah) and Deans of School of Life Sciences (**Prof. P. Reddanna**, Prof. Aparna Dutta Gupta, Prof. M. Ramanadham, Prof. A.S Raghavendra and Prof. R.P. Sharma) for allowing me to use all the central facilities of department and school.

I would like to thank all the faculty members of school of life sciences for their timely help.

I would also like to specially mention **Dr. Shekhar Mande** for his moral support, inspiration and encouragement during my tenure.

I express my gratitude to **Prof. K. Dharmalingam, Prof. K Veluthambi, Prof. R. Usha, Prof. S. Krishnaswamy** and **Prof. P. Palanivelu** for instilling both the scientific temper and attitude in me during my M.Sc. days.

I would like to thank Ms Nalini and Rachana for Confocal Microscopy and Chandrasekharan, Jalaja and Dr. Shiven for FACS analysis and their timely help.

I would also like to thank Dr. Shekhar Mande, Dr. Srikanth, Snigdha Dhali and Dr. Gaurang from NCCS, Pune for helping me with the proteomic data acquisition, identification analyses. I thank Dr. Sanjeev, CDFD, for timely help with Confocal microscopy. I also would like to thank Dr. Kanury Rao and Baseerat from ICGEB, New Delhi for helping me with the iTRAQ-based proteomic data acquisition and identification.

I thank Prof. Michael S. Glickman (*M. smegmatis*::Δrip1 and *M. smegmatis*::Δrip1-pMV-rip1), Prof. Eric J. Rubin (*M. smegmatis*::Δesx3), Dr. Rajesh S. Gokhale (*M. smegmatis*::Δpks) and Dr. Marcela Rodriguez (*M. smegmatis*::ΔIdeR) for providing the corresponding mycobacterial mutant strains. I thank Dr. Lalita Ramakrishnan and Dr. Deepak Saini for pTEC15 plasmid, Dr. Jayant Bhattacharya for pNL-ADA8 and Prof. Jaya S Tyagi for mycobacterial RNA isolation protocol.

I also thank my present and Ex- lab mates **Dr. Ronald, Dr. Atoshi, Dr. Harini, Harika, Arshad, Mahesh, Swetha, Kiran, Kannan, Suman, Dr. Krishnaveni Mohareer** for making my stay in the lab wonderful. I particularly thank Harika and Arshad for all their help during my PhD and also for all the 'Tom and Jerry' fights I and Harika had in the lab for every petty issue. I thank my juniors Kiran, Swetha, Kannan and Suman for helping whenever I ordered (with stern smile). I thank Mahesh for keeping the lab and culture room clean (Upon repeated reminders and persuasions). I relish all those lab parties we had together. Finally, I thank all of them for bearing with my terrible singing skills.

I thank **Mr. Prasenjit Banerjee** for his moral support and encouragement during my tenure.

I cannot imagine all these PhD years without my beloved friends: Jalaja, Harika, Prasad, Aadhi, Anji, Abdul, Madhavi, Shalu, Fareed, M. Swetha, Amina, Satyabala. These people have always been there to help me during my PhD. I also thank all my SLS friends.

I have been fortunate to have best friends: **Priyan, Raghuram, Sai Srinivas, Jalaja, Harika, Arshad, Prashanth, Chandoo** and **Anil**. They literally supported me all through my ups and downs during my Ph.D.

I am also fortunate to have friends like, Priyan, Sai Srinivas, Pavan, Jalaja, Sudhanshu, Avishek, Saroj, Jaya, Bhaba, Rahul, Ranjeet, Nagesh, Dr. Ajith and Dr. Padmanabhan with whom, other than the fun part, I could discuss Science and get critical suggestions.

I thank all the projects students (Ira, Saranya, Kannan, Harsha and others) who worked with me during the course of my PhD and had to bear my 'Kadoosipan'.

I acknowledge **CSIR** for my financial support through **CSIR-JRF and SRF**.

I also thank all the funding bodies (CSIR, UGC, ICMR, DBT, CREBB, DST, FIST, UPE, PURSE) for their financial assistance to the department and School.

I also acknowledge **Bill and Melinda Gates' foundation** for giving me the travel grant award to attend **15TH International Congress of Immunology-2013** at Milan, Italy.

I would like to thank my family for all the love and support. Their love and care always made me happy and forget the bad times.

ABBREVIATIONS

µg	micro gram
AIDS	Acquired Immune deficiency syndrome
ANOVA	Analysis of variance
AP-1	Activator protein 1
APC	Antigen presenting cell
APOBEC3G	apolipoprotein B mRNA editing enzyme, catalytic polypeptide-like 3G
ART	Anti-retroviral treatment
ATP	Adenosine triphosphate
BCG	Bacillus Calmette-Guerin
bp	base pair
BSA	Bovine serum albumin
C/EBP	CCAAT-enhancer binding protein
CCR5	C-C chemokine receptor type 5
CD	Clusters of Differentiation
cDNA	Complementary deoxyribonucleic acid
CFU	Colony forming unit
cfu units	Fold change in CFU with respect to CFU of mono-infection
cGAS	cyclic GMP-AMP synthase
CHCA	α-cyano-4-hydroxycinnamic acid
CTL	Cytotoxic-T-lymphocyte
CXCR4	Chemokine (C-X-C Motif) Receptor 4
DCs	Dendritic cells
DC-SIGN	Dendritic cell-specific intercellular adhesion molecule-3-grabbing non-integrin
DMEM	Dulbecco's Modified Eagle Medium
DMSO	Dimethyla Sulphoxide
DNA	Deoxyribonucleic acid
dNTP	Deoxynucleotide triphosphate
dsDNA	Double stranded DNA
DTT	Dithothreitol
E. coli	Escherichia coli
EDTA	Ethylene diamine tetraacetic acid
EGTA	Ethylene glycol tetraacetic acid
ELISA	Enzyme-linked immunosorbent assay
esx	Type VII secretion systems
FACS	Fluorescence-activated cell sorting
FBS	Fetal bovine serum
FITC	Fluorescein isothiocyanate
fmol	femtomole
FP	Forward Primer
GAPDH	Glyceraldehyde-3-phosphate dehydrogenase
GFP	Green fluorescent protein
GO	Gene Ontology
gp	Glycoprotein
GPL	Glycopeptidolipid
HAART	Highly active anti-retroviral treatment
HBS	HEPES buffered saline
HEK	Human embryonic kidney cells

HEPES	N-(2-hydroxyethyl) piperazine-N'-(2-ethanesulfonic acid)
HIV	Human Immunodeficiency virus
HIV+	HIV positive individual
hr	Hour
HRP	Horse radish peroxidase
hsp60 promoter	heat shock protein 60 promoter
iDCs	Interstitial dendritic cells
IFI16	Interferon inducible protein 16
IFN	Interferon
IL	Interleukin
iNOS	inducible Nitric oxide synthase
IRIS	Immune reconstitution inflammatory syndrome
iTRAQ	Isobaric tags for relative and absolute quantitation
kDa	Kilo Dalton
KO	Knock out
LC-MS/MS	Liquid Chromatography-Mass spectrometry/mass spectrometry
LTR	Long terminal repeat
M. avium	*Mycobacterium avium*
M. bovis	*Mycobacterium bovis*
M. kansasii	*Mycobacterium kansasii*
M. phlei	*Mycobacterium phlei*
M. smegmatis	*Mycobacterium smegmatis*
M.tb	*Mycobacterium tuberculosis*
MAC	*Mycobacterium avium* complex
MALDI	Matrix-assisted laser desorption ionization
MALDI-Tof	Matrix-assisted laser desorption ionization-Time of flight
mg	milli gram
MHC	Major Histocompatibility complex
min	minute
MIP	Macrophage inflammatory protein
mL	Milli Litres
mM	Milli Molar
MMTS	Methyl methane thiosulfonate
MOI	Multiplicity of infection
MOTT	Mycobacteria other than tuberculosis
mRNA	Messenger ribonucleic acid
MTBC	Mycobacterium tuberculosis complex
MX2	Myxovirus resistance 2
MΦ	Macrophage
Nef	Negative factor
NFAT	Nuclear factor of activated T-cells
NFκB	Nuclear factor kappa-light chain enhancer of activated B cells
NK	Natural Killer cell
NO	Nitric oxide
NP-40	Nonidet-P40
NTM	Non-tuberculous mycobacteria
OADC	Oleic acid Albumin Dextrose Catalase
^{o}C	Degree Celsius
OD	Optical density
PAMP	Pathogen associated molecular pattern

PCR	Polymerase chain reaction
PDB	Protein databank
pDCs	Plasmacytoid dendritic cells
PDIM	Phthiocerol Dimycocerosates
PEG	Polyethylene glycol
pg	pico gram
pks	Polyketide synthase
PMA	Phorbol myristate acetate
PMSF	Phenyl methane sulfonyl fluoride
PNK	Poly nucleotide kinase
PPD	Purified protein derivative
PRR	Pattern recognition receptor
qRT-PCR	Quantitative Real Time PCR
Rab	Ras-related protein
RANTES	Regulated on activation, normal T cell expressed and secreted
rip1	Regulated intramembrane proteolysis protein 1
RNA	Ribonucleic acid
RNS	Reactive Nitrogen Species
ROS	Reactive oxygen species
RP	Reverse Primer
RPM	Revolutions per minute
RPMI	Roswell Park memorial institute
RT	Room temperature
SAMHD1	Sterile alpha motif domain-C-terminal HD domain containing protein 1
SD	Standard deviation
SDS-PAGE	Sodium dodecyl sulphate-Polyacrylamide gel electrophoresis
sec	Second
ssDNA	Single stranded DNA
TA system	Toxin-antitoxin system
TAT	trans-activator of transcription
TB	Tuberculosis
TCEP	Tris-2-carboxyethy phosphine
TEAB	Triethylammonium bicarbonate
TEMED	N,N,N',N'-tetramethyl ethylene diamine
TFA	Trifluoro acetic acid
TGF	Tumor growth factor
TH1	T-helper cell 1
TH2	T-helper cell 2
TLR	Toll like receptor
TNF	Tumor necrosis factor
TNF-R	Tumor necrosis factor-receptor
Treg	Regulatory T cells
Tris	Tris (hydroxymethyl)aminomethane
UNAIDS	United Nations program on HIV/AIDS
VapBC	Virulence associated protein BC
vif	viral infectivity factor
Vpr	Viral protein R
Vpu	Viral protein U
Vpx	Viral protein x
WebGestalt	WEB-based GEneSeT Analysis Toolkit

WHO	World health organization
ZN staining	Ziehl-Neelsen staining

LIST FIGURES AND TABLES

Chapter 1

Introduction

Introduction

Human Immunodeficiency Virus (HIV), the lentivirus that weakens body's natural defense system causes a lifelong illness that culminates into Acquired Immunodeficiency Syndrome (AIDS), shortening the life expectancy. HIV infection is characterized by long asymptomatic incubation period referred to as clinical latency stage, where though asymptomatic, the infected host is susceptible to an over-abundance of infections. With no cure or early diagnosis in hand, inexorable high costs of treatment and patient care, associated co-infections and social stigma, HIV infection remains one of the most dreaded communicable disease worldwide, being responsible for a significant number of deaths (WHO report, 2014). WHO reported more than 35 million people infected with HIV across the world, which included 2.1 million registered new cases in 2013 (WHO report, 2014). The global epidemiology of HIV infection changed markedly owing to increased social awareness and expanding access to anti-retroviral therapy to low-income and middle-income countries. Although this has increased the life expectancy of HIV infected people, nearly 1.5 million HIV+ individuals reportedly died round the globe in 2013. In India, the percentage of AIDS related deaths decreased by 38% and newly diagnosed HIV+ cases fell by 19%. Despite the improvements, India stands third amongst total global HIV cases and first in the Asia-Pacific region (UNAIDS Gap report, 2014). This admissibly is unacceptable, given the fact that HIV infection can be prevented by public awareness.

HIV infects immune cells of myeloid origin, viz; T lymphocytes, monocytes, dendritic cells etc. that serve for viral propagation, spread and reservoir (Iordanskiy, Santos et al. 2013). This collapses the body's natural defense against many infections. The deaths in HIV infected individuals are mostly due to acquired secondary infections. Liver co-infections, the likes of hepatitis B and C, which follow related routes of transmission with HIV, are very common (Koziel and Peters 2007; Chen, Feeney et al. 2014). However, tuberculosis continues to be the foremost cause of morbidity and mortality in HIV infected population in low-income and middle-income countries, including India (WHO report, 2014).

1.1 HIV and Tuberculosis co-infection

Tuberculosis (TB) caused by bacillus *Mycobacterium tuberculosis* (*M.tb*), accounts for nearly 66% of co-infection within the total HIV positive cases. Tuberculosis, by itself, is a global health

problem, being responsible for the largest number of morbidity and mortality by a single infectious agent. In 2013, 9 million new TB cases were registered and resulted in 1.5 million deaths worldwide, only second to HIV (WHO report, 2014). India has the highest burden of TB in the world which accounts for nearly one-fourth of total TB cases worldwide. Nearly, 40% of Indian population is infected with TB, majority of which have latent infections (WHO report, 2014). TB is also the leading cause of deaths, accounted for 320,000 deaths in 2013 among HIV+ population, which is one-fourth of the total mortality associated with HIV infections (WHO report, 2014). The HIV-TB co-infection worsens the disease complications of both HIV and TB making the disease management highly challenging and expensive.

Clinical studies across the globe have recognized that HIV and TB during HIV-TB co-infection act in a synergistic manner accelerating the progression of both the diseases. It is reported that HIV patients have increased risk of acquiring primary TB or reactivation of latent TB (Suchindran, Brouwer et al. 2009; Naidoo, Padayatchi et al. 2011; Pawlowski, Jansson et al. 2012). In addition, pulmonary TB may also occur very early during HIV infection, even before T-cell depletion is apparent (Sonnenberg, Glynn et al. 2005). HIV patients are reported to progress to AIDS much faster if co-infected with TB than those without TB infection (Goletti, Weissman et al. 1996; Badri, Ehrlich et al. 2001; Collins, Quinones-Mateu et al. 2002). Disease management of HIV related TB is highly complex because of drug to drug interactions, side effects from both the anti-retroviral and the anti-TB regimens and increased incidence of Immune reconstitution inflammatory syndrome (IRIS) upon concomitant highly active anti-retroviral therapy (HAART) (Padmapriyadarsini, Narendran et al. 2011). IRIS is a condition where the compromised immune system recovers upon HAART and elicits an exaggerated inflammatory response towards TB, further worsening the symptoms of this opportunistic infection (Naidoo, Padayatchi et al. 2011; Sharma and Soneja 2011).

Apart from the pathogenic mycobacterial species, another emerging threat in the context of HIV infected population is the infections from the environmental non-tuberculous mycobacteria (NTM) (Juffermans, Verbon et al. 1998; Smith, Schnadig et al. 2001; Bachmeyer, Blum et al. 2002; Karakousis, Moore et al. 2004; Serra, Loi et al. 2007; Singh, Gopinath et al. 2007; Azzopardi, Bennett et al. 2009; Hesseling, Johnson et al. 2009). NTMs, which otherwise cannot establish infection in an immunocompetent individual (Zhang and Sugawara 2012), pose a serious threat to the HIV infected population, given the fact that they are not only abundantly present in

environment sharing common habitat with humans, but the infection remains asymptomatic, hard to diagnose and resistant to the conventional TB therapy (Primm, Lucero et al. 2004; Falkinham 2009; Brown-Elliott, Nash et al. 2012). There is a growing body of evidence suggesting infection by NTMs in HIV+ population as new emerging infectious diseases (Wagner and Young 2004). Although there are several ongoing attempts to understand the coalition between HIV and pathogenic strains of mycobacteria, the studies to understand the early establishment of infections by NTM in the HIV infected population are modest. A major impediment towards understanding co-infection biology has been the absence of simplified cell culture based co-infection models that simulate clinical observations. Given the severity of HIV-TB co-infection and emerging NTM infections in HIV+ population, there is a need of studies, *in vitro*, *ex vivo* and *in vivo* to develop a holistic understanding of co-infection biology.

This study is focused on understanding the modulation of host intracellular environment during HIV-mycobacteria co-infection for the establishment of infection by both non-pathogenic (opportunistic) and pathogenic mycobacteria and to comprehend the early adaptive response of mycobacteria with consequent impact on the HIV-1 propagation.

Three objectives were framed to address the same:

1. Developing an in vitro cell culture based co-infection model simulating reported clinical observations.
2. Studying the differential expression of the host proteins and the consequent early adaptive changes in the intracellular mycobacterial proteome during co-infection through comparative proteomics.
3. Quantitative proteomics to tabulate modulations in the phagosome enriched fractions of macrophages by pathogenic *Mycobacterium tuberculosis* H37Rv during mono-infection and HIV-H37Rv co-infection.

One must acknowledge the fact that both HIV and *M.tb* are very successful human pathogens on their own. In order to comprehend the complexity of the host-pathogen interactions during co-infection, this chapter briefly introduces the pathobiology, immune response and evasion strategies of HIV and *M.tb* before briefly discussing the existing literature on HIV-mycobacteria co-infection and emerging threat of NTM infections in the context of HIV infected population.

1.2 Human immunodeficiency virus (HIV)

1.2.1 Dynamics of HIV entry and viral life cycle

HIV is a lentivirus belonging to *retroviridae* family containing two copies of positive single stranded RNA as genome. The genome size is 9 kilobases carrying 9 genes coding for 15 proteins which include structural, regulatory and accessory proteins (Kirchhoff 2014). There are two types of HIV; HIV-1, the most prevalent and highly virulent and HIV-2, less virulent and confined to West Africa (Sharp and Hahn 2011). While the lifecycle of HIV is complex, a succinct overview is presented here to comprehend the same. HIV enters the cells using surface glycoprotein, gp120 that interacts with CD4 receptor and chemokine receptors, such as CXCR4 and CCR5, on host cells (Loetscher, Moser et al. 2000). The choice of co-receptors determines the tropism of HIV. Viruses utilizing the CCR5 receptor are called R5 viruses that primarily infect Macrophages (M-tropic), but can also infect CD4+ T cells. Viruses utilizing CXCR4 are called X4 viruses which are T-tropic and primarily infect and replicate inside CD4+ T cells (Loetscher, Moser et al. 2000; Suresh and Wanchu 2006; Naif 2013). However, one must add that the co-receptor preferences alone do not define the tropism of the virus. Upon interaction of gp120 with CD4 and co-receptors, the gp41 acts on the cell lipid bilayer, fusing virus envelope with the lipid bilayer leading to uncoating of virus and release of the viral RNA along with the lysine transfer RNA, reverse transcriptase, protease, capsid proteins and integrase into the cytoplasm of the cell (Weiss 2013). The virus enters at the lipid rafts in the lipid bilayer membrane which are rich in cholesterol. The viral entry is also through endocytosis but it does not result in the productive viral infection (Schaeffer, Soros et al. 2004). After entry, it is followed by the synthesis of double stranded DNA by viral reverse transcriptase, import of the dsDNA with viral proteins (pre-integration complex) into the nucleus and integration of the proviral DNA into the host genome by viral integrase. The unintegrated viral dsDNA in the cytoplasm is degraded (Kirchhoff 2014). Once integrated, the viral 5' Long terminal repeats (LTR) act as promoter and enhancer, and recruit host RNA polymerase II, transcription factors and other effectors for viral transcription. The transcribed viral spliced and unspliced RNA are exported into the cytoplasm with the help of host and viral factor, Rev. The viral proteins are synthesized and the virion is packaged. The mature assembled virions bud off from the cell and proceed further to infect other cells (Barre-Sinoussi, Ross et al. 2013;

Kirchhoff 2014). A schematic representation of various steps in the life cycle of HIV is presented in Figure 1.

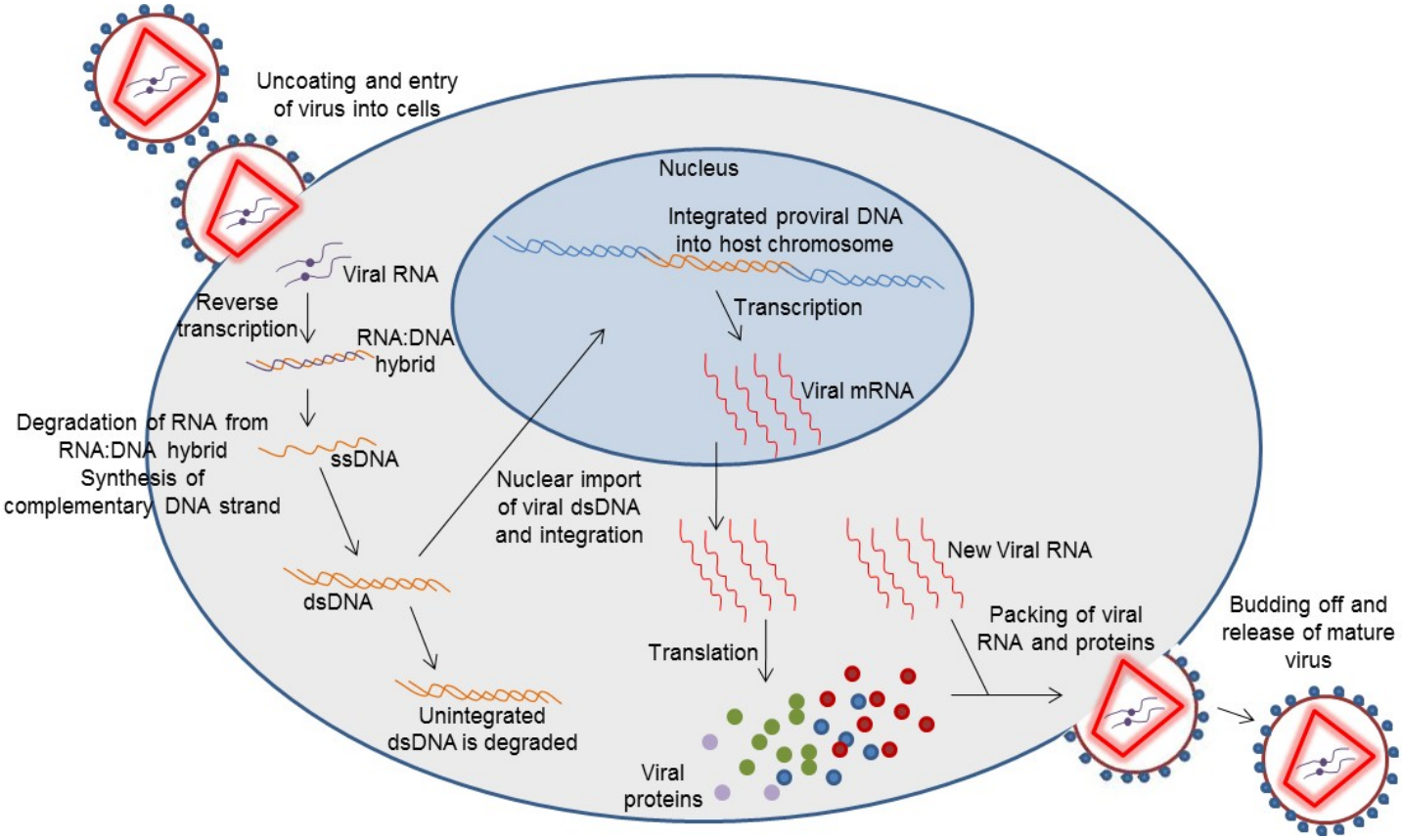

Figure 1: Schematic representation of the basic outline of HIV life cycle. After attaching to the cell surface through CD4 and co-receptors, the virus uncoats and fuses with the cell membrane and releases its genomic RNA and proteins into the cell. 1) The viral RNA is reverse transcribed using the viral reverse transcriptase. 2) The RNA in the RNA:DNA hybrid is degraded. 3) Second complementary strand of DNA is synthesized creating a double stranded viral DNA (dsDNA). 4) The viral dsDNA is imported into the nucleus and is integrated into the cell genome. 5) The proviral DNA is transcribed and viral mRNA is synthesized. 6) The viral mRNA is translated to produce viral proteins. 7) The viral RNA and proteins are packaged into virions. 8) The packaged, mature virions bud off from the membrane and are released. 9) Unintegrated viral dsDNA is degraded.

1.2.2 Host Innate and adaptive immune response to HIV infection and immune cells attacked by HIV

The infection of virus occurs in two stages namely, chronic infection and acute infection. Immediately after the infection, the viral load increases, but once the immune system is activated, an anti-viral immune response is initiated to counteract the virus and the increase in viral load is temporarily halted or stabilized through increasing the number of circulating CD4+ T cells. But, by then the virus establishes a chronic persistent infection during which the viral loads are stabilized and over a period of time, the number of CD4+ T cells decrease (Naif 2013). In the acute phase of HIV infection, the virus infects macrophages (M-tropic) and CD4+ T cells (T-tropic) and replicates. It then selectively and rapidly depletes the CD4+ T cells and cytotoxic CD8+ T cells (Figure 2). Since CD4+ and CD8+ T cells play a major role in cell mediated immune response to infections (McMichael, Borrow et al. 2010), the depletion of these cells makes the host susceptible to various opportunistic infections.

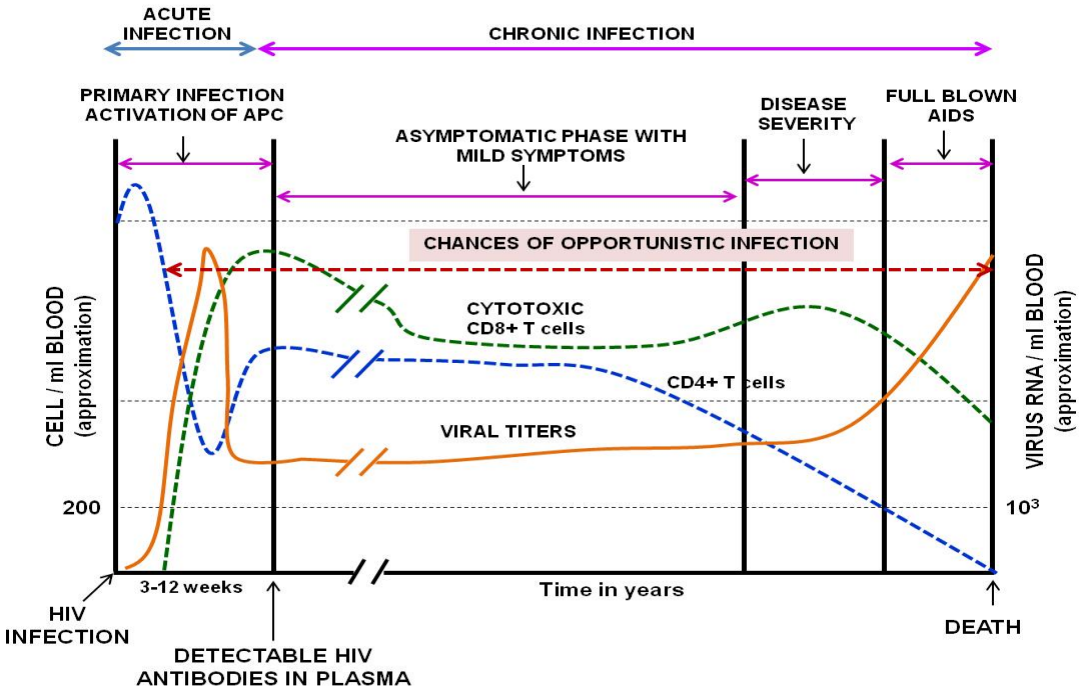

Figure 2: Graphical representation of the comparative levels of CD4+T cells, CD8+ T cells and viral titers during the course of HIV infection. The chances of opportunistic infection in HIV background span the entire period of infection. Representation adapted from Figure 1 in Munier, M.L., and Kelleher, A.D. (2007), *Immunol Cell Biol85*, 6-15 and Elsevier Science/Garland Publishing (Munier and Kelleher 2007).

The innate immune response against HIV infection forms the first line of defense. It mainly constitutes the macrophages, dendritic cells (DCs), natural killer cells (NK cells) and γδ-T cells (Medzhitov and Janeway 2000; Borrow, Shattock et al. 2010). HIV can infect both macrophages and DCs (Iordanskiy, Santos et al. 2013). The myeloid dendritic cells capture the virus through DC-SIGN (Geijtenbeek, Kwon et al. 2000; Geijtenbeek and van Kooyk 2003) and transmit the virus to the CD4+ cells in the lymphoid tissues where it helps in the initiation of adaptive anti-viral immune response (Groot, van Capel et al. 2006). The plasmacytoid DCs play a crucial role in the anti-viral immunity by releasing the type-I interferons which induce innate immune cells, including DCs to express the viral restriction factors by host (Groot, van Capel et al. 2006; Iwasaki and Medzhitov 2010). The activation of DCs results in the activation of NK cells that plays an important role in the early prevention of virus replication. It kills the virus-infected cells by perforin and granzymes through apoptosis and also modulates the function of DCs to control the viral spread (Cella, Jarrossay et al. 1999; Siegal, Kadowaki et al. 1999; Borrow and Bhardwaj 2008; Zhou, Kang et al. 2012). The innate immune cells also secrete chemokines such as, RANTES, MIP1α and MIP1β which block the CCR5 and prevent virus entry (Cocchi, DeVico et al. 1995; Lehner, Wang et al. 2000). The innate immune receptors involved in recognizing HIV pathogen associated molecular patterns (PAMPs) are: Toll like receptors (recognize the viral RNA) (Anderson 2000), C-type lectins such as DC-SIGN, dectin-1, mannose receptors (Recognize the viral glycoproteins) (Sallusto, Cella et al. 1995) and RIG-1 like receptors (Rustagi and Gale 2014). More recently identified pattern recognition receptors (PRRs) are interferon inducible protein 16 (IFI16) and cyclic GMP-AMP synthase (cGAS) which recognize the viral reverse transcriptase products (Jakobsen, Bak et al. 2013; Li, Wu et al. 2013). These PRRs upon recognition of the HIV antigens initiate intracellular anti-viral immune signaling cascade leading to the expression of type-I inteferons (IFN α and β) and host restriction factors, such as APOBEC3G (apolipoprotein B mRNA editing enzyme, catalytic polypeptide-like 3G), SAMHD1 (Sterile alpha motif domain-C-terminal HD domain containing protein 1), MX2 (Myxovirus resistance 2) and tetherin.

The adaptive immunity comprises of both humoral and cell-mediated responses. The humoral response is mainly directed in producing the neutralizing antibodies against the viral proteins,

especially viral capsid and envelope proteins but these have either little or no effect on the virus infectivity (Tomaras and Haynes 2009). The CD8+ T cells which form the major part in the cell-mediated immunity is quite effective against the virus. After gaining access into the host, virus is first detected by the dendritic cells and is attached onto the dendritic cell surface through the interaction with DC-SIGN receptor (Geijtenbeek and van Kooyk 2003). The dendritic cells carry the virus or present viral antigens to both the CD4+ T cells and CD8+ T cells in the lymphoid tissue through MHC-II and MHC-I complex leading to their activation (McMichael and Rowland-Jones 2001). The HIV-specific CD8+ T cells or cytotoxic T cells then recognize the virus infected cells and initiate apoptosis of virus-infected cells by secreting the perforin and granzymes. The activated CD4+ T cells secrete IL-2, IFNγ and TNFα which mediate cellular immune response. However, the activated CD4+ T cells are more susceptible to HIV infection as they express more co-receptors on their surface. The HIV-infected CD4+ T cells are compromised with respect to cytokine secretion, such as; they secrete IFNγ but not IL-2 (Younes, Yassine-Diab et al. 2003). The weakened CD4+ T cells do not support the anti-viral response of CD8+ T cells or formation of neutralizing antibodies by plasma cells. It thus leads to reduced CD8+ T cell function. Repeated activation of T cells with viral antigens lead to T cell exhaustion. Additionally, virus infection depletes TH17 pro-inflammatory cells and increases the regulatory T cells which further help in virus spread (Prendergast, Prado et al. 2010; Quaranta, Mattioli et al. 2012).

In summary, HIV attacks critical immune cells like Macrophages, Dendritic cells and CD4+ T lymphocytes impairing primarily the cellular wing of the immune system severely and indirectly the humoral wing through compromised activation of B lymphocytes.

1.2.3 Brief overview on immune evasion strategies of HIV

As mentioned earlier, the principle host restriction factors associated with helper T lymphocytes are APOBEC3G (apolipoprotein B mRNA editing enzyme, catalytic polypeptide-like 3G), SAMHD1 (Sterile alpha motif domain-C-terminal HD domain containing protein 1), MX2 (Myxovirus resistance 2) and tetherin. APOBEC3G, a cytidine deaminidase, is packaged into the budding virions and performs its retroviral restriction activity by causing Cytidine to Uridine mutations in the viral RNA (Sawyer, Emerman et al. 2004). Such mutations in the viral genome block the viral reverse transcription and finally viral replication. SAMHD1, a phosphodiesterase, is known to carry out its restriction activity by inhibiting the viral reverse transcription. It acts on

the deoxytrinucleotides (dNTPs) and thus decreases the intracellular pools of the dNTPs, which form the building blocks for the viral reverse transcription (Laguette, Sobhian et al. 2011). MX2 is a type-I interferon inducible gene which acts post viral reverse-transcription. It blocks the nuclear import of the viral DNA and destabilizes it (Goujon, Moncorge et al. 2013; Kane, Yadav et al. 2013). Tetherin, type-I interferon inducible gene, act late in the viral replication cycle. It tethers the virus onto the cell membrane and block viral release (Perez-Caballero, Zang et al. 2009; Sauter, Schindler et al. 2009). In parallel, HIV has developed numerous evasion strategies to overcome the defenses of the host. The innate immune responses, especially the host viral restriction factors are counteracted by the viral proteins. The APOBEC3G is counteracted by the HIV protein, viral infectivity factor (Vif). It blocks the recruitment of the APOBEC3G in the budding virions and directs it to the proteasomal degradation by exposing it for ubiquitination (Hultquist, Binka et al. 2012). The viral protein x (Vpx) is known to counteract the SAMHD1 mediated depletion of the dNTPs. The expression of Vpx results in the degradation of SAMHD1 (Laguette, Sobhian et al. 2011). Tetherin, that acts by blocking viral release is counteracted by viral protein u (Vpu) and Nef (Perez-Caballero, Zang et al. 2009; Sauter, Schindler et al. 2009; Simon, Bloch et al. 2015). The virus has also evolved defense strategies against host adaptive immune system. HIV envelope glycoprotein gp120 has low antigenicity and immunogenicity (Wyatt, Kwong et al. 1998). Additionally, to avoid detection by neutralizing antibodies, the epitopes are either hidden within the protein structures or masked by glycans making them inaccessible. HIV can also resist recognition as well as effector mechanisms of cytotoxic CD8+ T cells. Cytotoxic T cells (CTL) combat viral infections by inducing apoptosis in the infected cell (Petrovas, Mueller et al. 2005). HIV-1 can delay or prevent apoptosis in the residing cell. Fas and TNF-R mediated apoptosis of infected cells has been shown to be inhibited by viral protein Nef (Geleziunas, Xu et al. 2001; Yoon, Jeong et al. 2001). Nef and Tat are also reported to down-regulate MHC proteins and antigen processing (Goulder, Brander et al. 2001; Quaranta, Mattioli et al. 2012). HIV also mutates its epitopes frequently to avoid the recognition by MHC molecules or decrease binding affinity of the epitopes to these receptors (Back, Smit et al. 1994; Kamp, Berk et al. 2000).

Figure 3 summarizes some of the evasion strategies employed by HIV-1.

Suppositions are that HIV benefits from co-infections of the host by secondary pathogen-induced alterations in the host immune response, expression of HIV restriction factors or strengthening of HIV immune evasion strategies.

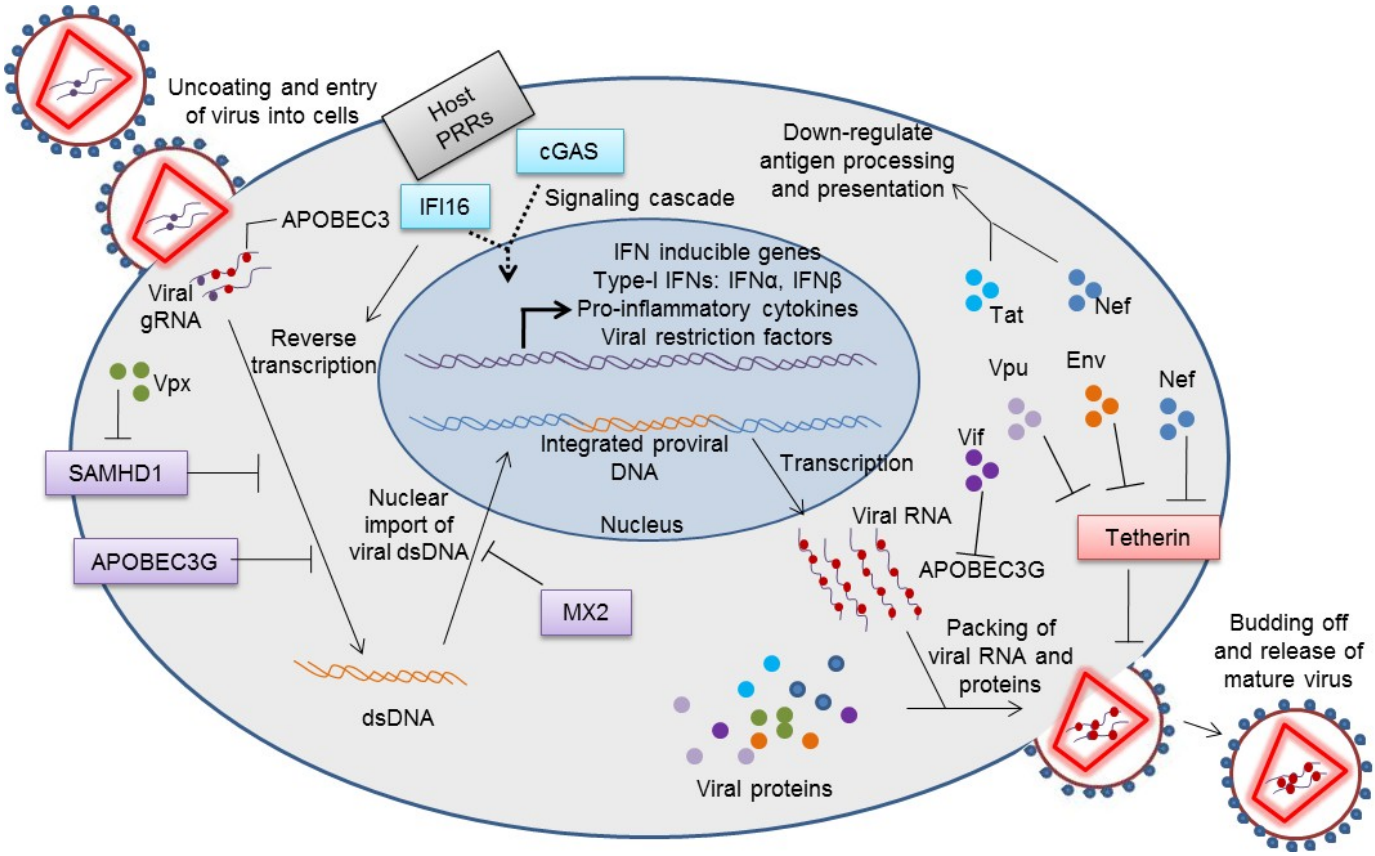

Figure 3: Overview of some of the evasion strategies employed by HIV. 1) The host pattern recognition receptors other than TLRs are IFI16 and cGAS. Both of them recognize the viral naked RNA and reverse transcriptase products and initiate signaling through STING followed by activation of IRF3 and NFκB which induce expression of pro-inflammatory cytokines, interferon inducible genes-MX2, type-1 interferons-IFNα and IFNβ and viral restriction factors-SAMHD1, APOBEC3G, tetherin. 2) SAMHD1 inhibits viral reverse transcription by depleting dNTPs. 3) APOBEC3G through its cytidine deaminidase activity converts C to U when packaged into virions and then inhibits reverse transcription. 4) MX2 inhibits the nulcear import of viral dsDNA. 5) Tetherin inhibits the release of virion from the cell. 6) SAMHD1 is inhibited by Vpx or Vpr or HIV-1 itself which initiate its degradation. 7) Tetherin is inhibited by Nef and also by Env and Vpu. 8) Vif inhibits APOBEC3G by directing it to proteasomal degradation. 9) Viral Tat and Nef are also reported to down-regulate antigen processing and presentation.

1.3 *Mycobacterium tuberculosis* (*M.tb*)-the tuberculosis (TB) causing bacteria

1.3.1 An outline of M.tb infection and host response

The disease tuberculosis (TB) is caused by *Mycobacterium tuberculosis* (*M.tb*) through bacteria containing aerosols. *M.tb* is a gram positive, obligate intracellular parasite which has a characteristic thick, lipid rich cell wall (Brennan 2003). It infects macrophages and resides in the phagosomes. *M.tb* has evolved to reside and propagate within the phagosomes of the macrophages by evading the defense strategies employed by macrophages, like fusion of lysosomes with phagosomes, preventing acidification, etc. (Cole, Brosch et al. 1998). After the aerosolic entry into a host, the bacteria are engulfed by the alveolar macrophages and interstitial dendritic cells forming the first line of defense against the pathogen. *M.tb* infection leads to secretion of cytokines by macrophages and DCs which prime T cells towards the TH1 kind of immune response characterized by secretion of pro-inflammatory cytokines such as IFNγ and TNFα, which further activate macrophages (O'Garra, Redford et al. 2013). *M.tb* can survive within the naïve or resting macrophages, but the IFNγ and TNFα stimulated macrophages or DCs can actively clear the mycobacterium. The mechanisms behind the clearance of mycobacteria by IFNγ-activated macrophages or DCs are not fully understood yet. Recently reported that, an IFNγ induced host factor LRG47, a guanosine triphosphatase, that associates with the phagosomes and promote phagosome maturation emphasizing the importance of phagosome maturation in containing mycobacteria (Weiss and Schaible 2015). Once inside the phagocytic cells there are two routes of spreading within the host; i) move into draining lymph nodes, priming the T cell responses; ii) enter the lung parenchyma and initiate the granuloma formation. Granuloma is a multi-cellular structure where the infected or uninfected macrophages and large multi-nucleated macrophages (called as epithelioid cells) are surrounded by the CD4+ and CD8+ T cells, B cells and fibroblast cells. Within the granuloma the *M.tb* is contained and cleared with the concerted immune functions of the macrophages, T cells (secrete IFNγ and TNFα to activate macrophages and CD8+ T cells act as CTLs) and fibroblast cells (form extracellular matrix shell). Occasionally, within granuloma the mycobacteria enter into a non-replicating and metabolically active dormant, asymptomatic state to avoid clearance by host and resurges when immune system is compromised (Flynn, Chan et al. 2011; O'Garra, Redford et al. 2013).

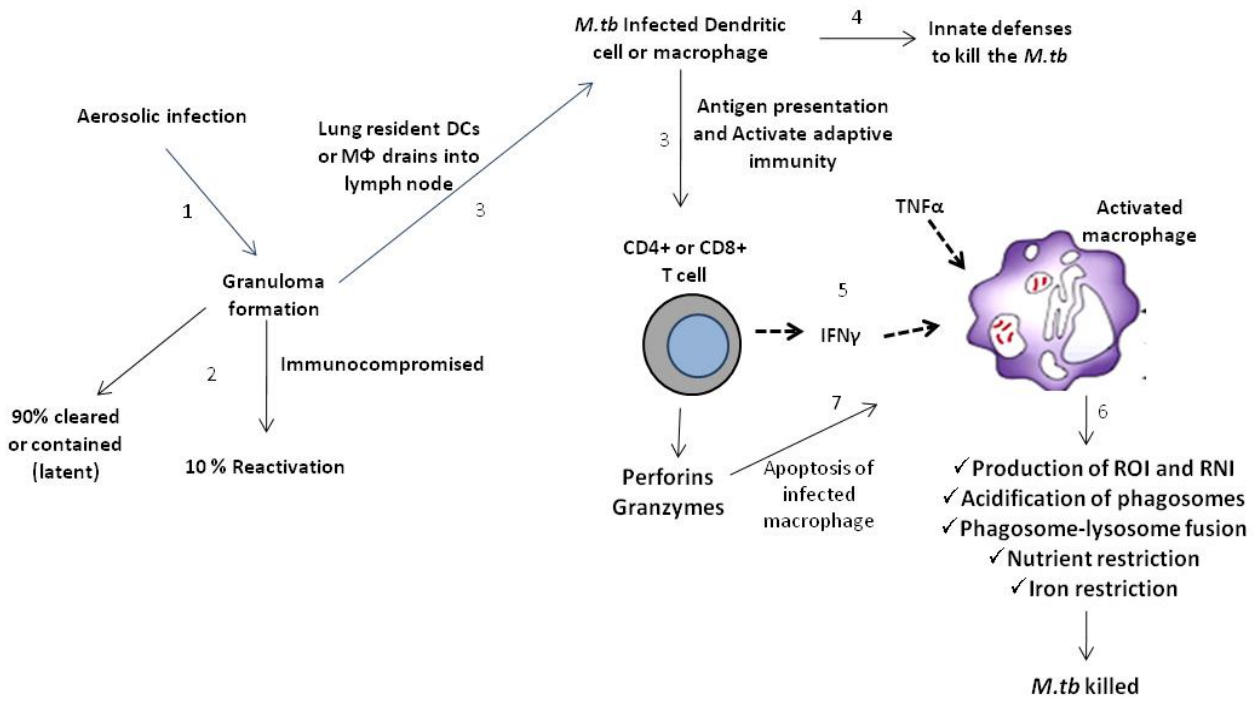

Figure 4: Overview of immune response against *Mycobacterium tuberculosis*. 1) Upon aerosolic infection, the host induces granuloma formation around the infected cells in the lungs. 2) Granuloma formation in 90% of the cases results in either clearance or containment of bacteria. In 10% of the infection cases, leads to disease or reactivation of contained bacteria which is due to either age related or other infection related immunocompromised state. 3) Upon infection, infected alveolar macrophages (MΦs) or Dendritic cells (DCs) drain into lymph node and prime adaptive immune response. 4) MΦ or DCs also employ innate defenses to kill the bacteria. 5) Activated adaptive immune response results in the secretion of pro-inflammatory cytokines which activate 6) MΦs that can kill the bacteria through phagosome maturation, oxidative burst or nutrient starvation. 7) Activated adaptive immune response also results in the killing of infected cells through apoptosis.

Mycobacterium also gains entry into the macrophages or DCs through phagocytosis using the complement receptors or Fc receptors or Scavenger receptors or mannose receptors where the bacterium is opsonized or the PAMPs on the bacterium is recognized by the cell surface PRRs and then phagocytosed (Vergne, Chua et al. 2004). Recently, it has been shown that aminopeptidase N (CD13) also acts as a receptor for mycobacterial entry and is thought to modulate the intracellular survival of mycobacteria (Ho, Tsai et al. 2014). Though, earlier it was speculated that the fate of mycobacterium intracellular trafficking inside the phagocytes, macrophages or DCs, is independent of the route of entry or the receptor used for entry into the cell, they may have distinct role in terms of initiating a signaling cascade and affect the mycobacterial survival. Once inside

the phagosomes, the phagocytes elicits the defense strategies, such as induction of reactive nitrogen or oxygen species (RNS or ROS) production or fusion of phagosomes to lysosomes and exposing to lysosomal hydrolases or acidification of the phagosome or directing the pathogen containing phagosome to autophagy to eliminate pathogen (Haas 2007). Approximately, 90% of the individuals infected with *M.tb* never acquire the disease because of a strong immune reaction (Kaufmann and McMichael 2005). However, *M.tb* has evolved to circumvent the host defense strategies and only a weak immune response leads to the disease state. Under immunocompromised state, these dormant bacteria are reactivated that may cause disease (Kaufmann 2005). As mentioned before, the life cycle and immune response of *M.tb*, like that of HIV, is equally complex, and the above description is a simplistic overview which is schematically represented and summarized in Figure 4.

1.3.2 Phagocytosis: a principal defense by macrophages to clear intracellular pathogens

M.tb primarily resides in the phagosomes/endosomal compartment of host macrophages, while phagocytosis is also the major defense by macrophages. Phagocytosis is a specialized process of ingestion of a particle by the biological cell. The process of uptake is receptor mediated endocytosis, elicited by specific cells called professional phagocytes, namely, macrophages, dendritic cells and neutrophils (Desjardins, Houde et al. 2005; Li, Jagannath et al. 2010). They ingest the bacteria and degrade them thus, playing a crucial role in the defense against bacterial infection (Tjelle, Saigal et al. 1998). Various defense strategies employed by the phagocytes are; acidification of the phagosomes by fusion of the phagosomes with lysosomes, exposing the bacteria to various lytic enzymes, production of reactive oxygen and nitrogen species, recruitment of the antimicrobial peptides such as defensins, granzyme, perforins, cationic peptides, etc. (Haas 2007). The macrophages and dendritic cells are also antigen presenting cells (APCs), that present *M.tb* antigens through MHC-II (Zhang and Sugawara 2012).

The phagosomes carry out the above processes through a controlled chain of events called phagosome maturation, the various stages of which; *viz*; early endosomes, late endosomes, phagolysosomes or mature phagosome, are characterized by procurement and/or loss of various surface markers (Haas 2007). Figure 5 depicts the maturation pathway of early phagosomes to phagolysosomes with the principal surface markers acquired and the change in compartmental pH.

Once a particle or microbe is internalized it enters the early endosome state where it acquires the early markers (Rab5, EEA1, etc) and is mildly acidified (pH 6 to 6.5). Then it loses the early markers and enters the late endosome state where it gains the late markers (Rab7) and acidified (pH 5 to 6). Then it fuses with acidic lysosomes, acquires the LAMPs and the cargo is degraded at acidic environment (pH 3.5 to 5). Disconcertion in acquisition of these markers is strongly correlated with deficiency in phagosome acidification and compromised pathogen clearance (Kinchen and Ravichandran 2008). These markers are also used to identify or isolate stage specific endosomal compartments.

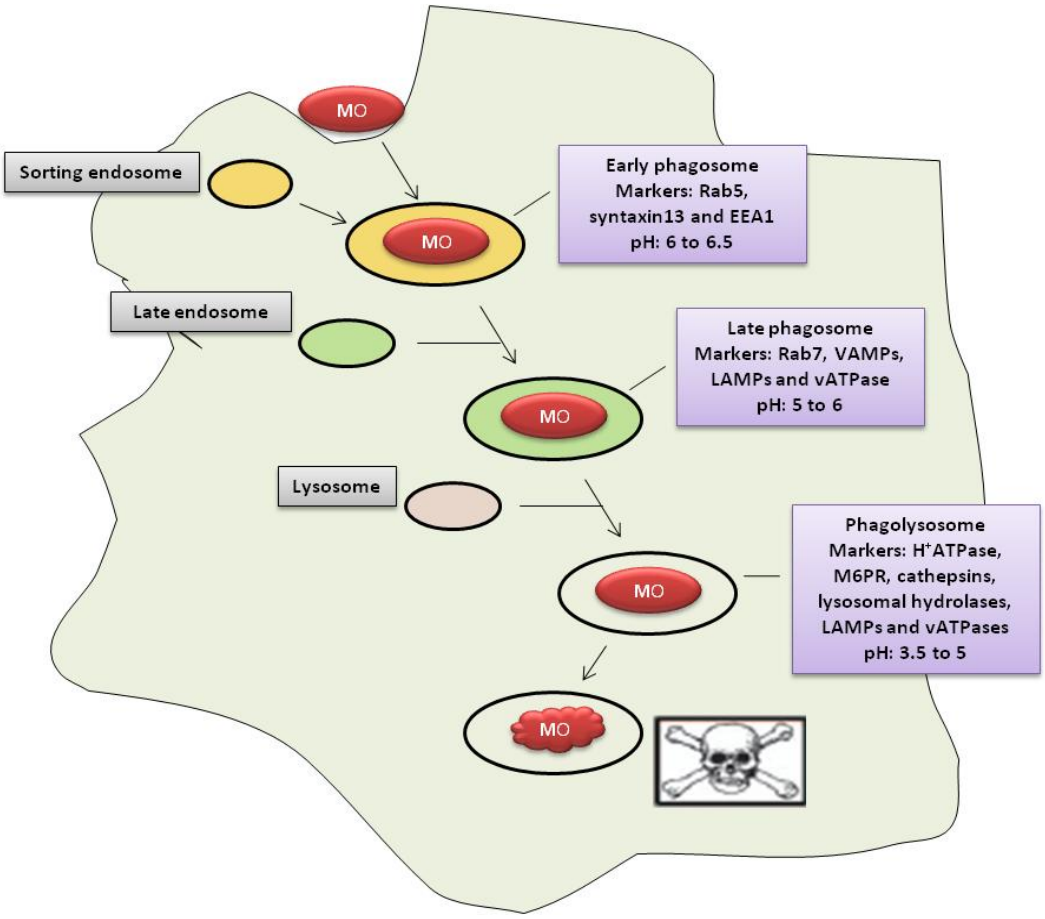

Figure 5: Outline of phagosome maturation process. The figure depicts the events of phagosome maturation indicating the pH of the specific compartment along with the corresponding surface markers in the cell after ingestion. MO: Micro-Organism. Adapted from Haas, 2007, Traffic. 2007 Apr;8(4):311-30, Wiley publishers (Haas 2007).

1.3.3 Overview of immune evasion strategies employed by Mycobacteria

One of the major immune evasion strategies exerted by *M.tb* is to arrest phagosome maturation, that is, inhibit the fusion of phagosome with lysosome to form phagolysosome and blocking acidification of phagosomes. By arresting phagosome maturation the pathogen containing vacuole exists in an early endosome state and gains access to the host metabolic intermediates to survive and replicate within the endosome (Vergne, Chua et al. 2004; Vergne, Chua et al. 2005). The key mechanisms of survival within the phagosomes are accounted by both the modulation of host response by mycobacteria and also the concomitant mycobacterial virulence factors expression. The pathogenic mycobacteria are able to block phagosome acidification, quench ROS and RNS, block fusion with lysosomes and maintain intrabacterial pH (Vergne, Chua et al. 2004; Vergne, Fratti et al. 2004; Vergne, Chua et al. 2005; Davis, Vergne et al. 2007; Vandal, Pierini et al. 2008; Vergne, Gilleron et al. 2014). Some of the host factors modulated towards this course are: Coronin 1a, a tryptophan-aspartate containing coat protein, is known to be involved in the actin-cytoskeleton remodeling and intracellular vesicular trafficking. It progressively associates with live mycobacteria containing phagosomes and interferes with the fusion of phagosome and lysosome, thus helping the survival of the mycobacteria. The same was not seen with the dead mycobacteria containing phagosomes or in the IFNγ-activated macrophages suggesting its role in the mycobacterial evasion and thus persistence of the pathogen (Ferrari, Langen et al. 1999; Pieters, Muller et al. 2013). Similarly, Hrs, a phospatidylinositol-3-phosphate binding protein, involved in regulating the endosomal pathway by associating with the late endosomes and directing them to the lysosomes, does not associate with the pathogenic mycobacteria containing phagosomes, interfering with its fusion with lysosomes (Vieira, Harrison et al. 2004). It has been reported that the pathogenic mycobacterial infection is associated with the low cytosolic Ca^{2+} levels (thought to be due to cell-wall associated Mannosylated Lipoarabinomannan) thus, hindering the phagosome-lysosome fusion (Malik, Denning et al. 2000; Malik, Thompson et al. 2003). In contrast, Mycobacterial infection in Coronin 1a expressing cells was associated with persistent increase in intracellular calcium levels and calcium dependent activation of calcineurin, a phosphatase, which help in blocking the fusion of phagosomes with lysosomes (Jayachandran, Sundaramurthy et al. 2007). Though, both the evidences contradict each other with respect to the relationship of calcium and mycobacterial infection, an in-depth study is required to better understand the modulation of host by mycobacteria. Galectin-3 was reported to be associated with

only live-mycobacteria containing phagosomes (Beatty, Rhoades et al. 2002). It was later reported to be interacting with mycolic acids (mycobacterial cell wall lipids) and is also reported to modulate the innate immune response by inhibiting the monocyte to dendritic cell differentiation and adaptive immune response by affecting the T cell antigen presentation (Chung, Sieling et al. 2013). But its exact role in mycobacterial infection is not yet known. The pathogenic mycobacteria, other than modulating the host protein functions or response, also employ its proteins for its survival inside the host. The pathogenic mycobacteria prevent acidification of phagosomes. Mycobacteria inhibit recruitment of proton-ATPase pumps into the phagosome membrane (Meena and Rajni 2010). For example, the secreted mycobacterial protein, PtpA, dephosphorylates the Vps33B protein involved in endosome membrane regulation and interacts with vacuolar H^+-ATPase and inhibit its recruitment to phagosome and resultant acidification (Wong, Bach et al. 2011). Mycobacterium is also an abundant producer of ammonia which help neutralize the acidic pH inside the phagosomes (Gordon, Hart et al. 1980). In addition to inhibiting the acidification of phagosomes, mycobacteria also maintains its intrabacterial pH which has been recently, attributed to three proteins through transposon mutant studies OmpATb, Rv3671c and Rv2136c (Molle, Saint et al. 2006; Vandal, Pierini et al. 2008; Vandal, Roberts et al. 2009). The mechanism by which they maintain the intrabacterial pH or proton homeostasis is not yet known.

The mycobacteria also possess the ability to resist the ROS and RNS inside macrophages manifested through several mycobacterial proteins such as, KatG (catalase-peroxidase quenches ROI) (Ng, Cox et al. 2004), SodA (Quenches ROS) (Edwards, Cynamon et al. 2001) and mycothiols, AhpC, AhpD, DlaT, Lpd (these protect from both ROS and RNS) (Buchmeier, Newton et al. 2003; Buchmeier, Newton et al. 2006; Shi and Ehrt 2006; Ehrt and Schnappinger 2009). It also expresses proteins that protect the mycobacterial targets (protein and DNA) of ROS such as, MsrA and MsrB (protect methionine of proteins) (Lee, Gold et al. 2009), MpaA, PafA and PrcBA (protect proteins from ROS and RNS mediated degradation) (Ehrt and Schnappinger 2009) and UvrB, DnaE2 and Lsr2 (Protect DNA from oxidative damage) (Colangeli, Haq et al. 2009; Ehrt and Schnappinger 2009). Mycobacteria also express several type-VII secretion systems (Esx Secretion systems) which secrete various virulent factors into the macrophage milieu and modulate the host response and confer survival advantage for mycobacteria (Houben, Korotkov et al. 2014). Additionally, *M.tb* possess 11 eukaryotic-like protein kinases (can alter host signaling cascades) such as PknG and PknE (Scherr, Muller et al. 2009; Pereira, Goss et al. 2011), and it

also possesses 88 Toxin-antitoxin modules which are known to act as stress responsive elements (Ramage, Connolly et al. 2009).

By and large, mycobacteria employ a vast array of strategies to overcome the host defenses and establish infection, some of them have been schematically represented in Figure 6. Unraveling more such pathogen survival strategies and pathogen-host interactions would help design intervention strategies to control the disease.

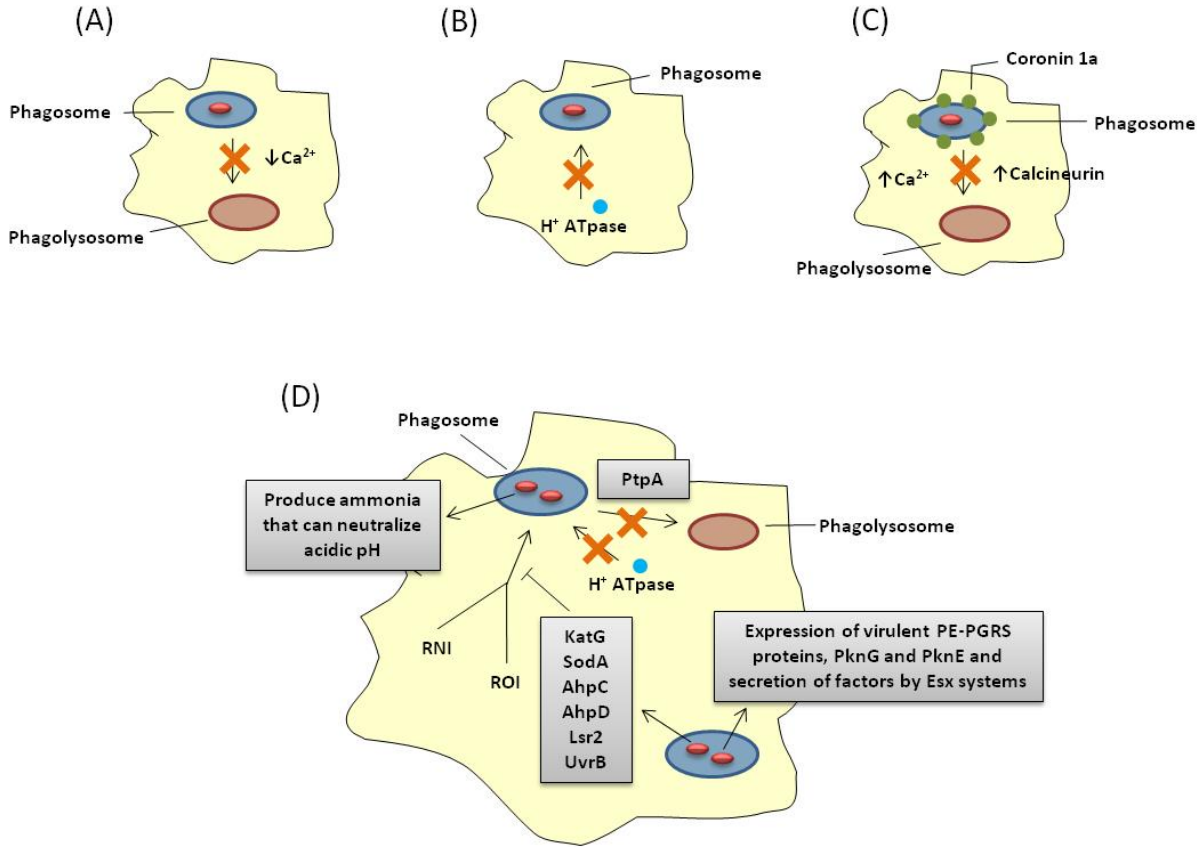

Figure 6: Schematic representation of some survival strategies of *Mycobacterium tuberculosis* inside macrophages. A) *M.tb* inhibits phagosome-lysosome fusion attributed to the waxy, lipid rich cell wall. B) *M.tb* inhibits the recruitment of H^+-ATPase pumps on phagosomes and thus the acidification. C) The *M.tb* phagosomes acquire Coronin 1a on it with persistent increase of cytosolic calcium leading to activation of calcineurin which inhibits phagosome maturation. D) *M.tb* expresses and secretes various proteins which can block phagosome maturation, quench ROI and RNI, prevents acidification of phagosome, maintain intrabacterial pH and also modulate host signaling cascades. For details, please refer section 1.3.3.

1.4 Mycobacterial infection in HIV+ population

HIV-1 targets two critical immune cells, macrophages and CD4+ T lymphocytes, which are also instrumental in controlling mycobacterial infections. *M.tb* complex, comprising of phylogenetically close groups of mycobacterium species, that infect humans causing tuberculosis (TB) colonize HIV+ population more frequently than other secondary infections (Bruchfeld, Correia-Neves et al. 2015). As mentioned before, apart from the pathogenic mycobacteria of *M.tb* complex, the immunocompromised HIV patients are also attacked by non-pathogenic and attenuated strains of mycobacteria. These mycobacteria, such as *Mycobacterium avium*, *M. kansasii*, *M. fortuitum*, *M. abscessus* and *M. bovis* Bacillus Calmette–Guérin (BCG), cause opportunistic pulmonary infections in HIV patients (Azzopardi, Bennett et al. 2009; Daley and Griffith 2010), even before T-cell depletion is apparent (Sonnenberg, Glynn et al. 2005). Not only TB is the most frequent co-infection, but amassing evidences, both at clinical and experimental levels, strongly point to synergism between these two pathogens.

1.4.1 Understanding the HIV-TB coalition

The immune response to *M.tb* infection is TH1 kind with release of pro-inflammatory cytokines and consequent increase in expression of transcription factors like NFκB, which are the factors that also support HIV propagation (Falvo, Ranjbar et al. 2011). Similarly, HIV infection is marked by increase in regulatory cytokines like IL-10, suggesting a strong TH2 immune response which cannot control secondary mycobacterial infection. Clinical studies show that HIV-TB co-infected patients could neither mount effective TH1 or TH2 response creating conducive environment for both the pathogens (Diedrich and Flynn 2011; Benjamin, Banerjee et al. 2013). There are few hypotheses laid down based on the evidences available so far, as to how the HIV-1 infection exacerbates TB or NTM infection risk. It has been observed that i) HIV replication is increased at sites of *M.tb* infection leading to increased pathology; ii) HIV manipulation of macrophage function prevents *M.tb* killing; iii) HIV induces functional changes in *M.tb*-specific T cells that decrease their ability to contain *M.tb*; iv) HIV induces primary or reactivated TB through killing of CD4+ T cells within granulomas (Diedrich and Flynn 2011) (Figure 7). HIV infection preferentially decreases the CD4+ T cells specific to *M.tb* (Geldmacher, Ngwenyama *et al.* 2010) and depletes CD4+ T cells from the granuloma compromising the containment of mycobacterium. HIV affects the function of macrophages and T cells. In HIV infected patients there are fewer IFNγ

and IL-2 producing cells thus affecting the immunity against bacteria and their containment. In HIV-TB co-infected patients high levels of IL-10 are observed, thus indicating compromised cell mediated immunity (Geldmacher, Ngwenyama et al. 2010; Geldmacher, Zumla et al. 2012). HIV-1 infection was recently reported to promote the secretion of a tryptophan-catabolizing enzyme which is involved in T cell suppression (Favre, Mold et al. 2010; Larsson, Shankar et al. 2013; Planes and Bahraoui 2013) and thus a compromised T cell response against *M.tb*. Also reported recently, that in HIV-TB patients, there is increased expression of co-inhibitory molecules on the T cells compared to healthy or TB alone infected patients suggesting a decreased cell mediated immunity during co-infection (Jurado, Pasquinelli et al. 2012; Larsson, Shankar et al. 2013). Several molecular mechanisms have been attributed to the synergistic impact of pathogenic mycobacteria on HIV propagation. HIV, during the early stages of infection, uses the CCR5 co-receptor on the cells for infection but as the disease progresses it utilizes the CXCR4 receptor. *M.tb* increases the levels of CXCR4 receptor thus facilitating the viral infection and progression (Rosas-Taraco, Arce-Mendoza et al. 2006). Mycobacterial components, directly or indirectly increase the expression of transcription factors such as NFκB, NFAT5, c/EBP or AP-1, ATF which in turn increase long terminal repeat (LTR) driven HIV replication (Ranjbar, Boshoff et al. 2009; Falvo, Ranjbar et al. 2011; Ranjbar, Jasenosky et al. 2012). Activation of these transcription factors also induces the expression of cytokines such as, TNFα, IL-1, IL-6, TGFβ, MCP1 and IFNγ which in turn through various signaling cascades upon binding to their cognate cell surface receptors drive the HIV transcription and propagation (Falvo, Ranjbar et al. 2011) (Figure 7). The viral replication is affected in a *M.tb* strain specific manner (Ranjbar, Boshoff *et al.* 2009) which is very sensitive to the transcriptional upregulation of HIV by *M.tb* and its Purified Protein Derivative (PPD) (Toossi, Xia *et al.* 1999).

In short, though the molecular mechanisms behind co-infection are not fully elucidated, HIV-1 during co-infection helps the persistence and survival of *M.tb* and *M.tb* in turn help increase the viral replication and propagation. Hence, there is an increased progression of both the diseases during co-infection.

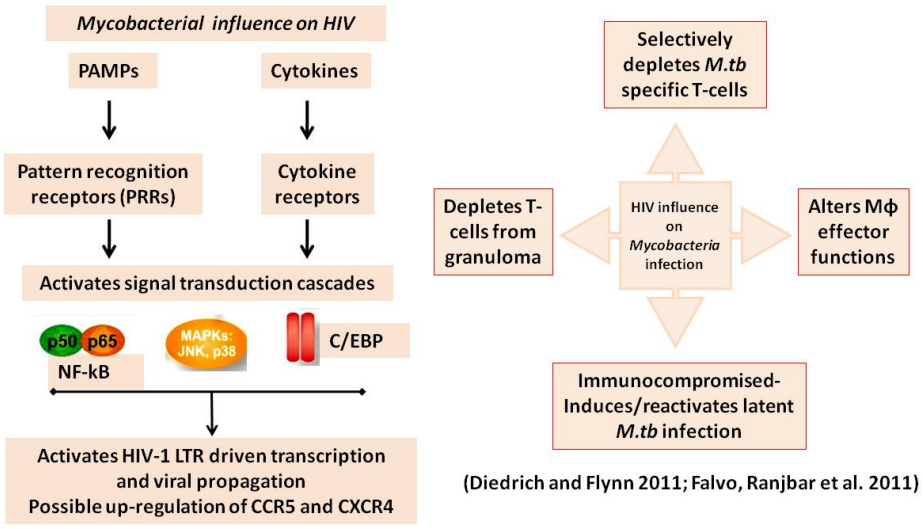

Figure 7: Flowchart giving the basic understanding of the HIV-TB coalition based on the reported evidences of co-infection. (A) Mycobacterial infection through PAMPs or cytokines leads to the activation of host transcription factors which drive the HIV-1 LTR driven transcription and thus viral propagation. Mycobacterial infection also increases the surface expression of co-receptors, CCR5 and CXCR4, helping the entry of virus into the cell. (B) HIV infection leads to depletion of CD4+ T cells from the granuloma and also decreases the *M.tb* specific CD4+ T cells. HIV infection also affects the MΦ effector functions helping the survival or persistence of mycobacteria.

1.5 Non-pathogenic, Non-tuberculous Environmental Mycobacteria and HIV co-infection

Mycobacterial species that do not belong to *Mycobacterium tuberculosis* complex (MTBC) or *M. leprae* are referred to as atypical or non-tuberculous mycobacteria (NTM) or mycobacteria other than tuberculosis (MOTT) (Primm, Lucero et al. 2004). Although information on MTBC and *M. leprae* are abundant, there is a paucity of data on NTMs. NTM are highly prevalent in environment and certain species of NTMs cause infections in humans other than tuberculosis. So far, over 150 species have been listed as NTMs and by days, the list is growing (Johnson and Odell 2014). NTMs are categorized based on the rate of growth as slow growers (*M. avium* complex (MAC), *M. kansasii*, etc.) and rapid growers (*M. fortuitum*, *M. abscesses*, etc.). They are ubiquitous in environment and heavily present in natural water, engineered water distribution systems, soil (Primm, Lucero et al. 2004; Johnson and Odell 2014). The highly ubiquitous nature of NTMs is attributed to their waxy, lipid-rich cell wall, slow growth, oligotrophy and ability to form biofilm that renders it resistant to coarse conditions such as disinfectants and antibiotics (Jarlier and

Nikaido 1994; Falkinham 2009). The hydrophobic nature of NTM cell surface makes them easy to aerosolize and gives tolerance for high temperature and low pH (Parker, Ford et al. 1983; Bodmer, Miltner et al. 2000). Their ubiquitous nature and overlap of habitat (engineered water systems and soil) with humans increases the chance of infections in humans (Primm, Lucero et al. 2004). The risk factors for the infections by NTM are immunocompromised state (due to old age or HIV infection or cancer or on immunosuppressive drugs during organ transplants), existing lung diseases or disorders, smoking and alcoholism (Primm, Lucero et al. 2004; Glassroth 2008; Taiwo and Glassroth 2010; Weiss and Glassroth 2012; Johnson and Odell 2014). The majority of the pulmonary infections, other than tuberculosis, in the humans are caused by NTMs which include, MAC followed by *M. kansasii* and *M. abscessus* (Glassroth 2008; Johnson and Odell 2014). NTMs may cause cervical lymphadenitis in children (route of infection is from soil) and hypersensitivity pneumonitis (route of infection is aerosols) in workers (metal industry) or individuals at home (hot tubs). NTM infections may be acquired from public swimming pools, water distribution supplies, hot tubs and hospitals. Due to their resistance to chlorine and disinfectants they are specifically enriched in the engineered water distribution systems and at hospitals (Falkinham 2009; Falkinham 2011). The rapid growers *M. fortuitum*, *M. chelonae* and *M. abscessus* and slow growers *M. avium* and *M. xenopi*, also cause nosocomial infections which include skin and soft tissue infections acquired at the hospitals. NTM infections cause intestinal infections similar to chronic bowel disease and the products of NTM or NTM infection leads to allergic responses. NTM (*M. vaccae*) is also known to interfere with BCG vaccination (Brown, Brown et al. 1985).

One must note that these mycobacteria can be easily cleared by robust and healthy immune system. Therefore, although exposed continuously to NTMs, most infections are not manifested as disease. Nevertheless, these seemingly harmless mycobacteria are adding to disease complications in HIV+ population.

1.5.1 NTM infections as emerging threat to HIV infected population

Recent reports on the prevalence of NTM infections in US has shown that since 1999 to 2010 there is an approximately 10% increase in their prevalence (Mirsaeidi, Machado et al. 2014). The reason behind these increased infections is not clear, but speculated to be due to the development or improvements in the diagnostic methods which were not detected efficiently earlier or an actual increase in infections due to the increase in the immune-compromised elderly population. Another

possible reason could be increased HIV epidemic where HIV infection impairs the immune system making the host susceptible to these opportunistic infections. Several reports exist on the incidences of NTM infections in the HIV infected populations (Mirsaeidi, Farshidpour et al. 2014; Mirsaeidi, Machado et al. 2014). The most common NTM infections observed in HIV infected populations is due to *M. avium*, *M. kansasii* and *M. fortuitum* (Carpenter and Parks 1991; Shafer and Sierra 1992; Juffermans, Verbon et al. 1998; Karakousis, Moore et al. 2004; Saritsiri, Udomsantisook et al. 2006; Azzopardi, Bennett et al. 2009; Herzmann, Esser et al. 2011; Lan, Yang et al. 2011). The complexities emerging from NTMs in HIV infected population are that they are (i) high exposure due to high prevalence in nature, (ii) mostly remain asymptomatic but slowly establishes infection (iii) difficult to diagnose and (iv) resistance to conventional TB therapy (Primm, Lucero et al. 2004; Brown-Elliott, Nash et al. 2012). While there is a growing body of evidences pointing to the increased incidences of the NTM infections worldwide in HIV infected population, the efforts to understand the molecular basis of NTM infections in HIV population is at its infancy. Systematic studies are called for to understand the molecular mechanisms behind these NTM infections and their impact on HIV disease progression to effectively control the co-infection situation worldwide.

Recapitulating the points of this chapter, while HIV-1 and *Mycobacterium tuberculosis* have independently evolved as efficient human pathogens, their co-epidemic has made the control of both the diseases difficult. Clinical evidences from the field suggest a strong coalition between these two pathogens where viral and mycobacterial loads are significantly higher in HIV-TB co-infected patients than patients with HIV or *M.tb* infection alone (Goletti, Weissman et al. 1998; Suchindran, Brouwer et al. 2009; Diedrich and Flynn 2011; Naidoo, Padayatchi et al. 2011; Pawlowski, Jansson et al. 2012; Bruchfeld, Correia-Neves et al. 2015). These observations are supported at molecular level by the fact that HIV-1 replication is differentially regulated by different pathogenic strains of *M.tb* and *M.tb* induced promotion of CXCR4 expression led to preferential X4 HIV-1 replication in human Macrophages. HIV, in turn has been shown to selectively deplete *M.tb* specific T cells and T cells from granuloma, making immune system vulnerable to *M.tb* pathogenesis or re-activation (Diedrich and Flynn 2011; Shankar, Vignesh et al. 2014). NTMs, which are otherwise cleared by healthy host, pose an emerging threat to the HIV+ population (Glassroth 2008; van Soolingen and van Ingen 2012). These non-pathogenic mycobacteria serve as opportunistic infections, but unlike earlier believes, can infect even at early

stages of HIV infection. While several studies pertaining to pathogenic mycobacteria are available, studies deciphering molecular and cellular events in establishment of non-pathogenic mycobacterial infections and their impact on HIV propagation and disease progression are limited. One of the major impedance towards this goal is the lack of simple yet efficient cell-culture based models that are field compliant to study co-infection.

1.6 Hypothesis and Objectives:

During co-infection, pathogenic or non-pathogenic mycobacteria, encounter altered macrophage environment due to prior HIV infection. The nature of intracellular phagosomal environment, inside which mycobacteria reside, is often the key to their pathogenesis and persistence. Hence comparative studies of the phagosomal environment from mycobacteria mono-infected and HIV-mycobacteria co-infected macrophages along with the concerted changes in the intracellular mycobacterial proteome will elucidate the molecular and cellular processes adapted/altered by mycobacteria during co-infection. This will help us understand the coalition between these two pathogens.

Towards this, the following **objectives** were drawn, which are discussed in ensuing chapters.

1. Developing an *in vitro* cell culture based co-infection model simulating reported clinical observations.

   This objective supported the subsequent proteomics studies. **[Chapter2]**
2. Studying the differential expression of the host proteins and the consequent early adaptive changes in the intracellular mycobacterial proteome during co-infection through comparative proteomics.

   This objective targeted to identify perturbations in the host and mycobacterial proteomes from phagosome-enriched fractions during co-infection and correlate the same to understand the molecular mechanisms behind persistence of opportunistic mycobacteria during co-infection. The objective also aimed to discover mycobacterial factors influencing HIV propagation during co-infection. **[Chapters 3 and 4]**
3. Quantitative proteomics to tabulate modulations in the phagosome enriched fractions of macrophages by pathogenic *Mycobacterium tuberculosis* H37Rv during mono-infection and HIV-H37Rv co-infection.

The chief intention of this objective was to tabulate quantitative differences in the proteome from phagosome-enriched fractions during virulent *M.tb* H37Rv and HIV-H37Rv infection for identification of leads to be pursued in context of HIV and pathogenic mycobacterial co-infections in the lab. **[Chapter 5]**

Chapter 2

In vitro HIV-Mycobacteria Co-infection model

2.1 Introduction:

The previous chapter introduced the concerns associated with the deadly nexus of HIV and mycobacteria which is further complicated by increasing numbers of infections by NTMs in HIV+ population. Efforts are being made in recognizing the basic biology behind the close association between these two diseases during co-infection to address diagnostics and treatment concerns. The major hindrance in addressing the needs for the diagnostics and therapeutics is the lack of proper models to understand the basic biology behind the HIV-TB synergism. The lack of proper models causes obstructions in the discovery of novel compounds to treat co-infection. So far, due to the lack of proper co-infection models, the inhibitors of either *M.tb* or HIV are studied independent of the other infection (Vijayakumar, Finney John et al. 2013). This does not account for the drug-drug interactions or the side-effects due to the combined intake of these drugs. Though macaques have been recognized as suitable animal model to study co-infection biology (Guo and Ho 2014), it poses a challenge in high-throughput screening of novel compounds and slows down the process of discovery. To address this, one needs to have a simple model and *in vitro* cell culture model, though with limitations, would be ideal to perform high-throughput screen of the novel compounds and also to understand co-infection biology. The inferences from such model can then be taken further to study in the macaque animal model. Based on the objectives of my study, I designed a THP-1cell line based co-infection model suitable for identification of intracellular mycobacterial proteome. The major challenges were to control cell death due to the infection by two pathogens and obtaining sufficient amounts of intracellular mycobacterial protein required for proteomics. These shortcomings were overcome by standardizing the conditions for both the infections, in terms of HIV titers, MOI for mycobacteria, time of infections and time of post-infection incubations for minimal cell death. At the same time MOI for mycobacteria was attempted to be kept as high as possible with minimum cell death for getting the sufficient amount of intracellular mycobacterial protein. Further, the model was validated for compliance with the clinical reports in terms of cytokine release and pathogen propagation to imitate field observations in context of co-infection.

The *in vitro* THP-1 cell culture based co-infection model is discussed.

2.2 Materials and methods:

Cell lines used:

- HEK293T (Human embryonic kidney) cell line was procured from NCCS, Pune, India.
- THP-1 monocyte leukemia cell line (Cat#TIB-202, ATCC).

Bacterial strain used:

- *Mycobacterium bovis* BCG

The virus strain used:

- Macrophage tropic HIV (NL-ADA8) was gifted by Dr. Jayant Bhattacharya.

2.2.1 Maintenance of cell lines:

The THP-1 cell line was maintained in RPMI 1640 media (Invitrogen, USA) supplemented with 10% FBS (South American origin, Gibco, USA) and incubated at 37ºC with 5% CO_2. The media was changed when the cells were 90% confluent. The HEK293T cell line was maintained in DMEM media (Invitrogen, USA) supplemented with 10% FBS and incubated at 37ºC with 5% CO_2. When the cells were 90% confluent, the cells were trypsinized with the Trypsin-EDTA (Sigma-Aldrich, USA) and washed with Phosphate buffered saline pH 7.4 (PBS) and fresh complete media was added.

2.2.2 Growth conditions of Mycobacteria:

The mycobacteria were grown on 7H10 agar media (Hi-media, India) supplemented with 10% Oleic acid, Albumin, Dextrose and Catalase (OADC, Hi-Media, India). The plate was incubated at 37ºC for 15 days. The colonies were picked into the 7H9 broth media supplemented with 10% OADC and the broth culture was incubated at 37ºC at 180 rpm until the $OD_{600\,nm}$ reached 0.8 to 1. The culture was examined for any contamination using Ziehl-Neelsen (ZN) staining procedure. Prior to the infection, centrifuged the bacterial suspension at 200 ×*g* for 10 min and washed the bacterial pellet with PBS and then with RPMI 1640 media. Suspension of single-bacillus was obtained by passing the suspension through 26G 1 mL syringe for 10-20 times and then withdrew from the top of the tube.

2.2.3 Preparation and quantification of infectious HIV-1 (NL-ADA8) particles:

Infectious HIV-1 particles were prepared by transfection of proviral DNA pNL-ADA8 into HEK293T cells by calcium phosphate method. Culture supernatants were collected at intervals of

24 hours post-transfection, filtered through 0.45 μm syringe filter (Millipore, USA), precipitated using Polyethylene glycol (Kutner, Zhang et al. 2009; Banerjee, Benjamin et al. 2014) and quantified by HIV-1 p24 antigen capture ELISA kit (Advanced BioScience Laboratories Inc, USA) according to the manufacturer's protocol. Cells were infected with 30 ng/mL of p24 equivalents of HIV.

2.2.4 Infection of macrophages and phagosome isolation:

THP-1 cells were PMA (10 ng/mL) differentiated to macrophages in RPMI 1640 media with 10% FBS in 150 mm culture dishes. After 24 hr the macrophages were washed, fresh media was added and kept for 48 hr rest. The macrophages were divided into two categories 1) for co-infection: First infected with HIV for 2 hr in incomplete RPMI media and followed by 24 hr incubation in complete RPMI media (Collman, Hassan et al. 1989; Sylwester, Wessels et al. 1993; Zhao, Thibault et al. 2006; Espert, Varbanov et al. 2009; Andreani, Gagnon et al. 2012). This was followed by infection with BCG at an MOI=100 for 4 hr which was modified from the protocol described earlier (Lee, Jethwaney et al. 2010). 2) For mono-infection: The cells were treated similar to co-infection but without virus and followed by BCG infection. After 4 hr of infection, fresh media with antibiotic was added and incubated for 24 hr. The phagosomes enter late endosome state at 24 hr post infection. After 24 hr the cells were harvested for fractionation to obtain enriched bacteria-*laden* phagosomes which was standardized in our laboratory using sucrose density gradient method as described earlier (Wandy Beatty and Russell 2001).

2.2.5 CFU enumeration and intracellular bacilli viability measurement:

For the CFU and Alamar blue assays, 24-well tissue culture plates carrying 0.2 million THP-1 per well was used. The mono- and co-infected cells after the incubation were washed thrice with PBS to remove any extracellular bacilli followed by lysis of macrophages with sterile water at 37^{o}C for 10 min. The lysates were diluted and were plated on 7H10 agar plates. The plates were incubated at 37^{o}C with 5% CO_2 and 95% humidity for 2-3 weeks (for BCG) and the colonies were enumerated.

2.2.6 Fluorescence microscopic studies:

For assessing percentage HIV infected cells, fluorescence microscopic studies were employed. After 2 hr of HIV infection, cells were washed, fixed in 2% paraformaldehyde for 10 min. The cells were permeabilized in 0.1% saponin in PBS containing 1% BSA, 10 mM HEPES and 0.5 mM EDTA (Shirvani, Achour et al. 2011). Anti-HIV-1 p24 mouse antibody was used at 1:50

dilution at RT for 1 hr. Washed and stained with anti-mouse FITC conjugated antibody at 1:150 dilution at RT for 45 min. Similar protocol was followed for mock infected or uninfected cells and used as control for the microscopic studies.

2.2.7 Flow Cytometry:

Percent of HIV infection of THP-1 was calculated using flow cytometry by staining for intracellular HIV Rev protein. The THP-1 macrophages were infected with HIV at 30 ng/mL for 2 hr. After 2 hr, the cells were washed, fixed in 2% paraformaldehyde for 10 min. The cells were permeabilized in 0.1% saponin in PBS containing 1% BSA, 10 mM HEPES and 0.5 mM EDTA (Shirvani, Achour et al. 2011). Anti-HIV-1 Rev mouse antibody was used at 1:50 dilution at RT for 1 hr. Washed and stained with anti-mouse FITC conjugated antibody at 1:150 dilution at RT for 45 min. Washed and cell populations were analyzed on BD FACS Canto instrument. Uninfected was used to normalize for the non-specific labeling and percent of HIV infected cells was calculated. The percent is the mean from three experiments and error values represent ±SD (Standard deviation). The FCS files were analyzed using the Flowing software (Version 2.5.1).

2.2.8 Cytokine measurement:

Cytokine profiles of the culture supernatants of Uninfected, BCG, HIV and HIV-BCG infected cells were measured using BD opti-eia capture ELISA kits according to the manufacturer's instructions. The absorbance at 450 nm was measured using the Biotek multi-well reader.

2.2.9 Statistical Analyses:

All the experiments were performed at the least three times. The data were analysed using SigmaPlot software version 11.0.0.77 (Systat Software, Inc., USA). The error bars represent the standard deviation (SD) from the mean of at least three independent experiments. Statistical analyses of the experimental data for comparing two groups were performed by Student's *t*-tests or paired *t*-test. Statistical analyses of the experimental data comparing more than two groups were performed by One-way repeated measures ANOVA with Holm-Sidak multiple pair-wise comparison method. $p<0.05$ was considered as significant.

2.3 Results and Discussion:

2.3.1 Cell-culture based HIV-mycobacteria co-infection model

The cell culture based model developed simulated a state where a HIV infected person acquires a secondary infection of non-pathogenic mycobacteria and the changes in the proteomes of the enriched phagosomal fractions of the host cell along with the intracellular *Mycobacteria* were studied. In this model, Phorbol myristate acetate (PMA) differentiated THP-1 derived macrophages (henceforth THP-1) were infected with either mycobacteria (mono-infection) or HIV and mycobacteria (co-infection) (Figure 8). *M. bovis* BCG was used to represent for the mycobacterial strain and HIV-ADA8 an M-tropic HIV strain was taken.

The model was simulated to represent the condition of acquisition of mycobacterial secondary infection in the HIV background. THP-1 monocytes were differentiated into macrophages using 10 ng/mL of PMA for 24 hr and given a rest of 48 hr to ensure that the maximum number of monocyte have differentiated into macrophages. The proteomic analyses require huge amounts of protein and to identify the differentially expressed phagosomal proteins and intracellular mycobacterial proteins, so one requires huge number of cells. Hence, THP-1 cells, a leukemia cell line, was chosen for the purpose which would be easy to culture in large amounts and it also can be infected by both HIV and mycobacteria. For the successful identification of phagosomal and intracellular mycobacterial proteins by LC-MALDI-MS/MS, 100×10^6 THP-1 monocytes per category were differentiated into macrophages using PMA. Upon differentiation the cells were first either mock infected or HIV infected with 30 ng/mL of p24 equivalents for 2 hr and then incubated for 24 hr. After 24 hr of post-virus-infection the cells were infected with *M. bovis* BCG for 4 hr and incubated for 24 hr infection. The 24 hr time point after the mycobacterial infection was chosen to study the early adaptive changes in the intracellular mycobacterial proteome that help mycobacteria to establish an infection during co-infection. Hence 24 hr time point was chosen which was also reported to be sufficient for BCG to enter late endosome state (Jordao, Bleck et al. 2008; Cardoso, Jordao et al. 2010).

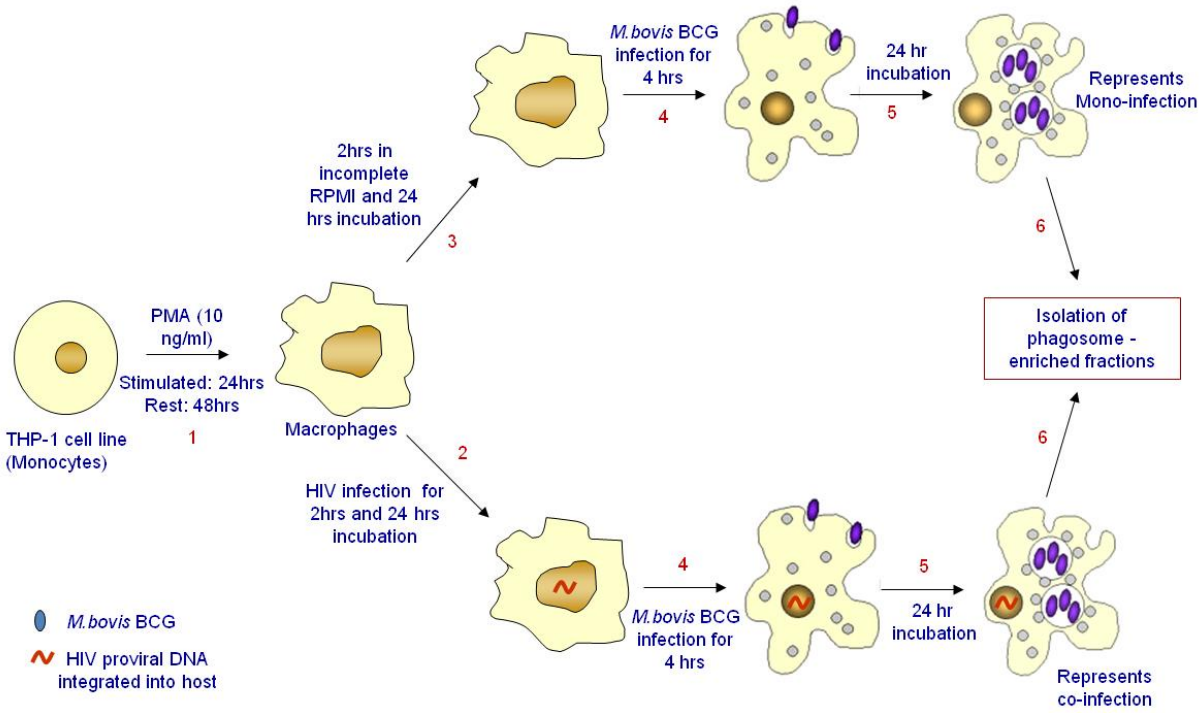

Figure 8: *In vitro* cell culture based model of HIV-BCG co-infection. 1) THP-1 monocytes differentiated into macrophages using PMA at 10 ng/mL for 24 hr. After 24 hr, fresh complete RPMI media was added and rested for 48 hr without PMA. 2) HIV infections: For co-infection condition, HIV infection was done prior to BCG infection. Macrophages were infected with HIV NL-ADA8 strain with 30 ng/mL p24 equivalents for 2 hr in RPMI media devoid of FBS, washed and incubated in fresh complete RPMI media for 24 hr. 3) The cells were kept for mycobacterial mono-infections in incomplete media and treated similarly, but without virus. 4) BCG infections: BCG was prepared as mentioned in methods and infected at an MOI=100 for 4 hr in RPMI media with FBS devoid of any antibiotics, washed and 5) incubated for 24 hr post-infection in RPMI media with FBS and antibiotics. 6) After 24 hr of BCG post-infection, the cells were processed for phagosome isolations.

In the model, the first criterion was to confirm the infection of macrophages by the HIV. To this end, the cells were assayed for the percentage of HIV infected cells immediately after the 2 hr of infection using flow cytometry for the intracellular presence of HIV-Rev protein and fluorescence microscopy for HIV-p24 protein using specific antibodies. The percent of HIV infected cells were calculated by flow cytometry using antibody against HIV protein, Rev after 2 hr of HIV-1 infection. THP-1 (39.05±3.27%) were infected with HIV under these conditions as assessed by FACS (Figure 9). The extent of HIV infected cells or the bystander effect of HIV infection was assessed by the fluorescence microscopic studies for the HIV-1 p24 protein by intracellular staining of infected cells. The intracellular staining for p24 as seen in the images confirmed the

infection of macrophages by HIV (Figure 10A). 47.27±11.06 % THP-1 were infected with HIV under these conditions as assessed by fluorescence microscopy (Figure 10B)

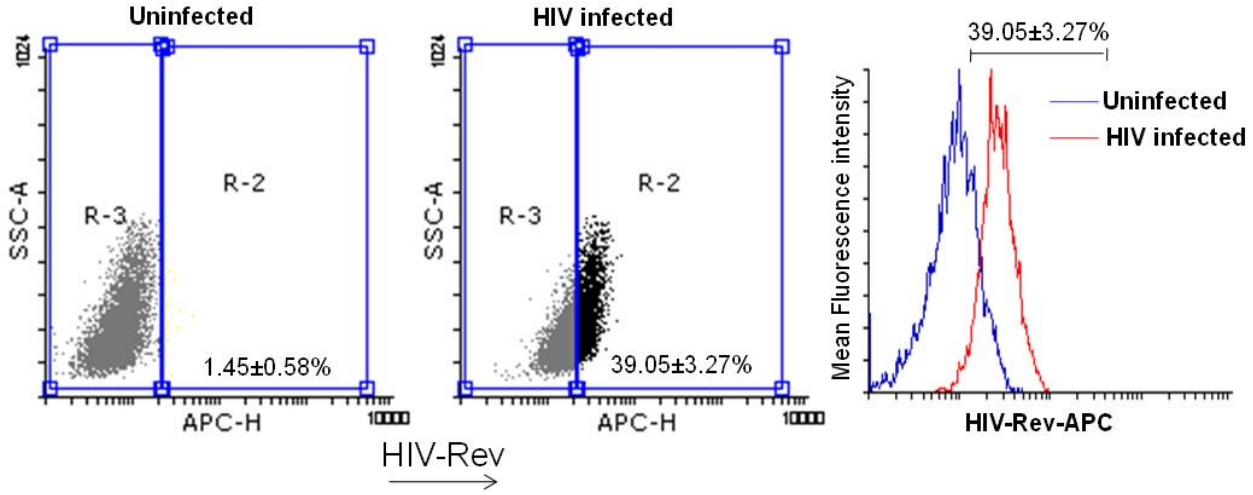

Figure 9: Percent of HIV infection of THP-1 was calculated using flow cytometry by staining for intracellular HIV-Rev protein. Representative dot plot from flow cytometric analysis depicting the percent HIV infected THP-1 population. Uninfected was used to normalize for the non-specific labeling and percent of HIV infected cells was calculated. The percent is the mean from three experiments and error values represent ±SD (Standard deviation). The FCS files were analysed using the Flowing software (Version 2.5.1).

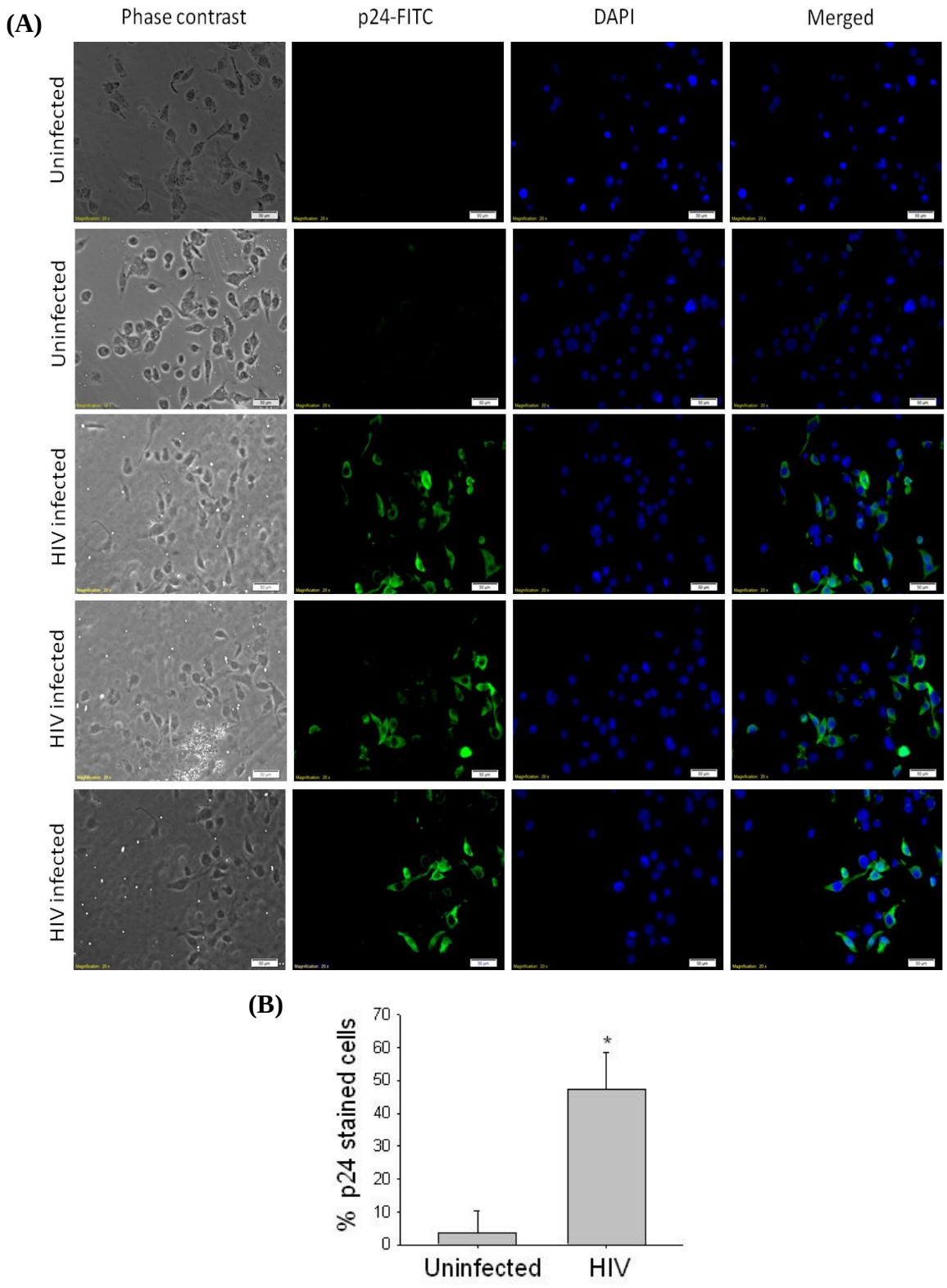

Figure 10: Percent of HIV infection of THP-1 was calculated using fluorescence microscopy by staining for intracellular HIV p24 protein. (A) THP-1 were infected with HIV at 30 ng/mL for 2 hr. After 2 hr, the cells were washed, fixed in 2% paraformaldehyde for 10 min. The cells were

permeabilized in 0.1% saponin in PBS containing 1% BSA, 10 mM HEPES and 0.5 mM EDTA (Shirvani, Achour et al. 2011). Anti-HIV-1 p24 mouse antibody was used at 1:50 dilution at RT for 1 hr. Washed and stained with anti-mouse FITC conjugated antibody at 1:150 dilution at RT for 45 min. Washed and cells were analyzed under fluorescence microscope (Olympus inverted microscope IX81, Make: Olympus). Uninfected was used to normalize laser exposure time for the non-specific labeling and (B) percent of HIV infected cells was calculated (at the least 10 microscopic fields (10 cells/field) per experiment from three experiments) represented as bar graph. The percent is the mean from three experiments and error values represent ±SD (Standard deviation). * represents $p<0.001$.

After HIV infection the cells were infected with mycobacteria/BCG. BCG infection was standardized in terms of Multiplicity of infection (MOI) because to identify the intracellular mycobacterial proteome through proteomics, very high MOI was required which should not have impact on the viability of the macrophages. MOI for *M. bovis* BCG was standardized and it was observed that up to an MOI of 100 (100 bacilli per macrophage) the viability of the cells was not affected significantly. Cell viability was determined 24 hr post BCG infection under these experimental conditions (Figure 11).

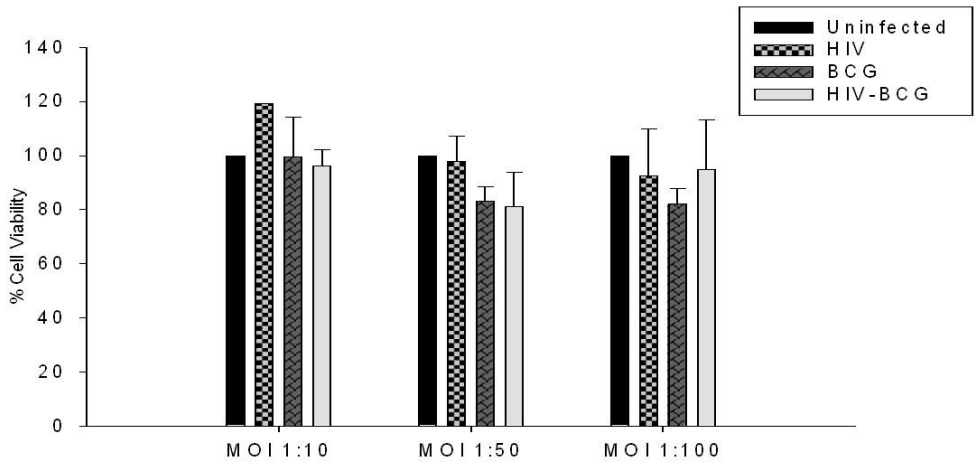

Figure 11: Multiplicity of infection (MOI) for BCG was standardized by cell viability assay. Cells were infected with BCG with increasing MOI of 10, 50 and 100. After 24 hr post BCG infection, the viability of the cells were assessed with respect to uninfected cells using MTT (3-(4, 5-dimethylthiazol-2-yl)-2, 5-diphenyltetrazolium bromide) assays. HIV titers of 30 ng/mL p24 equivalent were used wherever required. The error bars represent standard deviation from mean (± SD).

Once the MOI was standardized, phagosomes were isolated from the BCG mono- and HIV-BCG co-infected cells and checked for the presence of BCG in the fraction using acid-fast staining of the fractions. The Ziehl-Neelsen staining confirmed the presence of BCG in the fractions and infection of macrophages by BCG (Figure 12B). The infection of macrophages by BCG was also confirmed by colony forming units (CFU) plating of the intracellular mycobacteria upon infection on 7H10 agar plates (Figure 12C). Thus, the infection of macrophages by BCG was confirmed and hence the model was then tested for its fidelity with respect to its compliance with the field reports. The model was evaluated for three principle parameters; (i) the viral titers upon co-infection as against HIV mono-infection (ii) intracellular mycobacterial counts by colony forming units (CFU) on 7H10 agar plates and (iii) the secreted levels of cytokines TNFα, IL-12p70 and IL-10 to score for macrophage activation.

(i) HIV titers in the culture supernatants of HIV-BCG were 57.9% higher (27.59±1.3110 pg/mL) as compared to HIV mono-infection (17.47±4.387 pg/mL) (Figure 12A). These observations were similar to the clinical reports where HIV-TB co-infected patients registered higher viral titers compared to HIV patients without mycobacterial infection (Toossi, Mayanja-Kizza et al. 2001).

(ii) Intracellular mycobacteria were counted in terms of CFU by plating lysed cells on 7H10 agar plates at 24 hr post BCG infection. CFU counts from HIV-BCG ($10.27\pm1.43\times10^3$ CFU/mL) were higher than that of BCG alone ($7\pm0.5\times10^3$ CFU/mL) showing 46.71% increased survival of BCG in HIV infected THP-1 (Figure 12C). The CFU were normalized to that of BCG entered at 0 hr post-infection under both the conditions.

(iii) Cytokines released in the culture media during infections were measured to assess the stimulatory state of the THP-1. The levels of TNFα in HIV were 517.17±30.03pg/mL, BCG were 411.99±56.74pg/mL and HIV-BCG were 496.14±25.05 pg/mL (Figure 13A). BCG showed the least titers of released TNFα, since BCG is an attenuated strain. The regulatory cytokine, IL-10 levels during HIV-BCG (266.66±47.56 pg/mL) was marginally less than that of HIV mono-infection (307.39±65.77 pg/mL), however, significantly ($p<0.001$) higher than that of BCG (105.87±6.29 pg/mL) (Figure 13B). There was no significant change in IL-12p70 levels of BCG (101.76±25.28 pg/mL), HIV (89.23±22.25pg/mL) or HIV-BCG (89.46±19.76 pg/mL) co-infection (Figure

13C). Thus, the minimal cytokine profile in the culture supernatants were in the expected lines of stimulation by attenuated mycobacteria and HIV infections (Kindler, Sappino et al. 1989; Kindler and Sappino 1991; Kwon and Kaufmann 2010).

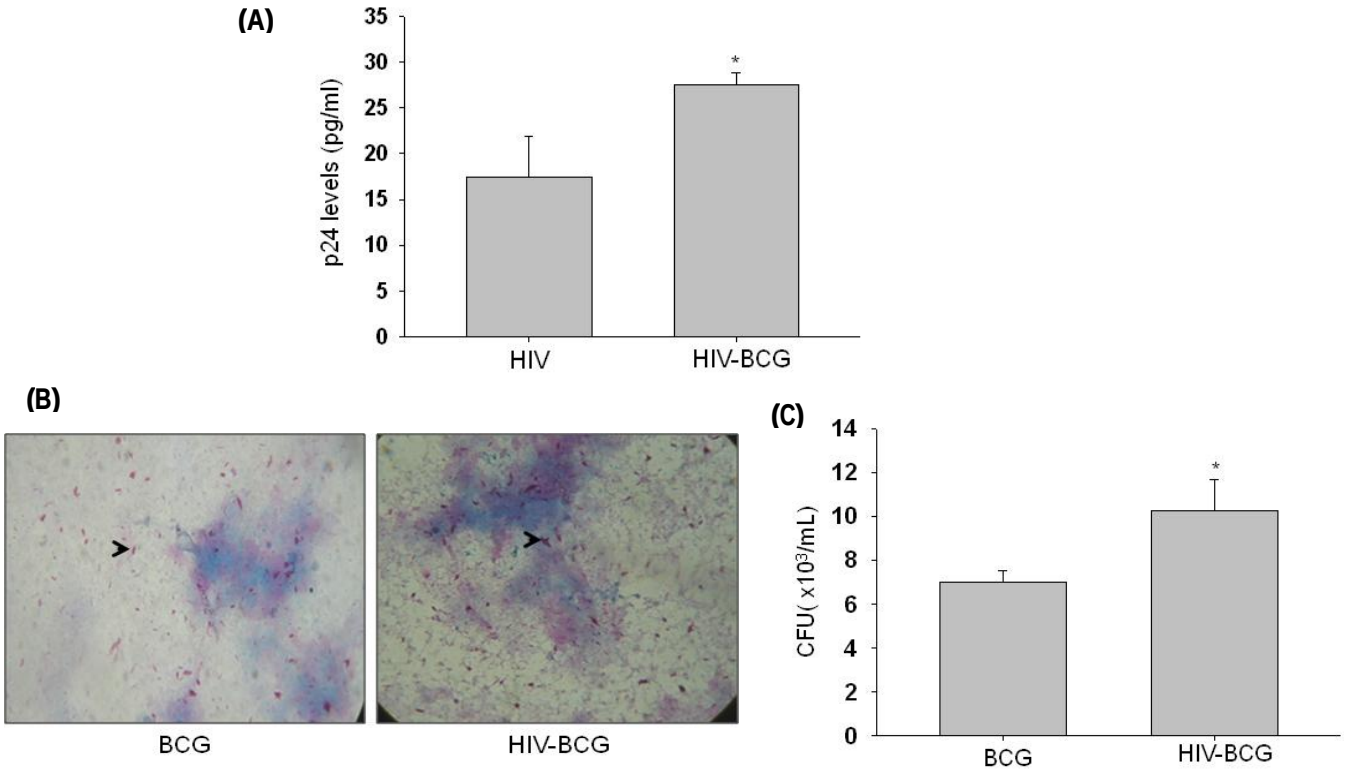

Figure 12: Viral and mycobacterial titers from THP-1 based co-infection model. A) HIV titers in the culture supernatants of HIV mono- and HIV-BCG co-infected cells at 24 hr post BCG infection as measured by p24 antigen capture ELISA; B) Ziehl-Neelsen staining of phagosomal fractions from BCG mono- and HIV-BCG co-infected cells. Black arrowheads indicate ZN stained mycobacteria (Red); C) CFU measurement of intracellular BCG during BCG mono- and HIV-BCG co-infections. All the experiments were performed more than three times. Statistical analyses were done with Student's *t*-test. Error bars represent ±SD (Standard deviation). * represents $p<0.05$.

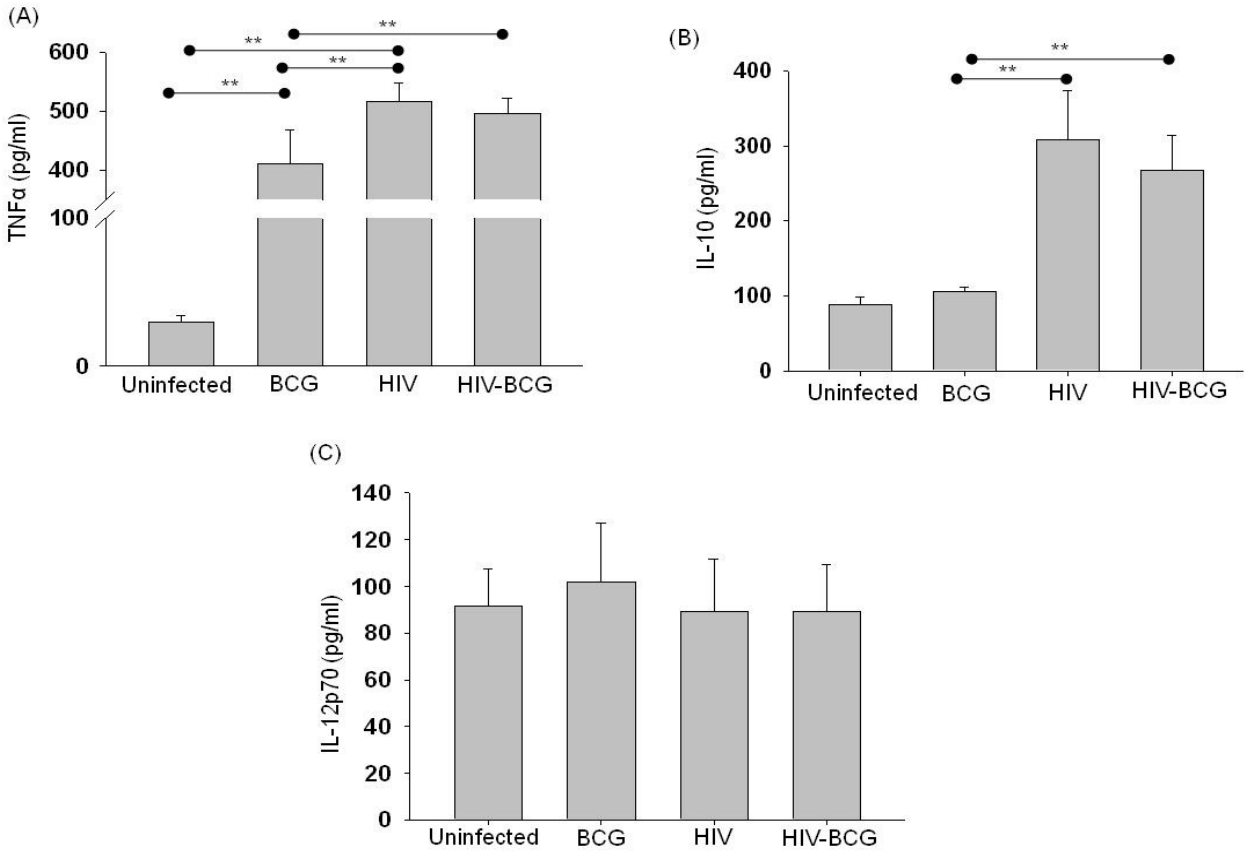

Figure 13: Cytokine profiles of the culture supernatants of Uninfected, BCG, HIV and HIV-BCG infected cells. (A) TNFα, (B) IL-10 and (C) IL-12p70 titers were measured using capture ELISA. All the experiments were performed more than three times. Statistical analyses were done using one-way repeated measures ANOVA with Holm-Sidak multiple pair-wise comparison method. Error bars represent ±SD (Standard deviation). ** represents $p<0.001$.

The model showed that infection by non-pathogenic mycobacteria promoted HIV proliferation with the simultaneous increase in the persistence of non-pathogenic mycobacteria during HIV-BCG. It also ensured that in the co-infection model, upon prior HIV exposure, THP-1 was in stimulated state, with respect to limited cytokine profile, when BCG infection occurred. Overall, the model was consistent with the hypothesis that the mycobacteria and HIV are mutually helped during co-infections (Diedrich and Flynn 2011). This model was used for further proteomics experiments and to understand the coalition between non-pathogenic mycobacteria and HIV.

2.4 Summary:

The *in vitro* cell culture model developed from THP-1 cells was standardized for the phagosome isolation and assayed for its fidelity by studying the impact of HIV infection on mycobacteria and vice versa. It was observed that during co-infection,

(i) HIV helped the persistence of the mycobacteria as observed by CFU counts and mycobacterial co-infection in turn had positive influence on the viral titers. This corroborates the various earlier evidences from the field (Newman, Kelley et al. 1993; Goletti, Weissman et al. 1996; Nakata, Rom et al. 1997; Imperiali, Zaninoni et al. 2001; Toossi, Mayanja-Kizza et al. 2001; Pathak, Wentzel-Larsen et al. 2010).

(ii) The model was also validated with respect to the cytokine profile. The purpose of assaying the cytokines, TNFα, IL-10 and IL-12, were to check if THP-1 were stimulated by the pathogens. It was earlier reported that, BCG and HIV increase TNFα secretion from macrophages as compared to uninfected cells (Kindler, Sappino et al. 1989; Molina, Scadden et al. 1989; Molina, Schindler et al. 1990; Kindler and Sappino 1991), HIV infection increases IL-10 (Brockman, Kwon et al. 2009; Kwon and Kaufmann 2010) and IL-12, in case of non-pathogenic mycobacteria and HIV-1 is not altered much (Ma and Montaner 2000; Mendez-Samperio 2010). Thus, the minimal cytokine profile of the model stands in compliance with the reported studies (Bordon, Plankey et al. 2011; Benjamin, Banerjee et al. 2013).

(iii) In view of the large amounts of the protein required for effective proteomic studies, the cell number was increased to 100 million cells per category and infection by BCG was performed at as high MOI as 100. MOI of 100 was determined based on two factors (a) the impact of the viability on macrophages and (b) the report by Lee *et al.*, 2010 where they were unsuccessful in identifying intracellular mycobacterial proteome even at MOI of 80 (Lee, Jethwaney et al. 2010).

(iv) The model can be used to study the biology behind the synergism during HIV-mycobacteria co-infection and also can be used to screen for the novel compounds against the HIV-mycobacteria co-infection. The model can be standardized or modified based on the study to be performed.

Thus, this model was used to identify the differential phagosomal proteomics of the host and intracellular mycobacteria during HIV-mycobacteria co-infection in comparision to the mycobacterial mono-infection.

Chapter 3

Proteomics of phagosome-enriched fractions from HIV-*M. bovis* BCG co-infected macrophages

3.1 Introduction:

In the chapter 1, the emergence of HIV-mycobacteria co-infection as a global health threat and the challenges associated with the disease management was introduced and highlighted the importance of understanding its pathobiology. In the recent times, AIDS epidemic has had an immense bearing on the clinical presentation, transmission and epidemiology of TB worldwide (Pawlowski, Jansson et al. 2012). TB is predominantly caused by pathogenic mycobacteria, *Mycobacterium tuberculosis* (*M.tb*), however non-tuberculous or attenuated strains of mycobacteria such as *Mycobacterium avium, M. kansasii, M. fortuitum, M. xenopi*, *M. bovis* Bacillus Calmette–Guérin (BCG), etc., cause opportunistic infections in HIV patients (Juffermans, Verbon et al. 1998; Smith, Schnadig et al. 2001; Bachmeyer, Blum et al. 2002; Karakousis, Moore et al. 2004; Serra, Loi et al. 2007; Singh, Gopinath et al. 2007; Azzopardi, Bennett et al. 2009; Hesseling, Johnson et al. 2009). These strains of mycobacteria can be successfully cleared by immune-competent macrophages (Zhang and Sugawara 2012).These are emerging as potential opportunistic pathogens in human, especially in immunocompromised HIV patients (Herzmann, Esser et al. 2011). The early molecular events that facilitate the establishment of infection by non-pathogenic strains of mycobacteria in HIV background are still not clear. At the same time, there are no experimental evidences towards molecular events explaining influence of non-pathogenic mycobacteria on HIV propagation during co-infection. The proteomic approach was undertaken to address the problem of co-infection and towards this a co-infection model was developed (Figure 8). The model was designed to simulate the field condition where a HIV patient acquires secondary mycobacterial infection. The fidelity of the co-infection model with respect to the field reports and the standardization of model for the phagosome isolation towards effective proteomics of phagosome and intracellular mycobacteria were discussed in the chapter 2. As mentioned, attenuated mycobacterial strain, BCG represented non-pathogenic mycobacterial co-infections. Using the model, phagosome fractions were obtained and by maintaining a stringent cut-off, followed by functional category enrichment analysis, differentially distributed phagosomal and mitochondrial proteins were identified revealing a highly altered host environment during co-infection. Overall, the proteomics data indicated interruption in phagosome maturation, extensive cytoskeletal rearrangement, alteration in fatty acid metabolism and increased energy state of the host cell during co-infection, making it conducive for mycobacterial persistence. The patronizing

impact of HIV on the persistence of non-pathogenic mycobacteria was reconfirmed using clinically relevant opportunistic mycobacterial strains *M. avium, M. kansasii* and *M. phlei.*

3.2 Materials and methods:

Cell lines used:

- HEK293T (Human embryonic kidney) cell line
- THP-1 monocyte leukemia cell line (Cat#TIB-202, ATCC)

Bacterial strains used:

- *Mycobacterium bovis* BCG
- *M. avium* (MTCC 1723) was procured from MTCC, IMTECH, India.
- *M. phlei* (MTCC 1724) was procured from MTCC, IMTECH, India.
- *M. kansasii* (MTCC 3058) was procured from MTCC, IMTECH, India.

Virus strain used:

- Macrophage tropic HIV (NL-ADA8) was gifted by Dr. Jayant Bhattacharya

The details of the protocols mentioned below are given in the chapter 2:

1) **Maintenance of the cell lines**
2) **Growth conditions of *Mycobacteria***

M. avium, M. phlei and *M. kansasii* were grown on 7H10 agar media (Hi-media, India) supplemented with 10% Oleic acid, Albumin, Dextrose and Catalase (OADC, Hi-Media, India). The plate was incubated at 37^{o}C until colonies appeared. The colonies were picked into the 7H9 broth media supplemented with 10% OADC and the broth culture was incubated at 37^{o}C at 180 rpm until the $OD_{600\ nm}$ reached 0.8 to 1. The culture was checked for any contamination using Ziehl-Neelsen (ZN) staining procedure. Prior to the infection, centrifuged the bacterial suspension at 200 ×*g* for 10 min and washed the bacterial pellet with PBS and then with RPMI 1640 media. Suspension of single-bacillus was obtained by passing the suspension through 26G 1 mL syringe for 10-20 times and then withdrew from the top of the tube.

3) **Preparation and quantification of infectious HIV-1 (ADA8) particles** (Kutner, Zhang et al. 2009; Banerjee, Benjamin et al. 2014)

3.2.1 Infection of macrophages and phagosome isolation:

THP-1 cells were PMA (10 ng/mL) differentiated to macrophages in RPMI 1640 media with 10% FBS in 150 mm culture dishes. After 24 hr the macrophages were washed, fresh media was added and kept for 48 hr rest. The macrophages were divided into two categories 1) for co-infection: First infected with HIV for 2 hr in incomplete RPMI media and followed by 24 hr incubation in

complete RPMI media (Collman, Hassan et al. 1989; Sylwester, Wessels et al. 1993; Zhao, Thibault et al. 2006; Espert, Varbanov et al. 2009; Andreani, Gagnon et al. 2012). This was followed by infection with BCG at an MOI=100 for 4 hr which was modified from the protocol described earlier (Lee, Jethwaney et al. 2010). 2) The MOI of 50 was used for *M. avium*, *M. kansasii* and *M. phlei* infections. For mono-infection: The cells were treated similar to co-infection but without virus and followed by BCG infection. After 4 hr of infection, fresh media with antibiotic was added and incubated for 24 hr. The phagosomes enter late endosome state at 24 hr post infection. After 24 hr the cells were harvested for fractionation to obtain enriched bacteria-*laden* phagosomes which was standardized in our laboratory using sucrose density gradient method as described earlier (Wandy Beatty and Russell 2001).

3.2.2 CFU enumeration and intracellular bacilli viability measurement:

For the CFU and Alamar blue assays, 24-well tissue culture plates carrying 0.2 million THP-1 per well was used. The mono- and co-infected cells after the incubation were washed thrice with PBS to remove any extracellular bacilli followed by lysis of macrophages with sterile water at 37^{o}C for 10 min. The lysates were diluted and were plated on 7H10 agar plates. The plates were incubated at 37^{o}C with 5% CO_2 and 95% humidity for 2-3 weeks (for BCG) and the colonies were enumerated. The intracellular viability of *M. avium*, *M. kansasii* and *M. phlei* was measured using the Alamar blue assay (Yajko, Madej et al. 1995; Kumar, Sahu et al. 2015) in a 24-well plate. The infected THP-1 were washed with PBS and lysed in 200 µL of sterile water at 37^{o}C for 10 min. To this, 40 µL of 1:1 mixture of 10% Tween-80 and 10% Alamar blue solution was added. The fluorescence was read in a fluorescence plate reader with excitation at 530 nm and emission at 590 nm.

3.2.3 Sample preparation and LC-MALDI-MS/MS Analyses:

Total 500 µg of phagosome-enriched protein fraction was trypsinized in each category (BCG fractions and HIV-BCG fractions) in presence of 0.1% SDS overnight at 37°C. The sample was then subjected to detergent removal using detergent removal spin columns (Thermo scientific Pierce, USA). A total of 2.5 µg digested peptides were separated using a Tempo Nano MDLC system (Eksigent) with 0.5 mm × 2 mm CapTrap™ C18 PepMap guard column (MichromBioresources, Auburn CA) and an Agilent 300 SB C18 0.075 µm × 150 mm, 3.5 µm, 300 Å Nano column (Agilent Technologies). The trap column was washed for 40 min with 0.1% aqueous TFA/2% Acetonitrile (ACN) at a flow rate of 15 µL/min. The Nano LC system was

operated at a flow rate of 300 nL/min. Desalted peptides were eluted using 98% water/2% ACN/0.1% TFA (Buffer A) and 2% water/98% ACN/0.1% TFA (Buffer B) with the following gradient: 5−50% B in 115 min, increase to 90% B in 12 min, decrease to 5% B in 13 min and equilibration at 5% B for 10 min. The eluent was mixed with MALDI matrix at 800 nL/min flow rate solution (2.5 mg/mL α-cyano-4-hydroxycinnamic acid [CHCA] in 80% ACN + 0.1% TFA) using a Ekspot Spotter (Eksigent) and spotted onto 28 × 44 spot arrays on 123 mm × 81 mm Opti-TOF LC/MALDI inserts (AB SCIEX). Spotting time was from 15 to 150 minutes, with 20 s spot intervals.

3.2.4 MALDI-TOF/TOF Analyses:

MS spectra were acquired on an AB SCIEX MALDI-TOF/TOF 4800 mass spectrometer equipped with a 200 Hz repetition rate Nd: YAG laser in positive ion mode in the mass range of 800−4000 m/z and 900 laser shots accumulation. MS spectra were internally calibrated using 4700 Proteomics Analyzer Standards Kit containing 6 peptide mix to 50 ppm accuracy. Laser intensity was set to 4000 for MS and 4600 for MS/MS acquisition. Precursor selection for MS/MS analysis was done by the 4000 Series Explorer Software (AB SCIEX, Darmstadt, Germany) in the strongest precursor first selection order using the following criteria: minimum S/N ratio, 60; maximum precursors per spot, 18. All MS/MS spectra were acquired with 2 kV collision energy by accumulation of 2500 laser shots.

3.2.5 Peptide Identification:

The data was analysed using GPS Explorer software (AB SCIEX) using MASCOT search engine in Human taxonomy with following parameters: MS tolerance: 150ppm; MS/MS tolerance: 0.5 Da; Enzyme used: Trypsin; Fixed modification: carbamidomethyl; Variable modification: oxidation (methionine), Deamidation (N,Q). I have reported only those proteins with a protein identification confidence interval of ≥95% ($p<0.05$).

3.2.6 Functional category enrichment analysis:

For functional category annotations, Uniprot accession number of the identified proteins was used. WEB-based GEneSeT Analysis Toolkit (WebGestalt) was used to annotate the predominantly represented biological processes or functions during mono- and co-infection (Zhang, Kirov et al. 2005; Wang, Duncan et al. 2013). The enrichments for GO (version 1.2, 11/11/2012), KEGG (03/21/2011) and Wiki pathways (11/11/2012) using WebGestalt with Hypergeometric statistical

test ($p<0.0001$), Benjamini and Hochberg Multiple test adjustment were considered with minimum three proteins per category (Zhang, Kirov et al. 2005; Wang, Duncan et al. 2013).

3.2.7 Immunoblot:

The phagosome fractions from mono- and co-infected cells were fractionated on 10% SDS-PAGE, transferred to Nitrocellulose membrane using GE-Amersham Western wet-transfer apparatus. The membrane was blocked with 5% non-fat milk powder in PBS with 0.1% Tween-20 at RT for 2 hr. The primary antibodies namely, Early phagosomal markers - Rabbit anti-Early phagosomal antigen-1 (EEA-1) (SantaCruz Biotechnology Inc., USA) and Rabbit anti-Rab5 (Cell Signaling Technology, USA) and Late phagosomal markers - Rabbit anti-LAMP-2 (Sigma Aldrich, USA) and rabbit anti-Rab7 (Cell Signaling Technology, USA) antibodies, rabbit anti-Tubulin and mouse anti-actin antibodies (kind gift by Prof. K.V.A.Ramaiah), prepared in PBS-T (PBS+0.1% Tween-20) with 2% BSA 1:1000 dilutions, were added and incubated at 4^{o}C on platform rocker overnight. After 3 PBS-T washes, added the corresponding HRP-conjugated secondary antibodies (Santa cruz Biotechnology Inc., USA), diluted 1:2000 in PBS-T with 2% BSA, incubated at RT for 2 hr. After 3 washes with PBS, ECL substrate (Femtolucent Plus-HRP, chemiluminiscent reagent from G-biosciences, USA) was added to the membranes and was scanned for chemiluminiscence using Versadoc Imaging system (Biorad). The Western blot images were quantified by Image-J software (NIH).

3.2.8 Fluorescence microscopic studies:

Wasabi-labeled BCG was generated by transformation of BCG with pTEC-15 plasmid (gift from Dr. Lalita Ramakrishnan and Dr. Deepak Saini). After the corresponding mono- and co-infections, acidophilic organelle dye Lysotracker Red DND-99 (Life Technologies, Invitrogen, USA) was added to cells at 75 nM prepared in pre-warmed media and incubated at 37^{o}C for 30 min as per the manufacturer's instructions (Life Technologies, Invitrogen, USA). The stained cells were washed with PBS and fixed with 3.7% paraformaldehyde. The co-localization of Wasabi-labeled bacteria and lysosomes were then monitored under fluorescence microscope. The co-localization was calculated using the Twin slicer tool from Huygens essential software (Huygens compute engine 4.4.6p3 32b; Huygens Essential for Win32). Using the Twin slicer tool, a line is drawn across the Wasabi-labeled BCG in the field image of fluorescence microscopy. Twin slicer tool measures the fluorescence intensity profile along the line drawn across the Wasabi-labeled BCG. If the intensity peaks for the two fluorochromes coincide then it was considered lysotracker

positive. More than 100 bacilli from at the least 10 fields (10cells/field) per experiment were taken into consideration for percentage colocalisation (Formula used: percentage colocalisation= [# of Co-localized bacilli/total # of bacilli]*100) calculations.

3.2.9 Intracellular ATP measurement:

The intracellular ATP was measured by colorimetric method at Abs_{570nm} using the colorimetric/fluorometric ATP assay kit as per the manufacturer's instructions (ab83355, Abcam Plc., UK).

3.2.10 Oil red O staining:

The cells were washed with PBS and fixed with 10% formalin at RT for 10 min. After fixing, the cells were washed with PBS and incubated with 60% isopropanol for 15 sec, followed by staining with 60% Oil red O stain at 37ºC for 1 min in dark. The excess stain was destained with 60% isopropanol for 15 sec and was followed by three PBS washes. At this stage representative images were taken under bright field microscopy. The cell densities in all the three infection conditions were checked microscopically before the colorimetric quantification of intracellular lipid bodies. The amount of lipid staining was quantified by eluting the intracellular Oil red O stain using 100% isopropanol at RT for 10 min and was measured at 500nm with 100% isopropanol as blank.

3.2.11 Whole cell RNA isolation:

After infections, cells were washed with Phosphate buffered saline (PBS) for three times and scraped into the RNase free micro centrifuge tubes. Cell pellet was resuspended in trizol and kept at RT for 5 min. To the trizol mix, $1/5^{th}$ volume of chloroform was added and vortexed vigorously for 5 min. Kept at room temperature for 5 min and centrifuged at 12000 rpm for 15 min. To the upper aqueous layer, equal volume of isopropanol was added and RNA was precipitated at 12000 rpm for 15 min at 4°C. The RNA pellet was washed with 70% ethanol and air-dried. The pellet was resuspended in 10-15 µL of DEPC treated water. The RNA was used for reverse transcription using SuperscriptIII reverse transcriptase as per manufacturer's protocol (Life Technologies, Invitrogen, USA).

3.2.12 Real-time PCR:

Equal amount of RNA was considered for equal loading and the corresponding cDNA was used for RT-PCR. As endogenous controls, β-actin gene was used (Annexure I). The 2X SyBr green mix (Takara Bio Inc., Japan) was used. The real-time PCR data analyses were done using the $2^{-\Delta\Delta Ct}$ method.

3.2.13 Statistical Analyses:

All the experiments were performed at the least three times. The data were analysed using SigmaPlot software version 11.0.0.77 (Systat Software, Inc., USA). The error bars represent the standard deviation (SD) from the mean of at least three independent experiments. Statistical analyses of the experimental data for comparing two groups were performed by Student's *t*-tests or paired *t*-test. Statistical analyses of the experimental data comparing more than two groups were performed by One-way repeated measures ANOVA with Holm-Sidak multiple pair-wise comparison method. $p<0.05$ was considered as significant.

3.3 Results and discussion:

The co-infection model, discussed in chapter 2, was consistent with the hypothesis that the mycobacteria and HIV mutually help each other during co-infections (Diedrich and Flynn 2011). After validating the fidelity of the model (Discussed in chapter 2), it was used for sucrose density gradient based phagosome fractionation from BCG mono- and HIV-BCG co-infected cells and performed LC-MALDI-MS/MS analyses to understand the coalition between non-pathogenic mycobacteria and HIV.

3.3.1 Identification of host proteins unique to BCG and HIV-BCG in phagosome-enriched fractions

Phagosome-enriched fractions from BCG mono- and HIV-BCG co-infected cells were obtained by 12-50% sucrose density gradient to minimize the presence of most cytosolic proteins and enrich the bacteria-*laden* phagosomes (Beatty, Rhoades et al. 2002). The protocol retained mitochondria in the enriched fractions, since mitochondria tend to surround mycobacteria-laden phagosomes (Jamwal, Midha et al. 2013). These fractions were then subjected to LC-MALDI-MS/MS for protein identification. Overall, a total of 189 phagosomal proteins and 71 mitochondrial proteins could be identified with more than 95% confidence ($p<0.05$) (Annexures II and III). Proteins detected exclusively in one but not in the other condition were considered for further analyses. The proteins were identified from three experiments of BCG mono-infected fractions and four experiments of HIV-BCG co-infected fractions. The proteins listed in the study were identified from at the least two independent experiments. Of the 189 phagosomal proteins, 27 (14.29%) proteins were exclusively present in the BCG fractions and 79 (41.80%) proteins in HIV-BCG fractions while 83 (43.91%) proteins showed a notable overlap in both the fractions (Figure 14 and Annexure II). For 71 mitochondrial proteins in the isolated fractions, 5 (7.04%) were exclusive to BCG, 15 (21.12%) in HIV-BCG and 51 (71.83%) proteins were found in the fractions from both the conditions (Figure 14 and Annexure III).

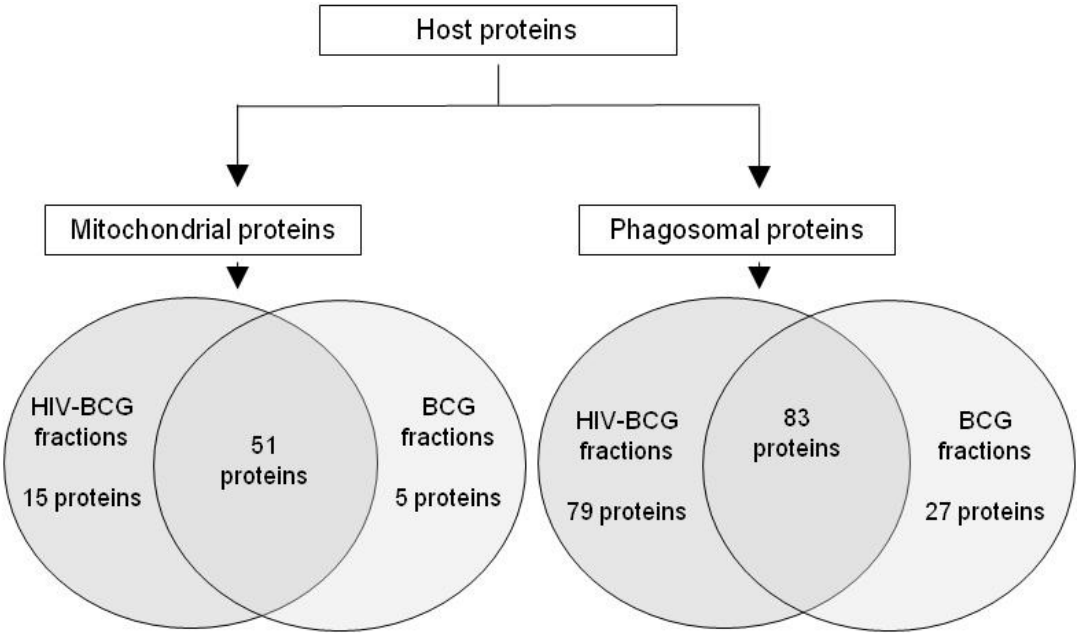

Figure 14: Venn diagram depicting the distribution of the phagosomal and mitochondrial proteins between BCG mono-infected and HIV-BCG co-infected cells.

Several of the proteins identified showed an overlap with the already reported BCG phagosome proteome identified by Lee et al., 2010. Of the total proteins, 86 (45.50%) phagosomal and 42 (59.14%) mitochondrial were also identified by Lee et al., 2010. When compared the proteins identified from our study for HIV-BCG fractions, there was an overlap of 34 (36.17%) proteins. 60 proteins, upregulated during HIV-BCG, were not identified in the already reported BCG phagosome proteome (Lee, Jethwaney et al. 2010).

Gene ontology (GO) annotations and enrichment analysis were performed to identify the major perturbations in the cell during co-infection using the WEB-based GeneSeT Analysis Toolkit (WebGestalt) as described (Zhang, Kirov et al. 2005; Wang, Duncan et al. 2013). Employed stringent cut-offs such as Hypergeometric statistical test with significance level to $p<0.0001$, and considering minimum 3 proteins per category of GO for the enrichment analyses. The enrichment analysis using GO, KEGG and Wiki pathways for BCG and HIV-BCG are summarized in Annexure IV. Cytoskeletal assembly and energy metabolism are affected during both BCG and HIV-BCG. Additionally, the enrichment analyses indicated that HIV-BCG appeared to impact mitochondrial activity, fatty acid beta oxidation, glycolysis-gluconeogenesis (prompting increased ATP synthesis) and peroxiredoxin activity (possibly to quench oxidative stress) more significantly

than the BCG (Annexure IV). Some of the leads from the above proteomics analyses were further investigated to understand the molecular mechanisms behind survival of the opportunistic mycobacteria during HIV co-infection.

3.3.2 Co-infection mediated alterations in the phagosome maturation supported the persistence of non-pathogenic mycobacteria

The proteomic data suggested perturbations in the phagosome maturation process during HIV-BCG. Host proteins that are involved in efficient phagosome maturation such as Ras-related protein Rab10 (Rab10), 185 kDa Golgi coiled-coil protein (GCC185), Sorting Nexin 9 (SNX9) and Wiskott Aldrich syndrome protein FAM21A (WASH) (Annexure II) were observed in fractions from BCG. Rab10 is shown to be involved in the early processes of phagosome maturation and drives the fusion of Mycobacteria containing phagosomes with lysosomes. Absence of Rab10 on phagosome is indicative of phagosome maturation arrest (Cardoso, Jordao et al. 2010). Absence of Rab10 in HIV-BCG, suggesting a possibility of obstructed phagosomal maturation during HIV-BCG. GCC185, an effector of Rab9, is involved in transit and recycling of lysosomal Mannose-6-phosphate receptor from the mature phagosomes (Reddy, Burguete et al. 2006). GCC185 was observed only in BCG fractions. Similarly, SNX9 and WASH are involved in the activation of actin polymerization for maintaining the structure and motility of the endocytic vesicles inside the cell, which were also absent in the fractions from HIV-BCG. WASH is also implicated in the efficient degradation of the phagosomal cargo (King, Gueho et al. 2013). Therefore, the absence or low expression of proteins involved in efficient phagosome maturation, cargo degradation and proper recycling for continual cycle of endocytosis during HIV-BCG suggested that the phagosomal maturation process is modified during the co-infection.

To test for compromised phagosome maturation during co-infection, I scored for the presence of the early phagosomal markers- EEA-1 and Rab5 and the late phagosomal markers- LAMP2 and Rab7 by immunoblotting (Figure 15A and 15B). The phagosomes in the fractions from HIV-BCG retained early markers, EEA-1 and Rab5 while they were detected at very low levels in the fractions from BCG (Figure 15A and 15B). Also, the phagosomes in the fractions from HIV-BCG have acquired low amounts of late markers, LAMP2 compared to the fractions from BCG which was evident from the Western blot for LAMP2 and corresponding densitometry plot (Figure 15A

and 15B). The corresponding post-nuclear supernatants (PNS) were taken as controls for the phagosome-enriched fractions (Figure 15A and 15B).

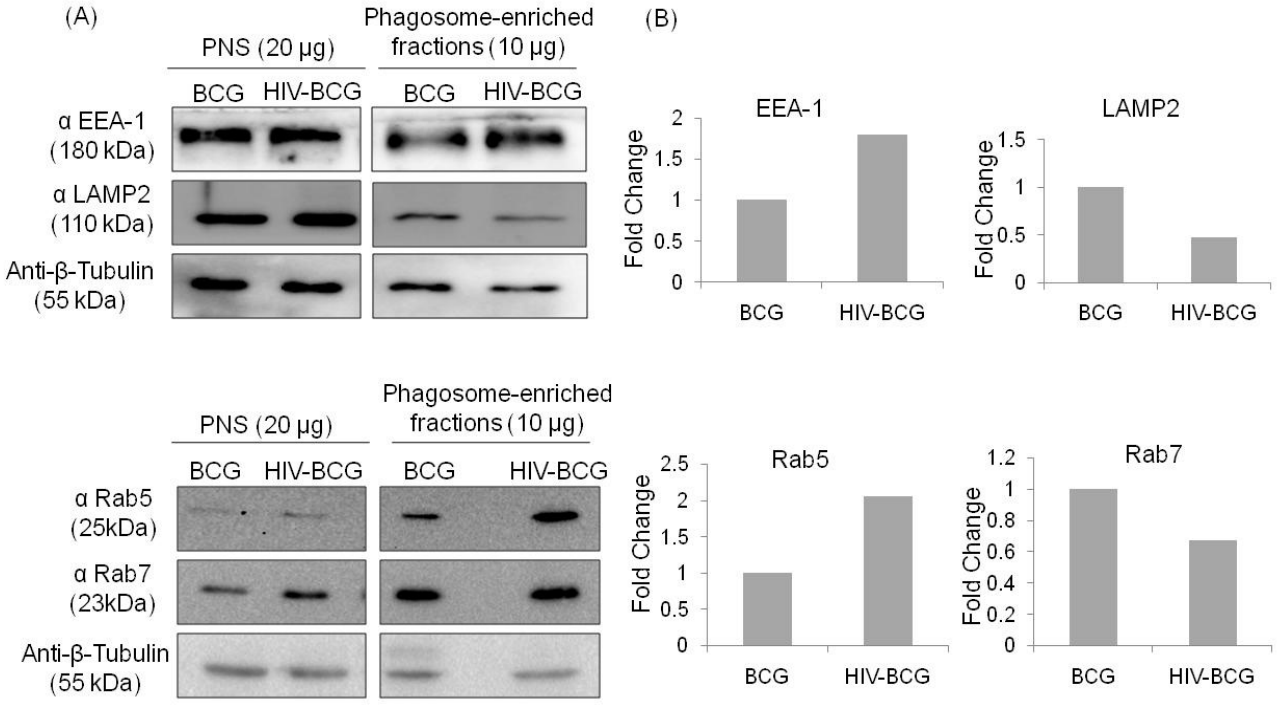

Figure 15: Phagosome maturation in BCG and HIV-BCG infected THP-1. The maturation states of the phagosomes were checked by A) Western blots for early phagosomal markers, EEA-1 and Rab5 and Late phagosomal markers, LAMP-2 and Rab7. 20 µg of PNS protein and 10 µg protein of phagosome-enriched fractions was taken for Western blot. β-Tubulin was used as a loading control; B) Corresponding densitometric analyses of the band intensities were performed using Image J software. The data were normalized to the band intensity of the loading control, β-Tubulin within a condition and then to that of PNS for the corresponding protein.

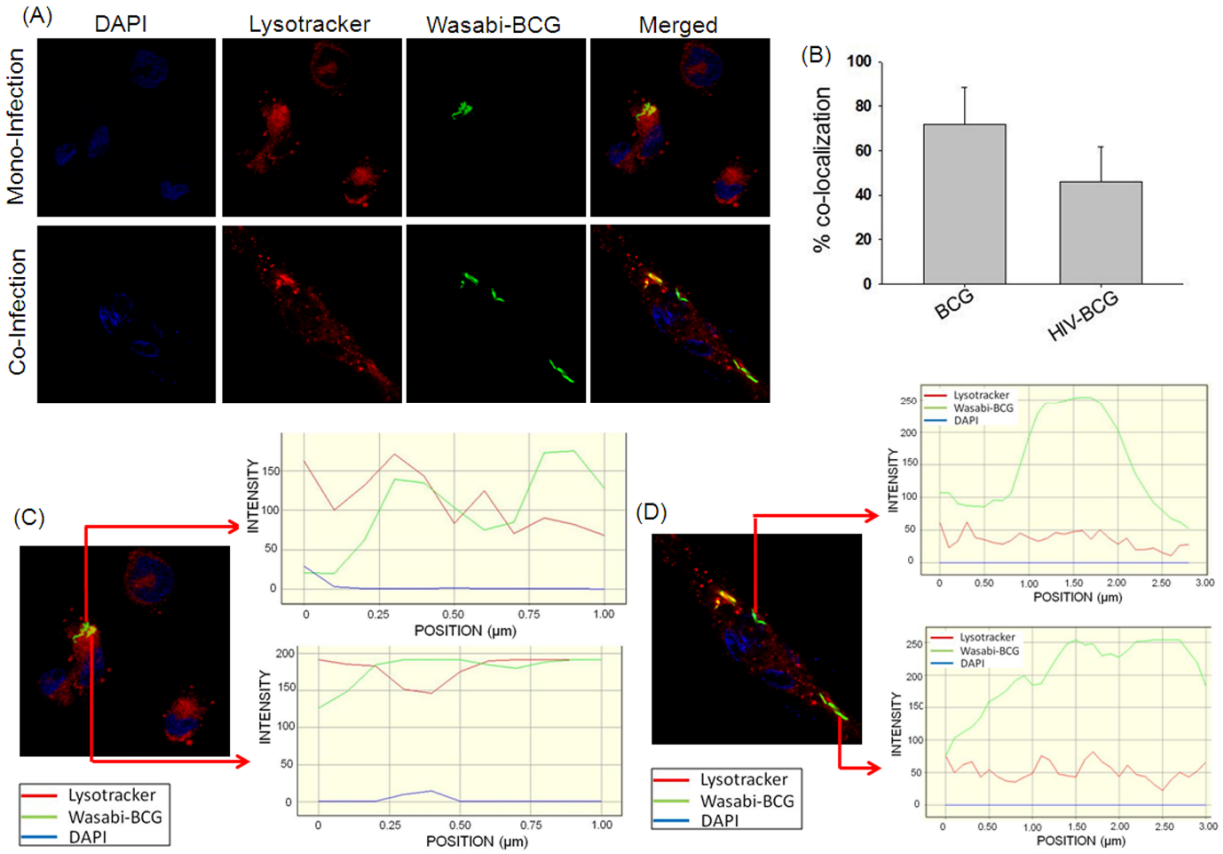

Figure 16: Co-localization of BCG in phagolysosomes of mono and co-infected cells using confocal microscopy. A) Representative image showing the localization of Wasabi-labeled BCG (Green) with respect to the Lysotracker Dye (Red). Macrophages were either mono-infected with Wasabi-labeled BCG (MOI=100) (Upper panel) or co-infected with HIV followed by Wasabi-labeled BCG (Lower panel). After 24 hr post BCG infection, the cells were stained with lysotracker dye, fixed and processed for confocal microscopy (Carl Zeiss 700). B) Bar graph representing the percent co-localization of Wasabi-labeled BCG and lysotracker. At least 10 fields (10 cells/field) per experiment were used to calculate the % co-localization using Huygens Essential software twin slicer tool (Formula used: % co-localization = [Co-localized BCG/Total BCG] ×100). The quantification was based on individual phagosomes within a cell. Graphical analyses of co-localization in BCG-infected (C) and HIV-BCG co-infected (D) THP-1 using Huygens Essential software twin slicer tool, where Blue line denotes DAPI, Red line denotes Lysotracker and Green line denotes Wasabi-labeled BCG. Co-localization is indicated by merging of Red line with the green line. All the experiments were performed more than three times. Statistical analyses were done with Student's *t*-test. Error bars represent ±SD (Standard deviation). ** represents $p<0.001$.

These results suggested that attenuated mycobacteria, BCG, continued to persist during HIV-BCG as result of improper maturation of phagosomes. To complement these observations, co-localization of Wasabi-labeled BCG with acidic phagosomal vesicles using lysotracker was monitored by fluorescence microscopy and images of at the least 10 fields (10 cells/field) of each experiment were taken to calculate the percentage co-localization. The BCG infected cells showed 71.69±16.98 % co-localization of BCG with the acidic lysosomes whereas the HIV-BCG infected cells showed 46.03±15.94 % ($p<0.001$) (Figure 16A and 16B) implying the breach in acidification of phagosomes during co-infection. The co-localization of BCG with acidic lysosomes was graphically analysed using Twin slicer tool of Huygens essential software and the representative images have been shown (Figure 16C and 16D; refer experimental procedures for details). In addition, Galectin-3, a protein known to be associated with only live-mycobacteria containing phagosomes (Beatty, Rhoades et al. 2002), was observed only in HIV-BCG and not in BCG (Annexure II). Based on these results, one could infer that co-infection blocked effective phagosomal maturation resulting in an improved persistence of non-pathogenic mycobacteria, which explained the higher CFU counts during HIV-BCG (refer Chapter 2; Figure 12C).

3.3.3 HIV-BCG *co-infected cells exhibited increased lipid bodies supporting mycobacterial persistence*

Mycobacterial or HIV infection leads to modulation in host metabolism towards increased lipid metabolism (Heaton and Randall 2011; Lee, VanderVen et al. 2013; Almeida, Roque et al. 2014). Macrophages infected with pathogenic mycobacteria like *M.tb*, exhibit foamy phenotype with increased presence of lipid droplets which provide an additional niche for pathogenic mycobacterium to escape from immune recognition and also nutrient reserve to persist inside the host (Russell, Cardona et al. 2009; Daniel, Maamar et al. 2011). However, non-pathogenic mycobacteria have not been reported to induce any such phenotype. GO enrichment analyses showed increased representation of lipid metabolism in HIV-BCG compared to BCG (Annexure IV). A higher number of lipid bodies were observed in THP-1 infected with HIV or HIV-BCG as compared to BCG alone using Oil red O staining under bright field microscopy (Figure 17A and 17B). Colorimetric quantification of the Oil red O stain suggested a 1.40±0.15 ($p=0.013$) fold increase in the lipid bodies in HIV-BCG compared to BCG (Figure 17C). The fold changes were normalized to BCG infection. As it is known that increased presence of lipid droplets (foamy

phenotype) provides additional niche for intracellular pathogen to escape from immune recognition and additionally serve as nutrient reserve for their persistence (Russell, Cardona et al. 2009; Daniel, Maamar et al. 2011), the results suggested that HIV infection alone or HIV-BCG provided a more conducive environment for the persistence of mycobacteria through lipid body biogenesis.

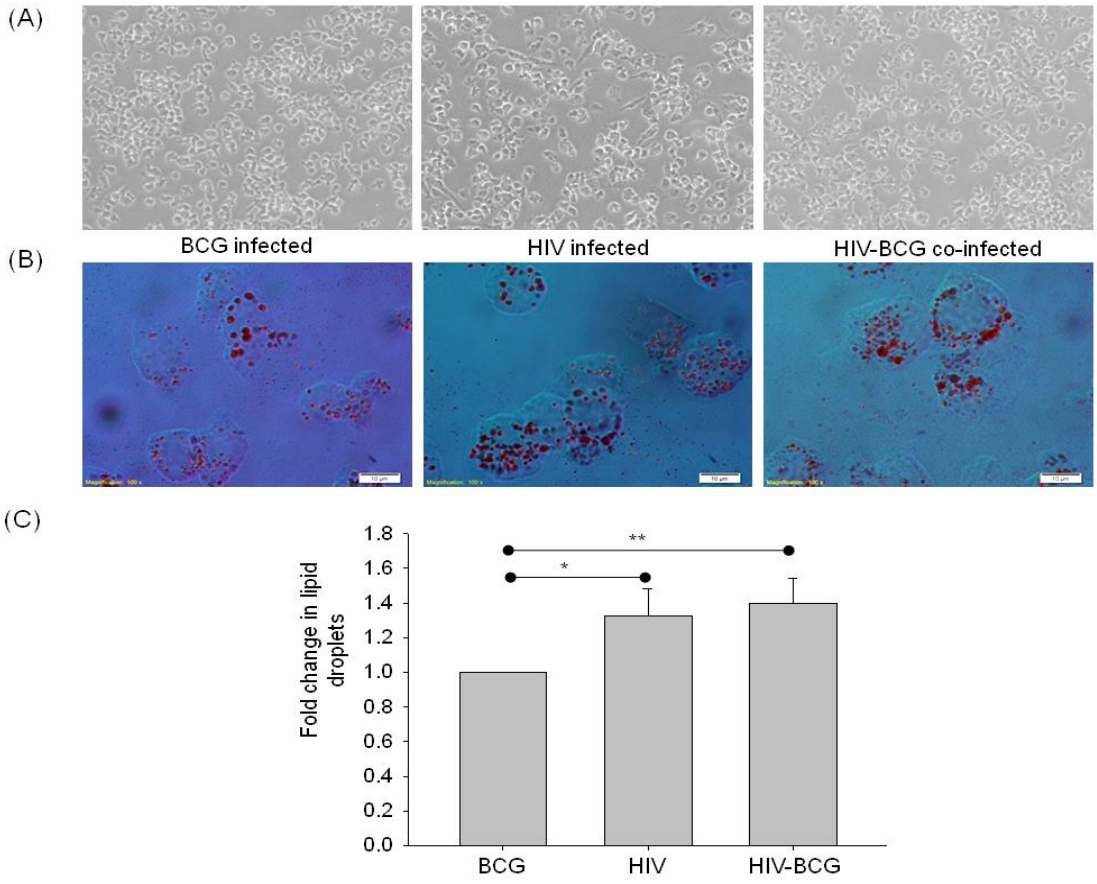

Figure 17: THP-1 exhibited lipid accumulation during co-infection. (A) Representative bright field images to show the density of the cells in all the three infection conditions for Oil-red-O staining. (B) Representative bright field microscopy image showing the accumulation of lipid bodies inside the infected cells by Oil Red O staining. 24 hr post BCG infection, the cells were fixed and stained with Oil Red O stain. The white bar indicates 10 µm scale. Images were taken at 100x magnification. The Oil red O stain accumulated by cells is measured by eluting intracellular stain using 100% isopropanol and measured at Absorbance at 500 nm; (C) Bar graph representing the fold change in the accumulation of Oil red O stain as measured at Abs_{500nm}. Fold changes were calculated with respect to the values of BCG. All the experiments were performed more than three times. Statistical analyses were done using one-way repeated measures ANOVA with Holm-Sidak multiple pair-wise comparison method. Error bars represent ±SD (Standard deviation). * represents $p<0.05$; ** represents $p<0.001$.

3.3.4 HIV-BCG *co-infected cells exhibited increased ATP synthesis by flux of nutrients through catabolic routes and exhibited higher expression of purinergic receptors*

The host metabolic response plays an important role in the pathogenesis and outcome of the infection which may be a host-*driven* or a pathogen-*driven* event. The objective of cell metabolism is to provide energy equivalents (ATP) and building blocks for the biosynthetic processes. Resting cells require optimal amounts of ATP and biosynthetic precursors but a stimulated or infected cell require increased amounts of energy and precursors for its adaptation to stimulation or to overcome the infection. Recent reports suggested that increased fatty acid beta oxidation drives the production of mitochondrial reactive oxygen species (ROS) for microbicidal activity (Hall, Boyle et al. 2013) and increased glycolysis with simultaneous glutamine metabolism provide biosynthetic intermediates (DeBerardinis, Lum et al. 2008; Rathmell 2012). The increase in fatty acid beta oxidation, glycolysis and mitochondrial activity during co-infection may result in high energy equivalents, biosynthetic precursors and mount defense against infection. However, this could be a double-edged sword, as these energy equivalents and precursors could also be exploited by mycobacteria and HIV for their survival and propagation.

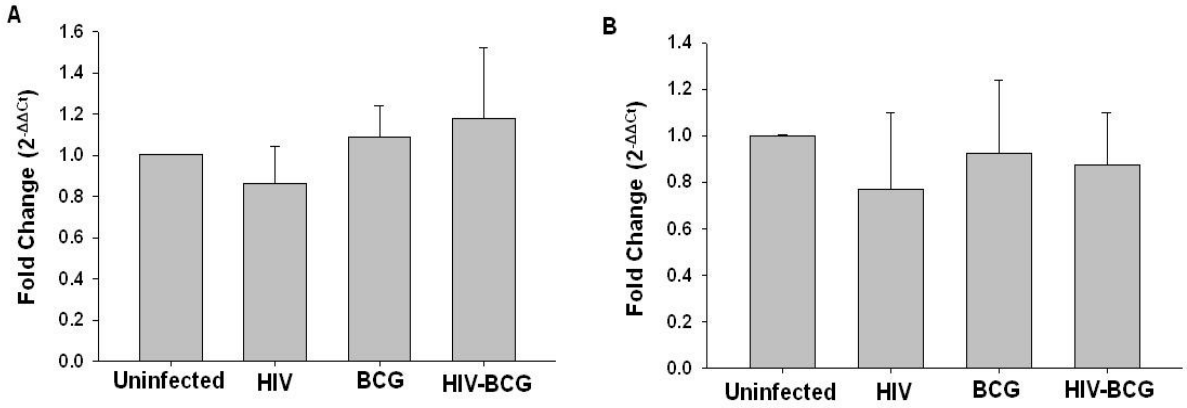

Figure 18: Real-time PCR of (A) Pyruvate kinase and (B) Glyceraldehyde-3-phosphodehydrogense. Fold change in transcript levels with respect to Uninfected. The transcript levels were quantified by relative $2^{-\Delta\Delta Ct}$ method with endogenous actin as loading control. All the experiments were performed more than three times. Statistical analyses were done using one-way repeated measures ANOVA with Holm-Sidak multiple pair-wise comparision method. Error bars represent ±SD (Standard deviation). * represents $p<0.05$; ** represents $p<0.001$.

Functional category enrichment suggested alterations in the TCA cycle, Electron Transport Chain (ETC), ATP synthesis by chemiosmotic coupling, oxidative phosphorylation and fatty acid beta oxidation during HIV-BCG (Annexure IV). It was also observed that glycolytic enzymes such as Enolase, 3-phosphogleraldehyde dehydrogenase, pyruvate kinase and 3-phosphoglycerate kinase were enriched in the fractions from HIV-BCG suggesting increased glycolysis. However, the change in the transcript levels of the 3-phosphoglyceraldehyde dehydrogenase (Figure 18B) and pyruvate kinase (Figure 18A), the first energy producing enzyme and enzyme involved in last step of glycolysis, respectively, were insignificant. This clearly indicated that though the overall expression of these proteins remains unaffected, the spatial distribution of the same is differential during mono and co-infection.

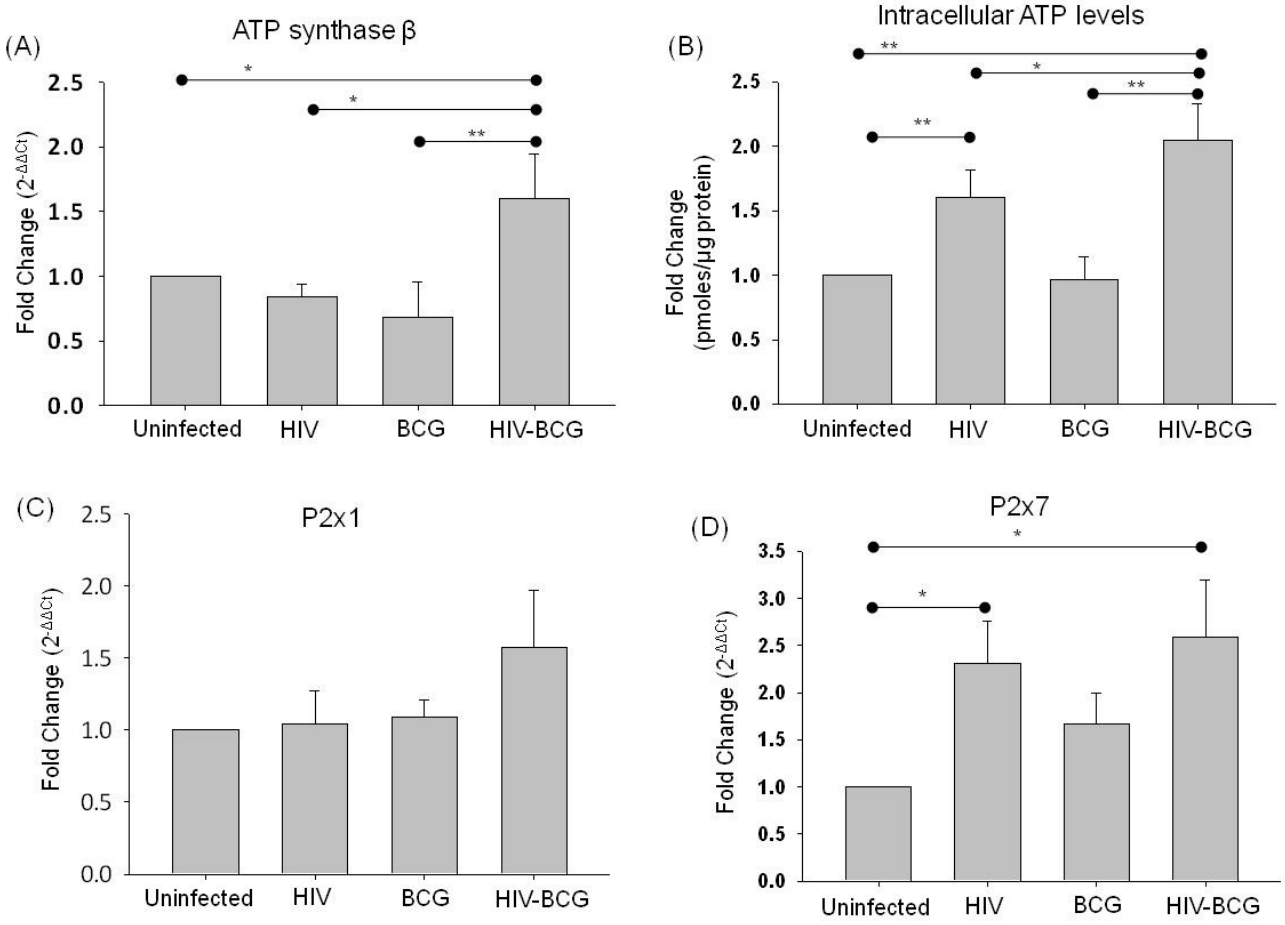

Figure 19: Alteration in energy metabolism of host during HIV-BCG co-infection. (A) Real-time PCR of ATP synthase beta. Fold change in transcript levels were calculated with respect to uninfected cells. The transcript levels were quantified by relative $2^{-\Delta\Delta Ct}$ method with endogenous actin gene as control; (B) Fold change in the intracellular ATP levels (pmoles/µg protein) normalized to the uninfected condition; Real-time PCR of (C) P2x1 and (D) P2x7 genes. Fold

change in transcript levels were calculated with respect to uninfected cells. The transcript levels were quantified by relative $2^{-\Delta\Delta Ct}$ method with endogenous actin gene as control. All the experiments were performed more than three times. Statistical analyses were done using one-way repeated measures ANOVA with Holm-Sidak multiple pair-wise comparison method. Error bars represent ±SD (Standard deviation). * represents $p<0.05$; ** represents $p<0.001$.

The differences in the spatial distribution of these proteins strongly supported a shift in the metabolism towards ATP synthesis via glycolysis, TCA cycle, Electron transport chain (ETC) and oxidative phosphorylation during co-infection. The transcript levels of ATP synthase beta subunit gene were 2.34±0.50 folds higher in HIV-BCG as compared to BCG (Figure 19A). This shift in the metabolism towards ATP synthesis was further supported by the presence of 3-phosphoglycerate dehydrogenase during HIV-BCG. To corroborate these observations, intracellular ATP levels during BCG and HIV-BCG were measured. ATP levels inside HIV-BCG infected cells were 2.04±0.28 fold ($p<0.001$) higher than the ATP levels in BCG-infected cell (0.97±0.18 fold) (Figure 19B). It is known that upon stress (here infection), released ATP binds to purinergic receptors in autocrine manner influencing several cellular mechanisms ranging from inflammasome activation to modulating aerobic glycolysis (Amoroso, Falzoni et al. 2012; Riteau, Baron et al. 2012). Purinergic receptors also help in HIV-1 entry (Hazleton, Berman et al. 2012). So, though not associated with either phagosome or mitochondrial proteome, the expression levels of purinergic receptors was checked. The transcript levels of P2x7 and P2x1 receptors in HIV-BCG were 1.55±0.37 and 1.44±0.36 fold higher as compared to BCG, respectively (Figure 19C and 19D). Increase in purinergic receptors during co-infection can be yet another explanation to increased viral titers as compared to HIV infection alone.

3.3.5 Cytoskeletal rearrangement and differential distribution of Vimentin and Septin in co-infected cells

Cytoskeletal reorganization plays diverse roles such as in , chemotaxis, trafficking of subcellular components such as lysosomes, phagosomes and secretory vesicles, macropinocytosis, signal transduction and autophagy (Fenteany and Glogauer 2004) but pathogens are also capable of modulating this reorganization for the persistence of infection. Various intracellular parasites are known to disrupt the actin filament network for their advantage and restrict the fusion events of the early phagosomes with the late endosomes or lysosomes, thus arresting the phagosome maturation process (Guerin and de Chastellier 2000). Similarly, HIV-1 infection is known to

modulate the cytoskeletal organization to facilitate the viral entry and syncytia formation (Iyengar, Hildreth et al. 1998; Pontow, Heyden et al. 2004; Harmon and Ratner 2008). Functional enrichment analysis of our proteome data suggested that the proteins involved in the regulation of cytoskeletal reorganization were significantly represented during mono- and co-infection (Annexure IV) (Zhang, Kirov et al. 2005; Wang, Duncan et al. 2013). However, during co-infection, cytoskeletal proteins such as actin, actin-related protein, actinin, myosin, septin-7, vimentin and tubulin were enriched in the phagosomal fractions from co-infected cells as compared to BCG mono-infection (Annexure IV). While several cytoskeletal proteins were represented in both the proteomes, our attention was drawn to vimentin and septin-7, as these proteins have been implicated in HIV infection and host immunity. HIV protease utilizes vimentin as substrate and is crucial for the pathogenesis of HIV, as cleaved intermediary filaments from vimentin are shown to disrupt the nuclear architecture and shape (Shoeman, Honer et al. 1990; Karczewski and Strebel 1996). The levels of vimentin in the phagosomal fractions of co-infected cells were observed to be higher than BCG mono-infected cells by Western blot (Figure 20), supporting the notion that mycobacterial co-infection reinforced conditions required for HIV pathogenesis.

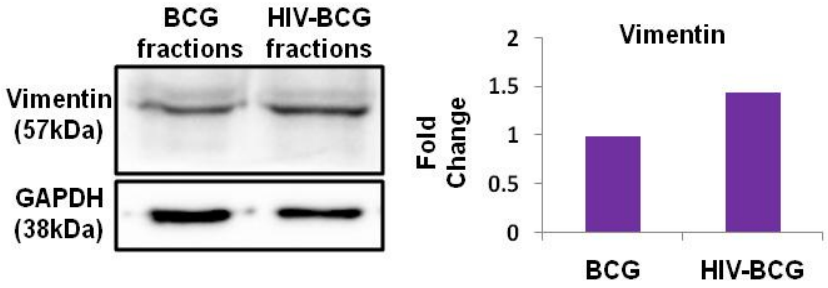

Figure 20: Western blot of phagosomal fractions from infected cells for Vimentin. Densitometric analysis was done using Image-J software with GAPDH as loading control.

Yet another important cytoskeleton protein, septin-7, appeared only in BCG phagosomal fractions but not in HIV-BCG co-infected phagosomal fractions. Septin fibres form cage around the intracellular pathogen that is employed as a defense strategy by the host cell for clearing the pathogen by signaling for autophagy (Haglund and Welch 2011). Below detectable levels of septin-7 during co-infection, indicated compromised self-defense by macrophages during co-infection. Decrease in septin-7 levels during HIV background additionally provided a supportive niche for the survival of the opportunistic Mycobacteria (Annexures II).

3.3.6 HIV co-infection assisted the persistence of clinically relevant opportunistic mycobacterial strains M. avium, M. kansasii and M. phlei

So far these observations indicated that, early adaptation of non-pathogenic strain of mycobacteria in the activated host macrophages during co-infection is supported by (i) altering phagosomal maturation, (ii) promoting foamy phenotype of macrophages characterized by the accumulation of lipid bodies and (iii) increasing energy synthesis and metabolism. In turn, infection by the attenuated mycobacterial strain up-regulated purinergic receptors that can be used by HIV for infecting new host cells, thereby, increasing viral titers during co-infection. The inferences made from proteomics of HIV-BCG co-infection were also checked with other clinically relevant opportunistic strains, *M. avium, M. kansasii* and *M. phlei*. The persistence of *M. avium, M. kansasii* and *M. phlei* strains during HIV-mycobacteria co-infection was followed at 0, 6, 16 and 24 hr post infection using Alamar blue assay (Yajko, Madej et al. 1995; Kumar, Sahu et al. 2015).

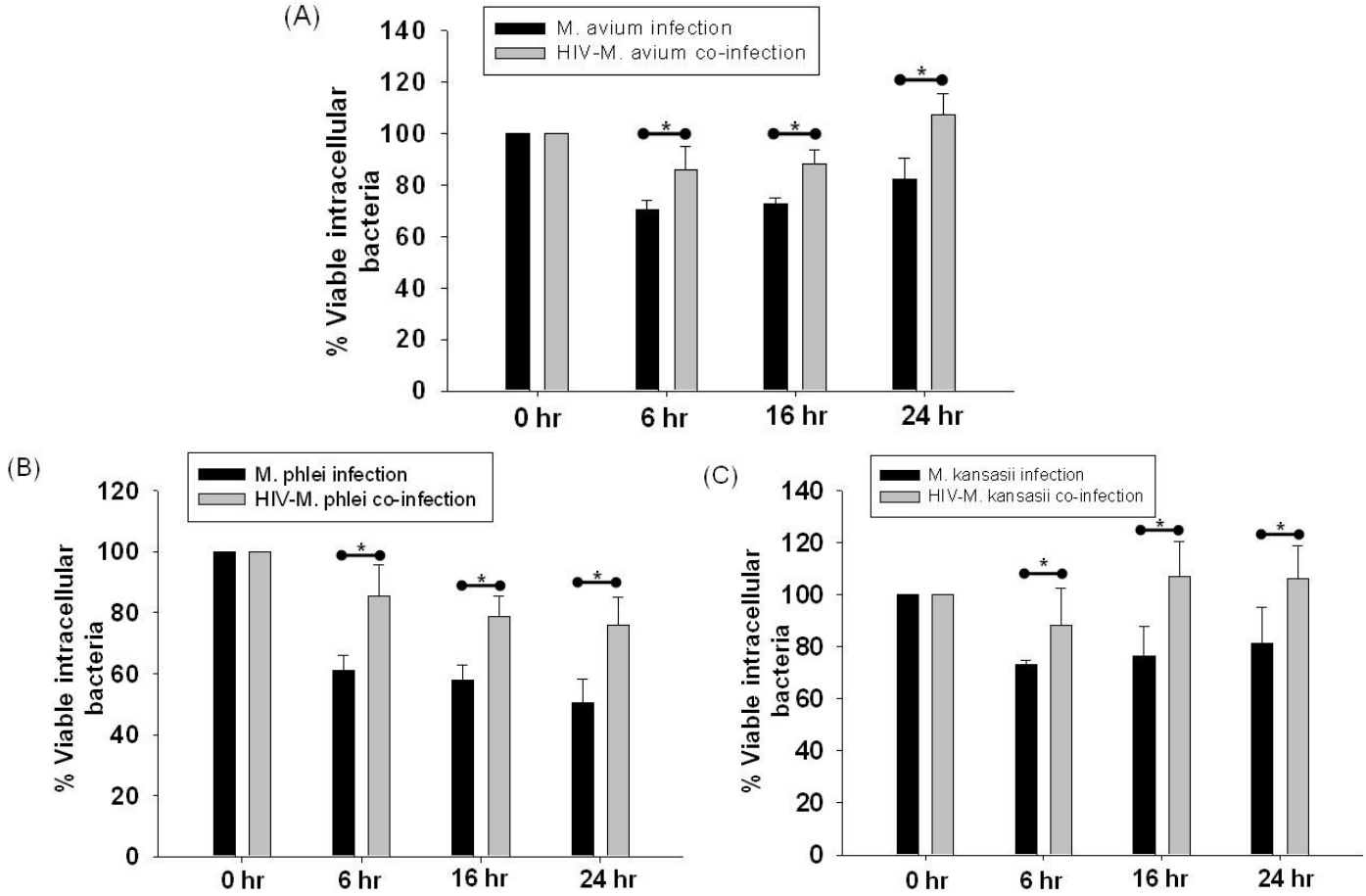

Figure 21: Co-infection supports the persistence of opportunistic mycobacterial strains inside THP-1. *M. avium, M. kansasii* and *M. phlei* infections were carried out at an MOI=50 for 4 hr. The viability of intracellular A) *M. avium,* B) *M. phlei* and C) *M. kansasii* at 0 hr, 6 hr, 16 hr and 24 hr upon respective mono- and HIV co-infection. The intracellular viable mycobacteria were measured using Alamar blue assay.

During HIV-*M. avium* co-infection, the percent viability of intracellular bacilli (107.15±8.34 %viable at 24 hr) was observed to be significantly higher than *M. avium* mono-infection (82.20±8.39 %viable at 24 hr) (Figure 21A). Similarly, the percent viability of intracellular bacilli during HIV co-infection for *M. kansasii* (106.17±12.69 %viable at 24 hr) (Figure 21B) and *M. phlei,* (75.82±9.48 %viable at 24 hr) (Figure 21C) were significantly higher than respective mono-infections (*M. kansasii*: 81.09±13.97 %viable at 24 hr and *M. phlei*: 50.57±7.71 %viable at 24 hr) (Figure 21B and 21C). The %viability was normalized to 0 hr for the infection conditions (Figure 21).

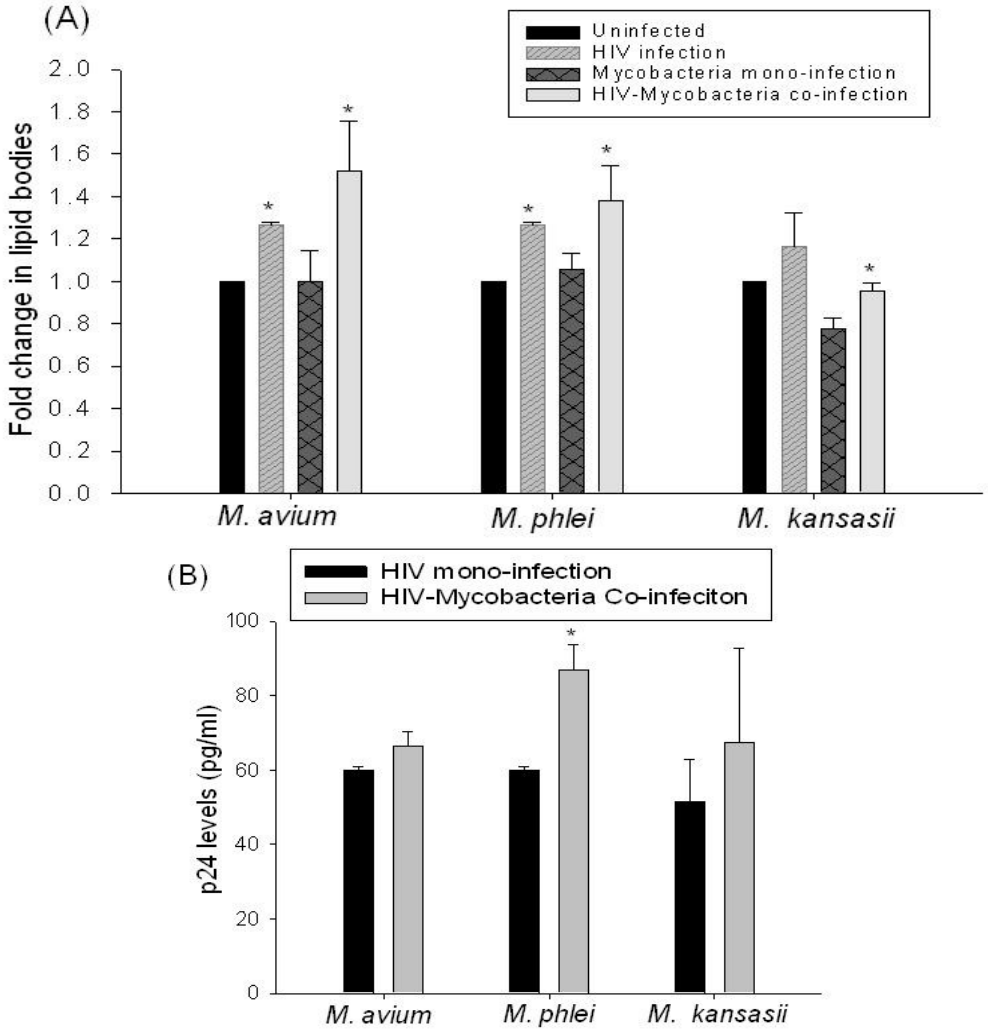

Figure 22: Co-infection by opportunistic mycobacteria increases HIV titers and accumulates lipids inside macrophages. *M. avium, M. kansasii* and *M. phlei* infections were carried out at an MOI=50 for 4 hrs. A) Oil red O staining of HIV- *M. avium*, HIV- *M. kansasii* and *M. phlei* co-infections. Bar graph representing the fold change in the accumulation of Oil red O stain as measured at Abs_{500nm}. Fold changes were calculated with respect to the values of respective mono-infections. B) HIV titers in the culture supernatants of HIV mono- and HIV- *M. avium*, HIV- *M. kansasii* and *M. phlei* co-infections at 24 hr post-infection as measured by p24 antigen capture ELISA. All the experiments were performed more than three times. Statistical analyses were done with Paired *t*-test. Error bars represent ±SD (Standard deviation). * represents $p<0.05$.

One of the parameters from the proteomics study, the lipid body accumulation, was then assessed for co-infections by these opportunistic mycobacteria. Similar to the HIV-BCG infections used for proteomics studies, THP-1 with HIV-*M. avium*; HIV-*M. kansasii* and HIV-*M. phlei* showed

increased accumulation of lipid body as compared to their respective mono-infections (Figure 22A). The lipid body accumulation in THP-1 as measured by Oil red O staining for each set of co-infection *vs* mono-infection were (i) HIV-*M. avium*: 1.52±0.24 fold, (ii) HIV-*M. kansasii*: 1.23±0.05 fold and (iii) HIV-*M. phlei*: 1.30±0.16 fold higher than their respective mono-infection (Figure 22A). Together with the HIV-BCG model, these results, thus, strengthen the notion that HIV infection assists the persistence of opportunistic infections by providing more conducive environment. It was also checked if these opportunistic mycobacteria influenced HIV titers during co-infection. It was observed that the co-infections by *M. avium*, *M. kansasii* and *M. phlei* increased the viral titers as compared to HIV mono-infection by 10.57 %, 30.76% and 44.85% respectively (Figure 22B). The viral titers in the culture supernatant as measured by p24 ELISA for each set of co-infection *vs* mono-infection experiments were (i) HIV-*M. avium*: 66.36±3.94 pg/mL and HIV: 60.02±1.05 pg/mL, (ii) HIV-*M. kansasii*: 67.29±25.60 pg/mL and HIV: 51.46±11.40 pg/mL and (iii) HIV- *M. phlei*: 86.93±6.70 pg/mL and HIV: 60.02±1.05 pg/mL (Figure 22B).

With these experiments, it was concluded that co-infection of HIV with opportunistic mycobacteria are mutually beneficial.

3.4 Summary:

While infection or resurgence of latent infection of pathogenic mycobacteria is common occurrence in HIV patients, infection by environmental mycobacteria is an emerging threat. The study showed that like the pathogenic mycobacteria, non-pathogenic and environmental mycobacterial stimulation of macrophages can promote HIV propagation. This is an important observation and requires to be reflected further as these infections can remain asymptomatic while silently promoting viral proliferation in a HIV patient.

Proteomics approach to catalog the changes in the host proteome helped us understand possible molecular mechanisms that explain how an opportunistic mycobacterial co-infection in HIV background mutually benefits both the pathogens. This also helped in establishing a culture based HIV-mycobacteria co-infection model that can be used for understanding various aspects of co-infection under laboratory conditions. Supported by experiments with clinically relevant opportunistic mycobacterial species, *M. avium*, *M. kansasii* and *M. phlei*, it was inferred that the early adaptation of non-pathogenic strains of mycobacteria in the activated host macrophages is supported by HIV through arresting phagosomal maturation, promoting accumulation of lipid bodies, increasing energy synthesis and cytoskeleton rearrangements. Upregulation of purinergic receptors during mycobacterial co-infection, in turn, is beneficial for HIV.

Apart from these principal mechanisms that were discussed above, the proteomic data also pointed out several interesting axes that can be deliberated to understand the synergistic impact of HIV and mycobacteria. Such as, Carnitine-O-palmitoyltransferase, that was absent in the fractions from BCG suggesting low levels of this enzyme during mono-infection. Carnitine deficiency promotes HIV propagation (De Simone, Famularo et al. 1994; Vilaseca, Artuch et al. 2003). Co-infection showed increased expression of peroxiredoxin proteins, which are known to quench the reactive oxygen species (ROS) (Tavender and Bulleid 2010) and thus, neutralize the microbicidal effects of ROS. The data also pointed towards the increased role of cytoskeletal proteins, as exemplified by Vimentin (substrate for HIV protease for nuclear entry) (Karczewski and Strebel 1996) and Septin7 (Signaling for autophagy) (Haglund and Welch 2011), and hence should not be overlooked owing to their ubiquitous nature.

Systematically pursuing such host-pathogen interactions at the molecular level would provide new insights into the mechanistic details of HIV-mycobacteria co-infection, helping decipher new intervention strategies and biomarker to overcome the synergism between HIV and mycobacteria.

Chapter 4

Intracellular mycobacterial proteome from HIV-*M. bovis* BCG co-infected macrophages

4.1 Introduction:

So far, proteomics of phagosome-enriched fractions were performed using the THP-1 based co-infection model (Chapter 2). Comparative proteomics of phagosome-enriched fractions from mycobacteria mono- and HIV-mycobacteria co-infected macrophages revealed that HIV altered the host macrophages environment providing conducive niche, in terms of altered phagosome maturation, lipid accumulation, increase in energy equivalents and purinergic receptors, which possibly helped mycobacterial infection and persistence. The same was validated by using clinically relevant opportunistc mycobacteria (Chapter 3).

The intraphagosomal mycobacterial proteomics from mycobacteria mono- and HIV-mycobacteria co-infected macrophages was studied next and is discussed in this chapter.

Mycobacteria reside inside the phagosomes of infected host macrophages. They adapt to the hostile intracellular conditions by concerted modulation of their protein expression and host signaling (Kaufmann and McMichael 2005). The adaptation of pathogenic mycobacterial proteome to the hostile intra-phagosomal environment has been studied using both transcriptomics and proteomics approaches (Li, Monahan et al. 2001; Monahan, Betts et al. 2001; Schnappinger, Ehrt et al. 2003; Mattow, Siejak et al. 2006; Rienksma, Suarez-Diez et al. 2015). These studies have been successful to a large extent in understanding the pathogenesis of TB bacteria. However, being restricted to mono-infection, these studies do not explain how a mycobacterium adapts to macrophages, where the cells have had a prior exposure to HIV. A population of monocytes/macrophages is colonized and used as reservoir by HIV during infection, but a large fraction of monocytes are also stimulated owing to immune environment generated by infected macrophages that makes them more aggressive phagocytes than usual (Mosser 2003; Carter and Ehrlich 2008; Guirado, Schlesinger et al. 2013; Tomlinson, Bell et al. 2014). In ideal conditions an activated macrophage, which is more aggressive in mounting both oxygen dependent and oxygen independent attacks, should be able to clear the non-pathogenic mycobacteria more efficiently than naïve macrophages, however, clinical reports state that these mycobacteria persist as opportunistic infections in HIV patients (Carpenter and Parks 1991; Shafer and Sierra 1992; Juffermans, Verbon et al. 1998; Karakousis, Moore et al. 2004; Saritsiri, Udomsantisook et al. 2006; Azzopardi, Bennett et al. 2009; Herzmann, Esser et al. 2011; Lan, Yang et al. 2011).

Mycobacteria, during co-infection, encounters altered, quite possibly, activated macrophages as the host is already infected with HIV-1 (Lawn, Butera et al. 2002) And so, looking at the changes in the early adaptive responses of mycobacteria for survival inside the phagosomes of infected macrophages during HIV-mycobacteria co-infections would help understand co-infection pathobiology. Earlier literature and also as discussed in chapter 3, mycobacteria co-infection increases HIV titers compared to mono-infection but it is not clear if mycobacterial factors or processes are directly or indirectly involved in increasing HIV titers during co-infection. In order to understand these two aspects of HIV-mycobacteria co-infection biology, proteomics approach was undertaken to understand the early adaptive changes in intraphagosomal mycobacterial protein during HIV-mycobacteria co-infection which is discussed in this chapter.

4.2 Materials and Methods:

Mycobacterium smegmatis mc^2155 strains used:

M. smegmatis harbouring pVV16	-	*M.smeg*-pVV16
M. smegmatis harbouring pVV- BCG3756c	-	*M.smeg*-pVV-BCG3756c
M. smegmatis harbouring pMV261	-	*M.smeg*-pMV261
M. smegmatis::Δ*IdeR*	-	*M.smeg*Δ*IdeR*
M. smegmatis::Δ*IdeR* harbouring pVV-IdeR	-	*M.smeg*Δ*IdeR*-pVV-IdeR
M. smegmatis::Δ*rip1*	-	*M.smeg*Δ*rip1*
M. smegmatis::Δ*rip1* harbouring pMV-rip1	-	*M.smeg*Δ*rip1*-pMV-rip1
M. smegmatis::Δ*pks*	-	*M.smeg*Δ*pks*
M. smegmatis::Δ*esx3*	-	*M.smeg*Δ*esx3*

The detailed protocol for Growth conditions of mycobacteria, Preparation and quantification of infectious HIV-1 (ADA8) particles, Infection of macrophages and phagosome isolation, CFU enumeration and intracellular bacilli viability measurement, Sample preparation and LC-MALDI-MS/MS Analyses, MALDI-TOF/TOF Analyses, Peptide Identification and Statistical Analyses have been described earlier in chapter 2 and chapter 3.

4.2.1 Intracellular Mycobacterial RNA isolation:

The monolayers of the infected cells after 24 hr were washed thrice with PBS. The cells were lysed in sterile water for 10 min at 37°C. The lysate was centrifuged at 1500rpm for 5 min to remove cell debris. The bacterium from the supernatant was pelleted at high speed (10000g) for 10 min and then the bacterial pellet was subjected to RNA isolation. The bacterial pellet was resuspended in Trizol and added to pre-chilled, acid washed 0.1 mm glass beads and lysed by bead beating - pulse on: 1 min and pulse off: 2 min on ice. Added glycogen to a final concentration of 200 µg/mL and kept at RT for 10 min. 1/10th volume of chloroform was added and vortexed vigorously for 15 sec and kept at RT for 10 min. Centrifuged at 12000 rpm for 15 min at 4°C and collected the upper aqueous layer. The RNA was precipitated using isopropanol in presence of glycogen (200 µg/mL) and pellet was washed with 75% ethanol. Air dried and resuspended in RNase free water. Prior to reverse transcription the RNA was subjected to DNase treatment to remove any residual DNA contamination. The DNase treated RNA was reverse transcribed using Superscript III

Reverse Transcriptase (Invitrogen) with random hexamers as primer. The reverse transcribed RNA was used for Real-time PCR.

4.2.2 Cloning and Expression of BCG3756c (VapC48) and IdeR gene into pVV16 shuttle vector:

The BCG3756c gene was PCR amplified from BCG genomic DNA and *IdeR* gene was PCR amplified from *M.tb* H37Rv genomic DNA (Annexure V). The mycobacterial shuttle vector, pVV16 (Stover, de la Cruz et al. 1991; Chatrath, Gupta et al. 2011), was amplified in *Escherichia coli* DH5α strain in Luria Bertani broth media with kanamycin at 100 µg/mL. The vector, BCG3756c and IdeR inserts were double digested with *NdeI* and *HindIII* (Fermentas, Thermo Fisher Scientific Inc., USA). The digested and insert and vector were ligated using T4 DNA ligase (Fermentas, Thermo Fisher Scientific Inc., USA) downstream of heat shock protein 60 (hsp60) promoter and transformed into *Escherichia coli* DH5α. The genes were cloned with C-terminus 6X Histidine tag. The recombinant plasmids carrying BCG3756c and IdeR were electroporated into *M. smegmatis* mc^2155 and *M. smegmatis::ΔIdeR,* respectively. The transformants were picked and grown in 7H9 broth media at 37°C and culture was harvested and lysed. Supernatant and cell pellet were separated and fractionated on SDS-PAGE followed by immunoblotting using anti-His antibody to confirm the expression of BCG3756c and IdeR. The growth curve for all the transformants was performed (Figure 23A and 23B).

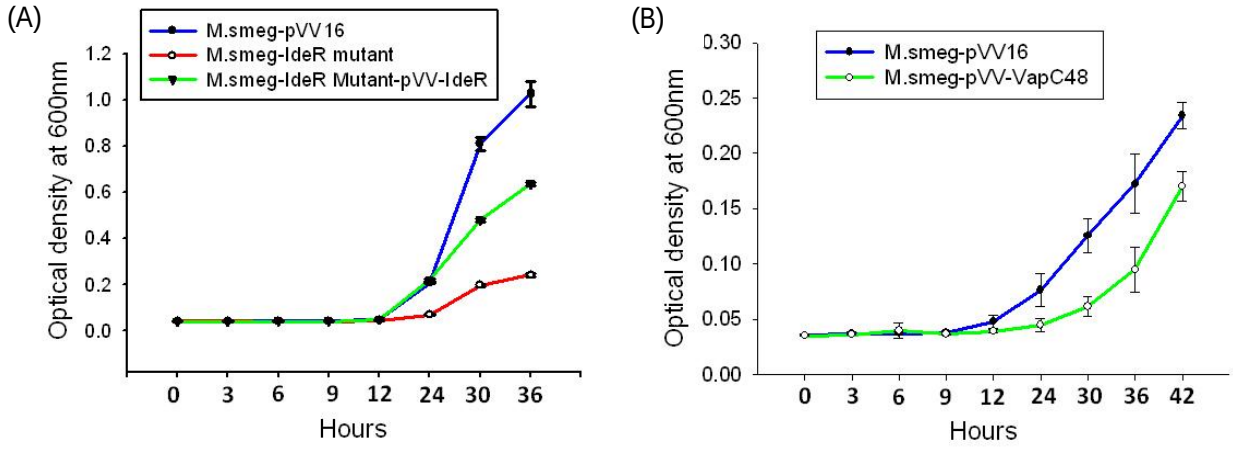

Figure 23: The growth curve of (A) *M.smegΔIdeR* along with the corresponding vector control and mutant complemented strain. (B) The growth curve of M.smeg-pVV-VapC48 along with the corresponding vector control.

4.2.3 Immunoblot:

The Mycobacterial cell lysates and supernatants were fractionated on 10% SDS-PAGE, transferred to Nitrocellulose membrane using GE-Amersham Western wet-transfer apparatus. The membrane was blocked with 5% non-fat milk powder in PBS with 0.1% Tween-20 at RT for 2 hrs. The primary antibody, Anti-His Tag mouse antibody (SantaCruz Biotechnology Inc., USA) was prepared in PBS-T (PBS+0.1% Tween-20) with 2% BSA 1:1000 dilutions, was added and incubated at 4^{o}C on platform rocker overnight. After 3 PBS-T washes, added the corresponding Anti-mouse HRP-conjugated secondary antibody (Santa cruz Biotechnology Inc., USA), diluted 1:2000 in PBS-T with 2% BSA, incubated at RT for 2 hr. After 3 washes with PBS, ECL substrate (Femtolucent Plus-HRP, chemiluminiscent reagent from G-biosciences, USA) was added to the membranes and was scanned for chemiluminiscence using Versadoc Imaging system (Biorad).

4.2.4 Real-time PCR:

Equal amount of RNA was considered for equal loading and the corresponding cDNA was used for RT-PCR. As endogenous controls, 16S rRNA gene was used (Annexure VI). The 2X SyBr green mix (Takara Bio Inc., Japan) was used. The real-time PCR data analyses were done using the $2^{-\Delta\Delta Ct}$ method with endogenous 16S rRNA gene as control.

4.2.5 Statistical Analyses:

All the experiments were performed at the least three times. The data were analysed using SigmaPlot software version 11.0.0.77 (Systat Software, Inc., USA). The error bars represent the standard deviation (SD) from the mean of at least three independent experiments. Statistical analyses of the experimental data for comparing two groups were performed by Student's *t*-test. $p<0.05$ was considered as significant. * represent $p<0.05$ and ** represents $p<0.001$.

4.3 Results and Discussion:

The perturbations in the macrophages upon HIV-mycobacteria co-infection and the supportive niche provided for mycobacteria by HIV were discussed in the chapter 3. In this chapter I sought to identify the early adaptive changes in the proteome of the intraphagosomal mycobacteria in the background of HIV infection concurrent to the host niche. High MOI of 100 was used to enrich mycobacteria laden phagosomes to identify the intraphagosomally expressed mycobacterial proteins.

4.3.1 Comparative Proteomes of intra-phagosomal mycobacteria from mono- and HIV co-infected THP-1 macrophages

To capture the early events, after 24 hr post-infection, phagosome-enriched fractions were isolated (to minimize the host background, from BCG mono- and HIV-BCG co-infected cells) and LC-MALDI-MS/MS of the fractions was performed. The results of proteomic data were from the three experiments of BCG mono-infected (n=3) fractions and four experiments of HIV-BCG co-infected (n=4) fractions. Proteins identified (95% confidence) from these experiments of a condition (mono- and co-infection) were pooled together into their respective categories. Then, the proteins identified in at the least two experiments per category were considered for further analyses. Overall, 92 differentially expressed proteins between BCG mono- and HIV-BCG co-infected fractions were identified (Annexure VII). Of these, 22 proteins overlapped, 30 and 40 proteins were exclusively present in BCG mono-infected and HIV-BCG co-infected fractions, respectively (Figure 24 and Annexure VII).

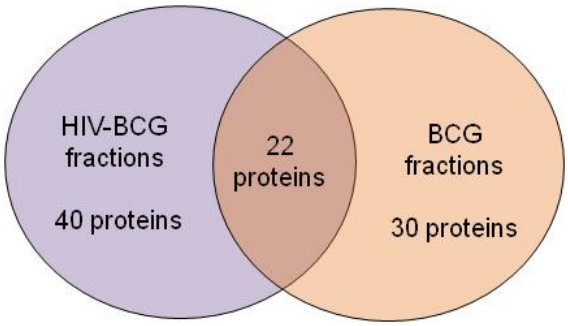

Figure 24: Distribution of mycobacterial proteins as identified by LC-MALDI-MS/MS from the phagosome enriched fractions of BCG mono- and HIV-BCG co-infected cells. Venn diagram representing the distribution of identified mycobacterial proteins between mono- and co-infections. Out of the 92 proteins, 30 (32.60%) were exclusive to mono-infected phagosomal

fractions, 40 (43.48%) to co-infected phagosomal fractions and 22 (23.91%) proteins show overlap in fractions from both the conditions.

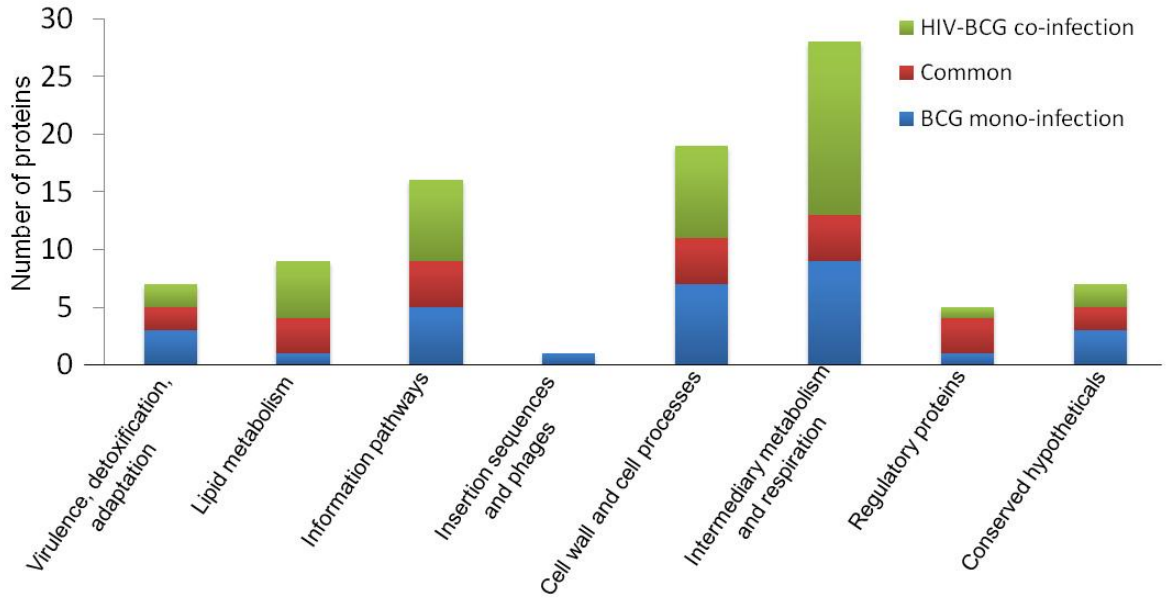

Figure 25: Distribution and functional categorization of mycobacterial proteins as identified by LC-MALDI-MS/MS from the phagosome enriched fractions of BCG mono- and HIV-BCG co-infected cells. Graph represents the distribution of proteins with respect to the functional categories between mono- and co-infections.

Proteins exclusively present in one condition but absent in the other condition were considered for further analyses. The proteins were categorized into different functional categories as described in *Tuberculist* (Lew, Kapopoulou et al. 2011) database (Figure 25). The proteins belonging to two major groups, that is, lipid metabolism and intermediary metabolism and respiration, were upregulated during co-infection. The other group that was categorically enriched during co-infection was information pathways.

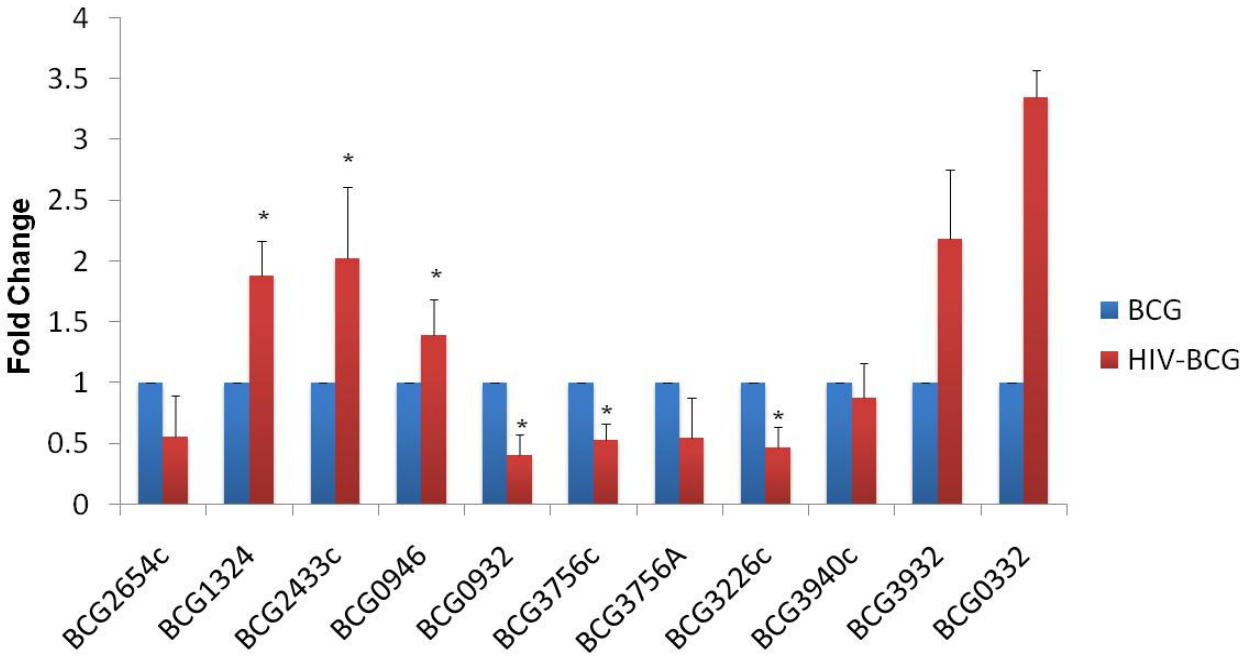

Figure 26: Real-time PCR of mycobacterial (BCG) genes reiterates the proteomic data. qRT-PCR was performed using the RNA isolated from intracellular BCG. The transcript levels were quantified by relative $2^{-\Delta\Delta Ct}$ method with endogenous 16S rRNA gene as control. Fold changes in transcript levels were normalized to mono-infection. All the experiments were performed more than three times. For genes, BCG3932, BCG0332 and BCG3940c data is representative of two experiments. Statistical analyses were done with Student's *t*-test. Error bars represent ±SD (Standard deviation). * represents $p<0.05$.

The proteomic data were further validated by Real-Time PCR of 10 randomly picked mycobacterial genes using the RNA isolated from the intraphagosomal BCG during BCG mono- and HIV-BCG co-infection (Figure 26). The Real-Time PCR results reiterated the proteomic data, where BCG0946 and BCG3940c were common for both mono- and co-infections, BCG2654c, BCG0932, BCG3756c and BCG3226c were observed up regulated in mono-infection and BCG3932, BCG0332 and BCG2433c were observed up regulated only in co-infection. The functional category analyses also revealed down-regulation of toxin-antitoxin (TA) modules, up-regulation of cation transporters, Type VII (Esx) secretion systems, proteins involved in cell wall lipid or protein metabolism, glyoxalate pathway and branched chain amino-acid synthesis during co-infection. Some of these important observations are discussed below. These observations are supported by co-infection studies with the knock-out/over-expression mutants of *M. smegmatis* to understand the synergistic impact of factors from mycobacteria on HIV propagation during co-infection.

4.3.2 Reduced expression of Toxin-Antitoxin systems in mycobacteria during co-infection

During mono-infection, expression of proteins belonging to Virulence-detoxification-adaptation category such as BCG3756c (VapC48) and BCG3477 (VapB47) were upregulated. BCG3756c (toxin) and BCG3477 (anti-toxin) belong to Toxin-Antitoxin (TA) family of proteins (Lew, Kapopoulou et al. 2011). Toxin-Antitoxin systems are expressed during stress and help in the viability of the bacteria by allowing the expression of stress responsive genes (Ramage, Connolly et al. 2009). The upregulation of BCG3756c during mono-infection was validated by qRT-PCR (Figure 26). As BCG3756c was over-expressed during BCG mono-infection, so expected that it may play a role in intracellular survival of mycobacteria. BCG3756c gene was expressed with N-terminus 6×His-tag in *M. smegmatis*, that does not have an ortholog of BCG3756c, using a mycobacterial shuttle vector, pVV16 (Figure 27A). The recombinant *M. smegmatis*-pVV-BCG3756c was used for mono- and HIV co-infections and scored for CFU by plating on 7H10 agar plates after 0, 6 and 24 hr post-infection. Accordingly, the recombinant strain survived better over time, 6 hr to 24 hr, inside macrophages as compared to *M. smegmatis*-pVV16 both during mono- and co-infection. The recombinant strain *M. smegmatis*-pVV-BCG3756c (6 hr: 1 cfu units; 24 hr: 0.97±0.45 cfu units) was cleared by 3% from 6 hr to 24 hr (Figure 27B) whereas the vector control, *M. smegmatis*-pVV16 (6 hr: 1 cfu units; 24 hr: 0.55±0.27 cfu units; $p<0.05$) was cleared by 45% from 6 hr to 24 hr time point during mono-infections (Figure 27B). During co-infection, *M. smegmatis*-pVV-BCG3756c (6 hr: 1 cfu units; 24 hr: 1.46±0.32 cfu units) was not cleared efficiently from 6 hr to 24 hr (Figure 27B) whereas *M. smegmatis*-pVV16 (6 hr: 1 cfu units; 24 hr: 0.52±0.03 cfu units; $p<0.05$) was cleared by 48% from 6 hr to 24 hr time point. The cfu units were normalized to that of 0 hr. Evident from these results, over-expression of BCG3756c, irrespective of mono- or co-infections, helped in the survival of mycobacteria.

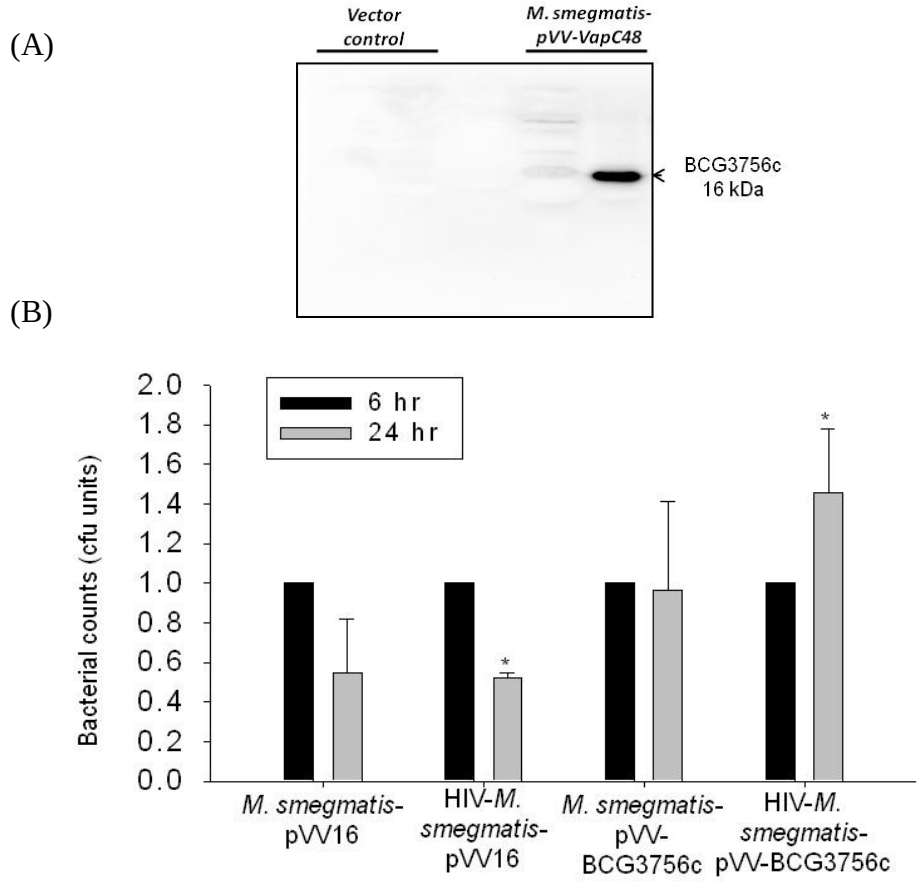

Figure 27: Expression of BCG3756c in *M. smegmatis* helps its persistence. (A) Western blot using anti-His antibody confirming the expression His-tagged BCG3756c in *M. smegmatis*. Lanes: 1-Vector control supernatant; 2-Vector control cell pellet; 3-pVV16-BCG3756c supernatant; 4-pVV16-BCG3756c cell pellet. (B) Plot representing *M. smegmatis*-pVV16 and *M. smegmatis*-pVV-BCG3756c persistence inside macrophages upon mono- and co-infections in cfu units at 0, 6 and 24 hr post *M. smegmatis* infection. cfu units = Fold change in CFU with respect to CFU of mono-infection. The cfu units were normalized to that of 0 hr. All the experiments were performed more than three times. Statistical analyses were done using Student's *t* test. Error bars represent ±SD (Standard deviation). * represents $p<0.05$.

Since BCG3756c was down-regulated during co-infection as per the proteomics data the impact of over-expression of this protein on HIV titers during co-infection was scored. It was observed that the co-infection with the Vector control increased the p24 equivalents of viral titers (HIV-*M. smegmatis*-pVV16: 14.36±0.36 pg/mL; $p<0.05$) compared to HIV infection (HIV: 8.21±0.91 pg/mL) alone (Figure 28), but co-infection with the recombinant strain failed to provide such

support to viral propagation (HIV-*M. smegmatis*-pVV-BCG3756c: 8.63±2.12 pg/mL) as compared to HIV infection (HIV: 8.21±0.91 pg/mL) (Figure 28).

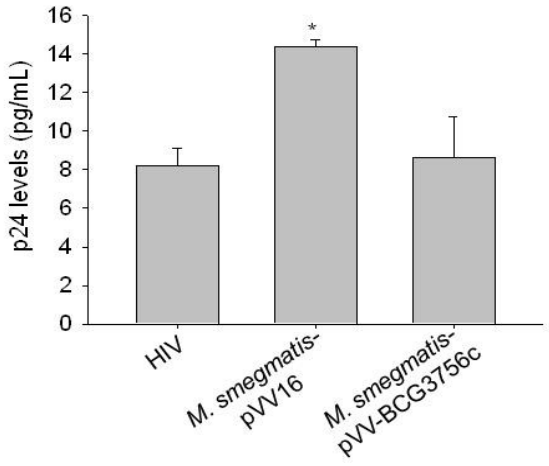

Figure 28: Expression of BCG3756c in *M. smegmatis* helps its persistence without affecting the HIV titers. Bar graph represents HIV p24 titers in the supernatants of HIV mono-, HIV-*M. smegmatis*-pVV16 and HIV-*M. smegmatis*-pVV-BCG3756c co-infected macrophages at 24 hr post infection. All the experiments were performed more than three times. Statistical analyses were done using Student's *t* test. Error bars represent ±SD (Standard deviation). * represents $p<0.05$.

VapBC TA systems are considered as stress responsive elements which help the bacteria persist during stress probably by decreasing the metabolic activity and activating the required pathways. This function is probably carried out by its annotated ribonuclease activity on mRNAs and thus inhibiting the translation of avoidable proteins during stress (Ramage, Connolly et al. 2009). During this process it is possible that toxin also inhibits the factors which can influence the viral titers. Therefore, expression of proteins belonging to TA systems helps in the persistence of mycobacteria upon infection but probably has no impact on HIV propagation during co-infection. This explained the down-regulation of this factor in the proteomics data during co-infection.

4.3.3 Mycobacterial iron dependent transcription regulator (IdeR) promoted viral titers during co-infection

Amongst the identified mycobacterial proteins upregulated during co-infection, BCG0332 (52% similar to MSMEG_0626), BCG1633 (76.5% similar to MSMEG_3200), BCG2957 (52% similar

to MSMEG_0408), BCG2636c (78.5% similar to MSMEG_3200), BCG2962 (75% similar to MSMEG_4727) belonged to IdeR regulon (Annexure VII) (Rodriguez, Voskuil et al. 2002). IdeR (91% similar to MSMEG_2750) is a global iron dependent transcriptional factor that regulates the expression of several critical proteins in mycobacteria (Rodriguez, Voskuil et al. 2002). Hence, using the mutant, *M. smegmatis* (*M.smegΔideR*) and complemented strain (*M.smegΔideR*-pVV-IdeR) (Dussurget, Rodriguez et al. 1996), the effect on mycobacterial survival and HIV titers during co-infection was determined. IdeR complemented strain was prepared by expressing the IdeR gene cloned into pVV16 shuttle vector in the mutant, *M.smegΔideR* (Figure 29).

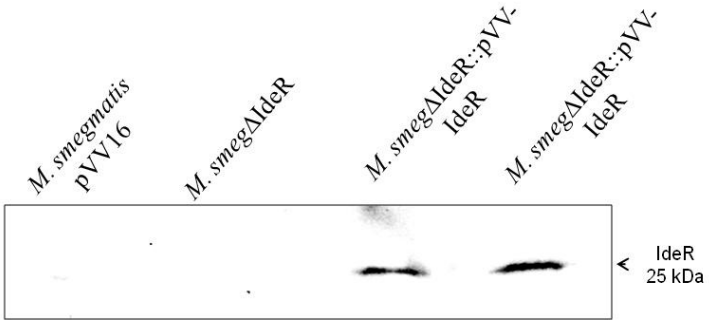

Figure 29: Western blot using anti-His antibody confirming the expression His-tagged IdeR in *M. smegmatis*. Lanes: Cell lysates of 1-Vector control *M. smegmatis*-pVV16; 2-*M.smegΔIdeR*; 3-protein marker; 4 and 5-*M.smegΔIdeR*-pVV-IdeR.

HIV co-infection helped in the survival of the wildtype mycobacteria (*M. smegmatis*-pVV16) as observed in terms of cfu units (*M. smegmatis*-pVV16 mono-infection: 1 cfu units; co-infection: 1.89±0.29 cfu units) (Figure 30A); however HIV co-infection could not support the survival of the IdeR mutant *M.smegΔideR* (Figure 30B), which was rescued in the complement strain *M.smegΔideR*-pVV-IdeR (Figure 30C), suggesting that IdeR is essential for HIV-supported survival of mycobacteria. The respective cfu units were normalized to cfu units at 0 hr, are *M.smegΔideR* mono-infection: 1 cfu units; co-infection: 0.41±0.08 cfu units and *M.smegΔideR*-pVV-IdeR mono-infection: 1 cfu units; co-infection: 4.40±0.93 cfu units) (Figure 30B and 30C).

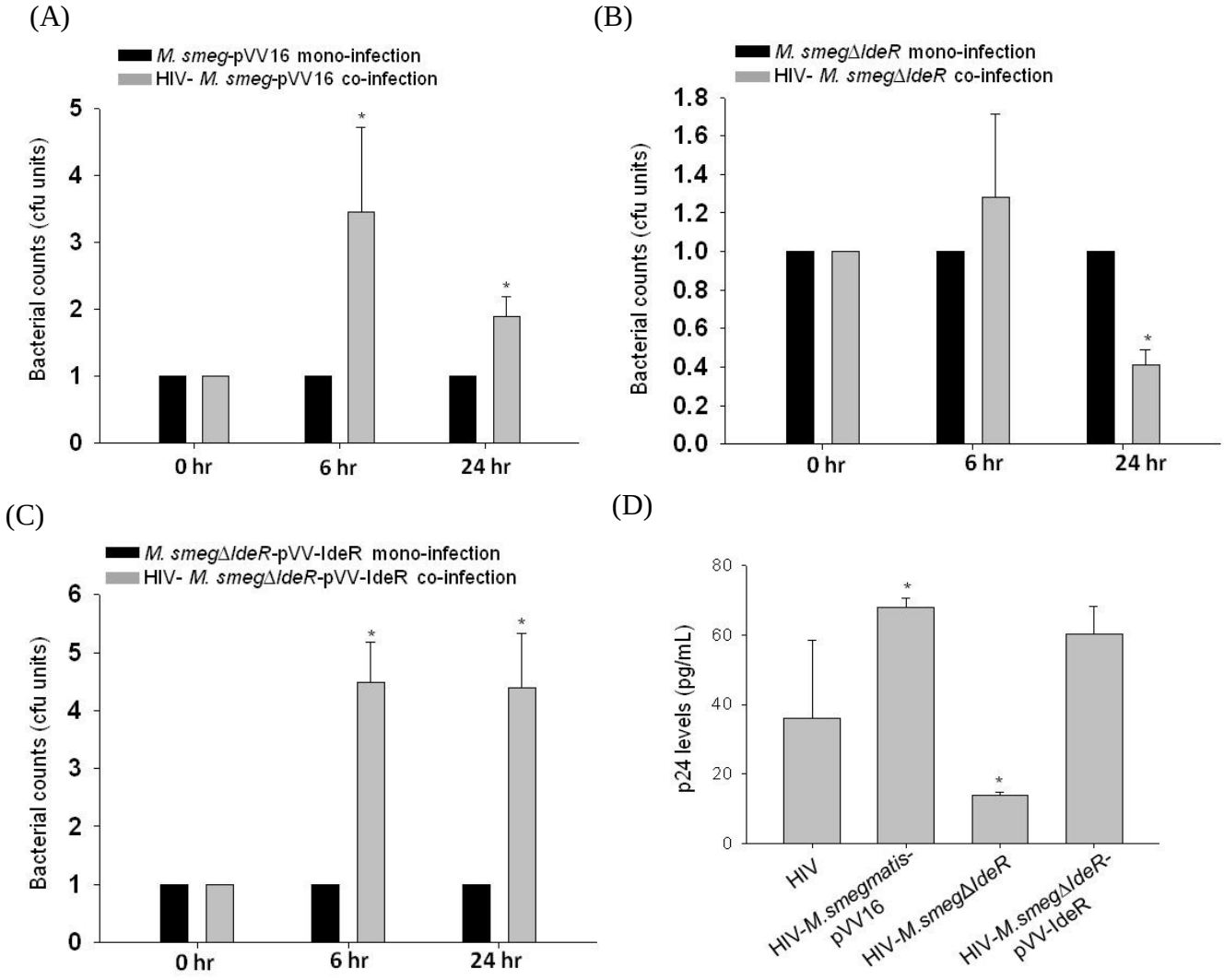

Figure 30: IdeR or IdeR dependent proteins help mycobacterial persistence during co-infection. (A) Plot representing (A)*M.smeg*-pVV16, (B) *M.smeg*Δ*IdeR* and (C) *M.smeg*Δ*IdeR*-pVV-IdeR persistence inside macrophages upon mono- and co-infections in cfu units (cfu units = %CFU of mono-infection/%CFU of co-infection) at 0, 6 and 24 hr post *M. smegmatis* infection. The CFU counts were normalized to 0 hr time point; (D) Bar graph represents HIV p24 titers in the supernatants of HIV mono-, HIV-*M.smeg*-pVV16, HIV-*M. smeg*Δ*IdeR* and HIV-*M. smeg*Δ*IdeR*-pVV-IdeR co-infected macrophages at 24 hr post infection. All the experiments were performed more than three times. Statistical analyses were done using Student's *t* test. Error bars represent ±SD (Standard deviation). * represents $p<0.05$.

Then, the p24 equivalent of viral titers was compared during co-infection using all the three strains, *viz*; with the vector control, HIV-*M. smegmatis*-pVV16 (HIV: 35.97±22.55 pg/mL; HIV-*M. smegmatis*-pVV16: 67.80±2.94 pg/mL; $p<0.05$), with the mutant, HIV-*M.smegΔideR* (HIV-

M.smegΔideR: 13.76±1.10 pg/mL; $p<0.05$) and with the complemented strain, HIV-*M.smegΔideR*-pVV-IdeR (HIV-*M.smegΔideR*-pVV-IdeR: 60.37±7.99 pg/mL) (Figure 30D). It was observed that the co-infection with the mutant strain decreased virus production as compared to the wild type. This decreased viral titers were restored upon complementation in the mutant (HIV: 35.97±22.55 pg/mL; HIV-*M.smegΔideR*-pVV-IdeR: 60.37±7.99 pg/mL) (Figure 30D). The defects in the survival of the IdeR mutant and the drastic decrease in the HIV p24 titers during co-infection compared to HIV mono-infection or HIV-*M.smeg*-pVV16 co-infection suggested that IdeR is essential for mycobacterial survival and also involved in the increase of viral titers during co-infection. This could be a direct effect of IdeR or by the proteins belonging to IdeR regulon. BCG2957 and BCG2636c are involved in the synthesis of cell wall lipids, phosphatidylinositol mannoside and lipoarabinomannans, respectively (Kordulakova, Gilleron et al. 2003; Daniel, Deb et al. 2004; Jain and Cox 2005). The alterations in the composition of mycobacterial cell wall lipids could alter the stimulation of the macrophages and thereby macrophage responses, which in turn can influence HIV propagation in a host (Ranjbar, Boshoff et al. 2009).

4.3.4 Alterations in the mycobacterial cell wall and lipid metabolism influence viral production and mycobacterial survival during co-infection

Mycobacterium relies on fatty acids as a source of energy and probably synthesizes triacylglycerols as energy reserves during infections for long-term sustenance inside the host (Russell 2003; Sirakova, Dubey et al. 2006). BCG proteome showed that expression of proteins that are involved in synthesis of Phthiocerol Dimycocerosates (PDIMs) during both mono- and co-infection conditions. PDIMs are key components of cell wall determining the virulence of mycobacteria (Goren, Brokl et al. 1974). These proteins included Long-chain-fatty-acid-CoA ligase FadD15/BCG2202, Mycocerosic acid synthase (BCG2962c), Phenolpthiocerol synthesis polyketide synthase PpsA/BCG2953 and probable enoyl-CoA hydratase echA6/BCG0957. However, Phenolpthiocerol synthesis polyketide synthase type I PpsE/BCG2957 (involved in the synthesis and translocation of PDIM to cell wall surface), Phosphatidylinositol mannoside acyltransferase/BCG2636c (involved in the synthesis of lipomannans and lipoarabinomannans) and Putative diacyglycerol O-acyltransferase/BCG3443 (involved in the synthesis of triacylglycerols) (Kordulakova, Gilleron et al. 2003; Daniel, Deb et al. 2004; Jain and Cox 2005) were upregulated during co-infection. A putative zinc metalloprotease (Rip1/BCG2891c), a

protein known to regulate the cell envelope lipid composition important for the virulence of mycobacterium (Makinoshima and Glickman 2005) was over-expressed during HIV-BCG co-infection. Rip1 was also shown to positively regulate transcription of other proteins BCG2962c and BCG2953 (Sklar, Makinoshima et al. 2010), which concurrently appeared in the proteomics data (Annexure VII). Together the over-expression of BCG2891c, BCG2962c and BCG2953 can regulate the composition of cell wall affecting the virulence of the mycobacterium.

The significance of the over-expression of mycobacterial proteins involved in the cell wall and lipid metabolism in the context of co-infection was studied next using *knock-out* (KO) mutants of *M. smegmatis* for the proteins, Rip1/MSMEG_2579 (81% similar to BCG2891c) and Polyketide synthase (Pks) (52% similar to BCG2957). As these proteins were over-expressed during co-infection, it was speculated that they may influence both mycobacterial survival and HIV titers during co-infection. The Pks was selected as it is reported to be involved in the synthesis of surface glycopeptidolipid (GPL) of mycobacteria (Vats, Singh et al. 2012). THP-1 cells were either infected with mutants *M. smegmatis*::*Δrip1* (*M.smegΔrip1*)/ *M. smegmatis*::Δ*pks* (*M.smeg*Δ*pks*) (Vats, Singh et al. 2012; Schneider, Sklar et al. 2014) alone or in the presence of HIV. As compared to mono-infection by vector control (*M.smeg*-pMV261), rip1 mutant (*M.smegΔrip1*) or the complemented strain (*M.smegΔrip1*-pMV-*rip1*), all the strains demonstrated increased survival upon co-infection with HIV (Figure 31A, 31B and 31C). The comparative % viability upon mono- and co-infections at 24 hr post mycobacterial infection are: *M.smeg*-pMV261: 78.10±3.24 % while HIV-*M.smeg*-pMV261: 91.14±4.96 % (Figure 31A); *M.smegΔrip1*: 53.77±6.69% while HIV-*M.smegΔrip1*: 72.48±10.80 % (Figure 31B) and *M.smegΔrip1*-pMV-*rip1*: 64.98±2.95 % while HIV- *M.smegΔrip1*-pMV-*rip1*: 78.47±3.20 % (Figure 31C).With this one can infer, that HIV background helped the survival of all the strains of mycobacteria, while deletion of *rip1* had no impact on survival. However, HIV-*M.smegΔrip1* co-infection showed significantly ($p<0.05$) lesser p24 levels (6.35±0.18pg/mL) compared to HIV mono-infection (8.01±0.57 pg/mL) and HIV-*M.smeg*-pMV261co-infection (14.07±2.65pg/mL) (Figure 31D). The expression of Rip1 in *trans* in the mutant (*M.smegΔrip1*-pMV-*rip1*) restored the HIV titers equivalent to the co-infection with the vector control (13.38±2.74 pg/mL) (Figure 31D). These experiments indicated that directly or indirectly, mycobacterial factor Rip1 definitely augmented HIV production during co-infection.

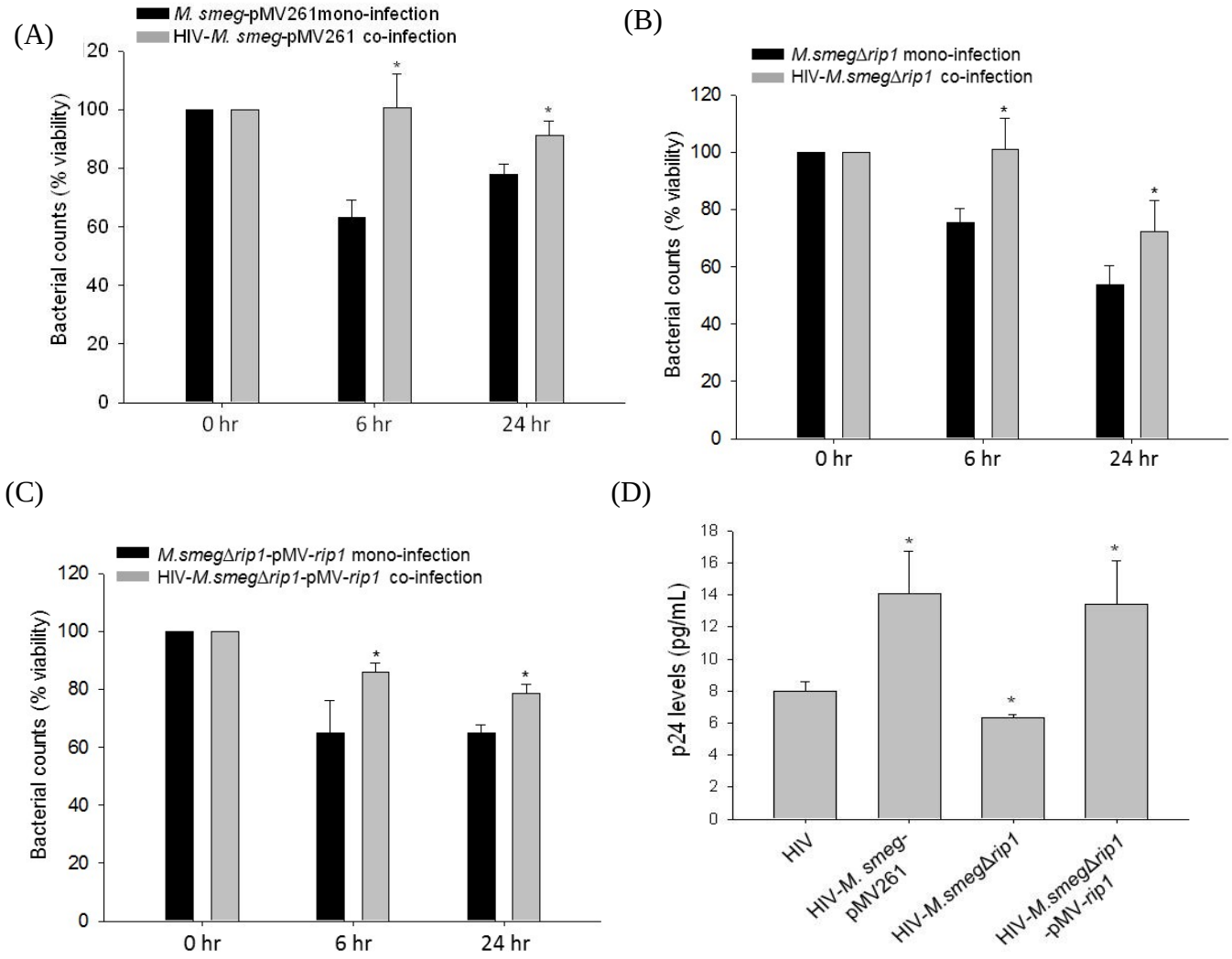

Figure 31: Mycobacterial Rip1 protein impacts the viral titers during co-infection. Plot representing (A) *M.smeg*-pMV261, (B) *M.smegΔrip1* and (C) *M.smegΔrip1*-pMV-*rip1*persistence inside macrophages upon mono- and co-infections in % viability (refer experimental procedures) at 0, 6 and 24 hr post *M. smegmatis* infection; (D) Bar graph represents HIV p24 titers in the supernatants of HIV mono-, HIV-*M.smeg*-pMV261, HIV-*M.smegΔrip1* and HIV-*M.smegΔrip1*-pMV-*rip1* co-infected macrophages at 24 hr post infection. All the experiments were performed more than three times. Statistical analyses were done using Student's *t* test. Error bars represent ±SD (Standard deviation). * represents $p<0.05$.

The Pks protein, involved in the synthesis of cell wall glycopeptidolipid, is a large multi-functional protein corresponding to 390 kDa with 11 active functional domains. The *M. smegmatis* pks mutant (*M.smegΔpks*) was used to score for the CFU and the impact on the viral titers. Cfu units of intracellular *M.smegΔpks* showed defect in survival during co-infection (0.64±0.45 cfu units at

24 hr) and mono-infection (1 cfu units at 24 hr) suggesting that it is required for the intracellular survival during co-infection (Figure 32A). Similarly, HIV-Δ*pks* (12.24±1.25 pg/mL) co-infection showed significantly ($p<0.001$) lesser p24 levels compared to both HIV mono-infection (17.94±2.22 pg/mL) and HIV-*wtM.smeg* co-infection (30.11±1.87 pg/mL) (Figure 32B). Due to the large size (390 kDa) of the Pks protein making a complement of the mutant was difficult. But, however, owing to the multi-functional domain structure of the Pks protein, it would be interesting to investigate the above impact on the viral titers by *M.smeg*Δ*pks* is due to the intact multi-functional Pks protein or due to individual domains, which is part of future investigations in the laboratory. One can thus infer that mycobacterial protein Pks supported both the survival of mycobacteria and viral titers during co-infection.

With this, one may hypothesize that the differences in the cell envelope proteins or lipid composition of mycobacteria modulate host cell response, increasing viral propagation during co-infection. This corroborates the earlier findings that the HIV propagation is differentially regulated by mycobacteria in a strain-dependent manner which was attributed to the differences in the cell wall composition (Ranjbar, Boshoff et al. 2009).

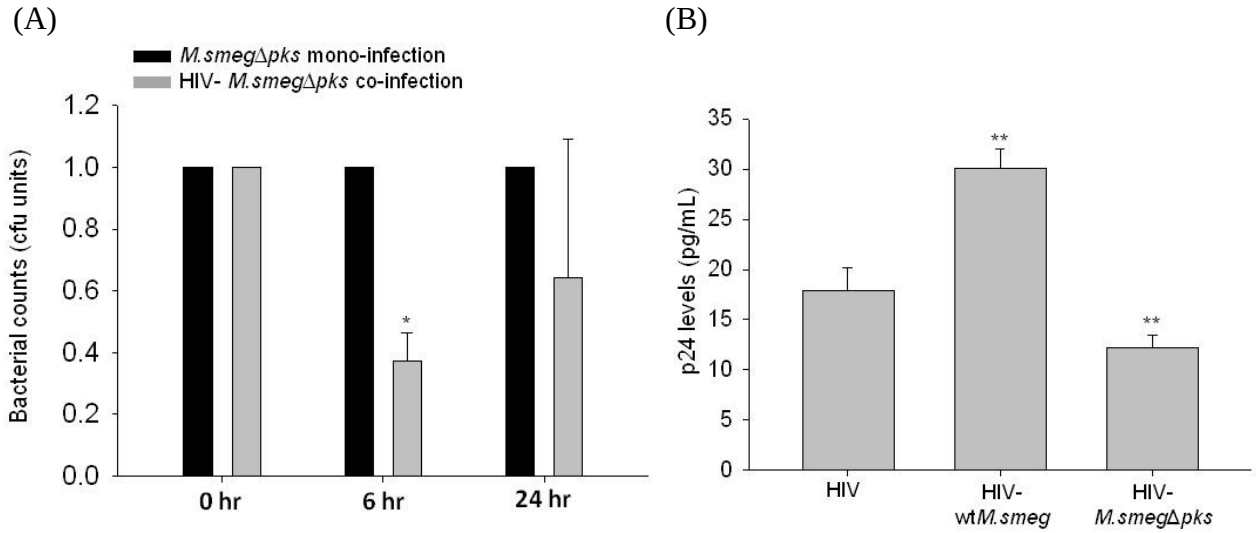

Figure 32: Validation of the inferences from the proteomics data using *M. smegmatis knock-out* (KO) mutant. The cells were infected with either *wtM. smegmatis* or *M. smegmatis::*Δ*pks* mutant for mono-infections and along with HIV for co-infection. (A) *M.smeg*Δ*pks* mono- or co-infected cells were lysed at 0, 6 and 24 hr post *M. smegmatis* infection and plated on 7H10 agar plates for CFU counts for scoring survival of mycobacterial strains, represented as bar plots. (B) HIV titers from the culture supernatants were measured as p24 equivalent by antigen capture ELISA and represented as bar graph. All the experiments were performed more than three times. Statistical

analyses were done using Student's *t* test. Error bars represent ±SD (Standard deviation). ** represents $p<0.001$.

4.3.5 Increased expression of Esx system and cation transporter proteins in mycobacteria during co-infection and impact on viral titers

Increased expression of components of Esx system (EccE3/BCG0332 and EccC5/BCG1816) along with cation transporter proteins (MntH/BCG0976c and BCG3299) was observed during co-infection as compared to mycobacterial mono-infection. Esx systems are Type VII secretion systems of mycobacteria and are implicated in both *in vitro* and intracellular survival (Feltcher, Gibbons et al. 2013). BCG0332 (EccE3) (52% similar to MSMEG_0626), a component of Esx-3 system, confirmed by qRT-PCR (Figure 26) was upregulated by 3.35±0.221 folds during co-infection. Esx-3 system has been reported to be essential for *in vitro* growth (Sassetti, Boyd et al. 2003) and sensed iron and zinc availability (Serafini, Pisu et al. 2013) in pathogenic mycobacteria. It may be speculated that the Esx-3 secretion system may indirectly be involved in iron and zinc acquisition for survival inside macrophages where these ions are limiting. This speculation was further strengthened by the concomitant increased expression of cation transporters, MntH (orthologue of eukaryotic Nramp) (Agranoff, Monahan et al. 1999; Papp-Wallace and Maguire 2006) and BCG3299 (probable cation transporter P type ATPase C) (Novoa-Aponte, Leon-Torres et al. 2012) during co-infection. Similarly, EccC5/ BCG1816, an Esx-5 system protein was present during co-infection. Esx-5 system, in pathogenic mycobacteria, has been implicated in the secretion of PPE proteins, maintenance of cell wall integrity and modulation of macrophage response (Abdallah, Savage et al. 2008; Bottai, Di Luca et al. 2012) and helps the survival of intracellular mycobacteria.

To understand the significance of these observations in the context of HIV-mycobacteria co-infection, Esx-3 as representative system was used and studied the *M. smegmatis esx3* deletion mutant (*M.smegΔesx3*) where the whole cassette of *esx-3* system was disrupted (Siegrist, Unnikrishnan et al. 2009). It was hypothesized that Esx-3 system, whose component protein (EccE3/BCG0332) was over-expressed selectively during HIV-mycobacteria co-infections may play a role not only in the intracellular survival of the attenuated mycobacteria, but also in inducing HIV production. THP-1 cells were either infected with *M.smegΔesx3* alone or co-infected with HIV. The cells were lysed after 0, 6 and 24 hr of *M.smegΔesx3* infection and plated onto 7H10

agar plates and CFU were counted. The cfu units were observed to be nearly similar for both *M.smegΔesx3* infection (1.00 cfu units at 24 hr) and HIV-*M.smegΔesx3* co-infection (0.76±0.05 cfu units at 24 hr) (Figure 33A). With these observations, it can be deduced that Esx-3 system may provide additional survival advantage to mycobacteria during co-infection. When HIV titers in the culture supernatants were compared between HIV-*wtM.smeg* co-infection and HIV-*M.smegΔesx3* co-infection, it was observed that deletion of *esx-3* reduced the mycobacterial induced increase in HIV titers by more than 50%. The viral titers in the culture supernatant for HIV mono-infection was 17.94±2.22 pg/mL, which significantly increased in HIV-*wtM.smeg* co-infection to 30.11±1.87 pg/mL, but HIV-*M.smegΔesx3* co-infection showed only 12.79±1.69 pg/mL of viral titers (Figure 33B). This provided an experimental evidence of factors (here, Esx 3 system) from mycobacteria involved in promotion of HIV propagation, explaining the alliance between HIV and mycobacteria.

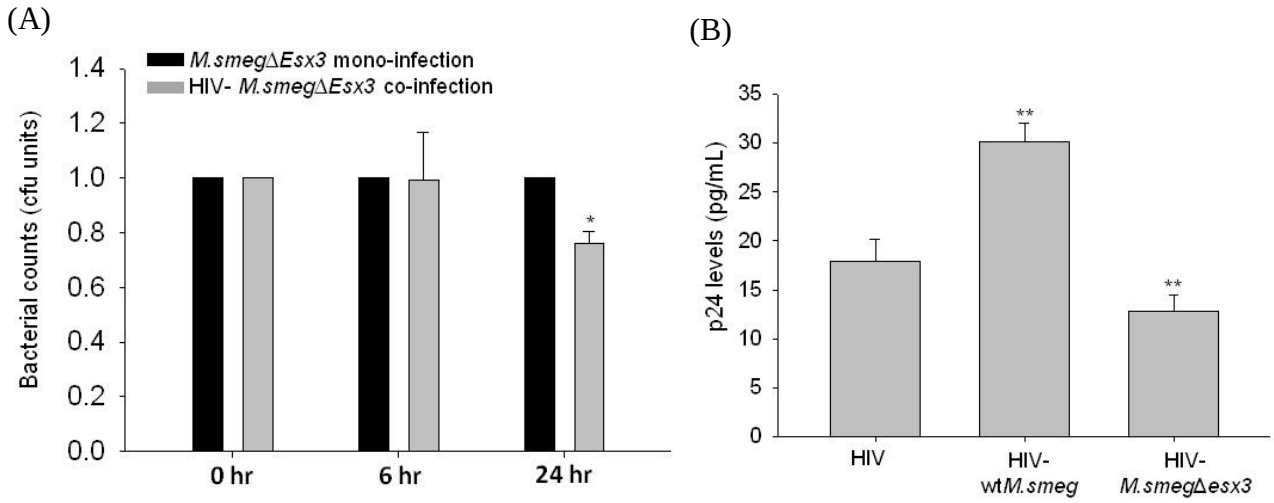

Figure 33: Validation of the inferences from the proteomics data using *M. smegmatis knock-out* (KO) mutant. The cells were infected with either *wtM. smegmatis* or *M. smegmatis::Δesx3* for mono-infections and along with HIV for co-infection. (A) *M.smegΔesx3* mono- or co-infected cells were lysed at 0, 6 and 24 hr post *M. smegmatis* infection and plated on 7H10 agar plates for CFU counts for scoring survival of mycobacterial strains, represented as bar plots. (B) HIV titers from the culture supernatants were measured as p24 equivalent by antigen capture ELISA and represented as bar graphs accordingly. All the experiments were performed more than three times. Statistical analyses were done using Student's t test. Error bars represent ±SD (Standard deviation). ** represents $p<0.001$.

A challenging but interesting quest would be to characterize the secretome of opportunistic mycobacteria either alone or in tandem with HIV co-infection, to identify the mycobacterial factors that make the macrophage environment more conducive, making these factors attractive for anti-mycobacterial drug targeting.

4.3.6 Heightened Intermediary metabolism and respiration in BCG *during co-infection to support intracellular survival*

Proteins belonging to intermediary metabolism and respiration category such as Malate synthase G (BCG1872c), Isopropylmalate synthase (BCG3770), Acetolactate synthase (BCG3025c and BCG1855), L-Aspartate oxidase (BCG1633), Glycerol-3-phosphate dehydrogenase (BCG3331c), pyruvate kinase (BCG1655) and probable L-lysine-epsilon-aminotransferase (BCG3319c and BCG3354c) were upregulated in the phagosomal fraction of co-infected cells. Malate synthase along with isocitrate lyase are the unique enzymes of glyoxylate shunt pathway. Earlier reports suggested that the glyoxylate shunt pathway is up regulated in pathogenic mycobacteria during the persistent phase *in vivo* and is important for the virulence (Sturgill-Koszycki, Haddix et al. 1997; McKinney, Honer zu Bentrup et al. 2000; Hou, Graham et al. 2002). Glyoxylate pathway utilizes the C2 substrates from fatty acids, which are abundantly found in mammalian cells, without generating carbon dioxide and help in the persistence of mycobacteria during nutrient stress (McKinney, Honer zu Bentrup et al. 2000). This was consistent with the observation (discussed in chapter 3) of increased lipid body accumulation in host during co-infection (Ganji, Dhali et al. 2015) and mycobacteria adaptation to the host niche by concomitant expression of malate synthase. Isopropylmalate synthase and Acetolactate synthase, which were upregulated during co-infection, are involved in the synthesis of branched chain amino acids, Leucine, Isoleucine and Valine which may provide survival advantage during co-infection (McAdam, Weisbrod et al. 1995; Bange, Brown et al. 1996). Glycerol-3-phosphate dehydrogenase and pyruvate kinase help bacteria utilize glycerol as carbon source (Ramakrishnan, Murthy et al. 1972). L-Aspartate oxidase (involved in the biosynthesis of NAD+) (Foster and Moat 1980) was expressed more during co-infection. NAD+ plays an essential role in cellular metabolism, given its involvement in almost all metabolic pathways; hence, biosynthesis of NAD+ can be used as a potential target against

pathogenic bacteria (Jang, Stella et al. 2010). Over-expression of these enzymes during co-infection may be supporting the survival of mycobacteria under co-infection conditions.

The above results clearly demonstrated that intra-phagosomal mycobacteria indeed adapted differently during mono- and co-infection and while adapting to the HIV induced-conducive intracellular niche of co-infected cells for persistence, the mycobacterial factors, possibly through influencing host responses, also influence the viral propagation.

4.4 Summary:

Proteomics approach to catalog changes in the pathogen proteome helped us understand possible molecular mechanisms that explain how mycobacterial factors may help HIV propagation during co-infection, mutually benefiting both the pathogens. The study, to my knowledge, is the first attempt to catalog the intracellular mycobacterial differential proteomics during co-infection.

- The intracellular mycobacterial proteomes during co-infection suggested modulations in key mechanisms like toxin-antitoxin systems, Type VII (Esx) secretory systems, cell wall and lipid metabolism pathways, intermediary metabolism and respiration and cation transporters whose importance in the pathogenesis was mentioned in the results section.
- The mycobacteria tend to adapt to the intracellular niche provided by HIV during co-infection by altering its protein complement. For instance, concurrent to the increased host lipid accumulation inside macrophages during co-infection (Ganji, Dhali et al. 2015), it increases the expression of lipid utilizing mycobacterial enzymes or pathways during co-infection. Transcriptional profiling studies reveal that the extensive modification of *Mycobacterium tuberculosis*' genes involved in carbon metabolism, presumably a metabolic adaptation to the host niche (Schnappinger, Ehrt et al. 2003; Timm, Post et al. 2003). A key finding in support of this is that *M.tb* relies on fatty acid metabolism through the glyoxalate cycle for in vivo growth (Munoz-Elias and McKinney 2005). This existing literature clearly is in line with observations made that there is an over-expression of glyoxalate pathway enzymes. Although there is no precedence to the observation of a further enhancement in the case of co-infection, it is one of the reason that possibly allow better survival of tubercle bacillus and *M.tb* infection following a HIV infection.
- Another significant observation from the data is the increased expression of proteins involved in altering the lipid and protein composition of the cell wall. The differences in the cell wall alter the macrophage signaling pathways probably influencing the viral replication and propagation. This corroborates the observation that different clinical strains affect viral replication in a strain-dependent manner during co-infection which was attributed to the differences in the cell wall composition (Ranjbar, Boshoff et al. 2009).
- All the proteins identified in the current study have homologues in the virulent Mtb H37Rv strain (Annexure VII). Upon comparisons with the intracellular mycobacterial proteome

from granuloma of guinea pigs infected with *M.tb* reported by Kruh *et al.,* group (Kruh, Troudt et al. 2010), the proteomic data has shown an overlap of only 22 proteins out of 92 (23.91 %). Elucidating their role would help understand the pathogenesis of *M.tb* during co-infection.

Thus, the leads from the study can be systematically pursued to understand host-pathogen interactions at the molecular level leading to new insights into the mechanistic details of HIV-mycobacteria co-infection, helping decipher new intervention strategies and biomarker to overcome the synergism between HIV and mycobacteria.

Chapter 5

Quantitative proteomics to tabulate modulations in the phagosome enriched fractions during HIV-*Mycobacterium tuberculosis* H37Rv co-infection

5.1 Introduction:

The second objective (Chapters 3 and 4) was focused on proteomics approach towards understanding the coalition between mycobacteria and HIV during co-infection, where I could identify some of the host processes that were affected during HIV co-infection, making it favourable for opportunistic and non-pathogenic mycobacteria to survive the hostile cellular environment of activated macrophages. I could also identify mycobacterial factors that promoted directly or indirectly through stimulating infected host cells, HIV propagation, thus explaining the synergistic influence on both HIV and mycobacterial titers during co-infection. These studies were performed using the field compliant cell culture based model of HIV-mycobacteria co-infection developed (Chapter 2).

Having investigated the coalition between HIV and non-pathogenic mycobacteria, the quest to understand co-infection biology was extended towards understanding the modulation of the phagosome proteome of macrophages by pathogenic *Mycobacterium tuberculosis* strain H37Rv during HIV-H37Rv co-infection. In this chapter, the differences in the proteomes from phagosome enriched fractions of macrophages infected with either H37Rv or HIV & H37Rv has been tabulated and described. The proteomics data has been further extrapolated on the basis of existing literature support to draw inferences and hypothesis. The main purpose of this objective was to have baseline information on quantitative differences in theproteome from phagosome-enriched fractions during virulent *M.tb* H37Rv and HIV-H37Rv infection for identification of leads to be pursued in context of HIV and pathogenic mycobacterial co-infections in the lab.

Virulent mycobacteria, such as H37Rv strain, are known to evade the macrophages defense strategies and survive within them (Cole, Brosch et al. 1998). Clinical reports have provided clear indicators of increased risk of primary tuberculosis or reactivation of latent tuberculosis and increased disease progression in HIV patients (Suchindran, Brouwer et al. 2009; Naidoo, Padayatchi et al. 2011; Pawlowski, Jansson et al. 2012). In similar note, tuberculosis infection in HIV patients is also associated with increased rate of progression towards AIDS (Goletti, Weissman et al. 1996; Badri, Ehrlich et al. 2001; Collins, Quinones-Mateu et al. 2002). Since, virulent *M.tb* by itself can reside and propagate inside phagosomes (Cole, Brosch et al. 1998), it

was hypothesized that the changes in the phagosomal proteome by a virulent mycobacteria will be different than those by non-pathogenic mycobacteria in HIV infected cells. A proteomics study recording changes in the host environment during HIV-TB co-infection, especially in the late endosomes/phagosomes harbouring virulent mycobacteria is not available so far. Towards, this iTRAQ based quantitative proteomics was performed on phagosome enriched fractions to tabulate the changes during co-infection. Further, emphasis has been given to and described in detail the differences that were observed in host mechanisms of phagosome maturation, fatty acid metabolism and response to oxidative stress during co-infection.

5.2 Materials and methods:

The cell lines used:

- HEK293T (Human embryonic kidney) cell line
- THP-1 monocyte leukemia cell line (Cat#TIB-202, ATCC)

Bacterial strains used:

- *Mycobacterium tuberculosis* H37Rv

Virus strain used:

- Macrophage tropic HIV (NL-ADA8) was gifted by Dr. Jayant Bhattacharya

The details of the protocols mentioned below are given in the chapter 1:

4) **Maintenance of the cell lines**
5) **Growth conditions of *Mycobacterium tuberculosis***

M. tuberculosis was plated on 7H10 agar media (Hi-media, India) supplemented with 10% Oleic acid, Albumin, Dextrose and Catalase (OADC, Hi-Media, India). The plate was incubated at 37^{o}C until colonies appeared. The colonies were picked into the 7H9 broth media supplemented with 10% OADC and the broth culture was incubated at 37^{o}C at 180 rpm until the $OD_{600\ nm}$ reached 0.8 to 1. The culture was checked for any contamination using Ziehl-Neelsen (ZN) staining procedure. Prior to the infection, centrifuged the bacterial suspension at 200 ×*g* for 10 min and washed the bacterial pellet with PBS and then with RPMI 1640 media. Suspension of single-bacillus was obtained by passing the suspension through 26G 1 mL syringe for 10-20 times and then withdrew from the top of the tube.

6) **Preparation and quantification of infectious HIV-1 (ADA8) particles** (Kutner, Zhang et al. 2009; Banerjee, Benjamin et al. 2014)

5.2.1 Infection of macrophages and phagosome isolation:

THP-1 cells were PMA (10 ng/mL) differentiated to macrophages in RPMI 1640 media with 10% FBS in 150 mm culture dishes. After 24 hr the macrophages were washed, fresh media was added and kept for 48 hr rest. The macrophages were divided into two categories 1) for co-infection: First infected with HIV for 2 hr in incomplete RPMI media and followed by 24 hr incubation in complete RPMI media (Collman, Hassan et al. 1989; Sylwester, Wessels et al. 1993; Zhao, Thibault et al. 2006; Espert, Varbanov et al. 2009; Andreani, Gagnon et al. 2012). This was

followed by infection with BCG at an MOI=100 for 4 hr which was modified from the protocol described earlier (Lee, Jethwaney et al. 2010). 2) The MOI of 10 was used for *M. tuberculosis* infection. For mono-infection: The cells were treated similar to co-infection but without virus and followed by *M.tb* infection. After 4 hr of infection, fresh media with antibiotic was added and incubated for 24 hr. The phagosomes enter late endosome state at 24 hr post infection. After 24 hr the cells were harvested for fractionation to obtain enriched bacteria-*laden* phagosomes which was standardized in our laboratory using sucrose density gradient method as described earlier (Wandy Beatty and Russell 2001).

5.2.2 CFU enumeration and intracellular bacilli viability measurement:

For the CFU assays, 24-well tissue culture plates carrying 0.2 million THP-1 per well was used. The mono- and co-infected cells after the incubation were washed thrice with PBS to remove any extracellular bacilli followed by lysis of macrophages with sterile water at 37ºC for 10 min. The lysates were diluted and were plated on 7H10 agar plates. The plates were incubated at 37ºC with 5% CO_2 and 95% humidity for 2-3 weeks and the colonies were enumerated.

5.2.3 Protein digestion and iTRAQ labeling:

Phagosome protein concentration of each sample was estimated by Bradford method (Bio-Rad, Hercules, CA). 100 µg of lyophilized protein from each sample was dissolved in 20 µL of dissolution buffer [0.5 M triethylammonium bicarbonate (TEAB)] and 1 µL of denaturant reagent [5%Sodiumdodecylsulfate (SDS)].The samples were reduced for 1 hr at 60 °C with 2 µL reducing reagent [5mM Tris-2-carboxyethy phosphine (TCEP)] and further, reduced cysteine residues were then blocked with 10 mM methyl methane thiosulfonate (MMTS) for 30 min at room temperature. 10 µL of enzyme trypsin (prepared as 1 µg/µL in water solution with enzyme and substrate ratio of 1:10) was added to initiate the digestion and incubated for 12−16 h at 37°C. The iTRAQ reagent labeling was performed according to manufacturer's protocol (SCIEX, Foster City, CA). iTRAQ reagents were thawed and reconstituted in 50 µl of isopropanol. Samples were labeled with respective isobaric tags (H37Rv fractions: 116 isobar and HIV-H37Rv fractions: 121 isobar) and incubated for 2 hr at room temperature. The peptide mixtures were then pooled and dried by vacuum centrifugation. The pooled labeled peptide mixture was cleaned post digestion by off-line strong cation exchange (SCX) chromatography using the SCX cartridge. Labeled peptides were reconstituted in SCX low ionic strength buffer [5 mM ammonium formate, 30% acetonitrile

(ACN)] pH 3 and loaded onto a cartridge. Peptides were eluted with high cationic exchange buffer [500mM ammonium formate, 30 % (ACN)] pH 3 and were lyophilized for LC-MS/MS analysis.

5.2.4 LC-MS /MS Analysis:

All samples were analyzed by reverse-phase high-pressure liquid chromatography electrospray ionization tandem mass spectrometry (RP-HPLC-ESI-MS/MS) using an NanoLC-Ultra 1D plus (Eksigent; Dublin, CA) and nanoFlex cHiPLC system (Eksigent) which is directly connected to an SCIEX 5600 Triple-TOF (SCIEX; Concord, Canada) mass spectrometer, referred as Triple TOF system. Reverse Phase-HPLC was performed via a elute configuration using two Nano cHiPLC columns (Eksigent) in tandem to make a long column set up for better separation with good resolution; the analytical column (75 µm × 15 cm) were manufacturer (Eksigent)-packed with 3 µm ChromXP C-18 (120 Å). Reverse-phase LC solvents included: mobile phase A: 2% acetonitrile/98% of 0.1% formic acid (v/v) in water, and mobile phase B: 98% acetonitrile/2% of 0.1% formic acid (v/v) in water. The auto-sampler was operated in full injection mode overfilling a 1 µl loop with 3 µl analyte for optimal sample delivery reproducibility. All samples were eluted in replicates from the analytical column at a flow rate of 400 nL/min using the gradient of 5% solvent B to 50% solvent B over duration of 300 min. The column was regenerated by washing with 90% solvent B for 10 min and re-equilibrated with 5% solvent B for 45 min.

Auto-calibration of spectra occurred after acquisition of every sample using dynamic LC–MS and MS/MS acquisitions of 50 fmol β-galactosidase. Mass spectra and tandem mass spectra were recorded in positive-ion and "high-sensitivity" mode with a resolution of ~35,000 full-width half-maximum. Peptides were injected into the mass spectrometer using 10 µm SilicaTip electrospray PicoTip emitter (New Objective Cat. No.FS360-20-10-N-5-C7-CT) and the ion source was operated with the following parameters: ISVF = 2600; GS1 = 25; CUR = 25. The data acquisition mode in DDA experiments was set to obtain a high resolution TOF-MS scan over a mass range 350–1250 m/z, followed by MS/MS scans of 30 ion candidates per cycle with activated rolling collision energy, operating the instrument in high sensitivity mode. The selection criteria for the parent ions included the intensity, where ions had to be greater than 150 cps, with a charge state between +2 to +5, mass tolerance of 50 mDa. Once an ion had been fragmented by MS/MS, its mass and isotopes were excluded from further MS/MS fragmentation for 12 sec and exclude former after 2 repeats. Collision-induced dissociation was triggered by rolling collision energy.

The ion accumulation time was set to 200 ms (MS) and to 100 ms (MS/MS) with total cycle time of 3.3 sec.

5.2.5 Database Search and Relative Quantification:

All automatic data analysis (MS and MS/MS) and database searching were conducted against the Uniprot database (version 04-25-2013) using the ProteinPilotTM software (version 4, revision 148085, Applied Biosystems) with the ParagonTM method utilizing the following search parameters: Homosapiens as species, Trypsin as enzyme (one missed cleavage allowed), with fixed modification of Methyl methane thiosulphonate (MMTS)-labeled cysteine parameter enabled, iTRAQ 8plex (peptide labeled) as sample type and the 'Search Effort' parameter 'Thorough ID', which provides a broad search of various protein modifications and multiple mass cleavages, were chosen. The raw peptide identification results from the ParagonTM Algorithm (Applied Biosystems) searches were further processed by the Pro *GroupTM* Algorithm (Applied Biosystems) within the ProteinPilot software before final display.

The parameters used for identification and quantification of differentially expressed proteins includes: 1) Threshold of 1% accepted Global False discovery rate (G-FDR) proteins; 2) At least one unique peptide with 95% confidence for identification and at least two peptides for the relative expression. The false positive rates of the aforementioned filter criteria were all below 1%, estimated by using an individual reversed (decoy) sequence database In brief, false positive rates were calculated by dividing the number of decoy hits by that of hits acquired in search against forward sequence database.

5.2.6 Functional category enrichment analysis:

For functional category annotations, Uniprot accession number of the identified proteins were used. WEB-based GEneSeT Analysis Toolkit (WebGestalt) was used to annotate the predominantly represented biological processes or functions during mono- and co-infection (Zhang, Kirov et al. 2005; Wang, Duncan et al. 2013). The enrichments for KEGG (03/21/2011) and Wiki pathways (11/11/2012) using WebGestalt with Hypergeometric statistical test ($p<0.000001$), Benjamini and Hochberg Multiple test adjustment were considered with minimum three proteins per category (Zhang, Kirov et al. 2005; Wang, Duncan et al. 2013).

5.2.7 Immunoblot:

The phagosome fractions from mono- and co-infected cells were fractionated on 10% SDS-PAGE, transferred to Nitrocellulose membrane using GE-Amersham Western wet-transfer apparatus. The

membrane was blocked with 5% non-fat milk powder in PBS with 0.1% Tween-20 at RT for 2 hr. The primary antibodies namely, Late phagosomal markers - Rabbit anti-LAMP-2 (Sigma Aldrich, USA) and rabbit anti-Rab7 (Cell Signaling Technology, USA) antibodies and mouse anti-GAPDH, prepared in PBS-T (PBS+0.1% Tween-20) with 2% BSA 1:1000 dilutions, were added and incubated at 4^{o}C on platform rocker overnight. After 3 PBS-T washes, added the corresponding HRP-conjugated secondary antibodies (Santa cruz Biotechnology Inc., USA), diluted 1:2000 in PBS-T with 2% BSA, incubated at RT for 2 hr. After 3 washes with PBS, ECL substrate (Femtolucent Plus-HRP, chemiluminiscent reagent from G-biosciences, USA) was added to the membranes and was scanned for chemiluminiscence using Versadoc Imaging system (Biorad). The Western blot images were quantified by Image-J software (NIH).

5.2.8 Statistical Analyses:

All the experiments were performed at the least three times. The data were analysed using SigmaPlot software version 11.0.0.77 (Systat Software, Inc., USA). The error bars represent the standard deviation (SD) from the mean of at least three independent experiments. Statistical analyses of the experimental data for comparing two groups were performed by Student's *t*-test. $p<0.05$ was considered as significant.

5.3 Results and Discussion:

Mycobacteria during co-infection modulate its protein expression in concurrent to the host intracellular niche during co-infection for its survival. To study the changes in the phagosome proteome between the virulent *Mycobacterium tuberculosis* H37Rv mono-infection and HIV-H37Rv co-infection, the THP-1 macrophages were either mono-infected with virulent H37Rv strain (MOI=1:10) or co-infected with HIV and Virulent H37Rv strain. To confirm the infection of macrophages with *M.tb* H37Rv CFU assay was performed. As expected, the virulent H37Rv showed marginally increased survival during co-infection compared to the mono-infection alone (Figure 34). The %CFU of H37Rv during mono-infection and co-infection were 287.74±136.51 %CFU and 376.58±47.08 %CFU at 24 hr post-mycobacterial infection, respectively. The %CFU were normalized to CFU at 0 hr (Figure 34).

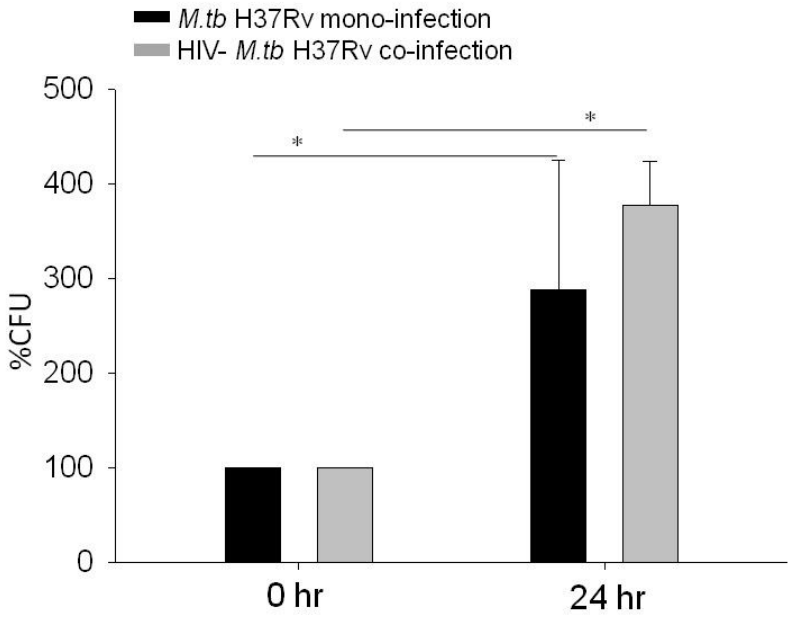

Figure 34: *Mycobacterium tuberculosis* H37Rv is provided additional survival advantage during HIV co-infection and thus survives better during co-infection. The graph represents the survival of H37Rv, in terms of %CFU, inside macrophages either H37Rv mono-infected or HIV-H37Rv co-infected cells at 0 hr and 24 hr post-mycobacterial infection. * represents $p<0.05$.

Upon confirmation of H37Rv infection by CFU assay, the phagosome-enriched fractions were isolated from the infected macrophages. The phagosome-enriched fractions were isolated at 24 hr post-infection where the mycobacteria *laden* phagosomes enter the late endosome state (Jordao, Bleck et al. 2008; Cardoso, Jordao et al. 2010) and sufficient time for *M.tb* to establish infection in macrophages. Thus, at this time-point one could assess the *M.tb* mediated early adaptive modulations in the phagosome proteome comparatively between *M.tb* mono- and HIV-*M.tb* co-infection to understand the co-infection pathogenesis. The isolated phagosome-enriched fractions were confirmed by Western blot for Rab7 and LAMP2 (Figure 35).

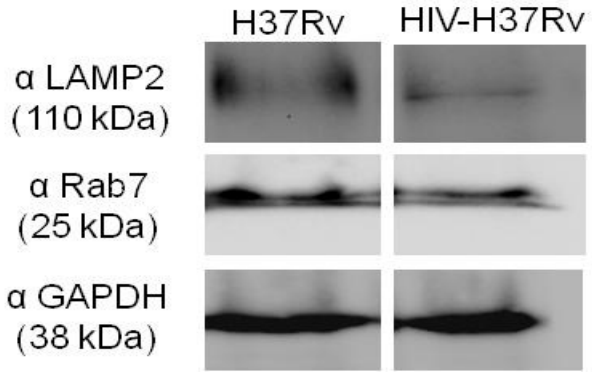

Figure 35: Western blot using anti-LAMP2 and anti-Rab7 antibodies for the phagosome-enriched fractions from H37Rv mono- and HIV-H37Rv co-infected cells.

The fractions were then subjected to quantitative LC-MS/MS using the isobaric Tags for Relative and Absolute Quantitation (iTRAQ) labels. Through iTRAQ LC-MS/MS of the phagosome samples, a total of 645 proteins were identified with more than 95 % confidence ($p<0.05$) which showed differential expression during H37Rv mono- and HIV-H37Rv co-infection (Annexure VIII). The proteins which showed more than 2 fold differences were only considered for further analyses.

5.3.1 Differences in the phagosome proteome of H37Rv mono- and HIV-H37Rv co-infected cells

Out of 645 proteins, 57 proteins (8.83 %) were upregulated in fractions from H37Rv mono-infected cells, 143 proteins (22.17 %) were upregulated in fractions from HIV-H37Rv co-infected cells and a commendable 445 (69 %) proteins' levels were unaltered between phagosome fractions of H3Rv mono and HIV-H37Rv co-infected cells (Figure 36 and Annexure VIII).

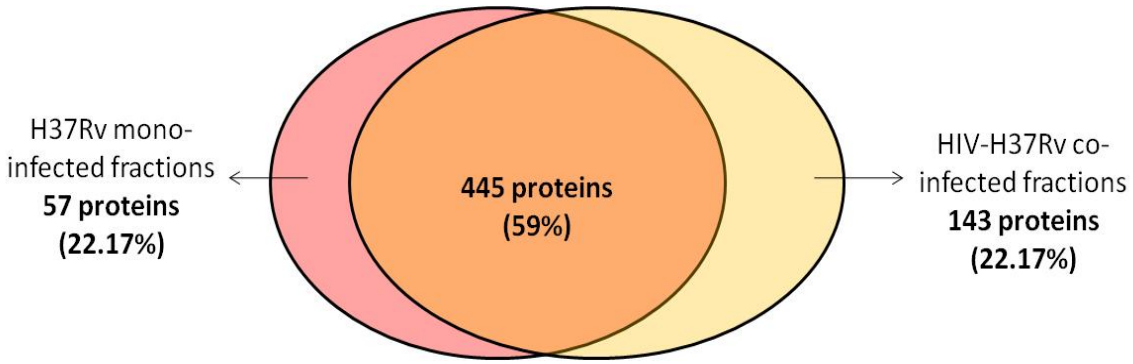

Figure 36: Venn diagram depicting the differential distribution of the phagosomal fraction proteins between H37Rv mono-infected and HIV-H37Rv co-infected cells.

GO enrichment analyses for the KEGG pathways and Wikipathways was performed using the WebGEstalt online tool (Zhang, Kirov et al. 2005; Wang, Duncan et al. 2013) with the human proteome as reference set (Figure 37 and Table 1). The enrichment was performed with stringent cut-offs (See materials and methods). The pathways altered between H37Rv infection and HIV-H37Rv co-infection were phagosome, lipid or fatty metabolism, energy metabolism and amino acid metabolism (Figure 37 and Table 1).

A

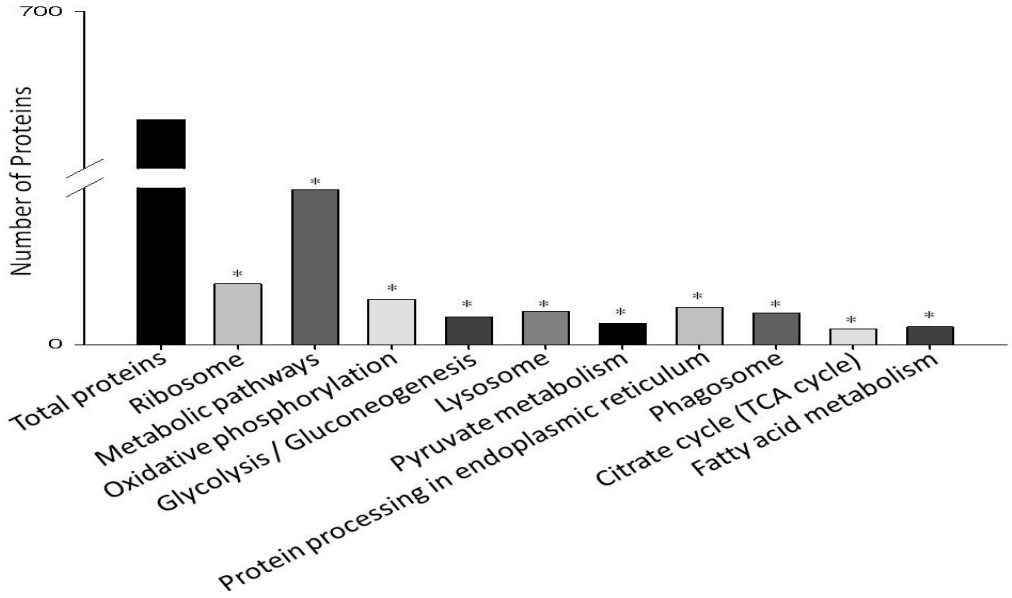

B

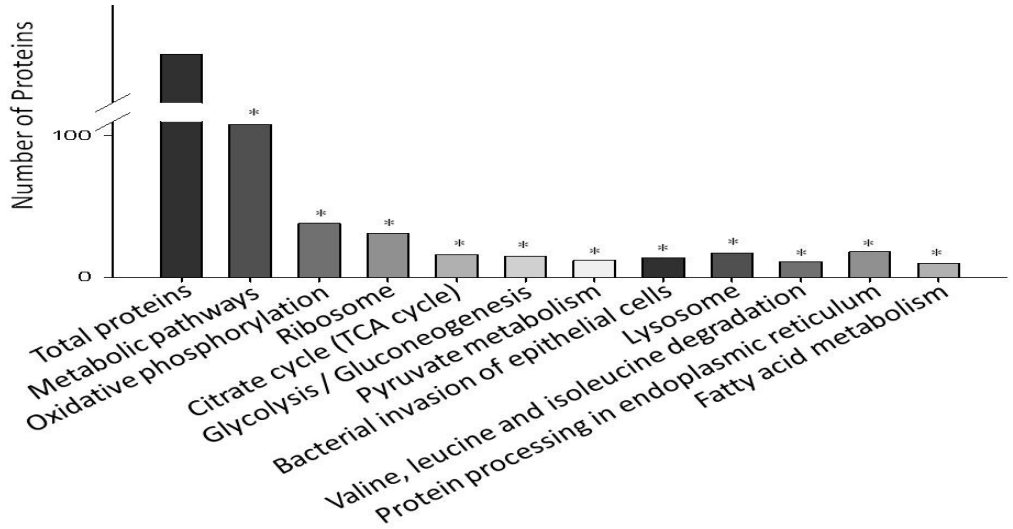

Figure 37: Bar graph represents the KEGG pathways enriched in the (A) H37Rv mono-infection and (B) HIV-H37Rv co-infection. * represents $p<0.000001$.

Pathways enriched in H37Rv mono-infection compared to HIV-H37Rv co-infection			
Pathway Name	**#Protein**	**Statistics**	**Enrichment type**
Ribosome	31	1.08E-29	KEGG
Metabolic pathways	79	6.11E-24	KEGG
Oxidative phosphorylation	23	5.9E-15	KEGG
Glycolysis / Gluconeogenesis	14	1.25E-10	KEGG
Lysosome	17	8.8E-10	KEGG
Pyruvate metabolism	11	9.65E-10	KEGG
Protein processing in endoplasmic reticulum	19	1.82E-09	KEGG
Phagosome	16	1.67E-07	KEGG
Citrate cycle (TCA cycle)	8	3.67E-07	KEGG
Fatty acid metabolism	9	4.79E-07	KEGG
Glycolysis and Gluconeogenesis	15	2.20E-13	Wikipathways
Electron Transport Chain	19	6.55E-13	Wikipathways
Pathways enriched in HIV-H37Rv co-infection compared to H37Rv mono-infection			
PathwayName	**#Protein**	**Statistics**	**Enrichment type**
Metabolic pathways	108	1.34E-38	KEGG
Oxidative phosphorylation	38	1.97E-30	KEGG
Ribosome	31	8.61E-28	KEGG
Citrate cycle (TCA cycle)	16	2.88E-18	KEGG
Cardiac muscle contraction	17	7.1E-12	KEGG
Glycolysis / Gluconeogenesis	15	7.41E-11	KEGG
Pyruvate metabolism	12	2.98E-10	KEGG
Bacterial invasion of epithelial cells	14	2.39E-09	KEGG
Lysosome	17	8.88E-09	KEGG
Valine, leucine and isoleucine degradation	11	1.34E-08	KEGG
Protein processing in endoplasmic reticulum	18	0.00000014	KEGG
Fatty acid metabolism	10	0.00000014	KEGG
Electron Transport Chain	34	2.84E-29	Wikipathways
Cytoplasmic Ribosomal Proteins	29	3.9E-25	Wikipathways
Glycolysis and Gluconeogenesis	18	1.83E-16	Wikipathways
Oxidative phosphorylation	18	5.76E-15	Wikipathways
TCA Cycle	12	1.44E-14	Wikipathways

Table 1: The table summarizes the KEGG and Wikipathways enriched in the H37Rv mono- and HIV-H37Rv co-infection.

5.3.2 Phagosome maturation impaired during HIV-H37Rv co-infection:

GO enrichment analyses of the iTRAQ data suggested a possible alteration in the maturation process of phagosome between H37Rv mono- and HIV-H37Rv co-infected cells. The phagosomes were fractionated at 24 hr post-mycobacterial infection at which the mycobacteria-*laden* phagosomes have entered the late endosome state. So, closely looking at the differential expression of proteins suggested that HIV-H37Rv fractions still retained the early endosome makers and acquired lesser amounts of late endosome markers on the phagosomes. Rab21 (0.95 fold in H37Rv), associates with early endosomes and regulate integrin association of endosomes (Roberts, Chua et al. 2006), Rab5c (1.20 fold in H37Rv), early endosomal marker (Haas 1998; Roberts, Chua et al. 2006; Haas 2007), Rab31 (0.68 fold in H37Rv), present on newly formed early endosomes (Yeo, Wall et al. 2015), and Rab10 (1.37 fold in H37Rv), associates with early endosomes and fuses mycobacteria-containing phagosomes with lysosomes (Cardoso, Jordao et al. 2010), were retained on phagosomes fractions of both H37Rv and HIV-H37Rv (Figure 38A). But EHD1 (4.48 fold on HIV-H37Rv) which associates with early endosome trafficking and recycling (Giridharan, Cai et al. 2012), was retained more on phagosomes during co-infection compared to H37Rv mono-infection (Figure 38A). The proteins specific for the late endosome state such as Rab7a (1.84 fold on H37Rv) and LAMP1 (0.62 fold on H37Rv) were unaltered during H37Rv and HIV-H37Rv co-infection. Similarly, the proteins such as, GDP-dissociation inhibitor 2 (1.46 fold on H37Rv), inhibits the release of GDP from Rab proteins (Pick, Gorzalczany et al. 1993) and subsequent phagosome maturation, Rab6a (0.86 fold on H37Rv), has many functions and considered to be pro-pathogenic (Rejman Lipinski, Heymann et al. 2009; Chen and Machner 2013) and Rab14 (1.60 fold in H37Rv), involved in blocking phagosome maturation (Kyei, Vergne et al. 2006) were unaltered during H37Rv and HIV-H37Rv co-infection. But the protein ADP-ribosylation factor 3 (6.25 fold in HIV-H37Rv), known to be involved in phagosome maturation arrest, was present in high levels on the phagosome fractions of co-infected cells compared to mono-infected cells (Figure 38A). Taken together in terms of phagosome maturation markers, although H37Rv mono-infection has the ability to compromise the phagosome maturation, HIV-H37Rv co-infection provided an additional advantage towards compromised phagosome maturation by increasing the levels of EHD1 (associated with early endosome) and ADP-ribosylation factor 3 (involved in phagosome maturation arrest) (Figure 38A).

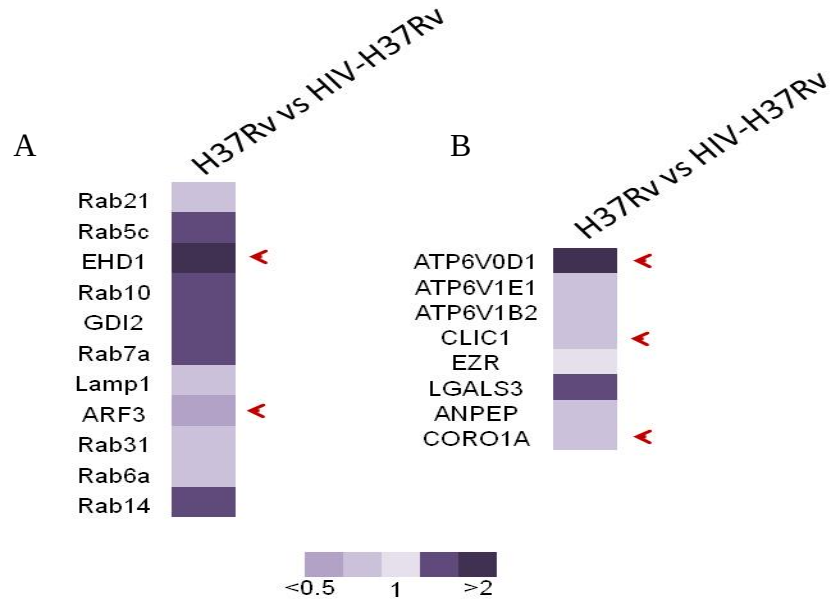

Figure 38: The expression profile of proteins involved in (A) phagosome maturation and (B) phagosome acidification in H37Rv mono-infected cell fractions compared to HIV-H37Rv co-infected cell fractions. Red arrows indicate proteins with more than 2 fold change in expression.

This arrest in phagosome maturation was further strengthened by the proteins involved in the acidification of phagosomes which showed differential expression during co-infection. The proteins involved in the acidification of phagosomes, except for one proton ATPase pump, were unaltered during both the infections. Proton ATPase pumps, such as ATP6V1E1 (0.87 fold in H37Rv), ATP6V1B1 (0.67 fold in H37Rv) (Mindell 2012), and Chloride Intracellular channel 1 (0.52 fold in H37Rv), involved in decrease of phagosomal pH (Jiang, Salao et al. 2012), Ezrin (0.99 fold in H37Rv), recruits iNOS to phagosomes (Miller, Fratti et al. 2004), levels were unaltered during both the infections on the phagosome fractions (Figure 38B). However, proton ATPase pump ATP6V0D1 (2.25 fold in H37Rv) shows higher expression in phagosome fractions of H37Rv mono-infected cells compared to fractions of HIV-H37Rv co-infected cells suggesting acidification of phagosomes of H37Rv mono-infected cells compared to HIV-H37Rv co-infected cells (Figure 38B). Other proteins such as, Galectin-3 (1.63 fold in H3Rv), associates with live mycobacteria-*laden* phagosomes (Beatty, Rhoades et al. 2002), Aminopeptidase N (0.73 fold in H37Rv), helps mycobacterial entry and survival (Ho, Tsai et al. 2014) and Coronin 1a (0.55 fold in H37Rv), associates with mycobacteria-*laden* phagosomes and inhibit phagolysosome formation

(Ferrari, Langen et al. 1999; Pieters, Muller et al. 2013) were present at similar levels on the fractions from both the infections but were marginally higher on co-infected fractions (Figure 38B). Overall, the phagosome maturation is compromised during both the infections with additional advantage provided by HIV co-infection.

Summarizing, when the available proteomics data on alteration in phagosomal maturation upon H37Rv infection (He, Li et al. 2012) was compared with our data on HIV-H37Rv co-infection, it could be concluded that infection by pathogenic strain of mycobacteria impairs phagosome maturation, which is further compromised during co-infection.

5.3.3 Some of the major differences in the phagosomal proteome during HIV-H37Rv co-infection:

Macrophages infected with pathogenic mycobacteria like *M.tb*, exhibit foamy phenotype with increased presence of lipid droplets which provide an additional niche for pathogenic mycobacterium to escape from immune recognition and also nutrient reserve to persist inside the host and similar increase in lipid metabolism are reported in case of HIV infections (Russell, Cardona et al. 2009; Daniel, Maamar et al. 2011; Heaton and Randall 2011; Lee, VanderVen et al. 2013; Almeida, Roque et al. 2014). GO enrichment analyses showed increased representation of lipid metabolism in both mono- and HIV co-infections (Table 1). During both the infections, levels of proteins involved in fatty acid degradation and fatty acid elongation were unchanged except for two proteins, namely, Acyl-CoA thoesterase 9 (2.61 fold in HIV-H37Rv) and Acyl-CoA synthetase long chain family member 1 (2.75 fold in HIV-H37Rv) which regulate the cellular free fatty acids and lipid levels (Jamwal, Midha et al. 2013) and were upregulated during co-infection (Figure 39A). Thus, a critical balance between free fatty acids and activated fatty acids determine either to accumulate lipids or help pathogen to utilize the lipids as nutrient source. As it is known that increased presence of lipid droplets (foamy phenotype) provides additional niche for intracellular pathogen to escape from immune recognition and additionally serve as nutrient reserve for their persistence (Russell, Cardona et al. 2009; Daniel, Maamar et al. 2011), the results suggested that HIV co-infection provided further more conducive environment for the persistence of mycobacteria through lipid body biogenesis.

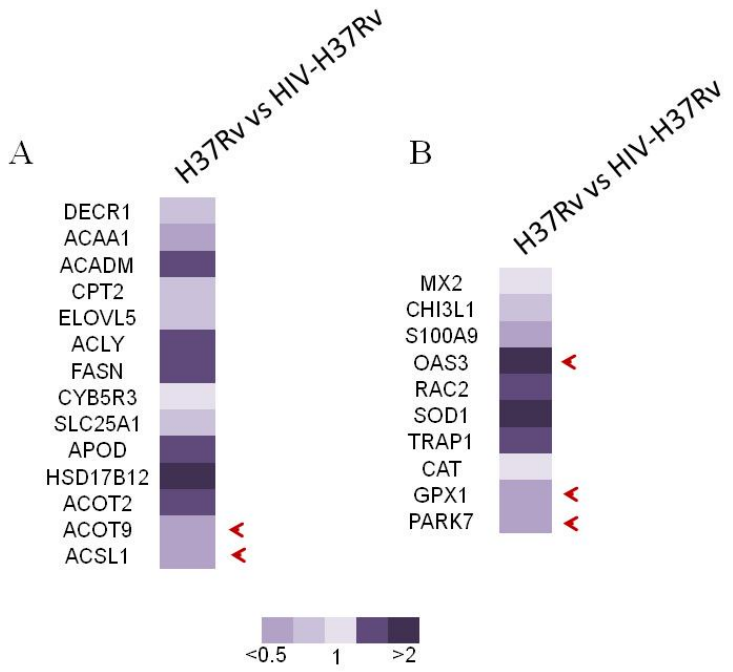

Figure 39: The expression profile of proteins involved in (A) fatty acid metabolism and (B) ROS/RNS inducers or quenchers in H37Rv mono-infected cell fractions compared to HIV-H37Rv co-infected cell fractions. Red arrows indicate proteins with more than 2 fold change in expression.

The other proteins which were expressed differentially during mono- and co-infection include 2'-5'-oligoadenylate synthetase 3 (2.21 fold in H37Rv) and Superoxide dismutase 1 (2.58 fold in H37Rv) were upregulated during H37Rv mono-infection and Glutathione peroxidase 1 (GPX1) (14.57 fold in HIV-H37Rv) and Parkinson protein 7 (PARK7) (5.30 fold in HIV-H37Rv) were upregulated during HIV-H37Rv co-infection (Figure 39B). 2'-5'-oligoadenylate synthetase 3 (OAS3) is an interferon-induced protein which is also implicated with the iNOS (Jamwal, Midha et al. 2013), produces Nitric oxide (NO) which can kill mycobacteria. It has already been reported that H37Rv is able to suppress OAS3 compared with avirulent H37Ra. From our proteomic data it was observed that HIV-H37Rv co-infection resulted in further suppression of OAS3 compared with H37Rv mono-infection suggesting an additional pro-survival mechanism provided during co-infection for mycobacteria. Similarly, co-infection resulted in the upregulation of GPX1 and PARK7 which are involved in relieving the cell from the oxidative stress (Gouaze, Andrieu-Abadie et al. 2002; Lee, Kim et al. 2003), thus probably help the pathogens to survive against the ROS/RNS during co-infection.

Overall, from the quantitative proteomic data we have seen that HIV-H37Rv co-infection possibly cause arrest of phagosome maturation, inhibit the acidification of phagosomes and also suppress factors which can synthesize NO to kill *M.tb* and upregulate factors which can quench the ROS/RNS and thus, may help better survival of *M.tb*.

5.4 Summary:

Broadly, HIV-H37Rv co-infection resulted in the recruitment of additional factors, other than the factors modulated by H37Rv alone, to arrest phagosome maturation, inhibit the acidification of phagosomes. The proteomic data suggested a possible increase in the fatty acid metabolism during HIV-H37Rv co-infection probably may have high levels of activated fatty acids, which either be utilized by mycobacteria as carbon source or can be used to accumulate more lipids. The quantitative data also suggested the possible downregulation of proteins which are indirectly involved in the Nitric oxide production during co-infection, which possibly H37Rv cannot achieve by itself. The proteins involved in the quenching of ROS are upregulated during co-infection compared to H37Rv mono-infection. Overall, HIV co-infection gave an additional advantage to the already well equipped *M.tb* to survive inside the macrophages.

Chapter 6

Summary and future prospects

6.1 Summary and future prospects

The study was an extension of the on-going quest in the laboratory to understand the synergistic existence of Mycobacteria and HIV during co-infection. It began with the collection of baseline information on the immune status of HIV-TB patients and correlation of the same with CD4+ T cell counts and viral loads at the point of detection before the initiation of either anti-TB or anti-HIV treatments. The field study from the laboratory inferred that Mycobacterial co-infection in HIV patients possibly results in discordance between CD4+ T cell levels and viral loads, owing to which CD4+ T cell levels as reference criteria to report the disease progression in terms of viral load in HIV-TB co-infected patients may be erroneous. It was further observed that TNFα and IL-4 levels in peripheral blood can possibly serve as indicators of hyper-inflammation in HIV-TB co-infected population prior to initiating the treatment (Benjamin, Banerjee et al. 2013). Further, towards understanding the coalition between Mycobacteria and HIV, the lab identified a host factor, human Zinc finger protein-134 (hZNF-134), that supported HIV propagation and was up-regulated upon mycobacterial infection, suggesting that up-regulation of such positive HIV-1 effectors upon mycobacterial stimulation can be one of the mechanisms by which mycobacteria facilitate HIV-1 propagation (Benjamin, Banerjee et al. 2014).

With these experimental evidences and field report from the lab, my objective was to understand the molecular and cellular events that assisted the initial phases of establishment of infection by mycobacteria, especially opportunistic mycobacteria, in HIV background. I targeted establishing a cell culture based model of HIV-mycobacteria co-infection in compliance with the field studies and use proteomics approach to identify the concurrent changes in both the host and intracellular mycobacterial proteomes to elucidate the molecular and cellular events underlying co-infection.

6.2 Highlights of the study

Objective 1: Developing an *in vitro* cell culture based co-infection model simulating reported clinical observations (Ganji, Dhali et al. 2015).

The *in vitro* cell culture model developed from PMA differentiated THP-1 simulated a state where a HIV infected person acquires a secondary infection of non-pathogenic/pathogenic mycobacteria.

The model used attenuated strain *M. bovis* BCG representing 'opportunistic infection by non-pathogenic mycobacteria. The model was found compliant with the earlier field studies, in terms of

(i) Limited cytokine profile, where BCG and HIV increase TNFα secretion from infected macrophages (Kindler, Sappino et al. 1989; Molina, Scadden et al. 1989; Molina, Schindler et al. 1990; Kindler and Sappino 1991) and HIV infection increases IL-10 secretion (Brockman, Kwon et al. 2009; Kwon and Kaufmann 2010). IL-12 secretion upon infection of non-pathogenic mycobacteria or HIV-1 is not altered distinguishably (Ma and Montaner 2000; Mendez-Samperio 2010).

(ii) Viral titers of HIV during co-infection in the model was similar to earlier clinical studies, where HIV-TB co-infected patients registered higher viral titers compared to HIV patients without mycobacterial infection (Toossi, Mayanja-Kizza et al. 2001).

(iii) Increased CFU counts of mycobacteria observed during co-infection corroborate the earlier reports (Newman, Kelley et al. 1993; Imperiali, Zaninoni et al. 2001; Pathak, Wentzel-Larsen et al. 2010).

The model showed that infection by non-pathogenic mycobacteria promoted HIV proliferation with the simultaneous increase in the survival of non-pathogenic mycobacteria during co-infection. It also ensured that in the co-infection model, before mycobacterial infection, THP-1 was in stimulated state, as indicated by the released cytokine levels due to HIV exposure. Overall, the model was consistent with the hypothesis that the Mycobacteria and HIV are mutually helped during co-infections (Diedrich and Flynn 2011).

The model represented the first THP-1 based cell culture model of HIV-mycobacteria co-infection.

Objective 2: Studying the differential expression of the host proteins and the consequent early adaptive changes in the intracellular mycobacterial proteome during co-infection through comparative proteomics.

The study is the first attempt to catalog the changes in the host proteome and the concerted changes in the intracellular mycobacterial proteome during co-infection. The differential proteins have been tabulated and attached as Annexures II, III and VII.

Host Proteome (Ganji, Dhali et al. 2015):

Some of the pathways that could be identified to be differentially affected are:

(i) Phagosome maturation pathways altered during co-infection.

(ii) Fatty acid metabolism pathways are enriched during co-infection.

(iii) Suggestive increase in energy metabolism during co-infection.

(iv) Extensive cytoskeletal rearrangements during co-infection.

(v) Increased representation of heat shock proteins during co-infection.

(vi) Impact on the transport of proteins across the mitochondrial membrane.

The differential expression of host proteome revealed possible alterations in the above mentioned pathways, out of which, based on the existing literature, I have pursued and validated three affected pathways, namely - phagosome maturation, fatty acid metabolism and energy metabolism. Supported by experiments with clinically relevant opportunistic mycobacterial species, *M. avium, M. kansasii* and *M. phlei,* it was inferred that the early adaptation of non-pathogenic strains of mycobacteria in the activated host macrophages is supported by HIV through arresting phagosomal maturation, promoting accumulation of lipid bodies, increasing energy synthesis and cytoskeleton rearrangements.

Intraphagosomal mycobacterial proteome (Manuscript under review):

Some of the pathways/proteins in mycobacteria that could be identified to be differentially affected are:

(i) The expression of TA system proteins were reduced during co-infection

(ii) During co-infection, mycobacteria showed increased expression Esx secretory system proteins (Esx3 and Esx5 systems) that are instrumental in secretion of virulent proteins.

(iii) During co-infection expression of proteins belonging to lipid metabolism were more expressed.

(iv) Mycobacteria from co-infected cell concomitantly increased the intermediary metabolism proteins which can utilize the fatty acid derived carbon sources from the host.

The inferences made from the intracellular mycobacterial proteome during co-infection were validated using the knock out and over-expressing *M. smegmatis* strains. The study shed light on the possible involvement of the mycobacterial factors that may help HIV propagation during co-

infection, mutually benefiting both the pathogens. The mycobacteria tend to adapt to the intracellular niche provided by HIV during co-infection by altering its protein complement. For instance, concurrent to the increased host lipid accumulation inside macrophages during co-infection (Ganji, Dhali et al. 2015), it increases the expression of lipid utilizing mycobacterial enzymes or pathways during co-infection. All the proteins identified in the current study have homologues in the virulent *M.tb* H37Rv strain. Elucidating their role would help understand the pathogenesis of *M.tb* during co-infection.

Objective 3: Quantitative proteomics to tabulate modulations in the phagosome enriched fractions of macrophages by pathogenic *Mycobacterium tuberculosis* H37Rv during mono-infection and HIV-H37Rv co-infection.

The differential proteins have been tabulated and attached as Annexure VIII.

The changes in the host cell proteome during infection by pathogenic mycobacteria H37Rv has been studied by several laboratories; however, this is the first study under co-infection. The ITRAQ based proteomics were performed for quantitative differentiation between the proteins expressed under the two conditions. The exercise primarily aimed to validate the co-infection model for pathogenic mycobacteria and make a base for further research on HIV-H37Rv co-infection biology in the lab. The pathways that were perturbed during opportunistic, non-pathogenic mycobacterial infections were revisited and the following additional differences were registered:

(i) As observed for opportunistic mycobacterial co-infection, the phagosome maturation was affected or arrested during the pathogenic strain co-infection, but the factors probably involved in the process were identified as ADP-ribosylation factor 3 and EH domain containing protein 1. This was also strengthened by the upregulation of phagosome acidifying factors, proton-ATPase pumps, during H37Rv mono-infection.

(ii) In context of lipid metabolism, the major difference during pathogenic strain co-infection is that there was increased expression of proteins that are involved in regulating the cellular activated fatty acid levels, which can be directed for lipid biogenesis or for utilization by the mycobacteria as carbon source.

(iii) The HIV-H37Rv co-infection also resulted in the upregulation of factors (GPX1 and PARK7) that can quench the ROS and downregulation of factor (OAS3) that is implicated in NO production would help better survival of *M.tb*.

Overall, it could be inferred that while pathogenic mycobacteria sufficiently modulate the host environment for its own survival, HIV background further helps by making the host macrophage severely compromised for phagosome maturation, oxygen-dependent pathogen clearance, like ROS and RNS production and fatty acid metabolism towards accumulation of fat in the cell that help *M.tb* by serving as carbon source or avoid immune recognition. Hence, HIV co-infection gave an additional advantage to the already well equipped *M.tb* to survive inside the macrophages.

6.3 Future prospects:

Mycobacterial co-infection in HIV patients accelerates both the disease progressions. The situation is challenged by toxicity burden and inadequate response to both the TB and HIV drugs increased incidence of Immune reconstitution inflammatory syndrome (IRIS) and additional threat of opportunistic infection by the environmental NTM (Juffermans, Verbon et al. 1998; Smith, Schnadig et al. 2001; Bachmeyer, Blum et al. 2002; Karakousis, Moore et al. 2004; Serra, Loi et al. 2007; Singh, Gopinath et al. 2007; Azzopardi, Bennett et al. 2009; Hesseling, Johnson et al. 2009). NTMs, which otherwise cannot establish infection in an immunocompetent individual (Zhang and Sugawara 2012), pose a serious threat to the HIV infected population given the fact that they are not only abundantly present in environment, but the infection remains asymptomatic, hard to diagnose and resistant to the conventional TB therapy (Primm, Lucero et al. 2004; Falkinham 2009; Brown-Elliott, Nash et al. 2012). Though, there are several ongoing attempts to understand the coalition between the HIV and pathogenic strains of mycobacteria but there exists little or no studies to understand the early establishment of infections by NTM in the HIV infected population.

6.3.1 Prospects of the Cell culture based co-infection model

Presence of a simple, *in vitro*, well validated, field-compliant cell culture based model, despite its limitations, tremendously helps high-throughput experiments, like screening of potential anti-mycobacterials, screening of mutants to identify biomarkers, perform trancriptomics, proteomics

or metabolomics etc. Though the macaques have been recognized as the suitable animal model to study HIV-mycobacteria co-infection (Guo and Ho 2014), it poses a challenge in high-throughput screening of novel compounds and slows down the process of discovery. The PBMC based *in vitro* co-infection model emphasized the utility of such models for the drug screening (Vijayakumar, Finney John et al. 2013). However, extracting PBMCs every time for drug-testing can be the limitation for such models. The *in vitro* cell culture based co-infection model developed in this study has the advantage of using a cell line based approach, hence is more user-friendly. It can be used for high-throughput screening of the potential drugs or study the drug to drug interactions or related cyto-toxicity or impact of drug on both the pathogens' infection. It also provides a simplistic platform to identify molecular mechanisms and cellular pathways for target and biomarker identification.

6.3.2 Leads from comparative proteomics

Apart from the mechanisms described in the thesis, the proteomic data also pointed out several interesting axes that can be deliberated to understand the synergistic impact of HIV and mycobacteria. Some of them are listed below.

<u>From the host proteome:</u>

(i) HIV infection and peroxiredoxins: co-infection showed increased expression of peroxiredoxin proteins, which are known to quench the ROS and thus, neutralize the microbicidal effects of ROS.

(ii) Pathogenic mycobacterial co-infection resulted in upregulation of ROS quenching factors, such as, GPX1 and PARK7 which were different from the peroxiredoxins observed during HIV-BCG co-infections. Earlier reports suggest that PARK7 is also implicated in maintenance of mitochondrial dynamics and autophagic response (McCoy and Cookson 2011). Studying its role would be interesting to understand the relation between mitochondria and autophagy in the context of co-infection.

(iii) Carnitine-O-palmitoyl transferase, that was absent in the fractions from BCG suggesting low levels of this enzyme during mono-infection. Carnitine deficiency

promotes HIV propagation (De Simone, Famularo et al. 1994; Vilaseca, Artuch et al. 2003).

(iv) The data also pointed towards the increased role of cytoskeletal proteins, as exemplified by Vimentin (substrate for HIV protease for nuclear entry) (Karczewski and Strebel 1996) and Septin7 (Signaling for autophagy) (Haglund and Welch 2011), and hence should not be overlooked owing to their ubiquitous nature.

From intracellular mycobacterial proteome:

Apart from the mycobacterial processes or factors discussed in the chapter 4, other mycobacterial factors/mechanisms which can be extended for further research in the terms of co-infection are:

(i) KstR1 (Tet-R family regulator) which is known to regulate expression of proteins (regulon of 80-100 proteins) involved in lipid metabolism is upregulated during co-infection. The proteins regulated by KstR1 are involved in utilization of cholesterol and other fatty acids. But the exact mechanism of regulation of KstR1 is still not known and deciphering its mechanism would help understand the adaptive transcriptional regulation of mycobacteria during co-infection.

(ii) The other transcriptional regulator of potency is Rv0894 (LuxR like regulator) is also differentially expressed. Earlier, in *M. avium paratuberculosis*, a luxR protein is shown to regulate the lipid metabolism and affect the infectivity (Alonso-Hearn, Eckstein et al. 2010). In *M.tb*, that possesses nearly seven luxR like regulators, out of which some are earlier reported to regulate key virulent pathways. These are RegX3 (regulates various virulent pathways), DevR (adaptation under Hypoxia) and Rv0195 (probable regulator involved in dormancy) (Parish, Smith et al. 2003; Fang, Yu et al. 2013; Bandyopadhyay, Biswas et al. 2014). Elucidating the function of Rv0894 may uncover yet another transcriptional regulator of *M.tb* and thus its survival tactics.

(iii) The other factors upregulated during co-infection are CtpC (Probable metal cation-transporting P-type ATPase C), MntH (Divalent cation-transport integral membrane protein) and Rv2850c (Possible magnesium chelatase) which can play important role

in acquiring the necessary metal ions or regulating the levels of metal ions inside the bacteria and thus help its survival.

(iv) Esx5 secretion system already known to be involved in PPE protein secretion (Abdallah, Savage et al. 2008) is upregulated during co-infection. Discovering the substrates of Esx5 system may help us understand the modulation of host response by mycobacteria during co-infection.

Overall, the study provides several new leads which can be pursued to understand host-pathogen interactions during HIV-mycobacteria co-infection that can be utilized to design intervention strategies to overcome the synergism between HIV and mycobacteria.

Annexures

Annexure I: Primers used for the qRT-PCR of the human genes.

Gene		**Primers (5'→3')**	**Melting Temperature (ºC)**	**Amplicon length (bp)**
P2x1	FP	CATGGGCTGTACGAAGAGAA	60.4	183
	RP	AGAGCCGATGGTGGTCATTG	62.45	
ATP synthase beta	FP	AGGAAATTCTGGTGACTGGTATC	60.99	212
	RP	ATAAATAGCAGTACATCTTGA	52.80	
P2X7	FP	AGACCTACGATGGACTTCACAG	62.02	317
	RP	AGCGCCAGCAAGGGCTC	62.02	
Actin	FP	AGCCTCGCCTTTGCCGA	62.32	181
	RP	CTGGTGCCTGGGGCG	60.4	
Pyruvate kinase	FP	AGAATCATGAGGGGGTTCGG	62	175
	RP	GAGTAGCACAGATGACAGGC	62	
Glyceraldehyde-3-phosphate dehydrogenase	FP	GAAGATGGTGATGGGATTTC	51	150
	RP	GAACGTGAAGGTCGGAGTCAA	58.8	

Annexure II: Summary of phagosomal proteins identified from fractions of mono- and co-infected cells and their distribution amongst the fractions.

Proteins Observed only in BCG fractions			
S#	**Protein Name**	**GENE ID**	**Uniprot Accession**
1	40S ribosomal protein S5	RPS5	P46782
2	40S ribosomal protein S8	RPS8	P62241
3	60S ribosomal protein L23	RPL23	P62829
4	Actin, alpha skeletal muscle	ACTA1	P68133
5	Afamin	AFM	P43652
6	ATP-dependent RNA helicase A	DHX9	O94761
7	Catechol O-methyltransferase	COMT	O95922
8	DENN domain-containing protein 4B	DENND4B	Q15434
9	Dynamin-1-like protein	DNM1L	O00429; O00635
10	Eukaryotic initiation factor 4A-II	EIF4A2	O15111
11	Eukaryotic translation initiation factor 3 subunit G	EIF3G	O75821
12	F-actin-capping protein subunit beta	CAPZB	P47756
13	Gonadotropin-releasing hormone receptor	GNRHR	P30968
14	HEAT repeat-containing protein 5B	HEATR5B	Q9P2D3
15	HLA class I histocompatibility antigen, A-2 alpha chain	HLA-A	P01892
16	Myosin light chain 1/3, skeletal muscle isoform	MYL1	P05976; P06741
17	Plexin-A1	PLXNA1	Q9UIW2; Q02363
18	Ras-related protein Rab-10	RAB10	P61026; Q9UIU6
19	Septin-7	SEPT7	Q16181
20	Serine/threonine-protein phosphatase 4 regulatory subunit 3A	SMEK1	Q6IN85
21	Signal recognition particle 14 kDa protein	SRP14	P37108
22	Sorting nexin-9	SNX9	Q9Y5X1
23	Tankyrase-2	TNKS2	Q9H2K2
24	Translocon-associated protein subunit alpha	SSR1	P43307
25	Tubulin beta-4B chain	TUBB4B	P68371
26	WASH complex subunit FAM21A	FAM21A	Q641Q2
27	Zyxin	ZYX	Q15942
Proteins Observed only in HIV-BCG fractions			
S#	**Protein Name**	**GENE ID**	**Uniprot Accession**
1	40S ribosomal protein S15	RPS15	P62841
2	60S ribosomal protein L3	RPL3	Q92985
3	60S ribosomal protein L4	RPL4	P36578

4	60S ribosomal protein L6	RPL6	Q02878
5	Actin, aortic smooth muscle	ACTA2	Q09428
6	Actin-related protein 2/3 complex subunit 2	ARPC2	O15144
7	Actin-related protein 2/3 complex subunit 4	ARPC4	P59998
8	Alpha-actinin-2	ACTN2	P35609; P28330
9	Alpha-actinin-3	ACTN3	Q08043
10	Alpha-enolase	ENO1	P06733
11	Ankyrin repeat domain-containing protein 35	ANKRD35	Q8N283
12	Basement membrane-specific heparan sulfate proteoglycan core protein precursor	HSPG2	P98160
13	Basigin	BSG	Q92974; P35613
14	Bassoon protein (Zinc-finger protein 231)	BSN	Q93100; Q9UPA5
15	B-cell receptor-associated protein 31	BCAP31	P51572
16	Beta-enolase	ENO3	P13929
17	Centrosomal protein 2 (Centrosomal Nek2-associated protein 1)	CEP250	Q9BV73
18	Chitinase-3-like protein 1	CHI3L1	P36222
19	Chloride intracellular channel protein 1	CLIC1	O00299; Q9H2W6
20	Ciliary dynein heavy chain 11 (Axonemal beta dynein heavy chain 11)	DNAH11	Q96DT5; Q9Y5H0
21	Collagen alpha 1(II) chain precursor [Contains: Chondrocalcin]	COL2A1	P02458
22	Collagen alpha 3(VI) chain precursor	COL6A3	P12111
23	D-3-phosphoglycerate dehydrogenase	PHGDH	O43175
24	Dynamin 3	DNM3	Q9UQ16
25	EH-domain containing protein 1	EHD1	Q9H4M9; O60779
26	ELAV-like protein 1 (Hu-antigen R)	ELAVL1	Q15717
27	Eosinophil peroxidase	EPX	P11678
28	Galectin-1	LGALS1	P09382
29	Galectin-3	LGALS3	P17931
30	Gamma-enolase	ENO2	P51800
31	Gamma-secretase subunit APH-1A	APH1A	Q96BI3
32	Golgi autoantigen, golgin subfamily A member 2 (Golgi matrix protein GM130)	GOLGA2	Q08379
33	Golgi autoantigen, golgin subfamily A member 3 (Golgin-160)	GOLGA3	Q08378
34	Golgin-45	BLZF1	Q9H2G9
35	Heat shock 70 kDa protein 1-like	HSPA1L	P34931
36	Heat shock protein HSP 90-alpha	HSP90AA1	P07900
37	Heat shock protein HSP 90-beta	HSP90AB1	P08238; P28324
38	HLA class I histocompatibility antigen, A-69 alpha chain	HLA-A	P10316

39	HLA class I histocompatibility antigen, Cw-12 alpha chain	HLA-C	P10321
40	HLA class I histocompatibility antigen, Cw-7 alpha chain	HLA-C	P10321
41	Huntingtin (Huntington's disease protein)	HTT	P42858
42	Importin subunit beta-1	KPNB1	Q14974
43	Integrin beta-4 precursor (GP150) (CD104 antigen)	ITGB4	P22455
44	Integrin beta-5	ITGB5	P18084; Q8N441
45	Interferon-regulated resistance GTP-binding protein MxA (Interferon-induced protein p78)	MX1	P20591
46	Keratin, type II cytoskeletal 5 (58 kDa cytokeratin)	KRT5	P13647
47	Leucine-rich repeat and calponin homology domain-containing protein 3	LRCH3	Q96II8
48	Low affinity cationic amino acid transporter 2	SLC7A2	P52569
49	Low-density lipoprotein receptor-related protein 10 precursor (SP220)	LRP10	Q9NX61
50	Lysosome-associated membrane glycoprotein 2 precursor (LAMP-2) (CD107b antigen)	LAMP2	P13473
51	Neurogenic locus notch homolog protein 3 precursor (Notch 3)	NOTCH3	Q9UM47
52	Neutral alpha-glucosidase AB	GANAB	Q14697
53	Protein Wnt-9b	WNT9B	O14905
54	Ryanodine receptor 2	RYR2	Q92736
55	Scaffold attachment factor B2	SAFB2	Q14151; Q14761
56	Semaphorin-6A	SEMA6A	Q9H2E6
57	Serine/threonine-protein phosphatase 6 regulatory subunit 2	PPP6R2	O75170
58	Serine/threonine-protein phosphatase 6 regulatory subunit 3	PPP6R3	Q5H9R7
59	Slit homolog 2 protein precursor (Slit-2)	SLIT2	O94813; P32119
60	Sperm associated antigen 5 (Astrin)	SPAG5	Q96R06
61	Translocon-associated protein subunit gamma	SSR3	Q9UNL2
62	Tubulin alpha-8 chain	TUBA8	Q9NY65
63	Tubulin alpha-ubiquitous chain (Tubulin K-alpha-1)	TUBAK	P68363
64	Tubulin beta chain	TUBB	P07437
65	Tubulin beta-2 chain (Tubulin beta-2 chain)	TUBB2A	A5D907
66	Tubulin beta-1 chain	TUBB1	Q9H4B7
67	Tubulin beta-3 chain	TUBB3	P04843; Q01726; Q13509
68	Tubulin beta-6 chain	TUBB6	Q9BUF5
69	Aminopeptidase N	ANPEP	P15144
70	Apolipoprotein B-100 precursor (Apo B-100)	APOB	P50052

71	Collagen alpha 1(XVII) chain	COL17A1	Q9UMD9; Q9Y3P4
72	Dystrophin	DMD	Q12864; P11532
73	Fibrillin 1 precursor	FBN1	P02458; P35555
74	Microtubule-actin crosslinking factor 1, isoform 4	MACF1	Q9UPN3; Q96PK2
75	Myosin XV (Unconventional myosin-15)	MYO15A	Q9UKN7
76	Proto-oncogene tyrosine-protein kinase ROS precursor (c-ros-1)	ROS1	P08922
77	Ras-related protein Rab-7	RAB7	Q8TC07
78	Serine/threonine-protein kinase 9	CDKL5	O76039
79	Spectrin beta chain, brain 4	SPTBN5	Q9NRC6
Proteins Observed in both fractions			
S#	**Protein Name**	**GENE ID**	**Uniprot Accession**
1	40S ribosomal protein S18	RPS18	P62269
2	60S ribosomal protein L12	RPL12	Q9UKX5; P30050
3	78 kDa glucose-regulated protein	HSPA5	P11021; P08246
4	Actin, alpha cardiac muscle 1	ACTC1	Q8NE71
5	Actin, cytoplasmic 1	ACTB	P60709
6	Actin-related protein 2/3 complex subunit 3	ARPC3	O15145
7	Actin-like protein 2 (Actin-related protein 2)	ACTR2	P61160
8	Actin-related protein 3	ACTR3	P61158
9	Adenylyl cyclase-associated protein 1	CAP1	Q01518
10	Alpha-actinin-1	ACTN1	P12814; Q9UKU7
11	Annexin A2	ANXA2	P07355
12	Armadillo repeat-containing protein 5	ARMC5	Q96C12
13	Atlastin-1	ATL1	Q8WXF7
14	Beta-1,4-galactosyltransferase 3	B4GALT3	O60512
15	Beta-actin-like protein 2	ACTBL2	Q562R1
16	CAAX prenyl protease 1 homolog	ZMPSTE24	O75844
17	Calmodulin	CALM1	P62158
18	Calnexin	CANX	P27824
19	Calreticulin	CALR	P27797
20	Cancer susceptibility candidate protein 1	CASC1	Q6TDU8; Q6TDU7
21	Cathepsin B	CTSB	P07858
22	Cathepsin D	CTSD	P07339
23	Collagen alpha-1(I) chain	COL1A1	P02452
24	Desmin	DES	P07766
25	Dolichyl-diphosphooligosaccharide--protein glycosyltransferase subunit 1	RPN1	P04843
26	Dolichyl-diphosphooligosaccharide--protein glycosyltransferase subunit 2	RPN2	P04844
27	Elongation factor 1-alpha 1	EEF1A1	O14646; P68104

28	Elongation factor 1-beta	EEF1B2	P24534
29	Elongation factor 1-gamma	EEF1G	P26641
30	Elongation factor 2 (EF-2)	EEF2	Q9Y259; P13639
31	Endoplasmin	HSP90B1	P14625
32	Exocyst complex component 3-like protein 2	EXOC3L2	Q2M3D2
33	Ezrin	EZR	P15311
34	F-actin-capping protein subunit alpha-1	CAPZA1	P52907
35	Fructose-bisphosphate aldolase A	ALDOA	P78563
36	Fructose-bisphosphate aldolase C	ALDOC	P09972
37	Glyceraldehyde-3-phosphate dehydrogenase	GAPDH	P04406; Q16678
38	Heat shock cognate 71 kDa protein	HSPA8	P11142
39	Heat shock protein beta-1	HSPB1	P04792
40	Heat shock-related 70 kDa protein 2	HSPA2	P54652
41	Hypoxia up-regulated protein 1	HYOU1	Q9Y4L1
42	Integrin beta-2	ITGB2	P05107
43	Lamina-associated polypeptide 2, isoforms beta/gamma	TMPO	P42166; P42167
44	Lamin-B1	LMNB1	P20700
45	Moesin	MSN	P26038; Q99677
46	Monocyte differentiation antigen CD14 precursor	CD14	P08571
47	Myosin light polypeptide 6	MYL6	P60660; P46439
48	Myosin regulatory light chain 12A	MYL12A	P19105
49	Myosin-10	MYH10	Q16772
50	Myosin-9	MYH9	P35579
51	Neurofilament medium polypeptide	NEFM	P07197
52	Palmitoyl-protein thioesterase 1	PPT1	P50897
53	Peptidyl-prolyl cis-trans isomerase A	PPIA	P62937
54	Peptidyl-prolyl cis-trans isomerase B	PPIB	P23284
55	Peripherin	PRPH	P41219
56	Phosphoglycerate kinase 1	PGK1	P00558
57	Plectin	PLEC	Q15149
58	Profilin-1	PFN1	P07737
59	Prostaglandin G/H synthase 1	PTGS1	P23219
60	Protein disulfide-isomerase A3	PDIA3	P30101
61	Protein disulfide-isomerase A6	PDIA6	Q15084
62	Protein disulfide-isomerase	P4HB	P07237
63	Protein LYRIC	MTDH	Q86UE4
64	Pyruvate kinase isozymes M1/M2	PKM2	P14618
65	Radixin	RDX	P35241
66	Ras-related protein Rab-7a	RAB7A	P51149
67	Ras-related protein Rap-1A	RAP1A	P62834

68	Receptor-type tyrosine-protein phosphatase C	PTPRC	P08575
69	Serine/threonine-protein kinase 10	STK10	O94804
70	SH3 domain and tetratricopeptide repeat-containing protein 2	SH3TC2	Q8TF17
71	SH3-domain binding protein 1 (3BP-1)	SH3BP1	Q9Y3L3; Q96GD0
72	Surfeit locus protein 4	SURF4	P46821
73	Talin-1	TLN1	Q9Y490
74	Torsin-1A-interacting protein 1	TOR1AIP1	Q5JTV8
75	Transketolase	TKT	P29401
76	Tripeptidyl-peptidase 1	TPP1	O14773
77	Tubulin alpha-1A chain	TUBA1A	Q71U36
78	Ubiquitin-40S ribosomal protein S27a	RPS27A	P48547; P62979; P62988
79	Vasodilator-stimulated phosphoprotein	VASP	P50552
80	Vesicle-trafficking protein SEC22b	SEC22B	O75396
81	Vimentin	VIM	P08670
82	Vitronectin precursor (Serum spreading factor)	VTN	P04004
83	Xylulose kinase	XYLB	O75191
84	Surfeit locus protein 4	SURF4	P46821
85	Talin-1	TLN1	Q9Y490
86	Torsin-1A-interacting protein 1	TOR1AIP1	Q5JTV8
87	Transketolase	TKT	P29401
88	Tripeptidyl-peptidase 1	TPP1	O14773
89	Tubulin alpha-1A chain	TUBA1A	Q71U36
90	Ubiquitin-40S ribosomal protein S27a	RPS27A	P48547; P62979; P62988
91	Vasodilator-stimulated phosphoprotein	VASP	P50552
92	Vesicle-trafficking protein SEC22b	SEC22B	O75396
93	Vimentin	VIM	P08670
94	Xylulose kinase	XYLB	O75191

Annexure III: Summary of mitochondrial proteins identified from the fractions of mono- and co-infected cells and their distribution amongst the fractions.

Proteins Observed only in BCG fractions			
S#	**Protein name**	**GENE ID**	**Uniprot Accession**
1	ADP/ATP translocase 1	SLC25A4	P12235
2	Glutaminase kidney isoform, mitochondrial	GLS	O94925
3	Leucine-rich PPR motif-containing protein, mitochondrial	LRPPRC	P42704
4	NADH dehydrogenase [ubiquinone] iron-sulfur protein 2, mitochondrial	NDUFS2	O75306
5	Sideroflexin-1	SFXN1	Q9H9B4
Proteins Observed only in HIV-BCG fractions			
S#	**Protein name**	**GENE ID**	**Uniprot Accession**
1	ATP synthase subunit g, mitochondrial	ATP5L	O75964
2	ATP synthase subunit gamma, mitochondrial	ATP5C1	P36542
3	Bcl-2 homologous antagonist/killer	BAK1	Q13014; Q16611; Q02410
4	Carnitine O-palmitoyltransferase 2, mitochondrial	CPT2	P23786
5	Heat shock protein 75 kDa, mitochondrial	TRAP1	Q12931
6	Isocitrate dehydrogenase [NAD] subunit alpha, mitochondrial	IDH3A	P50213
7	Isoleucine--tRNA ligase, mitochondrial	IARS2	Q9NSE4
8	Methylcrotonoyl-CoA carboxylase beta chain, mitochondrial precursor	MCCC2	Q9HCC0
9	Mitochondrial-processing peptidase subunit alpha	PMPCA	Q10713
10	Pyruvate dehydrogenase E1 component subunit beta, mitochondrial	PDHB	P11177
11	Serine hydroxymethyltransferase, mitochondrial	SHMT2	P34897
12	SRA stem-loop-interacting RNA-binding protein, mitochondrial	SLIRP	Q9GZT3
13	Peroxiredoxin 4	PRDX4	Q13162; Q9UBB4
14	Peroxiredoxin-6	PRDX6	P30041; P60484
15	Ubiquinol-cytochrome-c reductase complex core protein I, mitochondrial precursor	UQCRC1	P31930
Proteins Observed in both fractions			
S#	**Protein name**	**GENE ID**	**Uniprot Accession**
1	2,4-dienoyl-CoA reductase, mitochondrial	DECR1	Q16698
2	10 kDa heat shock protein, mitochondrial	HSPE1	Q14246
3	60 kDa heat shock protein, mitochondrial	HSPD1	P10809

4	Adenylate kinase 2, mitochondrial	AK2	P54819
5	ADP/ATP translocase 2	SLC25A5	P05141; P30520
6	ADP/ATP translocase 3	SLC25A6	Q6I9V5
7	ATP synthase-coupling factor 6, mitochondrial	ATP5J	P18859
8	ATP synthase subunit alpha, mitochondrial	ATP5A1	P25705
9	ATP synthase subunit beta, mitochondrial	ATP5B	P06576
10	ATP synthase subunit f, mitochondrial	ATP5J2	P56134
11	Bifunctional methylene tetrahydrofolate dehydrogenase/cyclohydrolase, mitochondrial	MTHFD2	P13995
12	Citrate synthase, mitochondrial	CS	O75390
13	Complement component 1, Q subcomponent binding protein, mitochondrial precursor	C1QBP	Q07021
14	Cytochrome b-c1 complex subunit 1, mitochondrial	UQCRC1	P31930
15	Cytochrome b-c1 complex subunit 2, mitochondrial	UQCRC2	P22695
16	Cytochrome b-c1 complex subunit 6, mitochondrial	UQCRH	P07919
17	Cytochrome b-c1 complex subunit 8	UQCRQ	O14949
18	Cytochrome c	CYCS	P99999
19	Cytochrome c oxidase subunit 4 isoform 1, mitochondrial	COX4I1	P13073
20	Cytochrome c1, heme protein, mitochondrial	CYC1	P08574
21	Delta(3,5)-Delta(2,4)-dienoyl-CoA isomerase, mitochondrial	ECH1	Q13011
22	Dihydrolipoyl dehydrogenase, mitochondrial	DLD	P09622
23	Dimethyladenosine transferase 1, mitochondrial	TFB1M	Q8WVM0
24	Electron transfer flavoprotein subunit alpha, mitochondrial	ETFA	P13804
25	Elongation factor Tu, mitochondrial	TUFM	P49411
26	Enoyl-CoA hydratase, mitochondrial	ECHS1	P30084
27	Glutamate dehydrogenase 1, mitochondrial	GLUD1	P00367
28	Glutamate dehydrogenase 2, mitochondrial	GLUD2	P26196
29	Isocitrate dehydrogenase [NADP], mitochondrial	IDH2	P48735
30	Malate dehydrogenase, mitochondrial	MDH2	P01275
31	Medium-chain specific acyl-CoA dehydrogenase, mitochondrial	ACADM	P11310; P78363
32	Mitochondrial import receptor subunit TOM22 homolog	TOMM22	Q9NS69
33	Mitochondrial import receptor subunit TOM70	TOMM70A	O94826
34	Mitochondrial inner membrane protein	IMMT	Q00325; Q16891
35	NADH-cytochrome b5 reductase 3	CYB5R3	P00387
36	Peptidyl-prolyl cis-trans isomerase F, mitochondrial	PPIF	P30405
37	Phosphate carrier protein, mitochondrial	SLC25A3	Q00325
38	Prohibitin-2	PHB2	Q99623
39	Protein ETHE1, mitochondrial	ETHE1	O95571

40	Serine/threonine-protein phosphatase PGAM5, mitochondrial	PGAM5	Q96HS1
41	Sideroflexin-3	SFXN3	Q9BWM7
42	Stress-70 protein, mitochondrial	HSPA9	P38646
43	Succinate dehydrogenase [ubiquinone] flavoprotein subunit, mitochondrial	SDHA	P31040
44	Sulfide:quinone oxidoreductase, mitochondrial	SQRDL	Q9Y6N5
45	Superoxide dismutase [Mn], mitochondrial	SOD2	P04179
46	Thioredoxin-dependent peroxide reductase, mitochondrial	PRDX3	Q05940; P30048
47	Trifunctional enzyme subunit alpha, mitochondrial	HADHA	P55039
48	Trifunctional enzyme subunit beta, mitochondrial	HADHB	Q13474; P55084
49	Voltage-dependent anion-selective channel protein 1	VDAC1	P21796
50	Voltage-dependent anion-selective channel protein2	VDAC2	P45880
51	Peroxiredoxin-1	PRDX1	Q06830

Annexure IV: The table represents the functional categories significantly enriched during the BCG and HIV-BCG. The Enrichment analysis was performed using the online WebGeStalt tool.

Enriched functional Category in HIV-BCG	**Adjusted p value after BH multiple test adjustment**	**Enrichment analysis**
Glycolysis / Gluconeogenesis	adjP=6.37e-06	KEGG
Citrate cycle (TCA cycle)	adjP=6.77e-06	KEGG
Arrhythmogenic right ventricular cardiomyopathy (ARVC)	adjP=1.38e-05	KEGG
Amoebiasis	adjP=2.42e-05	KEGG
Valine, leucine and isoleucine degradation	adjP=5.34e-05	KEGG
Parkin-Ubiquitin Proteasomal System pathway	adjP=1.29e-08	Wikipathways
Glycolysis and Gluconeogenesis	adjP=1.70e-06	Wikipathways
Fatty Acid Beta Oxidation	adjP=2.11e-05	Wikipathways
TCA Cycle	adjP=2.11e-05	Wikipathways
Protein polymerization	adjP=4.05e-07	GO
Establishment of protein localisation to organelle	adjP=1.70e-05	GO
Mitochondrial ATP synthesis coupled proton transport	adjP=4.30e-06	GO
Thiroredoxin peroxidase activity	adjP=4.32e-05	GO
ATPase activity	adjP=4.35e-05	GO
GTPase activity	adjP=4.32e-05	GO
Arp 2/3 protein complex	adjP=8.52e-08	GO
Mitochondrial proton-transporting ATP synthase complex	adjP=2.58e-06	GO
Enriched functional Category in BCG	**Adjusted p value after BH multiple test adjustment**	**Enrichment analysis**
Activation of signalling protein activity involved in unfolded protein response	adjP=3.56e-05	GO
ADP binding	adjP=6.18e-06	GO

Annexure V: Primers used for the cloning of *vapC48* and *ideR* gene into pVV16 shuttle vector.

Primers for cloning VapC48 into pVV16		**Primers (5'→3')**	**Melting Temperature**
Forward primer with *NdeI*	FP	ATCTCATATGAGCGAAACCTTTGACG	65ºC
Reverse primer with *HindIII*	RP	ACTCGGATCCAGCCGGAGAAGGGGTC	61ºC
Primers for cloning IdeR into pVV16		**Primers (5'→3')**	**Melting Temperature**
Forward primer with *NdeI*	FP	ATATATATGAACGAGCTGGTTGAT	52.2ºC
Reverse primer with *HindIII*	RP	TATAAGCTTTCAGACTTTTTCGACCTT	56.9ºC

Annexure VI: Primers for the qRT-PCR of the mycobacterial genes.

Gene		Primers (5'→3')	Melting Temperature (°C)	Amplicon length (bp)
16S rRNA	FP	TAGGCGTTCCCTTGTGGC	62.18	142
	RP	CAGTCTCTCACGAGTCCC	62.18	
BCG0946	FP	CGCTGTTACGTTCCTGTCC	62.32	212
	RP	GTCCAAGCGTCGGCAGAT	62.18	
BCG2433c	FP	GATGGGCGTCGGTTTCG	62.02	268
	RP	CGTCGCGTTGCTCACAG	62.02	
BCG2654c	FP	GTGCATGGGACGGCTCAA	62.18	248
	RP	ATCTTGACGGTGTGGCGG	62.18	
BCG3756c	FP	GCTGGGTTATCTACGGGTTG	62.45	213
	RP	ATGAGCGCGACGAGGTG	62.02	
BCG3226c	FP	GGTCAGCAGTTTGGTGGAG	62.32	157
	RP	CAGGTCAAACAGCAGTTCAG	60.4	
BCG0932	FP	GGGTGCGTTGGCGATTC	62	104
	RP	CGATGGGGTGTGGGG	61.6	
BCG3932	FP	TAGTGATCGGATCGGTCTTC	60.4	203
	RP	GGGTAGCGGTGAGGGGT	64	
BCG3940c	FP	CGCAGCTAGTCACCGAGAT	62.32	150
	RP	GAATCACGATCCTCTTGGC	60.18	
BCG0332	FP	ATCGGTTGGGAGGCTGGT	62	149
	RP	GTATCGGGCAACTCGGCA	62	

Annexure VII: Mycobacterial proteins identified by LC-MALDI-MS/MS from the phagosomal fractions of BCG mono- and HIV-BCG co-infected cells. *Note:**Corresponding protein belongs to IdeR regulon (Rodriguez, Voskuil et al. 2002)

Proteins Observed in fractions from BCG mono-infected cells						
S#	**BCG gene#**	**pI**	**MW (kDa)**	**Functional category**	**Product/Function (Known/probable/annotated)**	**Ortholog in *M.tuberculosis* H37Rv (Rv#)**
1	BCG1194c	4.9	81.5	intermediary metabolism and respiration	Involved *de novo* biosynthesis of Methionine	Rv1133c
2	BCG3477	10.7	11	virulence, detoxification, adaptation	Unknown; Possible Anti-toxin VapB47	Rv3407
3	BCG3226c	6.1	116.6	information pathways	Probable ATP-dependent DNA helicase/Has both ATPase and helicase activities	Rv3201c
4	BCG0136c	7.3	77.4	cell wall and cell processes	Probable cation-transporter P-type ATPase B CtpB/Cation-transporting ATPase	Rv0103c (ctpB)
5	BCG0422c	4.9	92.5	virulence, detoxification, adaptation	Probable endopeptidase ATP binding protein (chain B) ClpB (ClpB protein) (heat shock protein F84.1)	Rv0384c
6	BCG2367c	6.1	46.8	intermediary metabolism and respiration	Probable dGTP triphosphohydrolase	Rv2344c
7	BCG0677c	6.3	118.7	information pathways	Probable exonuclease V (beta chain) RecB/Involved in homologous recombination.	Rv0630c
8	BCG2238c	7.5	109.1	intermediary metabolism and respiration	Glutamate-ammonia-ligase adenylyltransferase GlnE/Regulatory protein involved in the regulation of glutamine synthetase activity	Rv2221c
9	BCG2457c	5.4	74.6	intermediary metabolism	Glutamine-dependent NAD(+) synthetase NadE (NAD(+) synthase/Involved in biosynthesis of NAD	RV2438c

				and respiration		
10	BCG1867	5.3	99.4	intermediary metabolism and respiration	Probable glycine dehydrogenase GcvB/The glycine cleavage system catalyses the degradation of glycine.	Rv1832
11	BCG1419c	5.9	33.9	conserved hypotheticals	Conserved hypothetical protein/Unknown	Rv1357c
12	BCG2119	6.5	58.9	insertion seqs and phages	Conserved hypothetical protein/Unknown	Rv2100
13	BCG0079c	7.5	30.8	cell wall and cell processes	Possible membrane protein/Unknown	Rv0048c
14	Mb2002c	4.5	24.8	cell wall and cell processes	Immunogenic protein Mpt64/Unknown.	Rv1980c
15	BCG3662c	10.7	12	information pathways	Iron-regulated H-NS-like protein Lsr2/Has DNA-bridging activity.	Rv3597c
16	BCG3174	5.2	85.3	intermediary metabolism and respiration	Probable NADH dehydrogenase I (chain G) NuoG/Involved in aerobic|anaerobic respiration	Rv3151
17	BCG1088	6.3	74.6	cell wall and cell processes	Probable potassium-transporting P-type ATPase B chain KdpB	Rv1030 (kdpB)
18	BCG1391c	6.5	70.1	information pathways	Probable ATP-dependent helicase DinG/Probable helicase involved in DNA repair and perhaps also replication.	Rv1329c
19	BCG1182	4.99	52.1	intermediary metabolism and respiration	Probable glucose-6-phosphate 1-dehydrogenase Zwf1 (G6PD)/Involved in pentose phosphate pathway (first step)	Rv1121
20	BCG3756c	9.6	16.3	virulence, detoxification, adaptation	Possible toxin VapC48/Unknown	Rv3697c

21	BCG0453c	6.1	23.2	intermediary metabolism and respiration	Thiamine-phosphate pyrophosphorylase ThiE/Involved in thiamine biosynthesis	Rv0414c
22	BCG3326; BCG3362	8.7	28.5	information pathways	Probable endonuclease VIII Nei/Involved in damage reversal of DNA	Rv3297
23	BCG1573	5	63.1	lipid metabolism	Probable fatty-acid-AMP ligase FadD25/Function unknown, but involvement in lipid degradation	Rv1521
24	BCG0932	10.9	15.5	Regulatory proteins	Possible transcriptional regulatory protein (possibly MarR-family)/Thought to be involved in transcriptional mechanism.	Rv0880
25	BCG1357	5.4	65.1	information pathways	Probable transcription termination factor Rho homolog/Facilitates transcription termination by a mechanism that involves rho binding to the nascent RNA, activation of rho'S RNA-dependent ATPase activity, and release of the mRNA from the DNA template	Rv1297
26	BCG0937	8.7	39.7	conserved hypotheticals	Conserved hypothetical protein/Unknown	Rv0885
27	BCG0788	5.2	19.1	conserved hypotheticals	Conserved protein/Unknown	Rv0738
28	BCG2654c	10	46.2	conserved hypotheticals	Conserved protein/Unknown	Rv2627c
29	BCG0489c *	7.11	105.2	cell wall and cell processes	Probable conserved transmembrane transport protein MmpL4/Unknown. Thought to be involved in fatty acid transport.	Rv0450c
30	*BCG2361; BCG2362*	6.5	89.9	cell wall and cell processes	Probable conserved transmembrane transport protein MmpL9/Unknown. Thought to be involved in fatty acid transport.	Rv2339

	Proteins Observed in fractions from HIV-BCG co-infected cells					
S#	**BCG gene#**	**pI**	**MW (kDa)**	**Functional category**	**Product/Function (Known/probable/annotated)**	**Ortholog in *M.tuberculosis* H37Rv (Rv#)**
1	BCG3770	4.78	70	intermediary metabolism and respiration	2-isopropylmalate synthase LeuA/Involved in leucine biosynthesis (at the first step)	Rv3710
2	BCG3025c	6.5	66	intermediary metabolism and respiration	Acetolactate synthase (large subunit) IlvB1/Involved in valine and isoleucine biosynthesis (at the first step)	Rv3003c
3	BCG0626	10.5	7.5	virulence, detoxification, adaptation	Possible antitoxin VapB26/Unknown	Rv0581
4	BCG0391	8.2	41.3	virulence, detoxification, adaptation	Probable chaperone protein DnaJ1/Acts as a co-chaperone.	Rv0352
5	BCG2216c	7.97	40.4	intermediary metabolism and respiration	Probable transmembrane cytochrome C oxidase (subunit II) CtaC/Involved in aerobic respiration.	Rv2200c
6	BCG3007c	12.4	22.1	Information pathways	DNA-binding protein HU homolog HupB (histone-like protein)/This protein belongs to the histone like family of prokaryotic DNA-binding proteins which are capable of wrapping DNA to stabilize it, and prevent its denaturation under extreme environmental conditions.	Rv2986c
7	BCG0006; BCG0036	5.2	92.2	Information pathways	DNA gyrase (subunit A) GyrA	Rv0006c
8	BCG3932	7.7	51	cell wall and cell processes	ESX conserved component EccB1/Unknown.	Rv3869
9	BCG0332*	10.5	35.9	cell wall and cell processes	ESX conserved component EccE3. ESX-3 type VII secretion system protein/Unknown.	Rv0292

10	BCG3331c	6.7	62	intermediary metabolism and respiration	Probable glycerol-3-phosphate dehydrogenase GlpD2/Involved in aerobic respiration and oxidation of glycerol.	Rv3302c
11	BCG3470	5.6	87	intermediary metabolism and respiration	Conserved protein/Function unknown; probably enzyme involved in cellular metabolism.	Rv3401
12	BCG2921c	7.7	84.5	intermediary metabolism and respiration	Possible formate dehydrogenase H FdhF/Decomposes formic acid to hydrogen and carbon dioxide under anaerobic conditions in the absence of exogenous electron acceptors	Rv2900c
13	BCG0535c	7.3	35.5	conserved hypotheticals	Conserved protein/Function Unknown.	Rv0493c
14	BCG2433c	6.5	28.4	conserved hypotheticals	Conserved protein/Function Unknown.	Rv2417c
15	BCG1633*	6.7	53.7	intermediary metabolism and respiration	Probable L-aspartate oxidase NadB/Quinolinate biosynthesis.	Rv1595
16	BCG1872c	4.8	80.4	intermediary metabolism and respiration	Malate synthase G GlcB/Involved in glyoxylate bypass (second step), an alternative to the tricarboxylic acid cycle	Rv1837c
17	BCG1689	4.9	88	information pathways	Probable phenylalanyl-tRNA synthetase, beta chain PheT/Charging PHE-tRNA	Rv1650
18	BCG0447	5.04	72.9	intermediary metabolism and respiration	Probable phosphate acetyltransferase Pta/Involved at the last step (of two) in the conversion of acetate to acetyl-CoA	Rv0408
19	BCG2957*	5.5	158	lipid metabolism	Phenolpthiocerol synthesis type-I polyketide synthase PpsE/Involved in phenolpthiocerol and phthiocerol dimycocerosate (dim) biosynthesis:	Rv2935
20	BCG1855	5.7	57.2	intermediary metabolism	Probable acetolactate synthase IlvG/Valine and	Rv1820

				and respiration	isoleucine biosynthesis (first step).	
21	BCG3661c	5.6	93.5	intermediary metabolism and respiration	Probable ATP-dependent protease ATP-binding subunit ClpC1/Hydrolyses proteins in presence of ATP.	Rv3596c
22	BCG3299	7.4	76.5	cell wall and cell processes	Probable metal cation-transporting P-type ATPase C CtpC/Metal cation-transporting ATPase	Rv3270
23	BCG0957	6.3	26	lipid metabolism	Possible enoyl-CoA hydratase EchA6/Could possibly oxidize fatty acids using specific components	Rv0905
24	BCG0976c	10.7	44.9	cell wall and cell processes	Divalent cation-transport integral membrane protein MntH (BRAMP)/H(+)-stimulated, highly selective, divalent cation uptake system.	Rv0924c
25	BCG2596	6.5	28.1	conserved hypotheticals	Conserved protein/Function Unknown.	Rv2573
26	BCG3443	9.7	48.8	lipid metabolism	Possible triacylglycerol synthase/May be involved in synthesis of triacylglycerol	Rv3371
27	BCG0992	7.8	83.5	Information pathways	ATP dependent DNA ligase LigD/Involved in DNA double-strand break repair, by non-homologous end joining (NHEJ).	Rv0938
28	BCG1479	8.4	24.2	cell wall and cell processes	Probable lipoprotein LprH/Function Unknown	Rv1418
29	BCG1655	5.3	50.5	intermediary metabolism and respiration	Probable pyruvate kinase PykA/Produces phosphoenol pyruvate in glycolysis	Rv1617
30	BCG2858c	5.3	18.9	information pathways	Probable ribosome-binding factor a RbfA/Associates with free 30S ribosomal subunits (but not with 30S subunits that are part of 70S ribosomes or polysomes).	Rv2838c
31	BCG2870c	8.5	66.9	intermediary metabolism and respiration	Possible magnesium chelatase/Function unknown; possibly introduces a magnesium ion	Rv2850c

					into specific substrate/compound.	
32	BCG1671	4.7	78	information pathways	Probable excinuclease ABC (subunit B - helicase) UvrB/Involved in nucleotide excision repair.	Rv1633
33	BCG1667	4.78	98.4	information pathways	Probable DNA polymerase I PolA/Involved in post-incision events.	Rv1629
34	BCG3633c	5.96	33.58	intermediary metabolism and respiration	3,4-DHSA dioxygenase/Catalyzes the extradiol cleavage of 3,4-dihydroxy-9,10-seconandrost-1,3,5(10)-triene-9,17-dione (3,4-DHSA)	Rv3568c
35	BCG1816	5.1	152.8	cell wall and cell processes	ESX conserved component EccC5. ESX-5 type VII secretion system protein/Function Unknown	Rv1783
36	BCG2636c *	8.96	35.16	lipid metabolism	Probable acyltransferase/Catalyzes the acylation of the 6-position of the mannose residue linked to position 2 of the myo-inositol in phosphatylinositol mono- and DI-mannosides.	Rv2611c
37	BCG3639	9.4	21.9	regulatory proteins	Transcriptional regulatory protein KstR (probably TetR-family)/Involved in transcriptional mechanism. Predicted to control regulon involved in lipid metabolism.	Rv3574
38	BCG2891c	8.69	42.9	cell wall and cell processes	Membrane bound metalloprotease/Controls membrane composition	Rv2869c
39	BCG0602	10.63	41.24	lipid metabolism	Mannosyltransferase MgtA/Involved in lipomannan (LM) biosynthesis	Rv0557

40	BCG0733	4.69	77.20	Information pathways	Probable elongation factor G FusA1 (EF-G)/This protein promotes the GTP-dependent translocation of the nascent protein chain from the A-site to the P-site of the ribosome.	Rv0684
	Proteins Observed in fractions from both mono- and co-infected cells					
S#	**BCG gene#**	**pI**	**MW (kDa)**	**Functional category**	**Product/Function (Known/probable/annotated)**	**Ortholog in *M.tuberculosis* H37Rv (Rv#)**
1	BCG1389c	5.3	78.6	intermediary metabolism and respiration	Unknown; probably involved in polysaccharide degradation	Rv1327c
2	BCG1368	4.7	59.2	intermediary metabolism and respiration	Probable ATP synthase alpha chain AtpA	Rv1308
3	BCG1370	4.5	53.09	intermediary metabolism and respiration	Probable ATP synthase beta chain AtpD	Rv1310
4	BCG1627	4.4	37.5	intermediary metabolism and respiration	Probable biotin synthetase BioB/ Involved in biotin synthesis.	Rv1589
5	BCG0389	4.5	66.8	virulence, detoxification, adaptation	Probable chaperone protein DnaK (heat shock protein 70)/Acts as chaperone	Rv0350
6	BCG2562c	6.5	41.7	intermediary metabolism and respiration	Probable chorismate synthase AroF/Involved in the synthesis of chorismate	Rv2540c
7	BCG2944c	4.9	130.6	cell wall and cell processes	Probable chromosome partition protein Smc/Plays an important role in chromosome structure and partitioning	Rv2922c
8	BCG0717	6	146.7	information pathways	DNA-directed RNA polymerase (beta' chain) RpoC	Rv0668
9	BCG0716	4.67	129.2	information pathways	DNA-directed RNA polymerase (beta chain) RpoB	Rv0667

10	BCG3940c	10.6	57.6	cell wall and cell processes	ESX conserved component EccE2. ESX-2 type VII secretion system protein/Function unknown	Rv3885
11	BCG0946	7.2	42.7	Regulatory proteins	Possible transcriptional regulatory protein (possibly LuxR-family)/Thought to be involved in transcriptional mechanism.	Rv0894
12	BCG2301c; BCG2302c	6.3	25.4	conserved hypotheticals	Possible membrane protein/Unknown	Rv2286c
13	BCG2962c *	4.8	224	lipid metabolism	Probable multifunctional mycocerosic acid synthase membrane-associated Mas/Catalyzes the elongation of N-fatty acyl-CoA with methylamalonyl-CoA (not malonyl-CoA) as the elongating agent to form mycocerosyl lipids	Rv2940c
14	BCG1539	9.3	49.8	virulence, detoxification , adaptation	Peptidoglycan hydrolase/Unknown	Rv1477
15	BCG2953	5	198.8	lipid metabolism	Phenolpthiocerol synthesis type-I polyketide synthase PpsA/Involved in phenolpthiocerol and phthiocerol dimycocerosate (dim) biosynthesis	Rv2931
16	BCG2112c	7.4	99.57	information pathways	ATP-dependent DNA helicase HelY/DNA helicase activity	Rv2092c
17	Mb2007c	9.3	32.8	Regulatory proteins	Probable transcriptional regulatory protein (probably LysR-family)/Involved in transcriptional mechanism.	Rv1985c
18	BCG1085c	5.8	92.7	Regulatory proteins	Probable sensor protein KdpD/Member of the two-component regulatory system KDPD/KDPE involved in the regulation of the KDP operon.	Rv1028
19	BCG0123	10.6	27.8	cell wall and cell processes	Possible membrane protein/Unknown	Rv0090
20	BCG1550	6.1	41.2	cell wall and cell processes	Possible exported conserved protein/Unknown	Rv1488

21	BCG3215c	9.2	107.4	cell wall and cell processes	Probable conserved transmembrane protein/Unknown	Rv3193c
22	BCG2500c	8.7	88.2	lipid metabolism	Probable glycerol-3-phosphate acyltransferase PlsB2/Involved in phospholipid biosynthesis	Rv2482c

Annexure VIII: The host proteins identified by iTRAQ based LC-MS/MS from the phagosome enriched fractions of H37Rv mono- and HIV-H37Rv co-infected cells. Fractions from H37Rv infected cell was labeled with 116 isobar and fractions from HIV-H37Rv co-infected cells was labeled with 121 isobar. The ratio of 116:121 representing H37Rv vs HIV-H37Rv gives the quantification of proteins between the conditions.

S#	% Sequence Coverage	Accession #_String	Name	Species	Peptides (95%)	116:121
1	79.7	Q60FE2	MYH9 variant protein	HUMAN	260	0.8472
2	61.7	Q9Y490	Talin-1	HUMAN	85	0.7943
3	45.5	Q14204	Cytoplasmic dynein 1 heavy chain 1	HUMAN	68	0.6486
4	92.5	P10809	60 kDa heat shock protein, mitochondrial	HUMAN	113	0.2655
5	90.5	P26038	Moesin	HUMAN	79	1.5276
6	92.3	P14618	Pyruvate kinase PKM	HUMAN	76	1.9055
7	92.3	P08670	Vimentin	HUMAN	90	0.263
8	91.4	Q01518	Adenylyl cyclase-associated protein	HUMAN	110	0.8954
9	43.3	Q15149	Isoform 7 of Plectin	HUMAN	41	0.9204
10	97.6	Q1KLZ0	HCG15971, isoform CRA_a	HUMAN	108	0.8872
11	84.4	P38646	Stress-70 protein, mitochondrial	HUMAN	58	0.3802
12	84.5	P25705	ATP synthase subunit alpha, mitochondrial	HUMAN	70	0.8091
13	76.8	P11021	78 kDa glucose-regulated protein	HUMAN	51	1
14	75.6	Q9Y6N5	Sulfide:quinone oxidoreductase, mitochondrial	HUMAN	51	1.1482
15	87.2	P06576	ATP synthase subunit beta, mitochondrial	HUMAN	69	0.3311
16	83.3	P07237	Protein disulfide-isomerase	HUMAN	38	0.7943
17	83.8	P07355	Isoform 2 of Annexin A2	HUMAN	39	0.4325
18	55.9	Q5CAQ5	Tumor rejection antigen (Gp96) 1	HUMAN	29	0.879
19	50.6	P15144	Aminopeptidase N	HUMAN	38	0.6855
20	49.1	A4QPB0	IQ motif containing GTPase activating protein 1	HUMAN	29	0.9817
21	68.5	P30101	Protein disulfide-isomerase A3	HUMAN	30	0.5248
22	60.2	Q6PJ75	Integrin beta (Fragment)	HUMAN	39	0.3802
23	74.9	Q6IPT9	Elongation factor 1-alpha	HUMAN	67	0.6081
24	71.8	P04075	Isoform 2 of Fructose-bisphosphate aldolase A	HUMAN	36	0.7047
25	65.7	P13639	Elongation factor 2	HUMAN	31	0.9036
26	82	P40926	Malate dehydrogenase, mitochondrial	HUMAN	49	0.673

27	80.8	P34897	Serine hydroxymethyltransferase, mitochondrial	HUMAN	35	0.6194
28	73.4	Q6NVC0	SLC25A5 protein (Fragment)	HUMAN	34	1.1695
29	50	P36776	Lon protease homolog, mitochondrial	HUMAN	24	0.4699
30	59.7	P00367	Epididymis tissue sperm binding protein Li 18mP	HUMAN	32	0.6668
31	64.6	P55084	Trifunctional enzyme subunit beta, mitochondrial	HUMAN	28	0.9036
32	61.8	Q53YD7	EEF1G protein	HUMAN	33	0.4446
33	56.3	P07339	Cathepsin D	HUMAN	42	0.5105
34	60.6	P13796	Plastin-2	HUMAN	24	0.3467
35	75.2	P49411	Elongation factor Tu, mitochondrial	HUMAN	26	0.5152
36	66.1	P48735	Isocitrate dehydrogenase [NADP], mitochondrial	HUMAN	23	0.2489
37	53.2	B4DGL0	cDNA FLJ53619, highly similar to Heat shock protein HSP 90-beta	HUMAN	27	1.2706
38	83.9	P06733	Alpha-enolase	HUMAN	23	1.0965
39	59.2	P11142	Heat shock cognate 71 kDa protein	HUMAN	28	0.7112
40	88.4	Q53G71	Calreticulin variant (Fragment)	HUMAN	34	0.879
41	62.9	B9A067	Mitochondrial inner membrane protein	HUMAN	16	0.3048
42	61.3	P04843	Dolichyl-diphosphooligosaccharide protein glycosyltransferase subunit 1	HUMAN	23	0.871
43	79.1	P21796	Voltage-dependent anion-selective channel protein 1	HUMAN	29	2.8054
44	62.6	B7Z452	Long-chain-fatty-acid--CoA ligase 1	HUMAN	23	0.3342
45	38.4	P05023	Sodium/potassium-transporting ATPase subunit alpha-1	HUMAN	21	1.2023
46	58.7	Q86UX7	Isoform 2 of Fermitin family homolog 3	HUMAN	23	0.7943
47	51.5	P12814	Alpha-actinin-1	HUMAN	19	0.1871
48	94.6	P62937	Peptidyl-prolyl cis-trans isomerase A	HUMAN	27	1.1482
49	57.7	O75390	Citrate synthase, mitochondrial	HUMAN	27	0.3837
50	60.1	P25311	Zinc-alpha-2-glycoprotein	HUMAN	29	1.4723
51	89.7	P54819	Adenylate kinase 2, mitochondrial	HUMAN	27	0.4246
52	63.5	Q59GY2	Ribosomal protein L4 variant (Fragment)	HUMAN	19	1.0765
53	93.2	P30405	Peptidyl-prolyl cis-trans isomerase F, mitochondrial	HUMAN	29	0.3076
54	38.7	Q2TB59	Nicotinamide nucleotide transhydrogenase	HUMAN	17	0.5702
55	55.4	P31930	Cytochrome b-c1 complex subunit 1, mitochondrial	HUMAN	25	0.7447
56	81.3	Q99623	Prohibitin-2	HUMAN	18	1.0864
57	35.8	O75844	CAAX prenyl protease 1 homolog	HUMAN	18	2.3121
58	40.1	Q9Y4L1	Hypoxia up-regulated protein 1	HUMAN	18	1.0471
59	86	P04406	Glyceraldehyde-3-phosphate dehydrogenase	HUMAN	29	0.52

60	99.6	P04179	Superoxide dismutase [Mn], mitochondrial	HUMAN	39	0.3192
61	36.3	Q14697	Isoform 2 of Neutral alpha-glucosidase AB	HUMAN	13	1.1272
62	79.6	P23284	Peptidyl-prolyl cis-trans isomerase B	HUMAN	20	1.9588
63	88	P61224	Ras-related protein Rap-1b	HUMAN	24	0.3908
64	58.2	B2R659	cDNA, FLJ92803, highly similar to Homo sapiens hydroxysteroid (17-beta) dehydrogenase 4 (HSD17B4), mRNA	HUMAN	17	0.7047
65	55.2	Q5SU16	Beta 5-tubulin	HUMAN	19	0.929
66	96.1	P61604	10 kDa heat shock protein, mitochondrial	HUMAN	18	0.3076
67	62.1	P09622	Dihydrolipoyl dehydrogenase, mitochondrial	HUMAN	21	0.5152
68	72.1	P13804	Electron transfer flavoprotein subunit alpha, mitochondrial	HUMAN	17	0.2051
69	33.6	P16615	Sarcoplasmic/endoplasmic reticulum calcium ATPase 2	HUMAN	15	0.6792
70	62.9	Q8NCF7	cDNA FLJ90278 fis, clone NT2RP1000325, highly similar to Phosphate carrier protein, mitochondrial precursor	HUMAN	19	0.631
71	66.3	Q06830	Peroxiredoxin-1	HUMAN	15	0.6486
72	60.6	B4DGP8	Calnexin	HUMAN	17	0.6427
73	48.4	B7ZB41	cDNA, FLJ79405, highly similar to Homo sapiens solute carrier family 25, member 24, transcript variant 1, mRNA	HUMAN	19	0.2938
74	67.7	Q8TAS0	ATP synthase subunit gamma (Fragment)	HUMAN	17	0.6427
75	68.9	P21281	V-type proton ATPase subunit B, brain isoform	HUMAN	16	0.7112
76	34.7	Q02218	2-oxoglutarate dehydrogenase, mitochondrial	HUMAN	14	0.5445
77	54.7	P30048	Thioredoxin-dependent peroxide reductase, mitochondrial	HUMAN	18	0.4831
78	53.9	Q15084	Protein disulfide-isomerase A6	HUMAN	20	2.3335
79	52.6	P23786	Carnitine O-palmitoyltransferase 2, mitochondrial	HUMAN	12	0.5395
80	52.8	Q53EM5	Transketolase variant (Fragment)	HUMAN	14	0.9462
81	44.5	O00754	Isoform 2 of Lysosomal alpha-mannosidase	HUMAN	18	0.9908
82	83.1	O14950	Myosin regulatory light chain 12B	HUMAN	17	0.6982
83	52.3	Q16836	Isoform 2 of Hydroxyacyl-coenzyme A dehydrogenase, mitochondrial	HUMAN	18	1.5136
84	61.4	P22695	Cytochrome b-c1 complex subunit 2, mitochondrial	HUMAN	22	0.3467
85	32.5	O94804	Serine/threonine-protein kinase 10	HUMAN	14	0.9462

86	54.4	P49748	Isoform 3 of Very long-chain specific acyl-CoA dehydrogenase, mitochondrial	HUMAN	10	1.3677
87	67.2	P61158	Actin-related protein 3	HUMAN	16	0.3802
88	49.8	Q5T4U5	Acyl-Coenzyme A dehydrogenase, C-4 to C-12 straight chain, isoform CRA_a	HUMAN	19	1.4191
89	55.2	Q16698	2,4-dienoyl-CoA reductase, mitochondrial	HUMAN	15	0.7244
90	49.7	P23368	NAD-dependent malic enzyme, mitochondrial	HUMAN	15	0.6855
91	54.9	P00558	Phosphoglycerate kinase 1	HUMAN	12	1.0965
92	53.6	B2R5U3	EH-domain containing 1, isoform CRA_b	HUMAN	12	0.2228
93	68	Q9H9B4	Sideroflexin-1	HUMAN	12	4.1305
94	66.5	P06753	Isoform 2 of Tropomyosin alpha-3 chain	HUMAN	12	0.912
95	51	Q8TAF6	Acyl-CoA synthetase 4	HUMAN	9	0.5702
96	74.1	B1ANK7	Fumarate hydratase, isoform CRA_c	HUMAN	11	0.4246
97	41.3	P36957	Dihydrolipoyl lysine-residue succinyl transferase component of 2-oxoglutarate dehydrogenase complex, mitochondrial	HUMAN	12	0.4786
98	82	O75947	ATP synthase subunit d, mitochondrial	HUMAN	14	0.6982
99	49.7	P50440	Glycine amidino transferase, mitochondrial	HUMAN	14	0.5058
100	42.7	P31146	Coronin-1A	HUMAN	11	0.5598
101	66.7	E9PK25	Cofilin-1	HUMAN	12	0.9727
102	47.1	Q9NVI7	Isoform 2 of ATPase family AAA domain-containing protein 3A	HUMAN	13	0.3532
103	63.1	P30084	Enoyl-CoA hydratase, mitochondrial	HUMAN	12	0.3597
104	35.6	Q59FD4	Hexokinase 1 isoform HKI variant (Fragment)	HUMAN	9	0.4169
105	60.7	P24752	Acetyl-CoA acetyltransferase, mitochondrial	HUMAN	11	0.597
106	40.6	P08195	4F2 cell-surface antigen heavy chain	HUMAN	10	0.5297
107	44.9	O95831	Apoptosis-inducing factor 1, mitochondrial	HUMAN	11	1.5417
108	27.9	Q00610	Clathrin heavy chain 1	HUMAN	9	1.1588
109	51.4	P55072	Transitional endoplasmic reticulum ATPase	HUMAN	11	1.1803
110	49.1	Q6NUK7	LYN protein (Fragment)	HUMAN	9	2.729
111	46.6	P07858	Cathepsin B	HUMAN	11	0.3133
112	44.4	P00505	Aspartate aminotransferase, mitochondrial	HUMAN	10	1.0186
113	57.6	P61160	Isoform 2 of Actin-related protein 2	HUMAN	13	0.6792
114	53	Q53G55	TNF receptor-associated protein 1 variant (Fragment)	HUMAN	12	1.9588
115	44.7	B4DZ87	cDNA FLJ57240, highly similar to Mitochondrial proteins import receptor	HUMAN	11	0.4365
116	85.5	P60660	Myosin light polypeptide 6	HUMAN	23	0.4571

117	35.2	P50570	Isoform 4 of Dynamin-2	HUMAN	12	0.4831
118	69.1	P00387	NADH-cytochrome b5 reductase 3	HUMAN	11	1.0666
119	39.9	B7Z6N2	cDNA FLJ56154, highly similar to Gelsolin	HUMAN	9	1.4322
120	22.8	P08575	Receptor-type tyrosine-protein phosphatase C	HUMAN	10	2.0701
121	71.4	Q9UJZ1	Stomatin-like protein 2, mitochondrial	HUMAN	12	0.5012
122	75.6	P48047	ATP synthase subunit O, mitochondrial	HUMAN	11	0.7727
123	32.8	B4DQJ8	6-phosphogluconate dehydrogenase, decarboxylating	HUMAN	9	0.9817
124	53.4	P49753	Acyl-coenzyme A thioesterase 2, mitochondrial	HUMAN	8	1.2942
125	49.7	O43707	Alpha-actinin-4	HUMAN	18	0.3597
126	43.4	Q6IB91	PCK2 protein	HUMAN	7	0.2535
127	64.1	P18124	60S ribosomal protein L7	HUMAN	10	0.8872
128	56.8	Q6NUR7	Ezrin	HUMAN	25	0.7798
129	42.4	A8K1Z2	cDNA FLJ78475, highly similar to Homo sapiens glycerol-3-phosphate dehydrogenase 2 (mitochondrial) (GPD2), mRNA	HUMAN	10	1.0093
130	39.2	Q9NSE4	Isoleucine--tRNA ligase, mitochondrial	HUMAN	7	0.5297
131	37.7	Q86YI5	Dihydrolipoamide S-acetyltransferase	HUMAN	8	0.4699
132	47.3	A8K4Z4	cDNA FLJ75549, highly similar to Homo sapiens ribosomal protein, large, P0 (RPLP0), transcript variant 1, mRNA	HUMAN	10	0.5861
133	64.7	A8K766	cDNA FLJ77343, highly similar to Homo sapiens electron-transfer-flavoprotein, beta polypeptide(ETFB), mRNA	HUMAN	8	1.0965
134	48.8	A7MAP1	Coronin	HUMAN	12	1.4997
135	58.8	P50897	Palmitoyl-protein thioesterase 1	HUMAN	17	0.5152
136	40.3	P13667	Protein disulfide-isomerase A4	HUMAN	11	1.0666
137	36.7	Q8TA92	Similar to AFG3 ATPase family gene 3-like 2 (Yeast) (Fragment)	HUMAN	9	0.7943
138	68.7	P63104	14-3-3 protein zeta/delta (Fragment)	HUMAN	11	1.2023
139	45	O00429	Dynamin 1-like, isoform CRA_c	HUMAN	8	0.5248
140	29.6	Q8NBJ5	Procollagen galactosyltransferase 1	HUMAN	9	0.5649
141	38.3	Q00653	Isoform 4 of Nuclear factor NF-kappa-B p100 subunit	HUMAN	8	0.413
142	80.8	P62158	Calmodulin (Fragment)	HUMAN	14	0.673
143	55.8	Q13011	Delta(3,5)-Delta(2,4)-dienoyl-CoA isomerase, mitochondrial	HUMAN	14	0.8872
144	41.6	Q9H7G6	cDNA: FLJ20897 fis, clone ADKA03573	HUMAN	15	0.7178
145	40.4	B3KT06	cDNA FLJ37398 fis, clone BRAMY2027467, highly similar to Tubulin alpha-ubiquitous chain	HUMAN	15	1.1588

146	41.7	O95202	LETM1 and EF-hand domain-containing protein 1, mitochondrial	HUMAN	8	0.863
147	40.6	O60313	Mitochondrial dynamin-like 120 kDa protein	HUMAN	11	0.9817
148	69.4	Q6IBS9	HADH2 protein	HUMAN	11	0.4406
149	58.2	P11177	Pyruvate dehydrogenase E1 component subunit beta, mitochondrial	HUMAN	10	1.3305
150	55.1	A8K4W2	cDNA FLJ78635, highly similar to Homo sapiens ATP synthase, H+ transporting, mitochondrial F0 complex, subunit b, isoform 1 (ATP5F1), transcript variant 1, mRNA	HUMAN	12	3.281
151	49.9	P08574	Cytochrome c1, heme protein, mitochondrial	HUMAN	17	0.4246
152	33.4	O94925	Isoform 3 of Glutaminase kidney isoform, mitochondrial	HUMAN	7	1.0568
153	51.5	O94905	Erlin-2 (Fragment)	HUMAN	7	2.1281
154	64.2	P21964	Catechol O-methyltransferase	HUMAN	8	0.9376
155	51.9	Q5NKV8	Intercellular adhesion molecule 1	HUMAN	9	0.8166
156	70.3	Q6F3I9	MHC class I antigen (Fragment)	HUMAN	12	1.5276
157	54.4	B4DRS6	cDNA FLJ58980, highly similar to Sideroflexin-3	HUMAN	16	0.9727
158	61.8	P45880	Isoform 1 of Voltage-dependent anion-selective channel protein 2	HUMAN	11	0.4529
159	48.3	P20592	Interferon-induced GTP-binding protein Mx2	HUMAN	8	0.9638
160	83	Q59EI9	ADP,ATP carrier protein, liver isoform T2 variant (Fragment)	HUMAN	35	0.3532
161	49.1	B3KM34	cDNA FLJ10132 fis, clone HEMBA1003046, highly similar to Mitochondrial-processing peptidase subunit beta, mitochondrial (EC 3.4.24.64)	HUMAN	8	0.8395
162	65.9	Q02878	60S ribosomal protein L6 (Fragment)	HUMAN	7	1.0666
163	34.8	P46459	Vesicle-fusing ATPase	HUMAN	8	2.208
164	37.1	P53007	Plasma membrane citrate carrier	HUMAN	6	0.631
165	57.6	Q6ICQ8	ARHG protein (Fragment)	HUMAN	10	1.5996
166	49	P00338	Isoform 3 of L-lactate dehydrogenase A chain	HUMAN	8	0.879
167	61.8	P51149	Ras-related protein Rab-7a	HUMAN	9	2.0324
168	29.1	P42224	Signal transducer and activator of transcription 1-alpha/beta	HUMAN	6	1.2134
169	32.7	B7Z1R5	V-type proton ATPase catalytic subunit A	HUMAN	8	0.631
170	49	P04181	Ornithine aminotransferase, mitochondrial	HUMAN	8	0.3532
171	54.2	A2RUM7	Ribosomal protein L5	HUMAN	10	0.6026
172	72.7	P30050	60S ribosomal protein L12	HUMAN	8	1.3305

173	50.5	A8K3Q9	cDNA FLJ76611, highly similar to Homo sapiens ribosomal protein L14 (RPL14), mRNA	HUMAN	5	0.9638
174	76	P20674	Cytochrome c oxidase subunit 5A, mitochondrial	HUMAN	10	0.3802
175	52.6	O75396	Vesicle-trafficking protein SEC22b	HUMAN	9	0.5754
176	22.2	Q9BSJ8	Extended synaptotagmin-1	HUMAN	8	1.0666
177	70.4	B2R7W0	cDNA, FLJ93628, Homo sapiens methylene tetrahydrofolate dehydrogenase (NAD+dependent), methenyl tetrahydrofolate cyclohydrolase (MTHFD2),nuclear gene encoding mitochondrial protein, mRNA	HUMAN	9	1.0666
178	52	Q15019	Isoform 2 of Septin-2	HUMAN	7	0.7798
179	44.2	O15533	Tapasin	HUMAN	7	2.6062
180	22.7	B0V043	Valine--tRNA ligase	HUMAN	9	1.3062
181	32.9	P11498	Pyruvate carboxylase, mitochondrial	HUMAN	7	0.2291
182	36.8	B7ZAF6	Succinate-CoA ligase, ADP-forming, beta subunit, isoform CRA_d	HUMAN	6	1.0666
183	46.8	P50552	Vasodilator-stimulated phosphoprotein	HUMAN	9	0.4613
184	58.5	Q92930	Ras-related protein Rab-8B	HUMAN	7	1.2474
185	76.2	P99999	Cytochrome c	HUMAN	10	2.2699
186	46.5	Q54A51	Basigin (Ok blood group), isoform CRA_a	HUMAN	7	0.6792
187	41.1	Q9BTT5	Similar to NADH dehydrogenase (Ubiquinone) 1 alpha subcomplex, 9 (39kD) (Fragment)	HUMAN	6	0.5495
188	54.1	P12273	Prolactin-inducible protein	HUMAN	8	4.2462
189	62.8	A8K651	cDNA FLJ75700, highly similar to Homo sapiens complement component 1, q subcomponent binding protein (C1QBP), nuclear gene encoding mitochondrial protein, mRNA	HUMAN	8	0.4365
190	42.6	Q59H77	Chaperonin containing TCP1, subunit 3 (Gamma) variant (Fragment)	HUMAN	6	1.0471
191	55.3	P62424	60S ribosomal protein L7a	HUMAN	5	1.0471
192	64.2	O15511	Actin-related protein 2/3 complex subunit 5	HUMAN	8	1.0186
193	29.7	B4DTU7	cDNA FLJ52076, highly similar to Homo sapiens aldehyde dehydrogenase 1 family, member L2 (ALDH1L2), mRNA	HUMAN	7	1.2823
194	54	P08567	Pleckstrin	HUMAN	7	0.7943
195	70.6	P62081	40S ribosomal protein S7	HUMAN	7	5.1051
196	40.9	C9JF17	Apolipoprotein D (Fragment)	HUMAN	12	1.4588
197	27.6	O95782	AP-2 complex subunit alpha-1	HUMAN	5	3.5318

198	27.5	P20020	Plasma membrane calcium-transporting ATPase 1	HUMAN	6	0.4742
199	59	Q53R19	Actin related protein 2/3 complex, subunit 2, 34kDa, isoform CRA_a	HUMAN	7	1.0965
200	53.4	B3KNP8	cDNA FLJ30111 fis, clone BNGH42000360, highly similar to 3-ketoacyl-CoA thiolase, mitochondrial (EC 2.3.1.16)	HUMAN	5	0.8017
201	39.7	P08559	Isoform 4 of Pyruvate dehydrogenase E1 component subunit alpha, somatic form, mitochondrial	HUMAN	6	1.1482
202	48.5	A8K7F6	cDNA FLJ78244, highly similar to Homo sapiens eukaryotic translation initiation factor 4A, isoform 1 (EIF4A1), mRNA	HUMAN	7	1.3305
203	38.6	P22307	Isoform 7 of Non-specific lipid-transfer protein	HUMAN	7	0.8395
204	35.8	Q59GW8	Succinate dehydrogenase complex, subunit A, flavoprotein variant (Fragment)	HUMAN	9	0.1923
205	67.2	Q99497	Protein DJ-1	HUMAN	5	0.2109
206	57.3	A4D2P1	Ras-related C3 botulinum toxin substrate 1 (Rho family, small GTP binding protein Rac1)	HUMAN	7	0.4093
207	37	Q13418	Integrin-linked protein kinase	HUMAN	7	0.4018
208	45.8	Q4GQP0	Cytochrome c oxidase subunit 2	HUMAN	7	0.7516
209	62.5	P04899	Guanine nucleotide-binding protein G(i) subunit alpha-2	HUMAN	8	1.1803
210	35.1	P25774	Cathepsin S	HUMAN	5	0.7379
211	33.1	P08758	Annexin A5	HUMAN	7	1.028
212	69.8	P10606	Cytochrome c oxidase subunit 5B, mitochondrial	HUMAN	6	0.2938
213	61.9	P00918	Carbonic anhydrase 2	HUMAN	5	2.6546
214	43.1	Q9H223	EH domain-containing protein 4	HUMAN	6	1.888
215	42.7	P50991	T-complex protein 1 subunit delta	HUMAN	7	0.871
216	46.7	P39023	60S ribosomal protein L3	HUMAN	5	0.3162
217	72.1	P14927	Cytochrome b-c1 complex subunit 7	HUMAN	5	0.2831
218	78.5	P09382	Galectin-1	HUMAN	6	0.8551
219	60.2	P30040	Endoplasmic reticulum resident protein 29	HUMAN	5	1.2942
220	26.7	Q9NVH1	DnaJ homolog subfamily C member 11	HUMAN	5	40.1791
221	33.1	P04844	Dolichyl-diphosphooligosaccharide--protein glycosyltransferase subunit 2	HUMAN	7	0.9908
222	57.3	P37802	Transgelin-2	HUMAN	8	1.803
223	73.6	P07737	Profilin-1	HUMAN	8	1.9231
224	38.9	Q9Y6C9	Mitochondrial carrier homolog 2	HUMAN	5	0.2679
225	55.8	P47985	Cytochrome b-c1 complex subunit Rieske, mitochondrial	HUMAN	6	1.3062

226	71.6	Q9BTQ7	Similar to ribosomal protein L23 (Fragment)	HUMAN	8	0.929
227	74	O95571	Persulfide dioxygenase ETHE1, mitochondrial	HUMAN	8	0.7656
228	35.3	Q16666	Gamma-interferon-inducible protein 16	HUMAN	7	0.1675
229	29.5	O14561	Acyl carrier protein, mitochondrial	HUMAN	5	0.3342
230	40	Q92947	Glutaryl-CoA dehydrogenase, mitochondrial	HUMAN	6	0.0115
231	68.2	Q9BSQ6	RPL13A protein (Fragment)	HUMAN	6	2.2699
232	65.7	P13073	Cytochrome c oxidase subunit 4 isoform 1, mitochondrial	HUMAN	7	0.8241
233	61.1	Q6NZ55	60S ribosomal protein L13	HUMAN	6	1.0186
234	17.1	P16070	CD44 antigen	HUMAN	5	0.3981
235	27.8	O95466	Isoform 2 of Formin-like protein 1	HUMAN	6	0.879
236	36.6	Q9HCC0	Methylcrotonoyl-CoA carboxylase beta chain, mitochondrial	HUMAN	6	1.0186
237	42.8	P51572	Isoform 2 of B-cell receptor-associated protein 31	HUMAN	5	0.9727
238	36	Q53GF9	Full-length cDNA 5-PRIME end of clone CS0DF013YM24 of Fetal brain of Homo sapiens (Human) variant (Fragment)	HUMAN	7	0.929
239	46.5	B3KQJ0	cDNA FLJ90530 fis, clone NT2RP4002187, highly similar to Homo sapiens hydroxysteroid (17-beta) dehydrogenase 12 (HSD17B12), mRNA	HUMAN	5	5.3951
240	41.3	B4DM63	cDNA FLJ51245, highly similar to Actin-related protein 2/3 complex subunit 3	HUMAN	6	1.3305
241	34.6	Q53FB6	Mitochondrial aldehyde dehydrogenase 2 variant (Fragment)	HUMAN	5	1.0093
242	32.5	Q6IAX9	SRPR protein	HUMAN	5	0.7244
243	37.3	P61586	Transforming protein RhoA	HUMAN	5	1.0186
244	52.9	B2R491	Ribosomal protein S4, X-linked, isoform CRA_c	HUMAN	4	3.3729
245	53.4	P30042	ES1 protein homolog, mitochondrial	HUMAN	4	0.7379
246	48.2	Q96AG4	Leucine-rich repeat-containing protein 59	HUMAN	5	0.7311
247	38.4	P40227	T-complex protein 1 subunit zeta	HUMAN	5	1.1066
248	35.1	Q9NQC3	Isoform 2 of Reticulon-4	HUMAN	6	1.0864
249	45.1	P28838	Cytosol aminopeptidase	HUMAN	4	0.871
250	29.3	Q96RP9	Mitochondrial elongation factor G	HUMAN	8	0.929
251	28.9	O43175	D-3-phosphoglycerate dehydrogenase	HUMAN	4	1.406
252	43.2	Q9BU08	Putative uncharacterized protein (Fragment)	HUMAN	8	0.1585
253	33.1	P14314	Glucosidase 2 subunit beta	HUMAN	5	0.787
254	56.8	Q07020	60S ribosomal protein L18 (Fragment)	HUMAN	4	1.7378
255	37.9	B4DWA6	cDNA FLJ60094, highly similar to F-actin capping protein subunit beta	HUMAN	5	0.6368

256	28.8	Q9P0V8	SLAM family member 8	HUMAN	5	0.5248
257	39.3	Q59E88	DnaJ (Hsp40) homolog, subfamily A, member 3 variant (Fragment)	HUMAN	6	2.9107
258	66.7	B2R4M6	cDNA, FLJ92148, highly similar to Homo sapiens S100 calcium binding protein A9 (calgranulin B) (S100A9), mRNA	HUMAN	5	0.2992
259	31.4	Q5JTV8	Torsin-1A-interacting protein 1	HUMAN	5	1.3932
260	63	P51148	Ras-related protein Rab-5C	HUMAN	11	1.3062
261	30.2	Q13557	Calcium/calmodulin-dependent protein kinase type II subunit delta	HUMAN	4	0.8318
262	54.8	Q9HAV7	GrpE protein homolog 1, mitochondrial	HUMAN	5	1.1912
263	38.9	Q99832	T-complex protein 1 subunit eta	HUMAN	5	1.1912
264	64.8	Q6IB54	ATP synthase-coupling factor 6, mitochondrial	HUMAN	4	0.9462
265	47.5	P50213	Isocitrate dehydrogenase [NAD] subunit alpha, mitochondrial	HUMAN	6	0.912
266	34.6	B4DZZ0	cDNA FLJ52128, highly similar to PRA1 family protein 3	HUMAN	6	0.5495
267	42.8	B4DU58	cDNA FLJ51488, highly similar to Macrophage capping protein	HUMAN	5	1.1482
268	42.9	Q10713	Mitochondrial-processing peptidase subunit alpha	HUMAN	4	0.4169
269	35.4	Q59GB4	Dihydropyrimidinase-like 2 variant (Fragment)	HUMAN	4	1.3804
270	20.1	B2R627	cDNA, FLJ92752, highly similar to Homo sapiens integrin, alpha 5 (fibronectin receptor, alphapolypeptide) (ITGA5), mRNA	HUMAN	5	1.1482
271	86.4	O75964	ATP synthase subunit g, mitochondrial	HUMAN	5	0.5346
272	33.9	Q96II6	NADH dehydrogenase (Ubiquinone) 1 beta subcomplex, 10, 22kDa, isoform CRA_a	HUMAN	4	1.7219
273	39	P39656	Dolichyl-diphosphooligosaccharide--protein glycosyltransferase 48 kDa subunit	HUMAN	4	0.5702
274	33.1	P08571	Monocyte differentiation antigen CD14	HUMAN	5	0.3733
275	50.7	Q53XJ5	Peptidyl-prolyl cis-trans isomerase	HUMAN	4	0.2333
276	54.7	P09669	Cytochrome c oxidase subunit 6C	HUMAN	5	0.3311
277	43.1	P50454	Serpin H1	HUMAN	5	0.6194
278	31.4	Q13740	CD166 antigen	HUMAN	4	1.8197
279	27.7	Q15067	Isoform 2 of Peroxisomal acyl-coenzyme A oxidase 1	HUMAN	4	0.7656
280	33.8	O96008	Mitochondrial import receptor subunit TOM40 homolog	HUMAN	5	0.6668
281	21.7	Q9NZM1	Myoferlin	HUMAN	4	3.5645

282	38.4	Q6IAL5	Putative uncharacterized protein tmp_locus_1	HUMAN	3	1.1588
283	39.2	Q6FGL0	LGALS3 protein (Fragment)	HUMAN	5	2.208
284	28.3	Q5JTZ9	Alanine--tRNA ligase, mitochondrial	HUMAN	4	2.0137
285	54.4	P61106	Ras-related protein Rab-14	HUMAN	8	5.0119
286	26	P20701	Isoform 3 of Integrin alpha-L	HUMAN	4	1.0093
287	20.7	P10253	Lysosomal alpha-glucosidase	HUMAN	7	1.1803
288	20.4	Q8IV08	Phospholipase D3	HUMAN	4	0.6368
289	37.9	Q0VAB1	Translocase of inner mitochondrial membrane 50 homolog (S. cerevisiae)	HUMAN	6	0.5754
290	25.3	Q59GX2	Solute carrier family 2 (Facilitated glucose transporter), member 1 variant (Fragment)	HUMAN	5	0.6081
291	63.9	Q7Z4Y4	GTP:AMP phosphotransferase	HUMAN	4	0.9204
292	68.6	P14854	Cytochrome c oxidase subunit 6B1	HUMAN	5	1.4859
293	54.9	P61247	40S ribosomal protein S3a	HUMAN	4	1.2359
294	47.7	O00560	Syntenin-1	HUMAN	4	0.2704
295	47.1	A4D1N4	Coiled-coil-helix-coiled-coil-helix domain containing 3	HUMAN	3	0.879
296	33.1	P07900	Isoform 2 of Heat shock protein HSP 90-alpha	HUMAN	11	0.929
297	45.3	Q53HU0	Chaperonin containing TCP1, subunit 8 (Theta) variant (Fragment)	HUMAN	3	2.6792
298	49	P61981	14-3-3 protein gamma	HUMAN	8	0.7656
299	59.1	P59998	Actin-related protein 2/3 complex subunit 4	HUMAN	3	1.9588
300	29.5	A2RRH1	Interleukin 4 induced 1	HUMAN	3	0.8091
301	56.8	C9J9K3	40S ribosomal protein SA (Fragment)	HUMAN	4	0.7516
302	62.3	P62888	60S ribosomal protein L30 (Fragment)	HUMAN	4	0.9817
303	43.4	Q9UNF0	Protein kinase C and casein kinase substrate in neurons protein 2	HUMAN	4	0.5346
304	17.5	Q8NF50	Dedicator of cytokinesis protein 8	HUMAN	3	0.7047
305	22.9	Q9BS26	Endoplasmic reticulum resident protein 44	HUMAN	3	0.7516
306	28.4	B4E100	cDNA FLJ61520, highly similar to Amyloid beta A4 protein-bindingfamily B member 1- interacting protein	HUMAN	3	0.7047
307	27.9	Q7L2E3	Putative ATP-dependent RNA helicase DHX30	HUMAN	6	0.5861
308	58.5	Q5U0I6	RAB1A protein	HUMAN	10	1.2134
309	22.5	P36222	Chitinase-3-like protein 1	HUMAN	3	0.8318
310	50.5	P15880	40S ribosomal protein S2	HUMAN	3	0.6982
311	37.7	Q9Y2Z4	Tyrosine--tRNA ligase, mitochondrial	HUMAN	3	0.0832
312	18.1	Q3HY29	Cyclooxygenase 1b2	HUMAN	4	0.863
313	34.2	Q9UL25	Ras-related protein Rab-21	HUMAN	3	0.9817

314	55.2	A8K0T9	cDNA FLJ75422, highly similar to Homo sapiens capping protein (actin filament) muscle Z-line, alpha 1, mRNA	HUMAN	5	0.8017
315	38.8	Q9P0J0	NADH dehydrogenase (Ubiquinone) 1 alpha subcomplex, 13	HUMAN	3	0.5012
316	25.8	Q13409	Isoform 2B of Cytoplasmic dynein 1 intermediate chain 2	HUMAN	3	0.879
317	23.9	P50281	Matrix metalloproteinase 14 (Membrane-inserted)	HUMAN	5	9.2897
318	38.5	P61916	Epididymal secretory protein E1 (Fragment)	HUMAN	5	0.6792
319	38.4	P32119	Peroxiredoxin-2	HUMAN	7	0.863
320	32.6	Q96IH1	Fascin (Fragment)	HUMAN	5	1.2823
321	35.8	Q53GX6	Nucleobindin 1 variant (Fragment)	HUMAN	3	4.0179
322	41.3	O95881	Thioredoxin domain-containing protein 12	HUMAN	3	1.6904
323	32.6	P49821	NADH dehydrogenase (Ubiquinone) flavoprotein 1, 51kDa, isoform CRA_c	HUMAN	3	0.5702
324	40	Q32Q10	RSU1 protein (Fragment)	HUMAN	3	0.4169
325	18.1	Q9BRR6	ADP-dependent glucokinase	HUMAN	3	0.7656
326	23.5	B7Z6S9	cDNA FLJ56157, highly similar to Glucosylceramidase (EC 3.2.1.45)	HUMAN	4	2.3335
327	29.4	Q53GU8	Transforming growth factor, beta-induced, 68kDa variant (Fragment)	HUMAN	3	6.4269
328	35.3	Q53G25	Ribosomal protein S5 variant (Fragment)	HUMAN	3	0.5546
329	13.7	Q6IBK3	SCAMP2 protein	HUMAN	3	0.8166
330	24.4	C9JSL2	Uncharacterized protein	HUMAN	3	0.7656
331	40	Q53EY4	RAB31, member RAS oncogene family variant (Fragment)	HUMAN	4	0.7244
332	44.3	Q96HS1	Serine/threonine-protein phosphatase PGAM5, mitochondrial	HUMAN	4	0.9817
333	34.1	Q14108	Lysosome membrane protein 2	HUMAN	5	0.9204
334	52.8	Q9Y2R0	Cytochrome c oxidase assembly protein 3 homolog, mitochondrial	HUMAN	3	0.4966
335	49	P61026	Ras-related protein Rab-10	HUMAN	8	1.3804
336	15.4	Q8WU79	Stromal membrane-associated protein 2	HUMAN	4	1.6596
337	35.9	B9EKV4	Aldehyde dehydrogenase 9 family, member A1	HUMAN	3	2.0324
338	39.5	P83731	60S ribosomal protein L24	HUMAN	4	3.4995
339	46.2	P60866	40S ribosomal protein S20	HUMAN	3	0.929
340	59.3	P61313	60S ribosomal protein L15	HUMAN	4	3.8019
341	29.8	P06744	Glucose-6-phosphate isomerase	HUMAN	4	1.556
342	20.4	O00186	Syntaxin-binding protein 3	HUMAN	4	1.1912
343	28.3	Q01432	Isoform 3 of AMP deaminase 3	HUMAN	5	1.0568
344	69.2	P07919	Cytochrome b-c1 complex subunit 6, mitochondrial	HUMAN	3	0.3281

345	45.2	P62906	60S ribosomal protein L10a	HUMAN	3	1.2246
346	36.8	Q5U077	L-lactate dehydrogenase	HUMAN	5	0.5445
347	57.6	P35241	Isoform 5 of Radixin	HUMAN	24	1.1695
348	73.8	P30049	ATP synthase subunit delta, mitochondrial	HUMAN	4	0.631
349	24.8	O14773	Tripeptidyl peptidase I, isoform CRA_a	HUMAN	5	0.871
350	20.5	P20292	Arachidonate 5-lipoxygenase-activating protein	HUMAN	4	1.2023
351	42.1	Q9UNX3	60S ribosomal protein L26-like 1	HUMAN	3	1.0375
352	47.5	P46779	60S ribosomal protein L28	HUMAN	3	1.0765
353	31.2	Q9Y305	Acyl-coenzyme A thioesterase 9, mitochondrial	HUMAN	4	0.4018
354	31.9	Q969V3	Nicalin	HUMAN	3	0.2805
355	20.4	Q00722	1-phosphatidylinositol 4,5-bisphosphate phosphodiesterase beta-2	HUMAN	3	1.406
356	45.8	Q96A35	39S ribosomal protein L24, mitochondrial	HUMAN	3	1.3428
357	32.9	P35914	Hydroxymethylglutaryl-CoA lyase, mitochondrial	HUMAN	2	0.4487
358	26.7	Q96TA1	Niban-like protein 1	HUMAN	3	1.6749
359	14.2	P46977	Dolichyl-diphosphooligosaccharide--protein glycosyltransferase subunit STT3A	HUMAN	3	4.7863
360	49.3	P46776	60S ribosomal protein L27a	HUMAN	5	1.6596
361	39.4	A6NI72	Putative neutrophil cytosol factor 1B	HUMAN	4	0.673
362	45.6	Q9P015	39S ribosomal protein L15, mitochondrial	HUMAN	4	1.3804
363	38.1	Q9P0L0	Isoform 2 of Vesicle-associated membrane protein-associated protein A	HUMAN	4	0.1213
364	36.5	Q9HDC9	Adipocyte plasma membrane-associated protein	HUMAN	2	0.4055
365	56.8	P15153	Ras-related C3 botulinum toxin substrate 2	HUMAN	7	1.1482
366	50.3	P62277	40S ribosomal protein S13	HUMAN	2	0.2188
367	60.7	Q53HJ8	PKCI-1-related HIT protein variant (Fragment)	HUMAN	3	0.2249
368	38.7	B2R5V2	Succinyl-CoA:3-ketoacid-coenzyme A transferase	HUMAN	4	1.3804
369	56.2	P20340	Ras-related protein Rab-6A (Fragment)	HUMAN	3	0.413
370	21	Q9UGE8	C1 protein	HUMAN	4	0.5297
371	33.2	P28331	Mitochondrial NADH-ubiquinone oxidoreductase 75 kDa subunit	HUMAN	2	0.2606
372	48.7	P62269	40S ribosomal protein S18	HUMAN	3	1.2706
373	24.7	Q96DR8	Mucin-like protein 1	HUMAN	2	1.7701
374	42.7	A8K878	cDNA FLJ77177, highly similar to Homo sapiens arginine-rich, mutated in early stage tumors (ARMET), mRNA	HUMAN	2	0.3733

375	29.8	Q9H845	Acyl-CoA dehydrogenase family member 9, mitochondrial	HUMAN	3	0.871
376	25.7	Q15942	Zyxin	HUMAN	5	0.5808
377	35	A8K517	Ribosomal protein S23, isoform CRA_a	HUMAN	3	2.0137
378	45.2	Q96DB5	Regulator of microtubule dynamics protein 1	HUMAN	3	1.6293
379	26.3	B7Z809	cDNA FLJ56016, highly similar to C-1-tetrahydrofolate synthase, cytoplasmic	HUMAN	4	0.0802
380	26.1	P22234	Multifunctional protein ADE2	HUMAN	3	2.421
381	16.4	Q5JPE7	Nodal modulator 3	HUMAN	2	0.7798
382	51.3	P62750	60S ribosomal protein L23a	HUMAN	3	0.2421
383	45.7	Q9NX40	OCIA domain-containing protein 1	HUMAN	2	1.1912
384	38.6	Q6IAM7	SPC18 protein	HUMAN	3	0.7516
385	47.2	O60664	Perilipin-3	HUMAN	2	0.7727
386	41.5	P78371	T-complex protein 1 subunit beta	HUMAN	3	1.0765
387	62	Q53G19	Mitochondrial ribosomal protein L11 isoform a variant (Fragment)	HUMAN	3	0.871
388	41.1	P02792	Ferritin light chain	HUMAN	3	0.7311
389	27.1	A8K940	cDNA FLJ77630, highly similar to Homo sapiens BPY2 interacting protein 1, mRNA	HUMAN	3	0.8241
390	55.2	Q16718	NADH dehydrogenase [ubiquinone] 1 alpha subcomplex subunit 5	HUMAN	3	0.1282
391	36.2	Q16181	Septin-7	HUMAN	3	0.787
392	43.5	Q96I99	Succinyl-CoA ligase [GDP-forming] subunit beta, mitochondrial	HUMAN	3	0.3733
393	27.4	P29350	Isoform 4 of Tyrosine-protein phosphatase non-receptor type 6	HUMAN	2	2.5823
394	31.9	Q8NBX0	Saccharopine dehydrogenase-like oxidoreductase	HUMAN	3	1.1695
395	23.7	Q9Y6G9	Cytoplasmic dynein 1 light intermediate chain 1	HUMAN	3	1.4454
396	62.6	P07203	Glutathione peroxidase	HUMAN	4	0.0679
397	24.6	Q9NYU2	UDP-glucose:glycoprotein glucosyltransferase 1	HUMAN	3	0.4831
398	26.1	Q7L0Y3	Mitochondrial ribonuclease P protein 1	HUMAN	2	0.177
399	30.2	Q53HG2	NADH dehydrogenase (Ubiquinone) Fe-S protein 2, 49kDa (NADH-coenzyme Q reductase) variant (Fragment)	HUMAN	4	0.7586
400	38.3	B4DMN1	cDNA FLJ61136, highly similar to Ras-related protein Rab-11A	HUMAN	3	1.4997
401	23.8	Q4LE58	EIF4G1 variant protein (Fragment)	HUMAN	2	1.1912
402	27	Q8NFW8	N-acylneuraminate cytidylyltransferase	HUMAN	2	0.673
403	47.1	P62917	60S ribosomal protein L8	HUMAN	4	1.2134

404	41.1	P06703	Protein S100-A6	HUMAN	2	0.4365
405	29.4	Q86UP2	Kinectin	HUMAN	2	1.1803
406	28.7	P56134	Pentatricopeptide repeat-containing protein 1, mitochondrial	HUMAN	4	0.9376
407	42.7	Q9BYD1	39S ribosomal protein L13, mitochondrial	HUMAN	2	1.3932
408	77.2	P68032	Actin, alpha cardiac muscle 1	HUMAN	61	1.3428
409	84.1	P56385	ATP synthase subunit e, mitochondrial	HUMAN	3	0.0904
410	28.5	B2R4W8	HCG1994130, isoform CRA_a	HUMAN	2	0.5248
411	23.3	B7ZM99	MTHFD1L protein	HUMAN	2	1.1066
412	51.4	Q9Y3U8	60S ribosomal protein L36	HUMAN	3	1.2823
413	32.4	B1PS43	Myosin heavy chain 11 smooth muscle isoform	HUMAN	27	1.1912
414	21.5	P00390	Glutathione reductase, mitochondrial	HUMAN	2	0.5297
415	40.2	Q53XZ9	Isovaleryl Coenzyme A dehydrogenase	HUMAN	2	1.1912
416	15.1	P14780	Matrix metalloproteinase-9	HUMAN	3	0.5395
417	31.7	P26447	Protein S100-A4	HUMAN	2	0.9462
418	37.1	Q6IS14	Eukaryotic translation initiation factor 5A-1	HUMAN	3	0.4093
419	22.6	P15586	N-acetylglucosamine-6-sulfatase	HUMAN	4	1.4723
420	16.8	Q9BR76	Coronin-1B	HUMAN	3	1.0965
421	20.6	B0UXB6	Abhydrolase domain-containing protein 16A	HUMAN	2	1.0666
422	36.3	A4D275	Actin related protein 2/3 complex, subunit 1B, 41kDa	HUMAN	5	0.4325
423	34.4	Q9UJS0	Calcium-binding mitochondrial carrier protein Aralar2	HUMAN	2	0.912
424	20.5	Q13510	N-acylsphingosine amidohydrolase (Acid ceramidase) 1, isoform CRA_c	HUMAN	2	1.1588
425	16.2	Q8TCT9	Isoform 2 of Minor histocompatibility antigen H13	HUMAN	2	0.0122
426	27.5	B2RDE8	cDNA, FLJ96580, highly similar to Homo sapiens hepatoma-derived growth factor (high-mobility group protein 1-like) (HDGF), mRNA	HUMAN	2	0.6486
427	52.7	Q5W0H4	Translationally-controlled tumor protein	HUMAN	2	0.6792
428	54.9	Q549C5	HCG2010808, isoform CRA_a	HUMAN	3	1.2823
429	43.2	P62851	40S ribosomal protein S25	HUMAN	2	0.8017
430	39.3	Q9Y6M9	NADH dehydrogenase [ubiquinone] 1 beta subcomplex subunit 9	HUMAN	2	0.0698
431	51.9	Q8IZ29	Tubulin, beta 2C	HUMAN	18	0.1445
432	71.5	Q6IBG1	MYL9 protein	HUMAN	10	0.2754
433	40	P14406	Cytochrome c oxidase subunit 7A2, mitochondrial	HUMAN	3	0.6546

434	46	A8K686	cDNA FLJ77316, highly similar to Homo sapiens interferon, gamma-inducible protein 30 (IFI30), mRNA	HUMAN	3	1.3804
435	30.9	P61088	Ubiquitin-conjugating enzyme E2 N	HUMAN	2	2.8054
436	47.2	Q6FGH9	DNCL1 protein	HUMAN	5	0.3664
437	34.1	O95168	NADH dehydrogenase [ubiquinone] 1 beta subcomplex subunit 4	HUMAN	2	1.8707
438	21.1	Q9NPA0	ER membrane protein complex subunit 7	HUMAN	2	1.7219
439	41	P49207	60S ribosomal protein L34	HUMAN	2	4.7424
440	31.8	P62263	40S ribosomal protein S14	HUMAN	2	1.1066
441	30.9	Q6FHT8	RNP24 protein	HUMAN	2	0.1282
442	24.4	Q96C36	Pyrroline-5-carboxylate reductase 2	HUMAN	2	0.7447
443	33.9	Q9UHL4	Dipeptidyl peptidase 2	HUMAN	3	0.5495
444	23.2	B4DVB8	ELAV-like protein 1	HUMAN	2	0.3373
445	38.5	Q04760	Isoform 2 of Lactoylglutathione lyase	HUMAN	2	0.8091
446	46.9	Q7Z4W8	Heparin-binding protein HBp15	HUMAN	2	1.0186
447	12.4	B3KRY3	cDNA FLJ35079 fis, clone PLACE6005283, highly similar to Lysosome-associated membrane glycoprotein 1	HUMAN	2	0.6607
448	26.4	O15260	Surfeit locus protein 4	HUMAN	3	1.8197
449	10.1	Q13488	V-type proton ATPase 116 kDa subunit a isoform 3	HUMAN	2	1.0471
450	25.5	P46013	Antigen KI-67	HUMAN	4	2.8314
451	34.8	Q9UFN0	Protein NipSnap homolog 3A	HUMAN	2	1.4454
452	50	P62899	60S ribosomal protein L31 (Fragment)	HUMAN	3	1.0666
453	18.6	Q96BY6	Dedicator of cytokinesis protein 10	HUMAN	5	0.6081
454	24	Q96F07	Cytoplasmic FMR1-interacting protein 2	HUMAN	4	0.6918
455	25	O95470	Sphingosine-1-phosphate lyase 1	HUMAN	2	0.15
456	29.5	A8K7T4	cDNA FLJ75774, highly similar to Homo sapiens lectin, mannose-binding 2 (LMAN2), mRNA	HUMAN	3	1.6444
457	21.2	P49792	E3 SUMO-protein ligase RanBP2	HUMAN	2	0.4055
458	25.2	P61204	ADP-ribosylation factor 3	HUMAN	2	0.1585
459	31.5	Q5SRT3	Chloride intracellular channel 1, isoform CRA_a	HUMAN	2	0.5598
460	43.9	P25398	40S ribosomal protein S12	HUMAN	2	0.0111
461	34.1	Q12905	NF45	HUMAN	3	1.0375
462	37.6	Q5U000	Cathepsin Z	HUMAN	2	0.3837
463	43.5	Q08ES8	Cell growth-inhibiting protein 34	HUMAN	2	0.3767
464	21.9	P61421	V-type proton ATPase subunit d 1	HUMAN	2	0.9727
465	56.6	B2R4D8	60S ribosomal protein L27	HUMAN	3	2.466
466	31.7	P46060	Ran GTPase-activating protein 1	HUMAN	3	0.2421

467	33.2	Q9BVK6	Transmembrane emp24 domain-containing protein 9	HUMAN	4	0.6427
468	34.1	P51553	Isocitrate dehydrogenase [NAD] subunit gamma, mitochondrial	HUMAN	2	1.1482
469	50.4	P60174	Triosephosphate isomerase	HUMAN	2	1.6596
470	26.3	Q9BTV4	Transmembrane protein 43	HUMAN	3	0.4325
471	52.7	P62249	40S ribosomal protein S16	HUMAN	2	1.3552
472	37.3	P61019	Ras-related protein Rab-2A	HUMAN	3	1.2589
473	38.4	A8K4I8	cDNA FLJ78131, highly similar to Homo sapiens nipsnap homolog 1 (C. elegans) (NIPSNAP1), mRNA	HUMAN	2	0.6982
474	31.7	Q6IAT1	GDI2 protein	HUMAN	2	1.4454
475	29.3	Q6NVY1	3-hydroxyisobutyryl-CoA hydrolase, mitochondrial	HUMAN	2	0.912
476	36.1	Q9H2U2	Isoform 2 of Inorganic pyrophosphatase 2, mitochondrial	HUMAN	6	0.9376
477	35.1	P09496	Clathrin light chain A	HUMAN	3	1.2134
478	49.8	P60903	S100 calcium binding protein A10 (Annexin II ligand, calpactin I, light polypeptide (P11)), isoform CRA_b (Fragment)	HUMAN	2	0.182
479	15.6	P36551	Coproporphyrinogen-III oxidase, mitochondrial	HUMAN	2	1.2474
480	22.1	Q99536	Synaptic vesicle membrane protein VAT-1 homolog	HUMAN	2	0.9727
481	14.7	B3KWH9	cDNA FLJ43108 fis, clone CTONG2021289, highly similar to Homo sapiens ELOVL family member 5, elongation of long chain fatty acids, mRNA	HUMAN	2	0.2128
482	46.8	O43399	Isoform 5 of Tumor protein D54	HUMAN	3	1.5417
483	44.7	P11233	Ras-related protein Ral-A	HUMAN	3	1.4723
484	89.1	A8KAH9	RAP1A, member of RAS oncogene family	HUMAN	17	1.2823
485	35.2	P10599	Thioredoxin	HUMAN	2	1.9588
486	54.7	B7Z4A1	cDNA FLJ50798, weakly similar to Ubiquinol-cytochrome c reductase complex ubiquinone-binding protein QP-C (EC 1.10.2.2)	HUMAN	3	0.302
487	34.6	Q96CW1	AP-2 complex subunit mu	HUMAN	2	1.3552
488	23.5	P53634	Dipeptidyl peptidase 1	HUMAN	2	0.6026
489	35.8	Q9Y2Q3	Isoform 2 of Glutathione S-transferase kappa 1	HUMAN	3	1.1066
490	18	Q68DN3	Putative uncharacterized protein DKFZp781F1414	HUMAN	2	2.6062
491	38.8	Q53G49	Ribosomal protein L19 (Fragment)	HUMAN	2	0.7112
492	23.5	P82675	28S ribosomal protein S5, mitochondrial	HUMAN	2	0.4656

493	70.6	Q5VTU8	ATP synthase subunit epsilon-like protein, mitochondrial	HUMAN	2	0.2884
494	34.2	P53680	AP-2 complex subunit sigma	HUMAN	2	1.4322
495	40	Q15388	Mitochondrial import receptor subunit TOM20 homolog	HUMAN	2	0.9462
496	56.4	Q5JQ44	Putative uncharacterized protein DKFZp547A0616 (Fragment)	HUMAN	2	0.227
497	40.2	A8K3M3	Tyrosine-protein phosphatase non-receptor type	HUMAN	2	0.8241
498	38.2	O43837	Isocitrate dehydrogenase [NAD] subunit beta, mitochondrial	HUMAN	1	0.0445
499	23.3	B0I1T2	Unconventional myosin-Ig	HUMAN	3	1.8365
500	20.9	P21730	C5a anaphylatoxin chemotactic receptor 1	HUMAN	3	0.7447
501	30.9	Q9Y512	Sorting and assembly machinery component 50 homolog	HUMAN	1	0.6792
502	63.1	P61769	Beta-2-microglobulin form pI 5.3	HUMAN	1	1.0666
503	43	Q01469	Fatty acid binding protein 5 (Psoriasis-associated)	HUMAN	2	1.2589
504	26.7	A8K4A8	cDNA FLJ76156, highly similar to Homo sapiens aspartyl-tRNA synthetase 2 (DARS2), mRNA	HUMAN	1	1.4454
505	32.2	Q8N2L6	cDNA FLJ90138 fis, clone HEMBB1000905, weakly similar to TRANSCRIPTIONAL REPRESSOR RCO-1	HUMAN	2	0.597
506	26.6	P07686	Beta-hexosaminidase subunit beta	HUMAN	1	1.0375
507	44.4	Q9Y277	Voltage-dependent anion-selective channel protein 3	HUMAN	7	6.1944
508	24.3	Q53EL3	C-src tyrosine kinase variant (Fragment)	HUMAN	2	0.955
509	42.8	Q32Q12	Nucleoside diphosphate kinase	HUMAN	2	0.879
510	35.6	O75251	NADH dehydrogenase [ubiquinone] iron-sulfur protein 7, mitochondrial	HUMAN	3	1.2134
511	32.3	B4DDB9	cDNA FLJ56339, highly similar to Signal peptidase complex subunit 2 (EC 3.4.-.-)	HUMAN	2	1.0093
512	15.7	P11215	Integrin alpha-M	HUMAN	1	2.1086
513	21.8	B3KM97	cDNA FLJ10554 fis, clone NT2RP2002385, highly similar to Synaptic glycoprotein SC2	HUMAN	1	1.5136
514	29.2	A1A508	PRSS3 protein	HUMAN	4	4.8753
515	33.7	Q5SZE4	Ceramide synthase 2 (Fragment)	HUMAN	2	1.0965
516	19.3	P49327	Fatty acid synthase	HUMAN	1	1.2706
517	45.5	Q16740	Putative ATP-dependent Clp protease proteolytic subunit, mitochondrial	HUMAN	2	0.5808
518	77.1	Q5XKP0	Protein QIL1	HUMAN	3	0.0126
519	32.4	B4DHU5	cDNA FLJ52495, highly similar to Calponin-2	HUMAN	2	0.3631

520	41.3	Q9NQ50	39S ribosomal protein L40, mitochondrial	HUMAN	1	1.6749
521	47	P69905	Hemoglobin alpha-1 globin chain (Fragment)	HUMAN	1	0.8551
522	40.6	Q504R6	RAB13 protein (Fragment)	HUMAN	6	4.8306
523	18.9	B4DW58	cDNA FLJ61429, highly similar to Ena/VASP-like protein	HUMAN	1	0.9817
524	42.4	P62280	40S ribosomal protein S11	HUMAN	1	0.863
525	21.8	Q9BUN6	MRPS30 protein (Fragment)	HUMAN	1	1.0765
526	59.5	P23396	Isoform 2 of 40S ribosomal protein S3	HUMAN	1	0.955
527	31.1	Q6P6D7	Phosphoglycerate mutase 1 (Brain)	HUMAN	1	0.8166
528	20.6	Q6UW68	Transmembrane protein 205	HUMAN	1	0.1786
529	30.7	B3KPC7	Actin-related protein 2/3 complex subunit 5	HUMAN	1	1.803
530	16.4	Q9UGQ3	Solute carrier family 2, facilitated glucose transporter member 6	HUMAN	1	1.0186
531	54.8	Q9GZT3	SRA stem-loop-interacting RNA-binding protein, mitochondrial	HUMAN	1	1
532	19.1	P14174	Macrophage migration inhibitory factor (Fragment)	HUMAN	3	0.6668
533	22.4	Q03405	Urokinase plasminogen activator surface receptor	HUMAN	3	0.9036
534	70.2	P01892	MHC class I antigen (Fragment)	HUMAN	6	1.803
535	22.6	P02452	Collagen alpha-1(I) chain	HUMAN	3	0.6138
536	15.2	Q12913	Receptor-type tyrosine-protein phosphatase eta	HUMAN	1	1.3677
537	16.5	P43155	Carnitine O-acetyltransferase	HUMAN	1	5.445
538	23	Q4LE36	ACLY variant protein (Fragment)	HUMAN	2	1.3305
539	26.6	P04040	Catalase	HUMAN	2	1.2706
540	29.1	P0CG39	POTE ankyrin domain family member J	HUMAN	20	0.8551
541	35	Q96C19	EF-hand domain-containing protein D2	HUMAN	1	1.2023
542	15.1	P04004	Vitronectin	HUMAN	2	0.2858
543	57.2	Q6FIG4	RAB1B protein	HUMAN	11	1.4859
544	40.5	Q96AB3	Isochorismatase domain-containing protein 2, mitochondrial	HUMAN	2	1.3305
545	26.5	B2RMW6	DnaJ (Hsp40) homolog, subfamily C, member 9	HUMAN	1	1.2823
546	22.4	Q9P107	GEM-interacting protein	HUMAN	2	0.2377
547	22.1	P25098	Beta-adrenergic receptor kinase 1	HUMAN	1	0.4093
548	19.4	Q59ET7	Thioredoxin reductase 2 isoform 1 variant (Fragment)	HUMAN	1	2.0893
549	23	P05161	Ubiquitin-like protein ISG15	HUMAN	1	1.6144
550	25.9	Q9NVA2	Septin 11, isoform CRA_b	HUMAN	2	1.5849
551	56.7	P51571	Translocon-associated protein subunit delta (Fragment)	HUMAN	3	0.1556

552	30.6	Q549N5	Signal recognition particle receptor beta subunit	HUMAN	2	0.2208
553	33.8	Q14318	Peptidyl-prolyl cis-trans isomerase FKBP8	HUMAN	2	1.0093
554	17.9	Q53EW8	Sulfurtransferase (Fragment)	HUMAN	1	0.8166
555	18.8	Q92619	Minor histocompatibility antigen HA-1	HUMAN	1	0.7244
556	33.8	P42126	Enoyl-CoA delta isomerase 1, mitochondrial	HUMAN	2	1.2942
557	20.6	B4E3D4	cDNA FLJ56293, highly similar to Transmembrane glycoprotein NMB	HUMAN	1	1.3804
558	14.3	P63244	Guanine nucleotide-binding protein subunit beta-2-like 1 (Fragment)	HUMAN	1	1.1169
559	27.5	Q8IXI1	Mitochondrial Rho GTPase 2	HUMAN	2	0.166
560	37.4	P42766	60S ribosomal protein L35	HUMAN	2	0.2148
561	66.7	Q6FG99	RPLP1 protein	HUMAN	1	0.9908
562	30.1	P11182	Lipoamide acyltransferase component of branched-chain alpha-keto acid dehydrogenase complex, mitochondrial	HUMAN	2	0.0207
563	44.6	Q86SX6	Glutaredoxin-related protein 5, mitochondrial	HUMAN	1	0.166
564	34.8	Q9UHQ9	NADH-cytochrome b5 reductase 1	HUMAN	1	0.7447
565	44.6	B4DZK8	cDNA FLJ61192, highly similar to Erythrocyte band 7 integral membrane protein	HUMAN	3	0.9727
566	21.4	B2R9T9	cDNA, FLJ94551	HUMAN	1	0.0466
567	32.1	C9JDE9	3-ketoacyl-CoA thiolase, peroxisomal	HUMAN	1	0.3251
568	41.7	P04259	Keratin, type II cytoskeletal 6B	HUMAN	14	1.4454
569	20.4	P48059	Isoform 5 of LIM and senescent cell antigen-like-containing domain protein 1	HUMAN	1	0.7447
570	31.8	P19971	Isoform 2 of Thymidine phosphorylase	HUMAN	1	0.9727
571	41.7	Q5JNZ5	Putative 40S ribosomal protein S26-like 1	HUMAN	1	3.4356
572	13.3	Q8NCN5	Pyruvate dehydrogenase phosphatase regulatory subunit, mitochondrial	HUMAN	1	1.1588
573	25.7	Q10471	Polypeptide N-acetylgalactosaminyltransferase 2	HUMAN	1	0.4246
574	25.7	Q53XC0	Eukaryotic translation initiation factor 2, subunit 1 alpha, 35kDa, isoform CRA_a	HUMAN	1	3.0479
575	63.2	Q9Y5L4	Mitochondrial import inner membrane translocase subunit Tim13	HUMAN	1	1.3183
576	45.3	Q9UII2	ATPase inhibitor, mitochondrial	HUMAN	1	0.1614
577	15.3	Q63HL5	Putative uncharacterized protein DKFZp686G12235	HUMAN	1	0.5916
578	21.1	P52565	Rho GDP-dissociation inhibitor 1	HUMAN	1	1.4191
579	26.9	Q12846	Syntaxin-4	HUMAN	1	0.3532

580	62.5	Q9Y2S6	Translation machinery-associated protein 7	HUMAN	1	0.1459
581	35.1	P00441	Superoxide dismutase [Cu-Zn]	HUMAN	1	2.5586
582	25.3	A8K750	cDNA FLJ78041, highly similar to Homo sapiens NADH dehydrogenase (ubiquinone) flavoprotein 2, 24kDa (NDUFV2), mRNA	HUMAN	1	1.1376
583	29.8	A5A3E0	POTE ankyrin domain family member F	HUMAN	37	1.556
584	30.4	Q59G70	Mannosyl (Alpha-1,3-)-glycoprotein beta-1,2-N-acetylglucosaminyltransferase variant (Fragment)	HUMAN	1	1.3677
585	65.2	P05387	60S acidic ribosomal protein P2	HUMAN	3	0.4656
586	25.6	Q9H061	Transmembrane protein 126A	HUMAN	1	0.2188
587	23	P78548	G18	HUMAN	1	0.4093
588	26.8	B2R6S5	Cytidylate kinase, isoform CRA_a	HUMAN	1	0.8318
589	14.4	A4D1C5	Protein tyrosine phosphatase, non-receptor type 12	HUMAN	1	0.052
590	28.2	Q9Y639	Neuroplastin	HUMAN	1	0.7943
591	22.3	Q6IBH0	SLC25A11 protein	HUMAN	1	1.0864
592	41.4	Q59GE4	Ribosomal protein S10 variant (Fragment)	HUMAN	2	1.3062
593	21.1	B2R4A5	cDNA, FLJ92019, highly similar to Homo sapiens mitochondrial ribosomal protein S14 (MRPS14), nuclear gene encoding mitochondrial protein, mRNA	HUMAN	1	0.8395
594	19.7	B4E2P2	Translocon-associated protein subunit gamma	HUMAN	1	0.6792
595	14.2	Q8NFF3	Pro-apoptotic protein BAKM variant	HUMAN	1	0.6081
596	25.3	P56556	NADH dehydrogenase [ubiquinone] 1 alpha subcomplex subunit 6	HUMAN	1	0.4875
597	22.1	P49006	MARCKS-related protein	HUMAN	1	0.7798
598	27.4	O43914	TYRO protein tyrosine kinase-binding protein	HUMAN	1	3.767
599	83.5	O43504	Ragulator complex protein LAMTOR5	HUMAN	1	1.8707
600	64.4	Q5TAQ0	Mitochondrial nucleoid factor 1	HUMAN	2	1.7701
601	31.8	O15173	Membrane-associated progesterone receptor component 2	HUMAN	2	1
602	17.9	Q4G0N4	NAD kinase 2, mitochondrial	HUMAN	1	1.7701
603	44.6	Q92665	28S ribosomal protein S31, mitochondrial	HUMAN	1	0.7798
604	20.8	Q8N5G0	Small integral membrane protein 20	HUMAN	1	1.3183
605	50	Q96EL3	39S ribosomal protein L53, mitochondrial	HUMAN	1	0.8954
606	18.9	Q56G89	Serum albumin	HUMAN	1	0.8872
607	21.9	B2R5H0	cDNA, FLJ92471, highly similar to Homo sapiens S100 calcium binding protein A11 (calgizzarin) (S100A11), mRNA	HUMAN	1	0.0111

608	31.8	Q8N4H5	Isoform 3 of Mitochondrial import receptor subunit TOM5 homolog	HUMAN	1	1.1066
609	19.4	O15427	Monocarboxylate transporter 4	HUMAN	2	1.3183
610	11.2	P01584	Interleukin-1 beta	HUMAN	1	1.2823
611	18.7	Q92544	Transmembrane 9 superfamily member 4	HUMAN	2	0.16
612	30.9	O00483	NADH dehydrogenase [ubiquinone] 1 alpha subcomplex subunit 4	HUMAN	1	0.4699
613	17.6	Q8TEL6	Short transient receptor potential channel 4-associated protein	HUMAN	1	3.4356
614	17.6	Q3ZCU9	STIP1 protein	HUMAN	1	1.0765
615	26.5	Q9H936	Mitochondrial glutamate carrier 1 (Fragment)	HUMAN	1	1.1912
616	17.6	Q8NBS9	Thioredoxin domain-containing protein 5	HUMAN	3	0.7447
617	27.3	B4E1J8	cDNA FLJ56285, highly similar to ADP-ribosylation factor-like protein 8B	HUMAN	2	1.3552
618	25.2	Q14197	Peptidyl-tRNA hydrolase ICT1, mitochondrial	HUMAN	1	0.6081
619	23.9	Q92835	Phosphatidylinositol 3,4,5-trisphosphate 5-phosphatase 1	HUMAN	1	0.6138
620	14.1	A8KA84	cDNA FLJ78682, highly similar to Homo sapiens 2'-5'-oligoadenylate synthetase 3, 100kDa (OAS3), mRNA	HUMAN	1	2.1878
621	24.7	Q14019	Coactosin-like protein	HUMAN	2	1.0093
622	20.5	B3KWR9	Toll-like receptor	HUMAN	1	1.0375
623	19	Q6IBU4	SDF2 protein	HUMAN	1	3.0761
624	29	P05109	Protein S100-A8	HUMAN	1	0.3664
625	24.9	P05556	Integrin beta-1	HUMAN	0	0.7586
626	12.1	Q92542	Nicastrin	HUMAN	1	0.8091
627	6.6	P00156	Cytochrome b	HUMAN	1	1.2823
628	28.7	B4E283	Apoptosis inhibitor 5	HUMAN	1	0.0575
629	21.3	O75037	Kinesin-like protein KIF21B	HUMAN	2	1.0093
630	11	Q9BPU6	Dihydropyrimidinase-related protein 5	HUMAN	1	1.2589
631	27.8	Q13136	Liprin-alpha-1	HUMAN	1	3.5975
632	24.8	B3KQQ3	cDNA PSEC0016 fis, clone NT2RM1001076, highly similar to Procollagen-lysine,2-oxoglutarate 5-dioxygenase 3 (EC 1.14.11.4)	HUMAN	1	0.6607
633	34.4	P83111	Serine beta-lactamase-like protein LACTB, mitochondrial	HUMAN	0	0.9036
634	34.1	Q53HD3	60S ribosomal protein L18a (Fragment)	HUMAN	1	0.6194
635	76.4	Q6IQ15	EEF1A1 protein	HUMAN	65	1.4322
636	30.1	P36268	Gamma-glutamyltranspeptidase 2	HUMAN	1	1.1066
637	31.1	P21912	Succinate dehydrogenase [ubiquinone] iron-sulfur subunit, mitochondrial	HUMAN	1	1.3062

638	11.6	A6NCQ8	High affinity immunoglobulin epsilon receptor subunit gamma	HUMAN	1	0.597
639	21.5	Q05655	Isoform 2 of Protein kinase C delta type	HUMAN	1	1.3428
640	32.7	B4DJV9	cDNA FLJ60607, highly similar to Acyl-protein thioesterase 1 (EC 3.1.2.-)	HUMAN	1	1.3305
641	14.6	Q6ZSA3	cDNA FLJ45695 fis, clone FEBRA2013570, highly similar to 2-oxoisovalerate dehydrogenase alpha subunit, mitochondrial (EC 1.2.4.4)	HUMAN	1	0.5754
642	22.2	P82933	28S ribosomal protein S9, mitochondrial	HUMAN	1	1.3932
643	25.4	Q9UHD8	Isoform 5 of Septin-9	HUMAN	2	0.6855
644	15.8	Q8WWC4	Uncharacterized protein C2orf47, mitochondrial	HUMAN	1	0.0619
645	26.2	A8KAH7	cDNA FLJ75444, highly similar to Homo sapiens protein kinase, cAMP-dependent, regulatory, type II, alpha (PRKAR2A), mRNA	HUMAN	1	2.0137

References

References

Abdallah, A. M., N. D. Savage, et al. (2008). "The ESX-5 secretion system of Mycobacterium marinum modulates the macrophage response." J Immunol **181**(10): 7166-7175.

Agranoff, D., I. M. Monahan, et al. (1999). "Mycobacterium tuberculosis expresses a novel pH-dependent divalent cation transporter belonging to the Nramp family." J Exp Med **190**(5): 717-724.

Almeida, P. E., N. R. Roque, et al. (2014). "Differential TLR2 downstream signaling regulates lipid metabolism and cytokine production triggered by Mycobacterium bovis BCG infection." Biochim Biophys Acta **1841**(1): 97-107.

Alonso-Hearn, M., T. M. Eckstein, et al. (2010). "A Mycobacterium avium subsp. paratuberculosis LuxR regulates cell envelope and virulence." Innate Immun **16**(4): 235-247.

Amoroso, F., S. Falzoni, et al. (2012). "The P2X7 receptor is a key modulator of aerobic glycolysis." Cell Death Dis **3**: e370.

Anderson, K. V. (2000). "Toll signaling pathways in the innate immune response." Curr Opin Immunol **12**(1): 13-19.

Andreani, G., D. Gagnon, et al. (2012). "An in vitro co-infection model to study Plasmodium falciparum-HIV-1 interactions in human primary monocyte-derived immune cells." J Vis Exp(66): e4166.

Azzopardi, P., C. M. Bennett, et al. (2009). "Bacille Calmette-Guerin vaccine-related disease in HIV-infected children: a systematic review." Int J Tuberc Lung Dis **13**(11): 1331-1344.

Bachmeyer, C., L. Blum, et al. (2002). "Mycobacterium xenopi pulmonary infection in an HIV infected patient under highly active antiretroviral treatment." Sex Transm Infect **78**(1): 60-61.

Back, N. K., L. Smit, et al. (1994). "An N-glycan within the human immunodeficiency virus type 1 gp120 V3 loop affects virus neutralization." Virology **199**(2): 431-438.

Badri, M., R. Ehrlich, et al. (2001). "Association between tuberculosis and HIV disease progression in a high tuberculosis prevalence area." Int J Tuberc Lung Dis **5**(3): 225-232.

Bandyopadhyay, A., S. Biswas, et al. (2014). "Analysis of DevR regulated genes in Mycobacterium tuberculosis." Syst Synth Biol **8**(1): 3-20.

Banerjee, A., R. Benjamin, et al. (2014). "Human protein Staufen-2 promotes HIV-1 proliferation by positively regulating RNA export activity of viral protein Rev." Retrovirology **11**: 18.

Bange, F. C., A. M. Brown, et al. (1996). "Leucine auxotrophy restricts growth of Mycobacterium bovis BCG in macrophages." Infect Immun **64**(5): 1794-1799.

Barre-Sinoussi, F., A. L. Ross, et al. (2013). "Past, present and future: 30 years of HIV research." Nat Rev Microbiol **11**(12): 877-883.

Beatty, W. L., E. R. Rhoades, et al. (2002). "Association of a macrophage galactoside-binding protein with Mycobacterium-containing phagosomes." Cell Microbiol **4**(3): 167-176.

Benjamin, R., A. Banerjee, et al. (2014). "Mycobacterial and HIV infections up-regulated human zinc finger protein 134, a novel positive regulator of HIV-1 LTR activity and viral propagation." PLoS One **9**(8): e104908.

Benjamin, R., A. Banerjee, et al. (2013). "Discordance in CD4+T-cell levels and viral loads with co-occurrence of elevated peripheral TNF-alpha and IL-4 in newly diagnosed HIV-TB co-infected cases." PLoS One **8**(8): e70250.

Bodmer, T., E. Miltner, et al. (2000). "Mycobacterium avium resists exposure to the acidic conditions of the stomach." FEMS Microbiol Lett **182**(1): 45-49.

Bordon, J., M. W. Plankey, et al. (2011). "Lower levels of interleukin-12 precede the development of tuberculosis among HIV-infected women." Cytokine **56**(2): 325-331.

Borrow, P. and N. Bhardwaj (2008). "Innate immune responses in primary HIV-1 infection." Curr Opin HIV AIDS **3**(1): 36-44.

Borrow, P., R. J. Shattock, et al. (2010). "Innate immunity against HIV: a priority target for HIV prevention research." Retrovirology **7**: 84.

Bottai, D., M. Di Luca, et al. (2012). "Disruption of the ESX-5 system of Mycobacterium tuberculosis causes loss of PPE protein secretion, reduction of cell wall integrity and strong attenuation." Mol Microbiol **83**(6): 1195-1209.

Brennan, P. J. (2003). "Structure, function, and biogenesis of the cell wall of Mycobacterium tuberculosis." Tuberculosis (Edinb) **83**(1-3): 91-97.

Brockman, M. A., D. S. Kwon, et al. (2009). "IL-10 is up-regulated in multiple cell types during viremic HIV infection and reversibly inhibits virus-specific T cells." Blood **114**(2): 346-356.

Brown-Elliott, B. A., K. A. Nash, et al. (2012). "Antimicrobial susceptibility testing, drug resistance mechanisms, and therapy of infections with nontuberculous mycobacteria." Clin Microbiol Rev **25**(3): 545-582.

Brown, C. A., I. N. Brown, et al. (1985). "The effect of oral Mycobacterium vaccae on subsequent responses of mice to BCG sensitization." Tubercle **66**(4): 251-260.

Bruchfeld, J., M. Correia-Neves, et al. (2015). "Tuberculosis and HIV Coinfection." Cold Spring Harb Perspect Med **5**(7).

Buchmeier, N. A., G. L. Newton, et al. (2006). "A mycothiol synthase mutant of Mycobacterium tuberculosis has an altered thiol-disulfide content and limited tolerance to stress." J Bacteriol **188**(17): 6245-6252.

Buchmeier, N. A., G. L. Newton, et al. (2003). "Association of mycothiol with protection of Mycobacterium tuberculosis from toxic oxidants and antibiotics." Mol Microbiol **47**(6): 1723-1732.

Cardoso, C. M., L. Jordao, et al. (2010). "Rab10 regulates phagosome maturation and its overexpression rescues Mycobacterium-containing phagosomes maturation." Traffic **11**(2): 221-235.

Carpenter, J. L. and J. M. Parks (1991). "Mycobacterium kansasii infections in patients positive for human immunodeficiency virus." Rev Infect Dis **13**(5): 789-796.

Carter, C. A. and L. S. Ehrlich (2008). "Cell biology of HIV-1 infection of macrophages." Annu Rev Microbiol **62**: 425-443.

Cella, M., D. Jarrossay, et al. (1999). "Plasmacytoid monocytes migrate to inflamed lymph nodes and produce large amounts of type I interferon." Nat Med **5**(8): 919-923.

Chatrath, S., V. K. Gupta, et al. (2011). "The Rv1651c-encoded PE-PGRS30 protein expressed in Mycobacterium smegmatis exhibits polar localization and modulates its growth profile." FEMS Microbiol Lett **322**(2): 194-199.

Chen, J. Y., E. R. Feeney, et al. (2014). "HCV and HIV co-infection: mechanisms and management." Nat Rev Gastroenterol Hepatol **11**(6): 362-371.

Chen, Y. and M. P. Machner (2013). "Targeting of the small GTPase Rab6A' by the Legionella pneumophila effector LidA." Infect Immun **81**(6): 2226-2235.

Chung, A. W., P. A. Sieling, et al. (2013). "Galectin-3 regulates the innate immune response of human monocytes." J Infect Dis **207**(6): 947-956.

Cocchi, F., A. L. DeVico, et al. (1995). "Identification of RANTES, MIP-1 alpha, and MIP-1 beta as the major HIV-suppressive factors produced by CD8+ T cells." Science **270**(5243): 1811-1815.

Colangeli, R., A. Haq, et al. (2009). "The multifunctional histone-like protein Lsr2 protects mycobacteria against reactive oxygen intermediates." Proc Natl Acad Sci U S A **106**(11): 4414-4418.

Cole, S. T., R. Brosch, et al. (1998). "Deciphering the biology of Mycobacterium tuberculosis from the complete genome sequence." Nature **393**(6685): 537-544.

Collins, K. R., M. E. Quinones-Mateu, et al. (2002). "Impact of tuberculosis on HIV-1 replication, diversity, and disease progression." AIDS Rev **4**(3): 165-176.

Collman, R., N. F. Hassan, et al. (1989). "Infection of monocyte-derived macrophages with human immunodeficiency virus type 1 (HIV-1). Monocyte-tropic and lymphocyte-tropic strains of HIV-1 show distinctive patterns of replication in a panel of cell types." J Exp Med **170**(4): 1149-1163.

Daley, C. L. and D. E. Griffith (2010). "Pulmonary non-tuberculous mycobacterial infections." Int J Tuberc Lung Dis **14**(6): 665-671.

Daniel, J., C. Deb, et al. (2004). "Induction of a novel class of diacylglycerol acyltransferases and triacylglycerol accumulation in Mycobacterium tuberculosis as it goes into a dormancy-like state in culture." J Bacteriol **186**(15): 5017-5030.

Daniel, J., H. Maamar, et al. (2011). "Mycobacterium tuberculosis uses host triacylglycerol to accumulate lipid droplets and acquires a dormancy-like phenotype in lipid-loaded macrophages." PLoS Pathog **7**(6): e1002093.

Davis, A. S., I. Vergne, et al. (2007). "Mechanism of inducible nitric oxide synthase exclusion from mycobacterial phagosomes." PLoS Pathog **3**(12): e186.

De Simone, C., G. Famularo, et al. (1994). "Carnitine depletion in peripheral blood mononuclear cells from patients with AIDS: effect of oral L-carnitine." AIDS **8**(5): 655-660.

DeBerardinis, R. J., J. J. Lum, et al. (2008). "The biology of cancer: metabolic reprogramming fuels cell growth and proliferation." Cell Metab **7**(1): 11-20.

Desjardins, M., M. Houde, et al. (2005). "Phagocytosis: The convoluted way from nutrition to adaptive immunity." Immunological Reviews **207**: 158-165.

Diedrich, C. R. and J. L. Flynn (2011). "HIV-1/mycobacterium tuberculosis coinfection immunology: how does HIV-1 exacerbate tuberculosis?" Infect Immun **79**(4): 1407-1417.

Dussurget, O., M. Rodriguez, et al. (1996). "An ideR mutant of Mycobacterium smegmatis has derepressed siderophore production and an altered oxidative-stress response." Mol Microbiol **22**(3): 535-544.

Edwards, K. M., M. H. Cynamon, et al. (2001). "Iron-cofactored superoxide dismutase inhibits host responses to Mycobacterium tuberculosis." Am J Respir Crit Care Med **164**(12): 2213-2219.

Ehrt, S. and D. Schnappinger (2009). "Mycobacterial survival strategies in the phagosome: defence against host stresses." Cell Microbiol **11**(8): 1170-1178.

Espert, L., M. Varbanov, et al. (2009). "Differential role of autophagy in CD4 T cells and macrophages during X4 and R5 HIV-1 infection." PLoS One **4**(6): e5787.

Falkinham, J. O., 3rd (2009). "Surrounded by mycobacteria: nontuberculous mycobacteria in the human environment." J Appl Microbiol **107**(2): 356-367.

Falkinham, J. O., 3rd (2011). "Nontuberculous mycobacteria from household plumbing of patients with nontuberculous mycobacteria disease." Emerg Infect Dis **17**(3): 419-424.

Falvo, J. V., S. Ranjbar, et al. (2011). "Arc of a vicious circle: pathways activated by Mycobacterium tuberculosis that target the HIV-1 long terminal repeat." Am J Respir Cell Mol Biol **45**(6): 1116-1124.

Fang, H., D. Yu, et al. (2013). "The LuxR family regulator Rv0195 modulates Mycobacterium tuberculosis dormancy and virulence." Tuberculosis (Edinb) **93**(4): 425-431.

Favre, D., J. Mold, et al. (2010). "Tryptophan catabolism by indoleamine 2,3-dioxygenase 1 alters the balance of TH17 to regulatory T cells in HIV disease." Sci Transl Med **2**(32): 32ra36.

Feltcher, M. E., H. S. Gibbons, et al. (2013). "Protein export by the mycobacterial SecA2 system is determined by the preprotein mature domain." J Bacteriol **195**(4): 672-681.

Fenteany, G. and M. Glogauer (2004). "Cytoskeletal remodeling in leukocyte function." Curr Opin Hematol **11**(1): 15-24.

Ferrari, G., H. Langen, et al. (1999). "A coat protein on phagosomes involved in the intracellular survival of mycobacteria." Cell **97**(4): 435-447.

Flynn, J. L., J. Chan, et al. (2011). "Macrophages and control of granulomatous inflammation in tuberculosis." Mucosal Immunol **4**(3): 271-278.

Foster, J. W. and A. G. Moat (1980). "Nicotinamide adenine dinucleotide biosynthesis and pyridine nucleotide cycle metabolism in microbial systems." Microbiol Rev **44**(1): 83-105.

Ganji, R., S. Dhali, et al. (2015). "Proteomics approach to understand reduced clearance of mycobacteria and high viral titers during HIV-mycobacteria co-infection." Cell Microbiol.

Geijtenbeek, T. B., D. S. Kwon, et al. (2000). "DC-SIGN, a dendritic cell-specific HIV-1-binding protein that enhances trans-infection of T cells." Cell **100**(5): 587-597.

Geijtenbeek, T. B. and Y. van Kooyk (2003). "DC-SIGN: a novel HIV receptor on DCs that mediates HIV-1 transmission." Curr Top Microbiol Immunol **276**: 31-54.

Geldmacher, C., N. Ngwenyama, et al. (2010). "Preferential infection and depletion of Mycobacterium tuberculosis-specific CD4 T cells after HIV-1 infection." J Exp Med **207**(13): 2869-2881.

Geldmacher, C., A. Zumla, et al. (2012). "Interaction between HIV and Mycobacterium tuberculosis: HIV-1-induced CD4 T-cell depletion and the development of active tuberculosis." Curr Opin HIV AIDS **7**(3): 268-275.

Geleziunas, R., W. Xu, et al. (2001). "HIV-1 Nef inhibits ASK1-dependent death signalling providing a potential mechanism for protecting the infected host cell." Nature **410**(6830): 834-838.

Giridharan, S. S., B. Cai, et al. (2012). "Trafficking cascades mediated by Rab35 and its membrane hub effector, MICAL-L1." Commun Integr Biol **5**(4): 384-387.

Glassroth, J. (2008). "Pulmonary disease due to nontuberculous mycobacteria." Chest **133**(1): 243-251.

Goletti, D., D. Weissman, et al. (1998). "The in vitro induction of human immunodeficiency virus (HIV) replication in purified protein derivative-positive HIV-infected persons by recall antigen response to Mycobacterium tuberculosis is the result of a balance of the effects of endogenous interleukin-2 and proinflammatory and antiinflammatory cytokines." J Infect Dis **177**(5): 1332-1338.

Goletti, D., D. Weissman, et al. (1996). "Effect of Mycobacterium tuberculosis on HIV replication. Role of immune activation." J Immunol **157**(3): 1271-1278.

Gordon, A. H., P. D. Hart, et al. (1980). "Ammonia inhibits phagosome-lysosome fusion in macrophages." Nature **286**(5768): 79-80.

Goren, M. B., O. Brokl, et al. (1974). "Lipids of putative relevance to virulence in Mycobacterium tuberculosis: phthiocerol dimycocerosate and the attenuation indicator lipid." Infect Immun **9**(1): 150-158.

Gouaze, V., N. Andrieu-Abadie, et al. (2002). "Glutathione peroxidase-1 protects from CD95-induced apoptosis." J Biol Chem **277**(45): 42867-42874.

Goujon, C., O. Moncorge, et al. (2013). "Human MX2 is an interferon-induced post-entry inhibitor of HIV-1 infection." Nature **502**(7472): 559-562.

Goulder, P. J., C. Brander, et al. (2001). "Evolution and transmission of stable CTL escape mutations in HIV infection." Nature **412**(6844): 334-338.

Groot, F., T. M. van Capel, et al. (2006). "Opposing roles of blood myeloid and plasmacytoid dendritic cells in HIV-1 infection of T cells: transmission facilitation versus replication inhibition." Blood **108**(6): 1957-1964.

Guerin, I. and C. de Chastellier (2000). "Pathogenic mycobacteria disrupt the macrophage actin filament network." Infect Immun **68**(5): 2655-2662.

Guirado, E., L. S. Schlesinger, et al. (2013). "Macrophages in tuberculosis: friend or foe." Semin Immunopathol **35**(5): 563-583.

Guo, M. and W. Z. Ho (2014). "Animal models to study Mycobacterium tuberculosis and HIV co-infection." Dongwuxue Yanjiu **35**(3): 163-169.

Haas, A. (1998). "Reprogramming the phagocytic pathway--intracellular pathogens and their vacuoles (review)." Mol Membr Biol **15**(3): 103-121.

Haas, A. (2007). "The phagosome: compartment with a license to kill." Traffic **8**(4): 311-330.

Haglund, C. M. and M. D. Welch (2011). "Pathogens and polymers: microbe-host interactions illuminate the cytoskeleton." J Cell Biol **195**(1): 7-17.

Hall, C. J., R. H. Boyle, et al. (2013). "Immunoresponsive gene 1 augments bactericidal activity of macrophage-lineage cells by regulating beta-oxidation-dependent mitochondrial ROS production." Cell Metab **18**(2): 265-278.

Harmon, B. and L. Ratner (2008). "Induction of the Galpha(q) signaling cascade by the human immunodeficiency virus envelope is required for virus entry." J Virol **82**(18): 9191-9205.

Hazleton, J. E., J. W. Berman, et al. (2012). "Purinergic receptors are required for HIV-1 infection of primary human macrophages." J Immunol **188**(9): 4488-4495.

He, Y., W. Li, et al. (2012). "Mycobacterium tuberculosis-specific phagosome proteome and underlying signaling pathways." J Proteome Res **11**(5): 2635-2643.

Heaton, N. S. and G. Randall (2011). "Multifaceted roles for lipids in viral infection." Trends Microbiol **19**(7): 368-375.

Herzmann, C., S. Esser, et al. (2011). "[Infections with non-tuberculous mycobacteria in HIV-infected patients]." Hautarzt **62**(4): 272-279.

Hesseling, A. C., L. F. Johnson, et al. (2009). "Disseminated bacille Calmette-Guerin disease in HIV-infected South African infants." Bull World Health Organ **87**(7): 505-511.

Ho, H. T., I. F. Tsai, et al. (2014). "Aminopeptidase N facilitates entry and intracellular survival of Mycobacterium tuberculosis in monocytes." Respirology **19**(1): 109-115.

Hou, J. Y., J. E. Graham, et al. (2002). "Mycobacterium avium genes expressed during growth in human macrophages detected by selective capture of transcribed sequences (SCOTS)." Infect Immun **70**(7): 3714-3726.

Houben, E. N., K. V. Korotkov, et al. (2014). "Take five - Type VII secretion systems of Mycobacteria." Biochim Biophys Acta **1843**(8): 1707-1716.

Hultquist, J. F., M. Binka, et al. (2012). "Vif proteins of human and simian immunodeficiency viruses require cellular CBFbeta to degrade APOBEC3 restriction factors." J Virol **86**(5): 2874-2877.

Imperiali, F. G., A. Zaninoni, et al. (2001). "Increased Mycobacterium tuberculosis growth in HIV-1-infected human macrophages: role of tumour necrosis factor-alpha." Clin Exp Immunol **123**(3): 435-442.

Iordanskiy, S., S. Santos, et al. (2013). "Nature, nurture and HIV: The effect of producer cell on viral physiology." Virology **443**(2): 208-213.

Iwasaki, A. and R. Medzhitov (2010). "Regulation of adaptive immunity by the innate immune system." Science **327**(5963): 291-295.

Iyengar, S., J. E. Hildreth, et al. (1998). "Actin-dependent receptor colocalization required for human immunodeficiency virus entry into host cells." J Virol **72**(6): 5251-5255.

Jain, M. and J. S. Cox (2005). "Interaction between polyketide synthase and transporter suggests coupled synthesis and export of virulence lipid in M. tuberculosis." PLoS Pathog **1**(1): e2.

Jakobsen, M. R., R. O. Bak, et al. (2013). "IFI16 senses DNA forms of the lentiviral replication cycle and controls HIV-1 replication." Proc Natl Acad Sci U S A **110**(48): E4571-4580.

Jamwal, S., M. K. Midha, et al. (2013). "Characterizing virulence-specific perturbations in the mitochondrial function of macrophages infected with Mycobacterium tuberculosis." Sci Rep **3**: 1328.

Jang, J., A. Stella, et al. (2010). "Functional characterization of the Mycobacterium tuberculosis serine/threonine kinase PknJ." Microbiology **156**(Pt 6): 1619-1631.

Jarlier, V. and H. Nikaido (1994). "Mycobacterial cell wall: structure and role in natural resistance to antibiotics." FEMS Microbiol Lett **123**(1-2): 11-18.

Jayachandran, R., V. Sundaramurthy, et al. (2007). "Survival of mycobacteria in macrophages is mediated by coronin 1-dependent activation of calcineurin." Cell **130**(1): 37-50.

Jiang, L., K. Salao, et al. (2012). "Intracellular chloride channel protein CLIC1 regulates macrophage function through modulation of phagosomal acidification." J Cell Sci **125**(Pt 22): 5479-5488.

Johnson, M. M. and J. A. Odell (2014). "Nontuberculous mycobacterial pulmonary infections." J Thorac Dis **6**(3): 210-220.

Jordao, L., C. K. Bleck, et al. (2008). "On the killing of mycobacteria by macrophages." Cell Microbiol **10**(2): 529-548.

Juffermans, N. P., A. Verbon, et al. (1998). "Mycobacterium xenopi in HIV-infected patients: an emerging pathogen." AIDS **12**(13): 1661-1666.

Jurado, J. O., V. Pasquinelli, et al. (2012). "ICOS, SLAM and PD-1 expression and regulation on T lymphocytes reflect the immune dysregulation in patients with HIV-related illness with pulmonary tuberculosis." J Int AIDS Soc **15**(2): 17428.

Kamp, W., M. B. Berk, et al. (2000). "Mechanisms of HIV-1 to escape from the host immune surveillance." Eur J Clin Invest **30**(8): 740-746.

Kane, M., S. S. Yadav, et al. (2013). "MX2 is an interferon-induced inhibitor of HIV-1 infection." Nature **502**(7472): 563-566.

Karakousis, P. C., R. D. Moore, et al. (2004). "Mycobacterium avium complex in patients with HIV infection in the era of highly active antiretroviral therapy." Lancet Infect Dis **4**(9): 557-565.

Karczewski, M. K. and K. Strebel (1996). "Cytoskeleton association and virion incorporation of the human immunodeficiency virus type 1 Vif protein." J Virol **70**(1): 494-507.

Kaufmann, S. H. (2005). "Recent findings in immunology give tuberculosis vaccines a new boost." Trends Immunol **26**(12): 660-667.

Kaufmann, S. H. and A. J. McMichael (2005). "Annulling a dangerous liaison: vaccination strategies against AIDS and tuberculosis." Nat Med **11**(4 Suppl): S33-44.

Kinchen, J. M. and K. S. Ravichandran (2008). "Phagosome maturation: Going through the acid test." Nature Reviews Molecular Cell Biology **9**(10): 781-795.

Kindler, V. and A. P. Sappino (1991). "The beneficial effects of localized tumor necrosis factor production in BCG infection." Behring Inst Mitt(88): 120-124.

Kindler, V., A. P. Sappino, et al. (1989). "The inducing role of tumor necrosis factor in the development of bactericidal granulomas during BCG infection." Cell **56**(5): 731-740.

King, J. S., A. Gueho, et al. (2013). "WASH is required for lysosomal recycling and efficient autophagic and phagocytic digestion." Mol Biol Cell **24**(17): 2714-2726.

Kirchhoff, F. (2014). HIV Life Cycle: Overview. Encyclopedia of AIDS. T. J. Hope, M. Stevenson and D. Richman, Springer New York**:** 1-9.

Kordulakova, J., M. Gilleron, et al. (2003). "Identification of the required acyltransferase step in the biosynthesis of the phosphatidylinositol mannosides of mycobacterium species." J Biol Chem **278**(38): 36285-36295.

Koziel, M. J. and M. G. Peters (2007). "Viral hepatitis in HIV infection." N Engl J Med **356**(14): 1445-1454.

Kruh, N. A., J. Troudt, et al. (2010). "Portrait of a pathogen: the Mycobacterium tuberculosis proteome in vivo." PLoS One **5**(11): e13938.

Kumar, M., S. K. Sahu, et al. (2015). "MicroRNA let-7 modulates the immune response to Mycobacterium tuberculosis infection via control of A20, an inhibitor of the NF-kappaB pathway." Cell Host Microbe **17**(3): 345-356.

Kutner, R. H., X. Y. Zhang, et al. (2009). "Production, concentration and titration of pseudotyped HIV-1-based lentiviral vectors." Nat Protoc **4**(4): 495-505.

Kwon, D. S. and D. E. Kaufmann (2010). "Protective and detrimental roles of IL-10 in HIV pathogenesis." Eur Cytokine Netw **21**(3): 208-214.

Kyei, G. B., I. Vergne, et al. (2006). "Rab14 is critical for maintenance of Mycobacterium tuberculosis phagosome maturation arrest." EMBO J **25**(22): 5250-5259.

Laguette, N., B. Sobhian, et al. (2011). "SAMHD1 is the dendritic- and myeloid-cell-specific HIV-1 restriction factor counteracted by Vpx." Nature **474**(7353): 654-657.

Lan, R., C. Yang, et al. (2011). "Mycobacterium tuberculosis and non-tuberculous mycobacteria isolates from HIV-infected patients in Guangxi, China." Int J Tuberc Lung Dis **15**(12): 1669-1675.

Larsson, M., E. M. Shankar, et al. (2013). "Molecular signatures of T-cell inhibition in HIV-1 infection." Retrovirology **10**: 31.

Lawn, S. D., S. T. Butera, et al. (2002). "Tuberculosis unleashed: the impact of human immunodeficiency virus infection on the host granulomatous response to Mycobacterium tuberculosis." Microbes Infect **4**(6): 635-646.

Lee, B. Y., D. Jethwaney, et al. (2010). "The Mycobacterium bovis bacille Calmette-Guerin phagosome proteome." Mol Cell Proteomics **9**(1): 32-53.

Lee, S. J., S. J. Kim, et al. (2003). "Crystal structures of human DJ-1 and Escherichia coli Hsp31, which share an evolutionarily conserved domain." J Biol Chem **278**(45): 44552-44559.

Lee, W., B. C. VanderVen, et al. (2013). "Intracellular Mycobacterium tuberculosis exploits host-derived fatty acids to limit metabolic stress." J Biol Chem **288**(10): 6788-6800.

Lee, W. L., B. Gold, et al. (2009). "Mycobacterium tuberculosis expresses methionine sulphoxide reductases A and B that protect from killing by nitrite and hypochlorite." Mol Microbiol **71**(3): 583-593.

Lehner, T., Y. Wang, et al. (2000). "Up-regulation of beta-chemokines and down-modulation of CCR5 co-receptors inhibit simian immunodeficiency virus transmission in non-human primates." Immunology **99**(4): 569-577.

Lew, J. M., A. Kapopoulou, et al. (2011). "TubercuList--10 years after." Tuberculosis (Edinb) **91**(1): 1-7.

Li, M. S., I. M. Monahan, et al. (2001). "cDNA-RNA subtractive hybridization reveals increased expression of mycocerosic acid synthase in intracellular Mycobacterium bovis BCG." Microbiology **147**(Pt 8): 2293-2305.

Li, Q., C. Jagannath, et al. (2010). "Analysis of phagosomal proteomes: From latex-bead to bacterial phagosomes." Proteomics **10**(22): 4098-4116.

Li, X. D., J. Wu, et al. (2013). "Pivotal roles of cGAS-cGAMP signaling in antiviral defense and immune adjuvant effects." Science **341**(6152): 1390-1394.

Loetscher, P., B. Moser, et al. (2000). "Chemokines and their receptors in lymphocyte traffic and HIV infection." Adv Immunol **74**: 127-180.

Ma, X. and L. J. Montaner (2000). "Proinflammatory response and IL-12 expression in HIV-1 infection." J Leukoc Biol **68**(3): 383-390.

Makinoshima, H. and M. S. Glickman (2005). "Regulation of Mycobacterium tuberculosis cell envelope composition and virulence by intramembrane proteolysis." Nature **436**(7049): 406-409.

Malik, Z. A., G. M. Denning, et al. (2000). "Inhibition of Ca(2+) signaling by Mycobacterium tuberculosis is associated with reduced phagosome-lysosome fusion and increased survival within human macrophages." J Exp Med **191**(2): 287-302.

Malik, Z. A., C. R. Thompson, et al. (2003). "Cutting edge: Mycobacterium tuberculosis blocks Ca2+ signaling and phagosome maturation in human macrophages via specific inhibition of sphingosine kinase." J Immunol **170**(6): 2811-2815.

Mattow, J., F. Siejak, et al. (2006). "Proteins unique to intraphagosomally grown Mycobacterium tuberculosis." Proteomics **6**(8): 2485-2494.

McAdam, R. A., T. R. Weisbrod, et al. (1995). "In vivo growth characteristics of leucine and methionine auxotrophic mutants of Mycobacterium bovis BCG generated by transposon mutagenesis." Infect Immun **63**(3): 1004-1012.

McCoy, M. K. and M. R. Cookson (2011). "DJ-1 regulation of mitochondrial function and autophagy through oxidative stress." Autophagy **7**(5): 531-532.

McKinney, J. D., K. Honer zu Bentrup, et al. (2000). "Persistence of Mycobacterium tuberculosis in macrophages and mice requires the glyoxylate shunt enzyme isocitrate lyase." Nature **406**(6797): 735-738.

McMichael, A. J., P. Borrow, et al. (2010). "The immune response during acute HIV-1 infection: clues for vaccine development." Nat Rev Immunol **10**(1): 11-23.

McMichael, A. J. and S. L. Rowland-Jones (2001). "Cellular immune responses to HIV." Nature **410**(6831): 980-987.

Medzhitov, R. and C. Janeway, Jr. (2000). "Innate immunity." N Engl J Med **343**(5): 338-344.

Meena, L. S. and Rajni (2010). "Survival mechanisms of pathogenic Mycobacterium tuberculosis H37Rv." FEBS J **277**(11): 2416-2427.

Mendez-Samperio, P. (2010). "Role of interleukin-12 family cytokines in the cellular response to mycobacterial disease." Int J Infect Dis **14**(5): e366-371.

Miller, B. H., R. A. Fratti, et al. (2004). "Mycobacteria inhibit nitric oxide synthase recruitment to phagosomes during macrophage infection." Infect Immun **72**(5): 2872-2878.

Mindell, J. A. (2012). "Lysosomal acidification mechanisms." Annu Rev Physiol **74**: 69-86.

Mirsaeidi, M., M. Farshidpour, et al. (2014). "Management of nontuberculous mycobacterial infection in the elderly." Eur J Intern Med **25**(4): 356-363.

Mirsaeidi, M., R. F. Machado, et al. (2014). "Nontuberculous mycobacterial disease mortality in the United States, 1999-2010: a population-based comparative study." PLoS One **9**(3): e91879.

Molina, J. M., D. T. Scadden, et al. (1989). "Production of tumor necrosis factor alpha and interleukin 1 beta by monocytic cells infected with human immunodeficiency virus." J Clin Invest **84**(3): 733-737.

Molina, J. M., R. Schindler, et al. (1990). "Production of cytokines by peripheral blood monocytes/macrophages infected with human immunodeficiency virus type 1 (HIV-1)." J Infect Dis **161**(5): 888-893.

Molle, V., N. Saint, et al. (2006). "pH-dependent pore-forming activity of OmpATb from Mycobacterium tuberculosis and characterization of the channel by peptidic dissection." Mol Microbiol **61**(3): 826-837.

Monahan, I. M., J. Betts, et al. (2001). "Differential expression of mycobacterial proteins following phagocytosis by macrophages." Microbiology **147**(Pt 2): 459-471.

Mosser, D. M. (2003). "The many faces of macrophage activation." J Leukoc Biol **73**(2): 209-212.

Munier, M. L. and A. D. Kelleher (2007). "Acutely dysregulated, chronically disabled by the enemy within: T-cell responses to HIV-1 infection." Immunol Cell Biol **85**(1): 6-15.

Munoz-Elias, E. J. and J. D. McKinney (2005). "Mycobacterium tuberculosis isocitrate lyases 1 and 2 are jointly required for in vivo growth and virulence." Nat Med **11**(6): 638-644.

Naidoo, K., N. Padayatchi, et al. (2011). "HIV-Associated Tuberculosis." Clin Dev Immunol **2011**.

Naif, H. M. (2013). "Pathogenesis of HIV Infection." Infect Dis Rep **5**(Suppl 1): e6.

Nakata, K., W. N. Rom, et al. (1997). "Mycobacterium tuberculosis enhances human immunodeficiency virus-1 replication in the lung." Am J Respir Crit Care Med **155**(3): 996-1003.

Newman, G. W., T. G. Kelley, et al. (1993). "Concurrent infection of human macrophages with HIV-1 and Mycobacterium avium results in decreased cell viability, increased M. avium multiplication and altered cytokine production." J Immunol **151**(4): 2261-2272.

Ng, V. H., J. S. Cox, et al. (2004). "Role of KatG catalase-peroxidase in mycobacterial pathogenesis: countering the phagocyte oxidative burst." Mol Microbiol **52**(5): 1291-1302.

Novoa-Aponte, L., A. Leon-Torres, et al. (2012). "In silico identification and characterization of the ion transport specificity for P-type ATPases in the Mycobacterium tuberculosis complex." BMC Struct Biol **12**: 25.

O'Garra, A., P. S. Redford, et al. (2013). "The immune response in tuberculosis." Annu Rev Immunol **31**: 475-527.

Padmapriyadarsini, C., G. Narendran, et al. (2011). "Diagnosis & treatment of tuberculosis in HIV co-infected patients." Indian J Med Res **134**(6): 850-865.

Papp-Wallace, K. M. and M. E. Maguire (2006). "Manganese transport and the role of manganese in virulence." Annu Rev Microbiol **60**: 187-209.

Parish, T., D. A. Smith, et al. (2003). "The senX3-regX3 two-component regulatory system of Mycobacterium tuberculosis is required for virulence." Microbiology **149**(Pt 6): 1423-1435.

Parker, B. C., M. A. Ford, et al. (1983). "Epidemiology of infection by nontuberculous mycobacteria. IV. Preferential aerosolization of Mycobacterium intracellulare from natural waters." Am Rev Respir Dis **128**(4): 652-656.

Pathak, S., T. Wentzel-Larsen, et al. (2010). "Effects of in vitro HIV-1 infection on mycobacterial growth in peripheral blood monocyte-derived macrophages." Infect Immun **78**(9): 4022-4032.

Pawlowski, A., M. Jansson, et al. (2012). "Tuberculosis and HIV co-infection." PLoS Pathog **8**(2): e1002464.

Pereira, S. F., L. Goss, et al. (2011). "Eukaryote-like serine/threonine kinases and phosphatases in bacteria." Microbiol Mol Biol Rev **75**(1): 192-212.

Perez-Caballero, D., T. Zang, et al. (2009). "Tetherin inhibits HIV-1 release by directly tethering virions to cells." Cell **139**(3): 499-511.

Petrovas, C., Y. M. Mueller, et al. (2005). "Apoptosis of HIV-specific CD8+ T cells: an HIV evasion strategy." Cell Death Differ **12**(S1): 859-870.

Pick, E., Y. Gorzalczany, et al. (1993). "Role of the rac1 p21-GDP-dissociation inhibitor for rho heterodimer in the activation of the superoxide-forming NADPH oxidase of macrophages." Eur J Biochem **217**(1): 441-455.

Pieters, J., P. Muller, et al. (2013). "On guard: coronin proteins in innate and adaptive immunity." Nat Rev Immunol **13**(7): 510-518.

Planes, R. and E. Bahraoui (2013). "HIV-1 Tat protein induces the production of IDO in human monocyte derived-dendritic cells through a direct mechanism: effect on T cells proliferation." PLoS One **8**(9): e74551.

Pontow, S. E., N. V. Heyden, et al. (2004). "Actin cytoskeletal reorganizations and coreceptor-mediated activation of rac during human immunodeficiency virus-induced cell fusion." J Virol **78**(13): 7138-7147.

Prendergast, A., J. G. Prado, et al. (2010). "HIV-1 infection is characterized by profound depletion of CD161+ Th17 cells and gradual decline in regulatory T cells." AIDS **24**(4): 491-502.

Primm, T. P., C. A. Lucero, et al. (2004). "Health impacts of environmental mycobacteria." Clin Microbiol Rev **17**(1): 98-106.

Quaranta, M. G., B. Mattioli, et al. (2012). "Glances in Immunology of HIV and HCV Infection." Adv Virol **2012**: 434036.

Ramage, H. R., L. E. Connolly, et al. (2009). "Comprehensive functional analysis of Mycobacterium tuberculosis toxin-antitoxin systems: implications for pathogenesis, stress responses, and evolution." PLoS Genet **5**(12): e1000767.

Ramakrishnan, T., P. S. Murthy, et al. (1972). "Intermediary metabolism of mycobacteria." Bacteriol Rev **36**(1): 65-108.

Ranjbar, S., H. I. Boshoff, et al. (2009). "HIV-1 replication is differentially regulated by distinct clinical strains of Mycobacterium tuberculosis." PLoS One **4**(7): e6116.

Ranjbar, S., L. D. Jasenosky, et al. (2012). "Regulation of Mycobacterium tuberculosis-dependent HIV-1 transcription reveals a new role for NFAT5 in the toll-like receptor pathway." PLoS Pathog **8**(4): e1002620.

Rathmell, J. C. (2012). "Metabolism and autophagy in the immune system: immunometabolism comes of age." Immunol Rev **249**(1): 5-13.

Reddy, J. V., A. S. Burguete, et al. (2006). "A functional role for the GCC185 golgin in mannose 6-phosphate receptor recycling." Mol Biol Cell **17**(10): 4353-4363.

Rejman Lipinski, A., J. Heymann, et al. (2009). "Rab6 and Rab11 regulate Chlamydia trachomatis development and golgin-84-dependent Golgi fragmentation." PLoS Pathog **5**(10): e1000615.

Rienksma, R. A., M. Suarez-Diez, et al. (2015). "Comprehensive insights into transcriptional adaptation of intracellular mycobacteria by microbe-enriched dual RNA sequencing." BMC Genomics **16**: 34.

Riteau, N., L. Baron, et al. (2012). "ATP release and purinergic signaling: a common pathway for particle-mediated inflammasome activation." Cell Death Dis **3**: e403.

Roberts, E. A., J. Chua, et al. (2006). "Higher order Rab programming in phagolysosome biogenesis." J Cell Biol **174**(7): 923-929.

Rodriguez, G. M., M. I. Voskuil, et al. (2002). "ideR, An essential gene in mycobacterium tuberculosis: role of IdeR in iron-dependent gene expression, iron metabolism, and oxidative stress response." Infect Immun **70**(7): 3371-3381.

Rosas-Taraco, A. G., A. Y. Arce-Mendoza, et al. (2006). "Mycobacterium tuberculosis upregulates coreceptors CCR5 and CXCR4 while HIV modulates CD14 favoring concurrent infection." AIDS Res Hum Retroviruses **22**(1): 45-51.

Russell, D. G. (2003). "Phagosomes, fatty acids and tuberculosis." Nat Cell Biol **5**(9): 776-778.

Russell, D. G., P. J. Cardona, et al. (2009). "Foamy macrophages and the progression of the human tuberculosis granuloma." Nat Immunol **10**(9): 943-948.

Rustagi, A. and M. Gale, Jr. (2014). "Innate antiviral immune signaling, viral evasion and modulation by HIV-1." J Mol Biol **426**(6): 1161-1177.

Sallusto, F., M. Cella, et al. (1995). "Dendritic cells use macropinocytosis and the mannose receptor to concentrate macromolecules in the major histocompatibility complex class II compartment: downregulation by cytokines and bacterial products." J Exp Med **182**(2): 389-400.

Saritsiri, S., N. Udomsantisook, et al. (2006). "Nontuberculous mycobacterial infections in King Chulalongkorn Memorial Hospital." J Med Assoc Thai **89**(12): 2035-2046.

Sassetti, C. M., D. H. Boyd, et al. (2003). "Genes required for mycobacterial growth defined by high density mutagenesis." Mol Microbiol **48**(1): 77-84.

Sauter, D., M. Schindler, et al. (2009). "Tetherin-driven adaptation of Vpu and Nef function and the evolution of pandemic and nonpandemic HIV-1 strains." Cell Host Microbe **6**(5): 409-421.

Sawyer, S. L., M. Emerman, et al. (2004). "Ancient adaptive evolution of the primate antiviral DNA-editing enzyme APOBEC3G." PLoS Biol **2**(9): E275.

Schaeffer, E., V. B. Soros, et al. (2004). "Compensatory link between fusion and endocytosis of human immunodeficiency virus type 1 in human CD4 T lymphocytes." J Virol **78**(3): 1375-1383.

Scherr, N., P. Muller, et al. (2009). "Survival of pathogenic mycobacteria in macrophages is mediated through autophosphorylation of protein kinase G." J Bacteriol **191**(14): 4546-4554.

Schnappinger, D., S. Ehrt, et al. (2003). "Transcriptional Adaptation of Mycobacterium tuberculosis within Macrophages: Insights into the Phagosomal Environment." J Exp Med **198**(5): 693-704.

Schneider, J. S., J. G. Sklar, et al. (2014). "The Rip1 protease of Mycobacterium tuberculosis controls the SigD regulon." J Bacteriol **196**(14): 2638-2645.

Serafini, A., D. Pisu, et al. (2013). "The ESX-3 secretion system is necessary for iron and zinc homeostasis in Mycobacterium tuberculosis." PLoS One **8**(10): e78351.

Serra, C., G. Loi, et al. (2007). "Unusual clinical presentation of Mycobacterium fortuitum infection in an immunocompetent woman." J Clin Microbiol **45**(5): 1663-1665.

Shafer, R. W. and M. F. Sierra (1992). "Mycobacterium xenopi, Mycobacterium fortuitum, Mycobacterium kansasii, and other nontuberculous mycobacteria in an area of endemicity for AIDS." Clin Infect Dis **15**(1): 161-162.

Shankar, E. M., R. Vignesh, et al. (2014). "HIV-Mycobacterium tuberculosis co-infection: a 'danger-couple model' of disease pathogenesis." Pathog Dis **70**(2): 110-118.

Sharma, S. K. and M. Soneja (2011). "HIV & immune reconstitution inflammatory syndrome (IRIS)." Indian J Med Res **134**(6): 866-877.

Sharp, P. M. and B. H. Hahn (2011). "Origins of HIV and the AIDS pandemic." Cold Spring Harb Perspect Med **1**(1): a006841.

Shi, S. and S. Ehrt (2006). "Dihydrolipoamide acyltransferase is critical for Mycobacterium tuberculosis pathogenesis." Infect Immun **74**(1): 56-63.

Shirvani, H., L. Achour, et al. (2011). "Evidence for internal stores of CCR5 in blood cells." Blood **118**(4): 1175-1176.

Shoeman, R. L., B. Honer, et al. (1990). "Human immunodeficiency virus type 1 protease cleaves the intermediate filament proteins vimentin, desmin, and glial fibrillary acidic protein." Proc Natl Acad Sci U S A **87**(16): 6336-6340.

Siegal, F. P., N. Kadowaki, et al. (1999). "The nature of the principal type 1 interferon-producing cells in human blood." Science **284**(5421): 1835-1837.

Siegrist, M. S., M. Unnikrishnan, et al. (2009). "Mycobacterial Esx-3 is required for mycobactin-mediated iron acquisition." Proc Natl Acad Sci U S A **106**(44): 18792-18797.

Simon, V., N. Bloch, et al. (2015). "Intrinsic host restrictions to HIV-1 and mechanisms of viral escape." Nat Immunol **16**(6): 546-553.

Singh, S., K. Gopinath, et al. (2007). "Nontuberculous mycobacterial infections in Indian AIDS patients detected by a novel set of ESAT-6 polymerase chain reaction primers." Jpn J Infect Dis **60**(1): 14-18.

Sirakova, T. D., V. S. Dubey, et al. (2006). "Identification of a diacylglycerol acyltransferase gene involved in accumulation of triacylglycerol in Mycobacterium tuberculosis under stress." Microbiology **152**(Pt 9): 2717-2725.

Sklar, J. G., H. Makinoshima, et al. (2010). "M. tuberculosis intramembrane protease Rip1 controls transcription through three anti-sigma factor substrates." Mol Microbiol **77**(3): 605-617.

Smith, M. B., V. J. Schnadig, et al. (2001). "Clinical and pathologic features of Mycobacterium fortuitum infections. An emerging pathogen in patients with AIDS." Am J Clin Pathol **116**(2): 225-232.

Sonnenberg, P., J. R. Glynn, et al. (2005). "How soon after infection with HIV does the risk of tuberculosis start to increase? A retrospective cohort study in South African gold miners." J Infect Dis **191**(2): 150-158.

Stover, C. K., V. F. de la Cruz, et al. (1991). "New use of BCG for recombinant vaccines." Nature **351**(6326): 456-460.

Sturgill-Koszycki, S., P. L. Haddix, et al. (1997). "The interaction between Mycobacterium and the macrophage analyzed by two-dimensional polyacrylamide gel electrophoresis." Electrophoresis **18**(14): 2558-2565.

Suchindran, S., E. S. Brouwer, et al. (2009). "Is HIV infection a risk factor for multi-drug resistant tuberculosis? A systematic review." PLoS One **4**(5): e5561.

Suresh, P. and A. Wanchu (2006). "Chemokines and chemokine receptors in HIV infection: role in pathogenesis and therapeutics." J Postgrad Med **52**(3): 210-217.

Sylwester, A., D. Wessels, et al. (1993). "HIV-induced syncytia of a T cell line form single giant pseudopods and are motile." J Cell Sci **106 (Pt 3)**: 941-953.

Taiwo, B. and J. Glassroth (2010). "Nontuberculous mycobacterial lung diseases." Infect Dis Clin North Am **24**(3): 769-789.

Tavender, T. J. and N. J. Bulleid (2010). "Peroxiredoxin IV protects cells from oxidative stress by removing H2O2 produced during disulphide formation." J Cell Sci **123**(Pt 15): 2672-2679.

Timm, J., F. A. Post, et al. (2003). "Differential expression of iron-, carbon-, and oxygen-responsive mycobacterial genes in the lungs of chronically infected mice and tuberculosis patients." Proc Natl Acad Sci U S A **100**(24): 14321-14326.

Tjelle, T. E., B. Saigal, et al. (1998). "Degradation of phagosomal components in late endocytic organelles." J Cell Sci **111 (Pt 1)**: 141-148.

Tomaras, G. D. and B. F. Haynes (2009). "HIV-1-specific antibody responses during acute and chronic HIV-1 infection." Curr Opin HIV AIDS **4**(5): 373-379.

Tomlinson, G. S., L. C. Bell, et al. (2014). "HIV-1 infection of macrophages dysregulates innate immune responses to Mycobacterium tuberculosis by inhibition of interleukin-10." J Infect Dis **209**(7): 1055-1065.

Toossi, Z., H. Mayanja-Kizza, et al. (2001). "Impact of tuberculosis (TB) on HIV-1 activity in dually infected patients." Clin Exp Immunol **123**(2): 233-238.

Toossi, Z., L. Xia, et al. (1999). "Transcriptional activation of HIV by Mycobacterium tuberculosis in human monocytes." Clin Exp Immunol **117**(2): 324-330.

van Soolingen, D. and J. van Ingen (2012). "On the road to unravelling the aetiology of non-tuberculous mycobacterial disease." Int J Tuberc Lung Dis **16**(10): 1279.

Vandal, O. H., L. M. Pierini, et al. (2008). "A membrane protein preserves intrabacterial pH in intraphagosomal Mycobacterium tuberculosis." Nat Med **14**(8): 849-854.

Vandal, O. H., J. A. Roberts, et al. (2009). "Acid-susceptible mutants of Mycobacterium tuberculosis share hypersusceptibility to cell wall and oxidative stress and to the host environment." J Bacteriol **191**(2): 625-631.

Vats, A., A. K. Singh, et al. (2012). "Retrobiosynthetic approach delineates the biosynthetic pathway and the structure of the acyl chain of mycobacterial glycopeptidolipids." J Biol Chem **287**(36): 30677-30687.

Vergne, I., J. Chua, et al. (2005). "Mechanism of phagolysosome biogenesis block by viable Mycobacterium tuberculosis." Proc Natl Acad Sci U S A **102**(11): 4033-4038.

Vergne, I., J. Chua, et al. (2004). "Cell biology of mycobacterium tuberculosis phagosome." Annu Rev Cell Dev Biol **20**: 367-394.

Vergne, I., R. A. Fratti, et al. (2004). "Mycobacterium tuberculosis phagosome maturation arrest: mycobacterial phosphatidylinositol analog phosphatidylinositol mannoside stimulates early endosomal fusion." Mol Biol Cell **15**(2): 751-760.

Vergne, I., M. Gilleron, et al. (2014). "Manipulation of the endocytic pathway and phagocyte functions by Mycobacterium tuberculosis lipoarabinomannan." Front Cell Infect Microbiol **4**: 187.

Vieira, O. V., R. E. Harrison, et al. (2004). "Acquisition of Hrs, an essential component of phagosomal maturation, is impaired by mycobacteria." Mol Cell Biol **24**(10): 4593-4604.

Vijayakumar, S., S. Finney John, et al. (2013). "In vitro model of mycobacteria and HIV-1 co-infection for drug discovery." Tuberculosis (Edinb) **93 Suppl**: S66-70.

Vilaseca, M. A., R. Artuch, et al. (2003). "Low serum carnitine in HIV-infected children on antiretroviral treatment." Eur J Clin Nutr **57**(10): 1317-1322.

Wagner, D. and L. S. Young (2004). "Nontuberculous mycobacterial infections: a clinical review." Infection **32**(5): 257-270.

Wandy Beatty and Russell, G. D. (2001). Analysis of Mycobacterium-Infected Macrophages by Immunoelectron Microscopy and Cell Fractionation. Mycobacterium tuberculosis protocols. Tanya Parish and Stoker,G.N. Totowa, New Jersey, Humana Press. **54:** 281-294.

Wang, J., D. Duncan, et al. (2013). "WEB-based GEne SeT AnaLysis Toolkit (WebGestalt): update 2013." Nucleic Acids Res **41**(Web Server issue): W77-83.

Weiss, C. H. and J. Glassroth (2012). "Pulmonary disease caused by nontuberculous mycobacteria." Expert Rev Respir Med **6**(6): 597-612; quiz 613.

Weiss, G. and U. E. Schaible (2015). "Macrophage defense mechanisms against intracellular bacteria." Immunol Rev **264**(1): 182-203.

Weiss, R. A. (2013). "Thirty years on: HIV receptor gymnastics and the prevention of infection." BMC Biol **11**: 57.

Wong, D., H. Bach, et al. (2011). "Mycobacterium tuberculosis protein tyrosine phosphatase (PtpA) excludes host vacuolar-H+-ATPase to inhibit phagosome acidification." Proc Natl Acad Sci U S A **108**(48): 19371-19376.

Wyatt, R., P. D. Kwong, et al. (1998). "The antigenic structure of the HIV gp120 envelope glycoprotein." Nature **393**(6686): 705-711.

Yajko, D. M., J. J. Madej, et al. (1995). "Colorimetric method for determining MICs of antimicrobial agents for Mycobacterium tuberculosis." J Clin Microbiol **33**(9): 2324-2327.

Yeo, J. C., A. A. Wall, et al. (2015). "Rab31 and APPL2 enhance FcgammaR-mediated phagocytosis through PI3K/Akt signaling in macrophages." Mol Biol Cell **26**(5): 952-965.

Yoon, K., J. G. Jeong, et al. (2001). "Stable expression of human immunodeficiency virus type 1 Nef confers resistance against Fas-mediated apoptosis." AIDS Res Hum Retroviruses **17**(2): 99-104.

Younes, S. A., B. Yassine-Diab, et al. (2003). "HIV-1 viremia prevents the establishment of interleukin 2-producing HIV-specific memory CD4+ T cells endowed with proliferative capacity." J Exp Med **198**(12): 1909-1922.

Zhang, B., S. Kirov, et al. (2005). "WebGestalt: an integrated system for exploring gene sets in various biological contexts." Nucleic Acids Res **33**(Web Server issue): W741-748.

Zhang, Q. and I. Sugawara (2012). "Immunology of tuberculosis." World J Exp Med **2**(4): 70-74.

Zhao, C., S. Thibault, et al. (2006). "In primary human monocyte-derived macrophages exposed to Human immunodeficiency virus type 1, does the increased intracellular growth of Leishmania infantum rely on its enhanced uptake?" J Gen Virol **87**(Pt 5): 1295-1302.

Zhou, D., K. H. Kang, et al. (2012). "Production of interferon alpha by human immunodeficiency virus type 1 in human plasmacytoid dendritic cells is dependent on induction of autophagy." J Infect Dis **205**(8): 1258-1267.

Publications

Cellular Microbiology (2015) doi:10.1111/cmi.12516

Proteomics approach to understand reduced clearance of mycobacteria and high viral titers during HIV–mycobacteria co-infection

Rakesh Ganji,[1] Snigdha Dhali,[2] Arshad Rizvi,[1] Swetha Sankati,[1] Mani Harika Vemula,[1] Gaurang Mahajan,[2] Srikanth Rapole[2] and Sharmistha Banerjee[1]*

[1]*Department of Biochemistry, School of Life Sciences, University of Hyderabad, Hyderabad, Telangana State, India.*

[2]*National Centre for Cell Science, Pune, Maharashtra, India.*

Summary

Environmental mycobacteria, highly prevalent in natural and artificial (including chlorinated municipal water) niches, are emerging as new threat to human health, especially to HIV-infected population. These seemingly harmless non-pathogenic mycobacteria, which are otherwise cleared, establish as opportunistic infections adding to HIV-associated complications. Although immune-evading strategies of pathogenic mycobacteria are known, the mechanisms underlying the early events by which opportunistic mycobacteria establish infection in macrophages and influencing HIV infection are unclear. Proteomics of phagosome-enriched fractions from *Mycobacterium bovis* Bacillus Calmette–Guérin (BCG) mono-infected and HIV–*M. bovis* BCG co-infected THP-1 cells by LC-MALDI-MS/MS revealed differential distribution of 260 proteins. Validation of the proteomics data showed that HIV co-infection helped the survival of non-pathogenic mycobacteria by obstructing phagosome maturation, promoting lipid biogenesis and increasing intracellular ATP equivalents. In turn, mycobacterial co-infection up-regulated purinergic receptors in macrophages that are known to support HIV entry, explaining increased viral titers during co-infection. The mutualism was reconfirmed using clinically relevant opportunistic mycobacteria, *Mycobacterium avium*, *Mycobacterium kansasii* and *Mycobacterium phlei* that exhibited increased survival during co-infection, together with increase in HIV titers. Additionally, the catalogued proteins in the study provide new leads that will significantly add to the understanding of the biology of opportunistic mycobacteria and HIV coalition.

Received 11 January, 2015; revised 27 July, 2015; accepted 20 August, 2015. *For correspondence. E-mail sbsl@uohyd.ernet.in; Tel. (+91)-40-23134573; Fax (+91)-40-23010120.

Introduction

Mycobacterium tuberculosis complex comprises of phylogenetically close groups of *Mycobacterium* species that infect humans causing tuberculosis (TB), a disease that despite being curable has re-emerged as a global pandemic (Kaufmann and McMichael, 2005). Multiple factors, including lack of effective vaccine, failure of early detection, emergence of drug resistance and, of late, the co-epidemics with HIV/AIDS, had limited the success of TB disease management. In the recent times, AIDS epidemic has had an immense bearing on the clinical presentation, transmission and epidemiology of TB worldwide (Pawlowski *et al*., 2012). TB is predominantly caused by the pathogenic mycobacteria *M. tuberculosis*; however, non-tuberculous or attenuated strains of mycobacteria such as *Mycobacterium avium*, *Mycobacterium kansasii*, *Mycobacterium fortuitum*, *Mycobacterium xenopi* and *Mycobacterium bovis* Bacillus Calmette–Guérin (BCG) cause opportunistic infections in HIV patients (Juffermans *et al*., 1998; Smith *et al*., 2001; Bachmeyer *et al*., 2002; Karakousis *et al*., 2004; Serra *et al*., 2007; Singh *et al*., 2007; Azzopardi *et al*., 2009; Hesseling *et al*., 2009) even before T-cell depletion is apparent (Sonnenberg *et al*., 2005). More than 90 species of *Mycobacterium* had been reported to inhabit natural (air, water, soil or other organisms) and artificial (chlorinated municipal water) reservoirs (Primm *et al*., 2004). These are emerging as potential opportunistic pathogens in human, especially in immunocompromised HIV patients (Herzmann *et al*., 2011), resulting in an increased risk of disease progression from both the pathogens in the individuals concurrently infected with mycobacteria and HIV as compared with those carrying single infections (Goletti *et al*., 1996).

Several molecular mechanisms have been attributed to the synergistic impact of pathogenic mycobacteria on HIV propagation. Mycobacterial components directly or indirectly increase the expression of transcription factors

Report of Plagiarism check

proteomics approach to understand hiv-mycobacteria co-infection

by Ganji Rakesh

proteomics approach to understand hiv-mycobacteria co-infection

ORIGINALITY REPORT

30%	8%	27%	3%
SIMILARITY INDEX	INTERNET SOURCES	PUBLICATIONS	STUDENT PAPERS

PRIMARY SOURCES

1	Ganji, Rakesh, Snigdha Dhali, Arshad Rizvi, Swetha Sankati, Mani Harika Vemula, Gaurang Mahajan, Srikanth Rapole, and Sharmistha Banerjee. "Proteomics approach to understand reduced clearance of mycobacteria and high viral titers during HIV-mycobacteria co-infection : Proteomics of HIV-mycobacteria co-infection", Cellular Microbiology, 2015. Publication	20%
2	informatics.yonsei.ac.kr Internet Source	1%
3	Chande, Ajit G., Zaved Siddiqui, Mukul Kumar Midha, Varsha Sirohi, Srikanth Ravichandran, and Kanury V. S. Rao. "Selective enrichment of mycobacterial proteins from infected host macrophages", Scientific Reports, 2015. Publication	1%
4	www.cbcp.at Internet Source	1%